THE INFLUENCE OF ROCK FABRIC ON EXCAVATION DAMAGE IN THE LAC DU BONNET GRANITE.

BY

RICHARD ALLEN EVERITT

A thesis
Submitted to the Faculty of Graduate Studies
In Partial Fulfillment of the Requirements
for the Degree of

DOCTOR OF PHILOSOPHY

Department Of Civil and Geological Engineering
University of Manitoba
Winnipeg, Manitoba

June 06, 2001

THE UNIVERSITY OF MANITOBA

FACULTY OF GRADUATE STUDIES

*****

COPYRIGHT PERMISSION

THE INFLUENCE OF ROCK FABRIC ON EXCAVATION DAMAGE IN THE LAC DU BONNET GRANITE.

BY

RICHARD ALLEN EVERITT

A Thesis/Practicum submitted to the Faculty of Graduate Studies of The University of Manitoba in partial fulfillment of the requirement of the degree

of

DOCTOR OF PHILOSOPHY

ABSTRACT

The Canadian concept for disposing of nuclear fuel waste involves placing and sealing it in excavations 500 to 1000 m deep in plutonic rocks of the Canadian Shield. Investigations pertaining to the Canadian concept for used nuclear fuel waste disposal in plutonic rocks were conducted at AECL's Underground Research Laboratory (URL). The URL is excavated within the Archean granite of the Lac Du Bonnet batholith (LDBB), approximately 120 km northeast of Winnipeg, Manitoba, at the western edge of the Canadian Shield.

At the URL, AECL has undertaken a wide range of experiments to test the feasibility of burying nuclear fuel waste in granitic rocks. The investigations have included detailed mapping of geological features, stress measurement, and a recording of excavation response.

The purpose of this thesis is to show how the geological conditions affect excavation stability, in particular how the fabric of granite influences excavation damage development including overbreak around tunnel or shaft perimeters.

Most of the design of the excavations has been based on the assumption that the host granite is homogeneous (i.e. texturally and mechanically homogeneous). This thesis demonstrates, through a program of field observations and laboratory testing, that the Lac

du Bonnet, and probably most granites, are highly heterogeneous and anisotropic at both the macro and the micro scale.

Field investigations included detailed mapping. This had four objectives:

1. to define the general site characteristics including: 1) the geology of the site, 2) the fault and fractures domains, and 3) the in-situ stress domains. This was supported by field and laboratory investigations including fracture, foliation and microcrack analyses. This work defined the nature and types of rock mass heterogeneities in the rock mass.
2. to locate and describe evidence where fabric anisotropy has influenced rock mass response. This was not restricted to only present-day excavation response, but also included observations from ancient faults and fractures, whose distribution and orientation provided the first hint of the anisotropic behaviour of the LDBB granite. In this regard, the ancient fractures provide a natural analogue for the long-term / large-scale response of the granite to stresses.
3. to characterize areas where excavation damage, including overbreak, occurred, and
4. to select and characterize areas where samples were collected for rock properties testing.

For this last purpose, three locations were selected at the 420 m depth (420 Level) to provide a representative sample of the range of the compositional and textural heterogeneity present in the LDBB, and its affect on rock strength and rock mass response. These are:

- a fine grained granite dyke with subvertical flow banding,

- a medium grained and weakly to moderately layered granite forming the main mass of the batholith, and
- a generally coarse grained and leucocratic unit that occurs as sills and recrystallized zones in the main phase.

For the sake of convenience, these are referred to as the fine, medium and coarse grained granites, respectively.

The three case studies were sited in newly excavated tunnels at the 420 Level (420 m depth of the URL) where the damage due to stress relief can be observed in the process of developing. The sites are in close proximity to each other. They are distant from faults or major fractures, and are in the same in-situ stress-domain. As such, they are subject to the same stress magnitudes and orientations.

At each of the three locations, the tunnel profile was surveyed, and the geology and excavation damage were then added to the profile. An array of boreholes was then designed for each of the three locations. The arrays were designed to intersect the most prominent foliation / microcrack set at 90°, and then at 20-30° increments until the core axis was parallel to the foliation. Boreholes, twelve in all, provided a total of 171 samples along these profiles.

The core was logged for foliations and microcracks, and then cut to provide oriented samples for uniaxial compression tests. Structure orientations were measured and converted from a relative (borehole) coordinate system to true orientations.

Strength anisotropy and the influence of foliation were then systematically investigated for each of the fine, medium and coarse grained granites using rock mechanics tests that are sensitive to planar anisotropy. This included: 103 Point Load tests to determine preferred microcrack directions and their relative strengths, and *57* Brazilian tests to determine the average tensile strength and any directional anisotropy. In addition to these tests, the borehole arrays provided samples at varying angles to the fabric with which to test for anisotropy in the uniaxial compressive strength of each rock type.

The excavations and boreholes at the URL site provide a unique cross section 1100 m deep through an Archean batholith. The underground mapping and boreholes clearly indicate that what appears on the surface to be a homogeneous Archean granite, is in fact coarsely layered with vertical gradations in lithology, in batholith structure, in the development of both natural and excavation-induced fractures, and in alteration.

Layering, grain size, foliation and microcrack alignment influence excavation damage development, including the depth and shapes of overbreak. The reason for this is that the tensile strength along layering, foliation and microcracks alignment is significantly lower than in direction unaffected by these. Similarly, grain size has a strong influence. Both the tensile and the compressive strength of granite are higher in the finer grained variety of the Lac du Bonnet granite.

ACKNOWLEDGEMENTS

I would first like to thank my wife, Maria, for her tireless support and encouragement and faith in my pursuit of a doctorate degree, and also my daughter Louisa, for being so patient while I was immersed in my university work.

This thesis represents a culmination of ideas and experience gained from working in a unique research environment. I am indebted to AECL Research for the financial support provided to pursue graduate studies at the University of Manitoba. AECL also funded my studies of the microfractures in the Lac du Bonnet granite, and the uniaxial compression testing of the pegmatite. These were initially components of this thesis, but are now presented separately owing to time limitations. Ontario Power Generation also provided financial support. I would particularly like to thank Mark Jensen and Frank King for their involvement. I would also like to acknowledge the advice and encouragement given to me by Anton Brown, Derek Martin, Cliff Davison, Ed Dzik, Jason Martino, Keith Nuttall, Rod Read, Denver Stone and Gary Simmons. Gig Hiltz, Ed Jacobs and Paul Gann provided invaluable assistance with figure preparation, and Dave Woodcock with the preparation and retrieval of the core samples used in this investigation.

Finally, I would also like to express sincere thanks to my advisor, Dr. Emery Lajtai, and to my examination committee (Drs. Brian Stimpson, Alexander Cruden, Neil Chandler Nash Soonawala, Nabil Bassim, and Vijay Chatoorgoon) for their guidance and recommendations that have helped in the completion of this thesis.

SYMBOLS AND NOTATION

x,y,z	*Rectangular Cartesian coordinates*
E	*Young's modulus*
G	*Shear modulus*
V	*Poisson's ratio*
σ_1	*Maximum principal stress component*
σ_2	*Intermediate principle stress component*
σ_3	*Minimum principle stress component*
σ_c	*Uniaxial compressive strength*
σ_t	*Tensile strength*
σ_{ci}	*Crack initiation stress*
σ_{cd}	*Crack damage stress (start of unstable crack growth)*
Is	*Point load strength index*
σ_{tB}	*Brazilian tensile strength*
k	*ratio of Young's moduli in tension and compression*
ε_v	*volumetric strain*
ε_a	*axial strain*
ε_c	*circumferential strain.*

CONTENTS

LIST OF FIGURES

LIST OF TABLES

Chapter 1

INTRODUCTION

The understanding of the mechanism of fracture development around underground openings is important for the design of a safe and stable openings in mining and civil engineering applications. In the design of nuclear waste disposal vaults, a special concern is the potential for significant propagation of existing fractures, or the creation of new fractures (excavation damage) through the construction of such a facility. Interconnected fractures could reduce the effectiveness of the rock as a barrier to contaminant movement by providing pathways for groundwater to transport contaminants released from a disposal vault.

The Canadian concept for disposing of nuclear fuel waste involves placing and sealing it in excavations 500 to 1000 m deep in plutonic rocks of the Canadian Shield. Investigations pertaining to the Canadian concept for used nuclear fuel waste disposal in plutonic rocks are being conducted at AECL's Underground Research Laboratory (URL). The URL is excavated within the Archean granite of the Lac Du Bonnet batholith (LDBB), approximately 120 km northeast of Winnipeg, Manitoba, at the western edge of the Canadian Shield (Figure 1). The main purpose of AECL's investigations at the URL is to develop geologic data and experience that can then be used in locating a permanent nuclear waste facility.

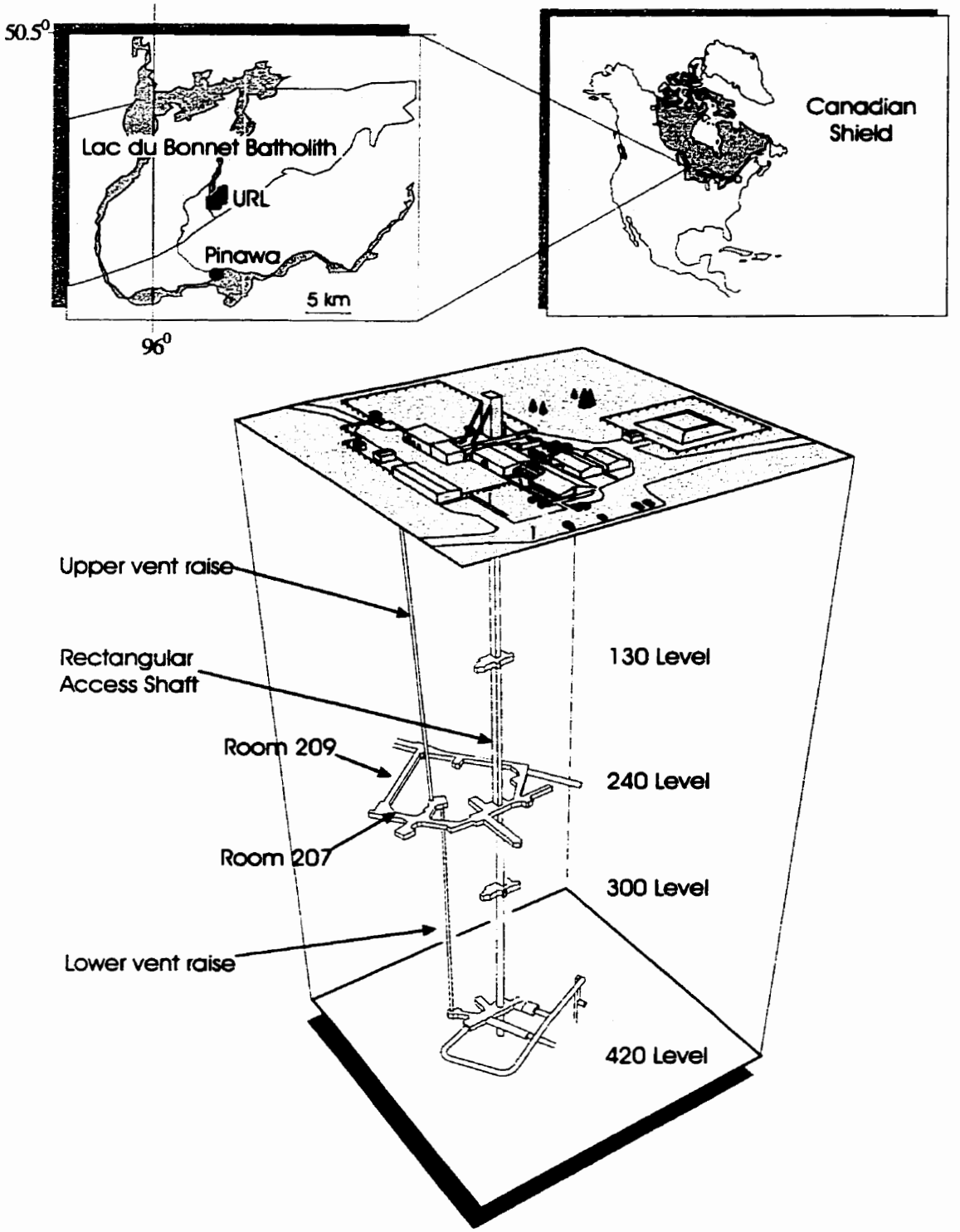

Figure 1. Regional setting of the Lac Du Bonnet batholith of Manitoba, the study area at AECL's Underground Research Laboratory (URL), and the excavations comprising the URL. Locations referred to in the text are shown.

1.1. Problem Statement

Mapping of the shafts and the various tunnels at the URL by the author, conducted during its construction, has indicated that excavation-induced fractures were far more numerous than natural fractures except within fault zones. In the shaft below Fracture Zone 2, in most of the 240 Level, and in all of the 420 Level, excavation-induced fractures are the only fractures present. Excavation-induced fractures are distinguished from natural fractures by the absence of mineral infilling or wall rock alteration, by their position and geometry relative to blasthole remnants, and by their position and geometry relative to the tunnel profiles or tunnel face. In general, they form an onion-skin pattern of surfaces, similar to the exfoliation fractures seen in surface outcrops, but in the subsurface their orientation and size is dependent on their location relative to the tunnel perimeter, and to the location of tunnel faces during excavation.

Prior to the excavations of the URL, there have been a number of studies to predict the response of the local granitic rocks to the new stress conditions imposed through the wide-ranging excavations, consisting of a central shaft and connecting tunnels and raises (Figure 1). Not one of these studies anticipated the massive fracture development (excavation damage of AECL terminology) that was later observed at compressive stress concentrations. There is one thing common to these and even to most of the later studies. They have all assumed that the granite is homogeneous, isotropic and relatively unfractured. From this flowed the next assumption that the in-situ strength of the granite should not be that much different from the intact rock strength determined in the laboratory using small drill core samples.

Although the in-situ stresses at the URL site have been found to be much higher than at comparable depths elsewhere in the Canadian Shield, the stresses are still not high enough to cause even minor fracture development in the intact rock samples used in the laboratory investigations. A one-half reduction of in-situ strength relative to the unconfined compressive strength due to environmental effects (heat, humidity and long-duration static loading) have been predicated by others (e.g. Lajtai et al., 1987) and some of the same factors have certainly been active at the URL site. This would explain some excavation damage, especially in the highest stress environment at 420 m depth. They do not however explain:

1. the fact that failure in the form of slabbing also exists under the much lower stresses present at the 240 m level, and
2. that documented differences in excavation damage within a single tunnel or shaft subject to the same in-situ stresses and excavated by the same means and schedule.

Examples of the excavation damage include:

1. slabbing and spalling of rock about tunnel perimeters at the 240 m depth (Figure 2; also Figure 3 and Figure 4)
2. slabbing and spalling of rock about the shaft perimeter at 300 m depth (Figure 2; also Figure 5),
3. breakout notches around the tunnels, bored vent raises, and the conventionally excavated (i.e. drill-and-blast) shafts (Figure 2), and
4. blast- or stress-relief fractures radiating away from the blasthole remnants preserved on tunnel faces (Figure 2).

None of the above can be explained while assuming homogeneous and isotropic conditions. Evidence that anisotropy of rock structure (i.e. average grain size, variation in

grain size, number and type of foliations, microcrack alignments and their orientations) was contributing to excavation damage development was first obtained during routine mapping of the shaft and tunnels during the most early phases of construction by the author, in his role as the URL site geologist. Damage development has been observed to vary in response to textural and structural variations in the granite in both the vertical (Figure 4) and horizontal planes (Figure 5).

The tunnels at the 240 Level demonstrate the influence of subtle fabric on excavation damage development in tunnels (Figure 4). The axis of tunnel (Room) 207 is parallel to the maximum principal stress and to the strike of the gneissosity, while Room 209 is oriented perpendicular to them. There was hardly any damage around the tunnel oriented parallel to the intermediate principal stress, despite that fact that this orientation would be the most critical. One would expect the least damage in Room 207 which is oriented parallel to the maximum principal stress. Nevertheless, a 1 x 1.5 m slab spalled from the area where the perimeter is parallel to the layering in the medium grained granite.

The tunnel profile of Room 207 is asymmetric, with induced fractures paralleling the gneissosity being not only more frequent, but also larger than those in other directions. Damage here also includes a 1 x 1.5 m slab spalled from the area where the perimeter is parallel to the layering in the medium grained granite. In Room 209, the layering is not favourably oriented to serve as exfoliation (i.e. failure) planes, and as a result, the damage profile is symmetrical. The orientation and magnitudes of the in-situ stress at this location are listed in Table 1. In this example, it is also noteworthy that the greatest

damage developed not in the tunnel subject to the higher $\sigma_1 - \sigma_3$ stress difference (25.5 – 12.8), but in the tunnel subject to the lower $\sigma_2 - \sigma_3$ stress difference (16.8 – 12.8). In fact, the perimeter stress calculated from the Kirsch stress equation should vary between 20 – 40 MPa only. No fracture would be expected for a rock that has uniaxial compressive strength of about 200 MPa. Clearly, while the damage is initiated by stress release about the tunnel profile, the geometry and extent of this damage is very dependent upon the presence of the low-dipping layering.

Table 1.

In-situ stresses measured at the 240 Level.

(Martin and Kozak, 1992)

	Magnitude	trend	plunge
σ_1	25.5 MPa	228°	8°
σ_2	16.8 MPa	135°	23°
σ_3	12.8 MPa	335°	65°

The cross section of the shaft excavation damage zone (provided by the floor of the 300 Level shaft station) further demonstrates the influence of subtle fabric on excavation damage development (Figure 5). Incipient breakout notches are developing in the NE and SW quadrants of the tunnel perimeter, in response to the stress orientations shown. Damage development varies with rock type, being best developed in the fine grained granite, and is weak or absent in the medium grained granite. This is the opposite of what would be expected based on the published strength data on these two rock types

(e.g. Martin, 1993), and from what would be expected based on the excavation response observations from the 420 Level (Read and Martin, 1990; 1991; 1992; and 1996). Mapping by the author, of the damage zone and geology at the 300 Level has revealed that the "anomalous damage" in the fine grained granite is due to the separation of slabs along a vertical foliation (planes of aligned biotite). Again, the conclusion is that while damage is initiated by stress release about the tunnel profile, the geometry and extent of this damage is very dependent upon the presence of a suitably oriented fabric element. The purpose of this thesis is to show how the geological conditions affect excavation stability, in particular how the fabric of granite influences excavation damage development including overbreak around tunnel or shaft perimeters. Fabric refers to natural planes of weakness in the form of pre-excavation microcrack alignments, compositional layering, foliation and changes in average grain size.

This space intentionally left blank for effective pagination.

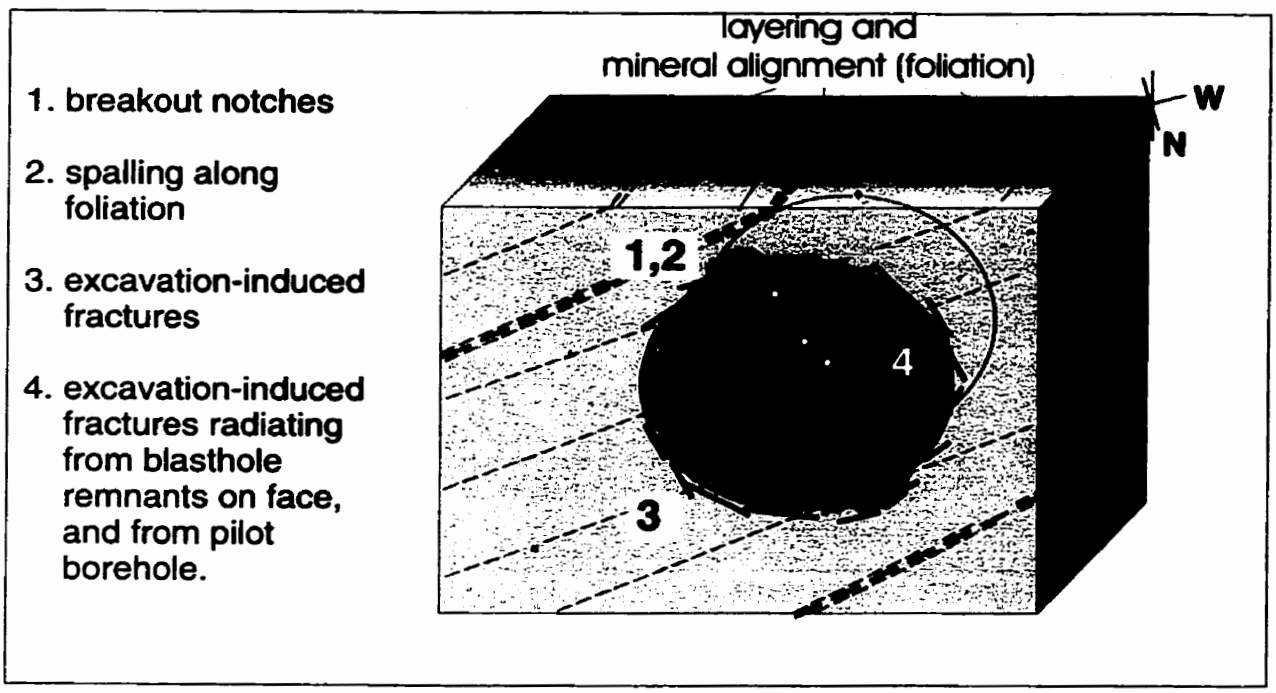

Figure 2. Schematic representation of excavation damage types observed in the URL. Breakouts (1) occur in all shafts and tunnels below 300 m, whether bored or blasted. Spalling and other excavation-induced fractures (2,3,4) occur at all levels in the URL, but are most intensely developed in the highly stressed rock below 300 m.

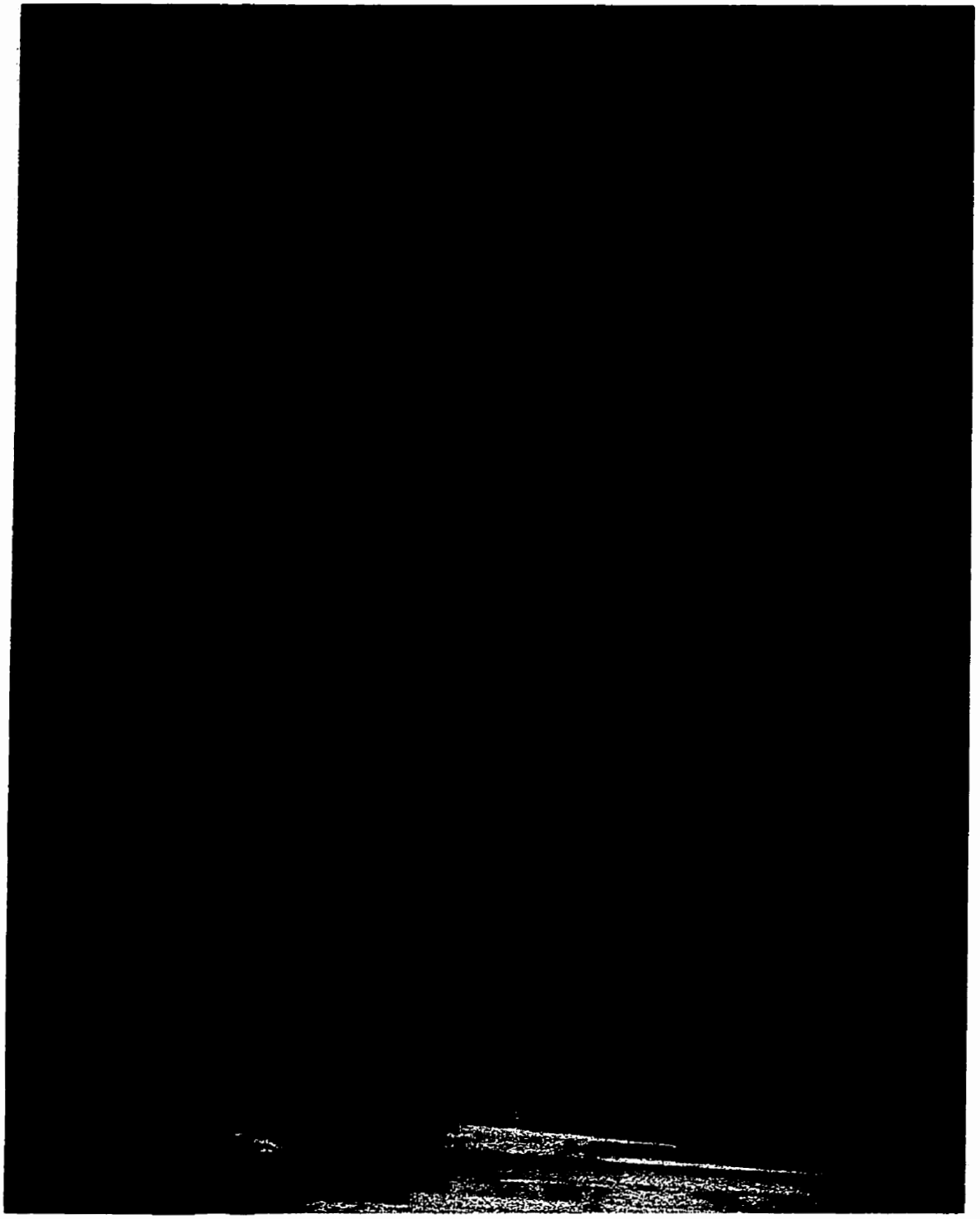

Figure 3. Spalling developed along a tunnel wall at the 240 Level of the URL during its construction. The tunnel axis is parallel to σ_1 (25.8 MPa), σ_2 (16.8 MPa) is nearly horizontal while σ_3 (12.8 MPa) is nearly vertical.

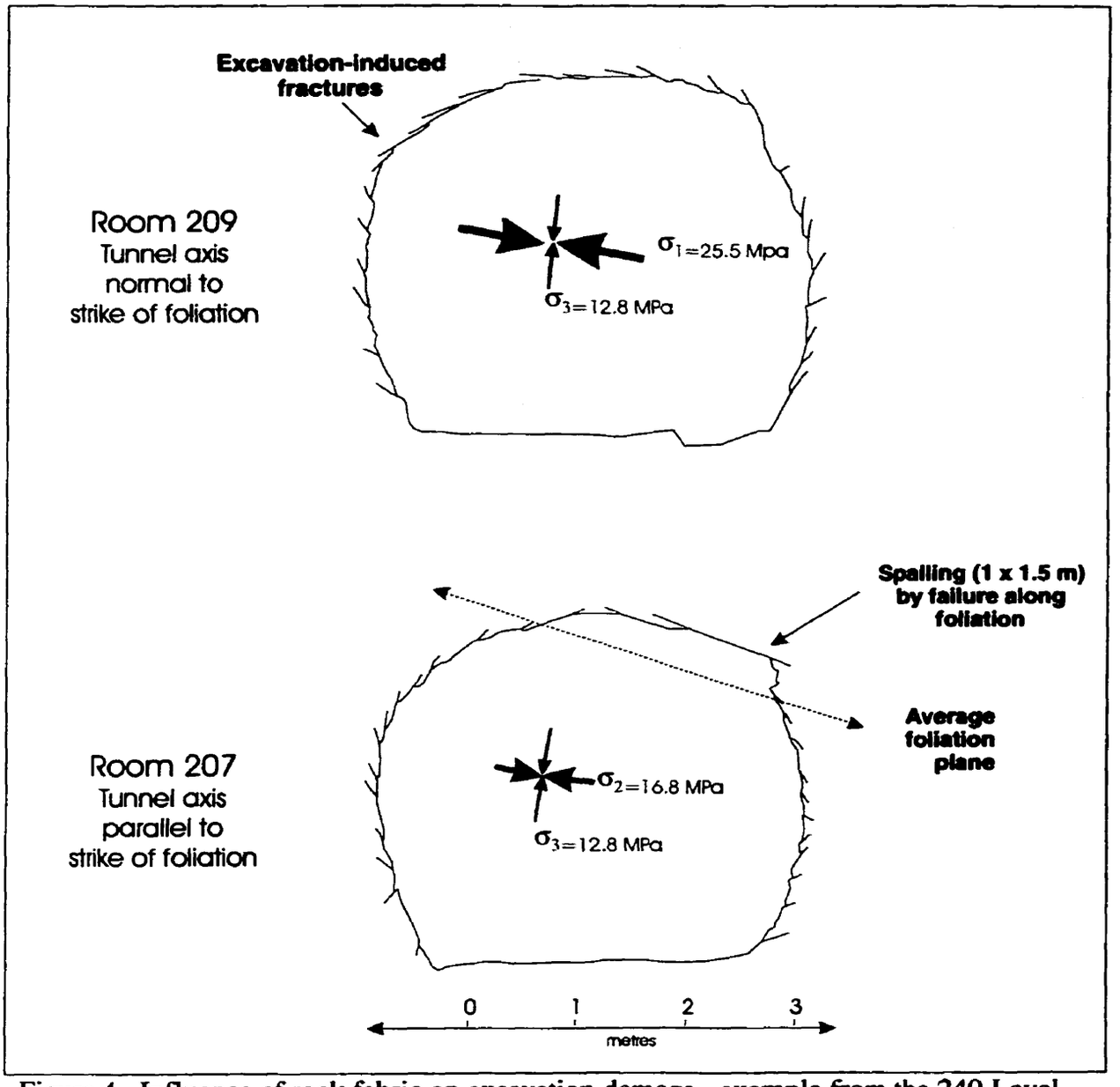

Figure 4. Influence of rock fabric on excavation damage - example from the 240 Level. This figure presents a schematic view of the fabric elements present at the 240 Level, and the damage associated with different tunnel orientations. Both tunnels are constructed in the same medium grained, coarsely layered granite, but differ in their orientation. The profile of Room 209 is in the σ_1 / σ_3 plane, while the profile of Room 207 is in the σ_2 / σ_3 plane. Mapping of the two tunnel profiles revealed that the damage about Room 209 is limited to minor surface exfoliation, with a symmetrical distribution of excavation-induced (stress-relief) fractures. In contrast, the damage about Room 207 is more extensive, with a markedly asymmetrical distribution of excavation-induced (stress-relief) fractures. A 1x 1.5 m slab spalled from the tunnel in the area where the perimeter is parallel to the layering.

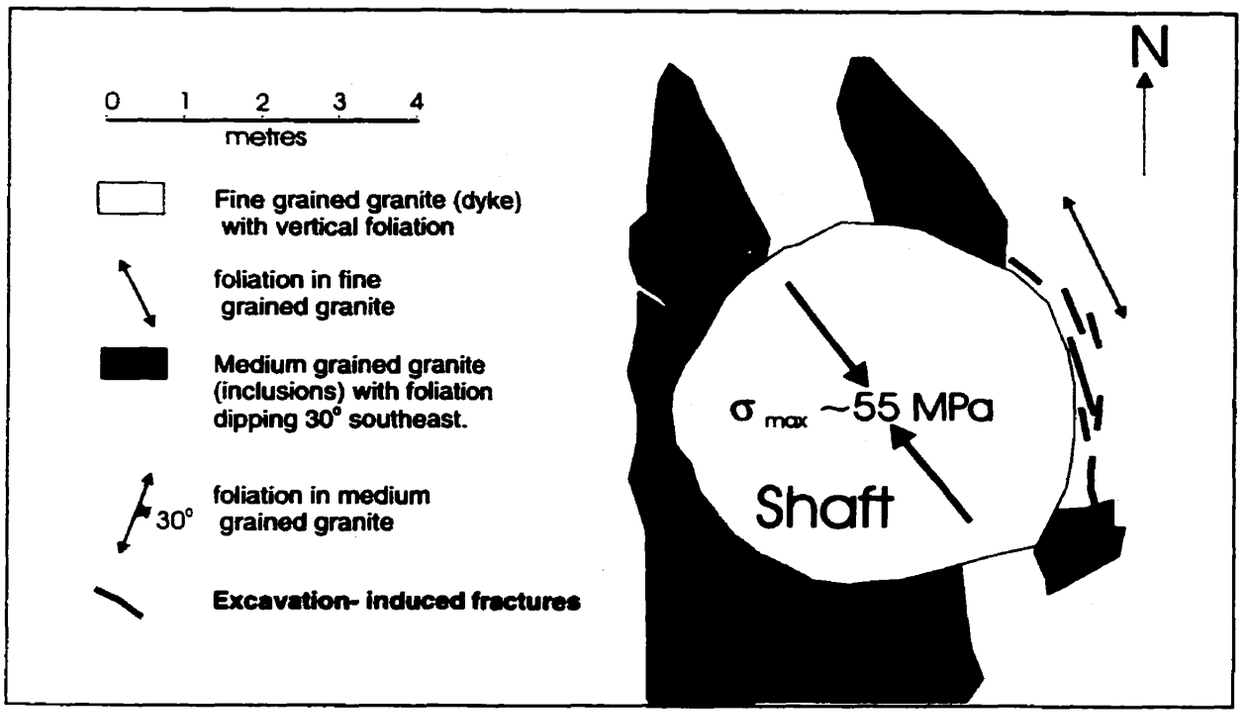

Figure 5. Influence of rock fabric on excavation damage - example from the 300 Level. At this depth, weak or incipient breakouts were occurring in the NE and SW quadrants of the shaft, due to spalling of slabs from the shaft wall. Most spalling occurred in the NE quadrant, and the presence of additional "loose" (incipient or partially spalled slabs) was indicated by a hollow sound when hit hard with a scaling bar. The corresponding breakout in the SW quadrant was, in comparison, insignificant and intact (no loose). Mapping of the station floor at this depth provided a cross section of the damage about the shaft, and an explanation for the difference in breakout development described above. In the NE quadrant, spalling was enhanced by parting along the subvertical foliation in the fine grained granite. In the SW quadrant, the foliation was subhorizontal, and therefore not favourably oriented to promote fracture development under these stress conditions.

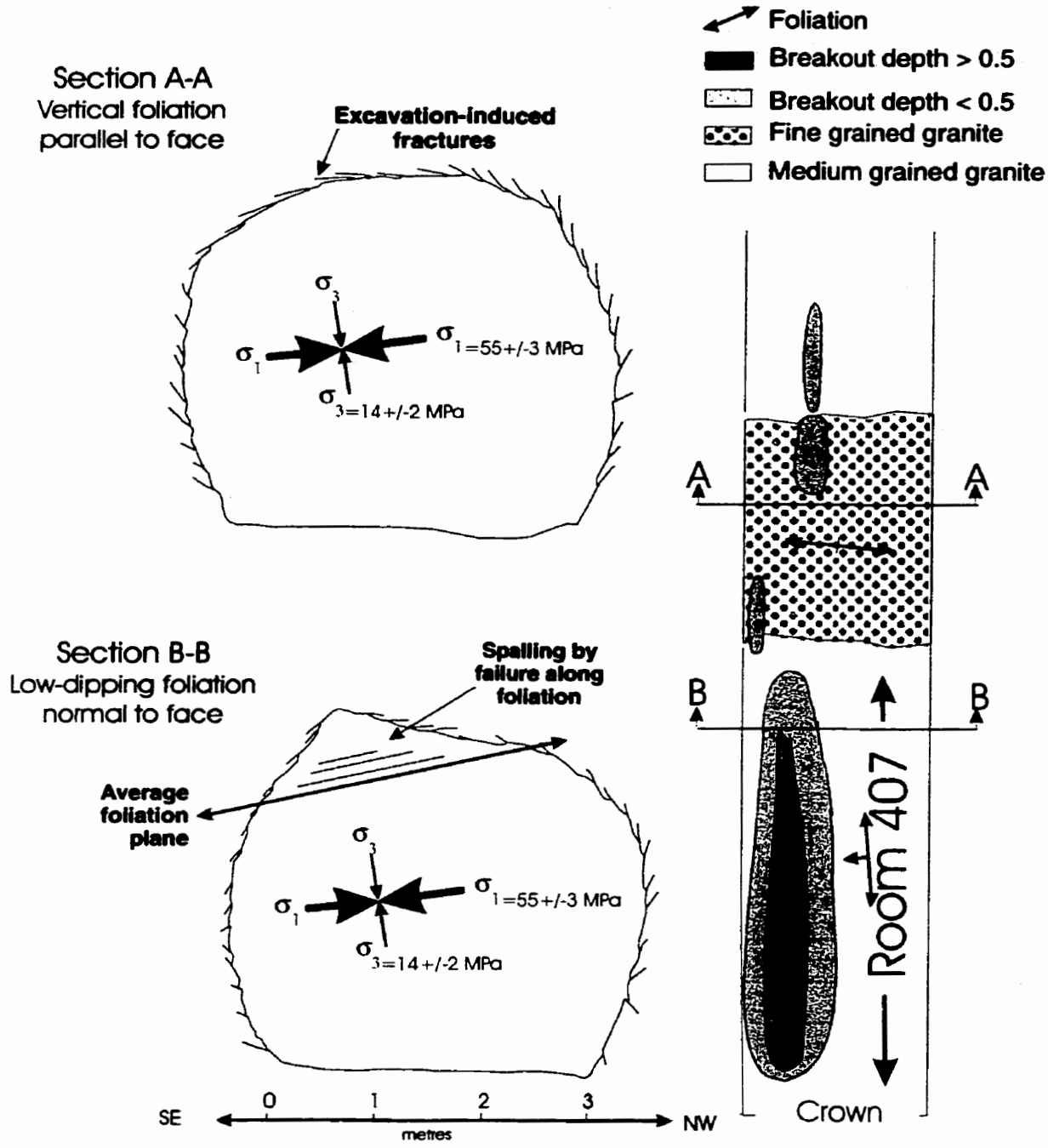

Figure 6. Influence of geology on breakout development within a single drill-and-blast tunnel. Room 407 at the 420 Level of the URL provides an example of the influence of subtle differences in geology on breakout development in granite where conventional excavation is used. The tunnel profiles developed in the medium grained and fine grained granites are shown in A and B, respectively. In the medium grained granite, the parting of the rock along planes of biotite facilitates breakout development. In the fine grained granite, a biotite foliation also exists but it is subvertical and normal to the tunnel axis. As such, its presence does not influence breakout development for this excavation orientation and geometry.

Figure 7. Influence of geology on breakout development within a single drill-and-blast tunnel. Room 421 at the 420 Level of the URL provides an example of the influence of subtle differences in geology on breakout development in the fine grained granite where conventional excavation is used. In the previous figure it was noted that ... "a biotite foliation also exists in the fine grained granite, but it is subvertical and normal to the tunnel axis. As such, its presence does not influence breakout development for this excavation orientation and geometry". In Room 421 however, the tunnel axis is parallel to the strike of the foliation, and spalling now occurs along this structure.

1.2. Objective, Scope of Work, and Thesis Organization

The objective of this research is to investigate and document the contribution of rock fabric on excavation damage development. This thesis demonstrates, through a program of field observations and laboratory testing, that foliation and other seemingly minor textural variations in the rock are major contributors to the observed variations in excavation damage, and the lower than expected strength.

The rock properties testing conducted in this study was intended to define the influence of foliation and preferred microcrack orientations in creating strength anisotropies, which in turn influence excavation damage development. Techniques sensitive to planar anisotropy in rock were identified from the literature. It is recognized that fabric is just one of the factors contributing to lowering of strength from what is observed under laboratory conditions. Other factors include e.g. saturated versus unsaturated conditions, the duration of loading, the rate of loading, and whether loading is cyclic. Treatment of these factors is outside the scope of this investigation.

This investigation is the first of its kind in both scope and emphasis. The essential contribution of this work is to take the data from AECL's Underground Research Laboratory (URL) and document the contribution of rock fabric in granite to the observed excavation damage. This damage includes overbreak due to stress relief, and to visible excavation-induced fractures. This work presents a unique and unprecedented data set on:

1. the considerable fabric variations present within what was previously thought to be a type example of a homogeneous granite, and
2. the relationships between excavation damage and geology,

This thesis will summarize:

1. what was learned from the URL that is useful in future site characterization,
2. how geological features in granite influence excavation damage (i.e. the link between geology and engineering), and
3. the role of rock fabric on rock mass response (including rock properties testing and in-situ stress measurement).

An outline of the scope of work and the organization of this thesis is provided in Table 2, with details provided in the following sections.

Table 2.

Scope of Work

Literature Review. ..... (Chapter 2)

Rock Mass Description.

- General Geology, Fault and Fractures, In-situ stress domains ..... (Chapter 3)
- Fracture, foliation and microcrack mapping ..... (Chapter 4)

Field Evidence of Fabric Anisotropy on Rock Mass Response.

- Ancient Faults and Fractures ..... (Chapter 5)
- Excavation Induced Fractures ..... (Chapter 5)

Selection of detailed study areas for sampling. ..... (Chapter 6)

- Excavation damage mapping ..... *3 linescan samples and tunnel profiles.*
- Drilling ..... *3 arrays, 12 boreholes.*
- Sampling ..... *171 samples.*
- Characterization of sample structure and texture. ..... *171 sample surface maps.*
- Classification of Fabric elements ... *foliations, lineations, and microcrack sets.*
- Measurement of fabric orientations ..... *~500 orientations.*

Rock Properties Testing ..... (Chapter 7)

- for preferred microcrack directions and their relative strengths. ..... *103 Point Load Tests..* (Chapter 8)
- for tensile strength and anisotropy. ..... *57 Brazilian tests..* (Chapter 9)
- for rock strength. ..... *11 uniaxial compression tests.* (Chapter 10)

Summary and Conclusions ..... (Chapter 11)

The site description (Chapter 3) provides a summary of the general geology, with emphasis on the foliations, natural microcracks, and other structures present in the granite. Also included is a summary of the in-situ stresses. The range of site characterization work previously completed by the author is summarized in Table 3. For the most part the work listed in Table 3 defines the general geology, excavation damage, petrography, natural microcracks, and the influence of rock structure on rock mass response.

The site characterization work and the determination of the ancient or natural microcracks (Chapter 4) were major elements of the scope of work, providing new data on these important structures and their variation with depth in a granite pluton. The results of the analysis of natural microcracks is provided in Chapter 4. In Chapter 5, field evidence for anisotropic behaviour of the rock mass is presented. The case is made that the rock mass behaved as an anisotropic medium when first subject to brittle deformation in the Precambrian, and that the present-day excavation response is simply a continuation of this behaviour.

Locations (sample areas) selected to examine the interaction between rock fabric, rock mass anisotropy, and excavation damage are described in Chapter 6. Three locations were chosen for mapping of excavation damage and for collection of a suite of samples for rock properties testing. These provide a representative sample of the range of the

compositional and textural heterogeneity present in the Lac du Bonnet granite, and their affect on rock strength and rock mass response. These are:

1. fine grained granite dykes with subvertical flow banding,
2. medium grained and weakly to moderately layered granite which forms the main mass of the batholith, and
3. generally coarse grained and leucocratic unit that occurs as sills and recrystallized zones in the main phase.

For the sake of convenience, these are referred to as the fine, medium and coarse grained granites, respectively.

The three study areas were sited in newly excavated tunnels at the 420 Level (420 m depth of the URL) where the damage due to stress relief can be observed in the process of developing. The sites are in close proximity to each other. They are distant from faults or major fractures, and are in the same in-situ stress-domain. As such, they are subject to the same stress magnitudes and orientations.

Excavation damage mapping was conducted at each of the study areas. "As-built" and "final" tunnel cross-sections were obtained to show progressive damage development, and to indicate the overbreak due to spalling. A linescan survey was then done for each study area, along the line of the surveyed tunnel profiles. Excavation induced fractures encountered along this profile were mapped and their orientation and surface characteristics noted. The rock types and the local structures were also mapped. Examples of excavation-induced fractures formed by parting along compositional

layering or other fabrics present at each case study site were noted. This mapping revealed those visible differences in excavation response (damage development) correlated with variations in the average grain size, the structure type and structure orientation. For example: the degree of excavation damage, including breakout development, follows the progression shown in Table 4. Within a given rock unit, the damage in the form of breakout notches is most pronounced in tunnels constructed along the strike of the layering.

At each study area, oriented core was obtained from an array of boreholes as listed in Table 5. The arrays were designed to intersect the most prominent foliation / microcrack set at 90°, and then at 20-30° increments until the core axis was parallel to the foliation. All samples are segments of HQ- sized core (46 mm diameter), the choice of specimen diameter being largely dictated by budget constraints. Specimens were prepared in accordance with the procedure described by Gyenge and Ladanyi (1977a,b), Gyenge (1980), and the method suggested by the International Society for Rock Mechanics (Brown, 1981). The end surfaces of each of the specimens were ground flat to 0.015 mm to ensure that they were parallel to each other and perpendicular to the axis of the specimen. The average dimensions and bulk densities of samples from each of the three rock types are listed in Table 6. The bulk density ranged from 2.54 to 2.72 gm/cm^3, these corresponding to the leucocratic and melanocratic layers in the coarse grained granite. Additional information on sample properties is presented in the individual chapters on rock properties testing.

Sample locations within the boreholes were chosen to minimize the possibility of damage caused by proximity to the excavation. Such damage is represented by discing of the core (which is relatively easy to see), and by the opening of microcracks along grain boundaries or other directions (which is not easily detected). The term "discing" refers to the tendency for core to split spontaneously into thin discs by the formation of closely spaced fractures perpendicular to the core axis. In general, discing is the result of tensile failure, which occurs wherever stresses radial to the borehole are high relative to: 1) the stresses along the borehole axis, and 2) the unconfined compressive strength of the rock (Engelder, 1993). According to the author, core discing occurs only in a high stress environment, which he defines as greater than 1 km depth on average, but which can be found at any depth in the URL. The extent of discing in any given area is a function of the room geometry (stress concentrations around the tunnel perimeter), and of the rock type, the fine grained granite being less susceptible to discing than the coarser grained types.

To avoid core damage, either from discing or from the opening of grain boundaries, samples were taken from the ends of each borehole as shown in Figure 9, a schematic representation of the general area affected by discing in core as seen in arrays surrounding the tunnels of the 420 Level (D.R. Woodcock, unpublished data).
To test for non-visible damage, rock properties tests results (such as tensile strength from the Brazilian Tests), were plotted against the specific gravity of the sample on scatterplots. If reduced tensile strengths were associated with lowered specific gravity, and these in turn correlated with distance from the excavation, it would be assumed that

damage, in the form of microcracking, was present. The results (presented in Chapters 6 and 7), showed no correlation with distance from the tunnel wall, and as such, are assumed to be free of damage due to proximity of the excavation.

The core was logged for foliations and microcracks, and then cut to provide oriented samples for rock properties testing. Logging procedures, particularly those relevant to distinguishing natural and induced fractures, followed recommendations by Kulander et al. (1980). Each of the 171 samples were also mapped individually for: foliations, microcracks, alteration products along grain boundaries, nature of grain boundaries including microcracking along boundaries, mineralogy variations, and mineral orientations. The sample maps for each specimen are presented in Appendices A and B.

The rock properties testing program is described in Chapters 7 to 9. Evidence for natural weakness planes (mechanical anisotropy) was defined by the preferred orientations of fractures induced by 103 axial Point Load tests (Chapter 7). Directional anisotropy in tensile strength was determined by the 57 Brazilian tests (Chapter 8) and in compressive strength by 11 uniaxial compression tests (Chapter 9). In each of these chapters, correlations between the rock properties tests and measured foliations and natural microcrack orientations are presented. To better examine the complex geometries between these data and the various structural elements in each rock type, all the above were plotted in their proper three-dimensional context using stereographic projections.

A summary of results is provided in Chapter 10. A relative ranking of rock strength correlating with average grain size is presented. The results are then compared with field observations of excavation damage development, and with published rock strengths. Directional anisotropies in rock strength are compared to the orientation of known fabric elements such as natural microcracks directions and some foliations. The results are consistent with tunnel mapping observations regarding preferential development of excavation damage in some rock types and in certain directions.

Table 3. Summary of Site Characterization by the Author

General Geology

Everitt, R., McMurry, J., Brown, A. and Davison, C. 1996. Geology of the Lac du Bonnet Batholith, Inside and Out: AECL's Underground Research Laboratory, Southeastern Manitoba. Field Excursion B-5: Guidebook. Geological Association of Canada - Mineralogical Association of Canada Joint Annual Meeting 1996, Winnipeg, Manitoba, Canada. 1996 May 30.

Everitt, R.A., Gann, P., Brown, A., Woodcock, D.R., Sikorsky, R.L. and R. B. Ejeckam. 1998. Subhorizontal Layering in the "Homogeneous" Lac du Bonnet Batholith at the Underground Research Laboratory, South Eastern Manitoba. In: Special Symposium on Extraction, Transport and Emplacement of Granitic Magmas, Ottawa '97 GAC-MAC Annual Meeting. Journal of Structural Geology. Volume 20, No. 9/10, p. 1291-1304.

Everitt, R.A. and Brown A. 1996. Geological Mapping of AECL Research's Underground Research Laboratory. A Cross Section of Thrust faults and Associated Fractures in the Roof Zone of an Archean batholith. Proceedings of Fractured and Jointed rock masses, a regional conference of the International Society for Rock Mechanics. June 1-6th 1992. Granlibakken, California. Vol. 1, p. 1-11.

Everitt, R.A., Gann, P., and Boychuk, D.M. 1993. Mine-by Experiment: Part 7 - Geological Setting and General Geology. AECL Technical Record RC-1080.1.

Excavation Damage - shaft

Everitt, R.A. and Passmore W. 1993. Shaft Extension Data Report - Wall Topography and Geology Map.

Everitt, R.A., Chernis, P.J., Good, D.H., and Grogan, A. 1989. Mapping of the Excavation Damage Zone around the Circular Access Shaft at Atomic Energy of Canada Limited's Underground Research Laboratory. In: Excavation Response in Geological Repositories for Radioactive Waste. Proceedings of an NEA Workshop, April 1988, Winnipeg, Canada, p. 271-282.

Excavation Damage - 240 Level

Everitt, R.A. and Read, R.S. 1989. Geology of the 240 Level of the Underground Research Laboratory, Volume I, General Geology. AECL Technical Record TR 491- 1, URL EXP 006 R001.

Everitt, R.A., Chernis, P.J. and Good, D.H. 1989. Geology of the Room 209 Floor. Contributions to the Excavation Damage Assessment Experiment. 5 p., 4 figures, 4 tables and 2 maps.

Lang, P. A., R. A. Everitt, E. T. Kozak and C. C. Davison. 1988. Underground Research Laboratory Room 209 Instrument Array: Pre - Excavation Information for Modellers. 1988 December, AECL 9566-1.

Lang, P.A., Babulic, P.J., Bilinsky D.M., Everitt, R.A., Spinney, M.H., Kozak, E.T. and Davison, C.C. 1990. Underground Research laboratory Room 209 Instrument Array: Measured Response to Excavation, Volumes 1 and 2, Atomic Energy of Canada Limited Report AECL 9566-3.

Excavation Damage - 420 Level

Everitt, R.A. and Woodcock, D.R. 1994. Contribution to the HFT Characterization Summary Report. Mapping Results for the 600 mm Heated Failure Test Borehole. Unpublished AECL Internal Memorandum. URL-01.84.41, AGB-94-190.

Everitt, R.A., Brown, D., A. Boychuk, D.M., and Gann, P. 1994. Excavation damage and organic growth in a 1.2m diameter borehole. Poster presentation at the 5th Annual International High-Level Radioactive Waste Management Conference & Exposition. May 22-26th 1994.

Everitt, R.A., Gann, P., and Boychuk, D.M. 1993. Mine-by Experiment: Part 7 - Geological Setting and General Geology. AECL Technical Record RC-1080.1

Petrography and Petrofabrics

Everitt, R.A. 1993b. Petrography of Granitic Rock Samples from the 420m Level of the Underground Research Laboratory, Pinawa, Manitoba. Prepared by Dana Kelly, David S. Peck and Richard S. James, Department of Geology, Laurentian University, Sudbury, Ontario, P3E 2C6. URL Library Identifier 01.73.03.

Correlations between Mineralogy and Crack Initiation

Everitt, R. A. 1995. Unpublished internal memorandum. URL-01.84.41, R-3002-07-00, Status of Pegmatite Testing Study. (A draft report on the testing results). Fracture Initiation and Propagation by Compressive Loading and Unloading in Component Mineral Phases of the Lac du Bonnet Batholith.

Natural Microcracks

Everitt, R.A. 2000. Synopsis of natural microcrack work at the Underground Research Laboratory. Unpublished report.

Table 4. Rationale for Selection of the Sample Sites

Variations in Excavation Damage with Average Grain Size and Foliation.
1. Coarse Grained Granite (Room 418) • Strong low dipping foliation and compositional layering • Variable but significant damage developing within hours
2. Medium grained Granite (Room 417) • Weak low dipping foliation • Significant damage developing within hours
3. Fine Grained Granite (Room 421) • Strong subvertical foliation and subhorizontal natural microcracks • Least damage, developing over a period of days or weeks.

Table 5. Sample and Testing Summary

Granite Type	Borehole	Orientation		test type and number		
		Trend	Plunge	Uniaxial compression	Brazilian	Point Load
1. Coarse Grained	418-051-RT1	324.90°	77.10°		*discing**	
	418-051-RT2	143.61°	54.76°	1	8	15
	418-051-RT3	143.40°	35.40°	1	8	6
	418-051-RT4	143.56°	19.70°	1	7	6
	418-051-RT5	143.38°	0.40°	1	4	12
2. Medium Grained	403-014-MB2	225°	00°	1		
	417-071-RT1	Not drilled.				
	417-071-RT2	190.43°	59.44°		*discing*	
	417-071-RT3	190.20°	39.48°		*discing*	
	417-071-RT4	189.10°	19.50°	1	6	6
	417-071-RT5	189.70°	-0.20°	1	4	8
3. Fine Grained	421-032-RT1	133.99°	0.23°	1	4	10
	421-032-RT2	157.61°	0.46°	1	6	7
	421-032-RT3	175.81°	0.80°	1	5	10
	421-034-RT4	199.05°	0.00°	1	6	13

* The term "discing" refers to the tendency for core to split spontaneously into thin discs by the formation of closely spaced fractures perpendicular to the core axis. For further information on discing see page 20.

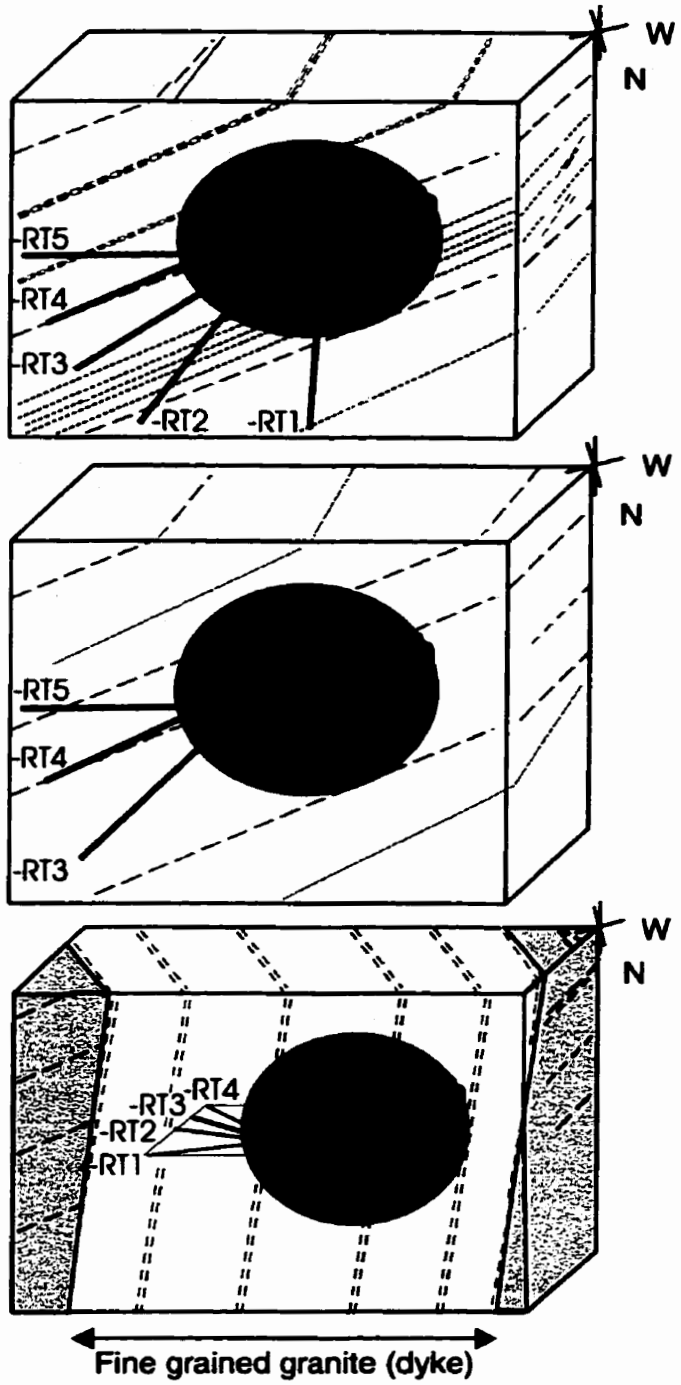

Coarse grained Granite

strong low-dipping fabric

4 uniaxial compression tests

27 Brazilian Tests

40 Point Load Tests

Medium grained Granite

weak low-dipping fabric

3 uniaxial compression tests

9 Brazilian tests

20 Point Load Tests

Fine grained Granite

subvertical fabric

4 uniaxial compression tests

21 Brazilian tests

43 Point Load Tests

Figure 8. Distribution of measurements relative to rock structure. The orientation of the arrays relative to the local rock structure is shown (layering / foliation indicated by the line symbols). The influence of the subhorizontal layering is tested by the arrays in the coarse and medium grained granite, while the influence of the subvertical layering in the fine grained granite is tested by the third array in the fine grained granite, which occurs as dykes intruding the medium and coarse grained granites. The geometry of the complete sample array at each location is also shown.

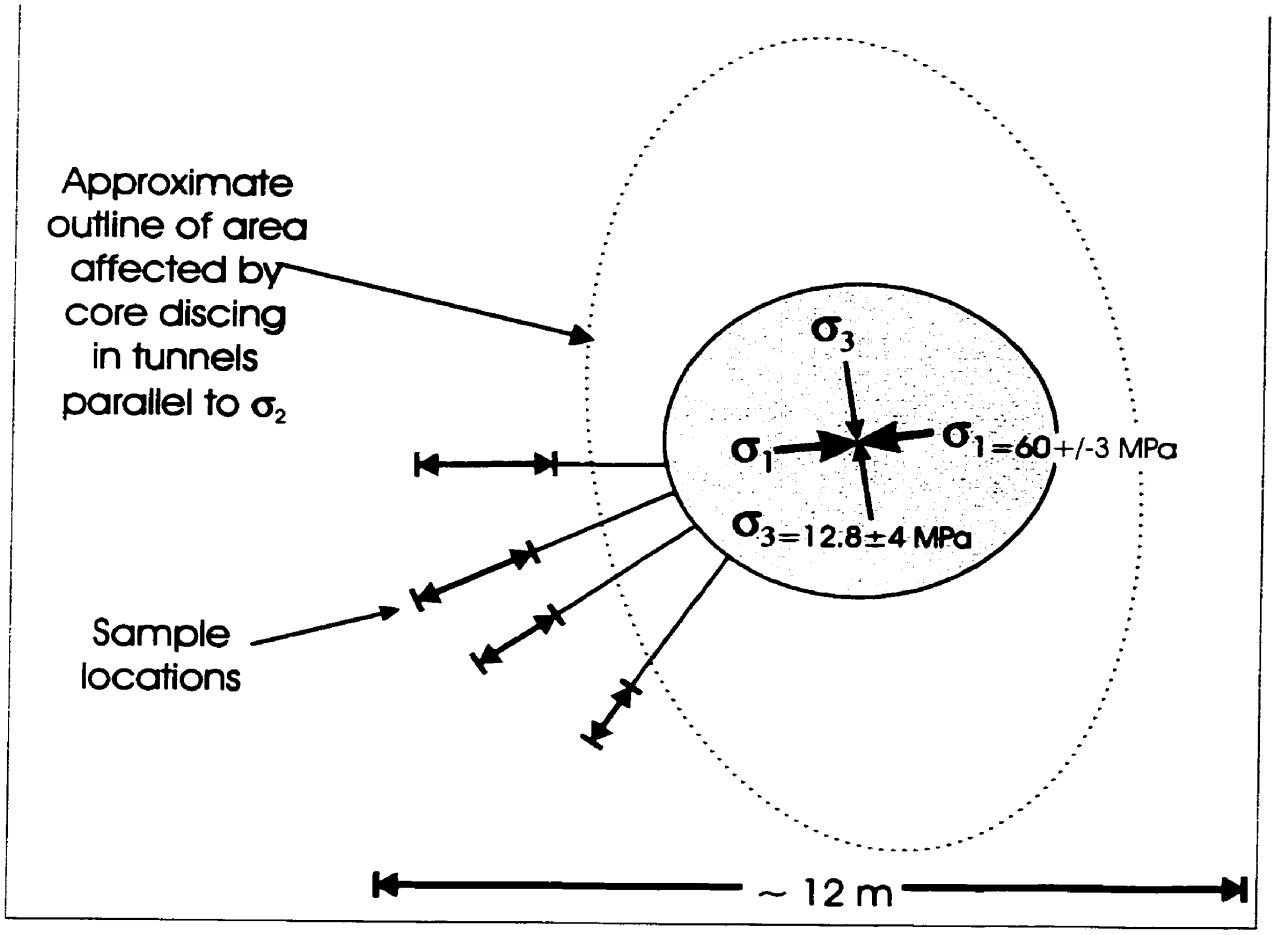

Figure 9. Approximate extent of the zone of core discing around a tunnel at the 420 Level.

Table 6. Sample Properties

Granite type	Number of samples	Diameter (mm)	Thickness (mm)	T/D	Density gm/cm^3
		max	max		max
		mean	mean	(average)	mean
		min	min		min
Fine grained granite	21	44.91	28.36		2.67
			24.93	0.56	2.64
		44.86	22.24		2.61
		44.82			
Medium grained granite	10	44.80	25.86		2.63
		44.77	22.56	0.58	2.62
		44.73	28.06		2.60
Coarse grained granite	27	44.81	27.55		2.72
		44.60	25.05	0.56	2.65
		44.43	22.03		2.54

Chapter 2

LITERATURE REVIEW

2.1. Introduction

Understanding the mechanism of fracture development around underground openings is important for the design of a safe and stable opening. This understanding applies to mining and civil engineering works as well as nuclear waste disposal vaults. The Canadian concept for disposing of nuclear fuel waste involves placing and sealing it in excavations 500 to 1000 m deep in plutonic rocks of the Canadian Shield. Of concern is the potential for significant propagation of existing fractures or the creation of new fractures (excavation damage) during construction. Interconnected fractures could reduce the effectiveness of the rock as a barrier to contaminant movement by providing pathways for groundwater to transport contaminants released from a disposal vault.

The literature was reviewed for studies that considered the role of rock mass anisotropy in excavation-induced displacements around tunnels with particular emphasis on cylindrical tunnels in highly stressed brittle rock masses. More specifically, the objectives of this literature review were to identify information relevant to the objectives of this thesis regarding:

1. the factors affecting rock strength,
2. the influence of foliation and other fabrics on strength and excavation response in rocks where these structures are well developed and first tested (slates, schists, etc.), and for granites in general,
3. the laboratory methods designed to test for and quantify anisotropy in rock mass response at a variety of scales and in different rock types,
4. the recognition of primary and secondary fabrics within plutons, and
5. previous related work within the Lac du Bonnet Batholith.

A recent compilation by the United States National Research Council (1993) reviewed the state of the art regarding the stability problems that occur in sediments and metamorphic rocks, with less emphasis on granite or other crystalline intrusives or extrusives. The editors concluded that field observations on circular openings of varying scales have highlighted the complex interrelationship between:

1. the stress field (either static or transient),
2. the geometry of the opening (radius and time dependence), and
3. the in-situ material characteristics (strength, discontinuities, and rockmass anisotropy).

Factors inducing strength reduction in rock include:

1. time-dependence,
2. influence of pore fluid on strength,
3. influence of specimen size, and
4. influence of anisotropy.

The first three factors, although important in predicting rock mass response to excavation, are of secondary importance to this thesis, affecting only the collection of samples and the rock properties testing. Each of these is examined in the sections 2.2.1 to 2.2.4 following. The influence of anisotropy, the subject of this thesis, is reviewed in the most detail.

2.1.1. Influence of pore fluid on strength

The presence of water in the pores of a rock causes a reduction in its uniaxial compressive strength. Hoek and Brown (1985, p. 155) showed that the presence of water caused the strength of samples of shale and sandstone to reduce by a factor of 2 from oven dried to saturated specimens. The following ratios between the uniaxial compressive strengths of dry and saturated specimens were reproduced by Hoek and Brown (1985), from Broch (1974), and Colback and Wild (1965).

Quartz diorite	1.5:1
Gabbro	1.7:1
Gneiss (normal to foliation)	2.1:1
Gneiss (parallel to foliation)	1.6:1
Sandstone	2:1
Shale	2:1

Lajtai et al. (1987), on the other hand, found that a reduction in strength for Lac du Bonnet granite due to moisture was strongly time-dependent. In a fast uniaxial

compression test, the change in strength was negligible. However the strength reduction in long-term loading tests was considerable, corresponding to a ratio of 2:1.

Application to this thesis: As a precaution, samples for this thesis were stored and tested under the same conditions (i.e. dry), and tested at the same time. Accordingly, the differences observed between rock types are considered to be intrinsic differences between the rock types and different sample orientations, rather than to differences in moisture content.

2.1.2. Influence of specimen size

One of the most common explanations given for the difference between the laboratory strength of rock, and the rock strength found in-situ, is the effect of specimen scale (Martin, 1993). However, the rock mechanics literature contains a number of conflicting observations on the effect of specimen size upon the strength of rock. As noted by Hoek and Brown (1985, p.157) for the general case involving all rock types:

1. some authors report no change in rock strength with change in specimen size (e.g. Hodgson and Cook, 1970; and Obert et al., 1946), while
2. others note significant strength reductions with increasing specimen size (e.g. Mogi 1962, Bieniawski, 1972; Pratt et al., 1972; Protodiakonov and Koifman, 1963; and Hoskins and Horino, 1969).

The case for scale-dependence specific to the Lac du Bonnet granite, was examined in a comprehensive study conducted by Jackson and Lau (1990), Lau and Gorski (1991 a,b,c) and Martin (1993).

Uniaxial compressive strength and scale-dependence

The study by Jackson and Lau (1990) was conducted specifically to study the effect of specimen size on the ambient-temperature uniaxial mechanical properties of the Lac du Bonnet grey granite. According to the authors:

1. Specimens up to 63 mm, while showing some variation, indicated no trends with increasing specimen size.
2. However, as specimen diameters increased from 63 mm to 294 mm, the uniaxial compressive strength and tangent modulus of elasticity decreased.

Jackson and Lau (1990) concluded that " ..This decrease is well explained by the increased probability of the existence of a critical flaw or flaws in larger specimens (Weibull's "weakest link" theory) and is adequately described by any of the Hoek and Brown, Gyenge and Herget or Weibull models". Martin (1993) concluded, " the effect of scale on the compressive strength of Lac du Bonnet granite is not very significant" for the normal core diameter range (i.e. below 63 mm).

Field evidence collected by the author for this thesis supports the interpretation by Jackson and Lau 1990. The samples for the study by Jackson and Lau (1990) and also by

Lau and Gorski (1991 a, b, c) were taken from what was described as "massive grey granite". In reality, the granite from which their samples were taken is layered, with the layering varying between 100 and 300 mm in thickness, and the layers separated by thin planes of aligned biotite (Everitt and Read, 1989, also Figures 10, 12 and 13 of this thesis). It is suggested by the author that the decrease in strength in the larger samples obtained by Jackson and Lau (1990), reflects the increasing likelihood that these samples contain more than one layer and layer boundary (i.e. their critical flaw or flaws interpretation).

For this thesis, the diameter (43 mm) for uniaxial compression test samples is in the mid-range where no size effect was noted by Jackson and Lau (1990) or Martin (1993), and was small enough to keep the samples as texturally and structurally homogeneous as possible. This last point was a concern as samples chosen for this thesis were specifically chosen to avoid having multiple orientations of foliations.

Tensile strength and scale-dependence.

Hodgson and Cook (1970), and Martin (1993) showed that under uniform stresses, tensile strength would be independent of size. However, in situations with high stress gradients, such as are created by Brazilian testing, strength will be a function of sample size, with Brazilian tensile strength showing an increase at the smaller scales. This was based on a comparison of test results from samples with diameters of 25 mm, ~30 mm, ~35 mm, 43 mm, ~ 50 mm, ~55 mm, 63 mm and ~105 mm. Nevertheless, it has been shown that tensile strength is independent of sample size for the most common core diameters (35 –

63 mm). For the LDBB, Martin (1993) concluded that samples larger than 63 mm diameter were beyond any scale effect and provided an accurate measure of tensile strength for granite from the Lac du Bonnet granite. Similar results were obtained by Wijk et al. (1978) for the Bohus granite.

In this authors view, the caution about sample size relative to the scale of textural / structural domains in the rock also applies here. That is, the decrease in strength in the larger samples may reflect, at least in part, the increasing likelihood that these samples contain more than one layer and layer boundary (i.e. critical flaw). Given this caveat, the sample size (43 mm) used for this study is regarded as acceptable, especially as the objective of the testing is to test for directional anisotropy related to fabric within a given suite of samples. The absolute tensile strength of the LDB granite is of secondary importance, and as this study demonstrates – tensile strength is rock unit and orientation specific anyway.

2.1.3. Influence of anisotropy

A rock is mechanically anisotropic when the mechanical behaviour changes for different stress orientations. Foliations or lineations formed by the parallel alignment of micaceous minerals, or of rod-like minerals like hornblende, impart a strong textural and mechanical anisotropy. Thus, metamorphic rocks like schist and slate are often markedly directional in their behaviour (Davis, 1984; Goodman, 1989; and Behrestaghi, 1998). Anisotropy also occurs in layered mixtures of different components, as in banded gneisses, or in alternating sequences of sandstone, shales, cherts, and limestones (United

States National Research Council 1993, Hoek and Brown). In all such rocks, strength varies continuously with direction and demonstrates pronounced minima when the planes of symmetry of the rock structure are oblique to the major principal stress.

According to Goodman (1989), strength anisotropy can be evaluated best by systematic laboratory testing of specimens drilled in different directions from an oriented block sample.

Experimental deformation studies of the Martinsburg slate by Donath (1961), and a oil shale (intercalated marlstone and kerogen). McLamore (1966) demonstrated the mechanical effect of well developed mechanical anisotropy, by rotating the loading axis relative to the fabric in increments from 0° to 90°, the angle between the two being referred to as ψ. The results indicate that a strong mechanical anisotropy will control the orientation of the failure plane over a broad range of loading geometries, and that this control is reflected by the variation in breaking strengths. Donath (1961) concluded:

$\psi < 45°$ failure is preferentially developed along the plane of the slaty cleavage, with breaking strength at its lowest when the fabric is at 30° to the loading axis.

$\psi = 45°$ to 75° the failure planes reach a maximum of about 60° to the loading axis, and the breaking strength continued to increase.

P = 90° the plane of failure returns to about 30° (considered the ideal angle as would exist in a homogeneous rock), and the breaking strength reaches its maximum at this geometry.

The ratio of minimum to maximum unconfined compressive strength in the slate was approximately 25% (Donath, 1961), and approximately 17% in the oil shale (McLamore, 1966). The minimum strength occurred at approximately 30° to the fabric plane in both examples. Similar results in sandstones were noted by Hoek and Brown (1980), and in metamorphic rocks – with the lowest axial strength (at various confining pressures) at 30° to loading axis.

Examples of structural or textural anisotropies affecting rock mass response in sedimentary or metamorphic rocks are common in the literature (Hoek and Brown, 1980; Goodman et al., 1993). The causative structures include: 1) spaced singular discontinuities at the tunnel-scale, such as bedding planes and joints, and 2) fabrics such as foliation, slaty cleavage, or lineations which are pervasive at the tunnel and hand - specimen scales. The latter should be considered as an intrinsic characteristic of the intact portion of jointed rock (Behrestaghi et al., 1996).

The anisotropic strength behaviour of four varieties of schists was examined by Behrestaghi et al. (1996), through the testing of specimens with varying orientation of schistosity with respect to the major principal stress under uniaxial and triaxial conditions. The results of this study were anisotropic deformation properties and natural planes of fracture defined by foliations. This structural anisotropy influences rock mass

response through either the development of unstable block geometries, and by anisotropic response of the intact rock including the development of fractures in orientations related to the fabric (also USNRC, 1993; Goodman et al., 1993).

The role of bedding in controlling breakouts in excavations has been described by Komar and Frohne (1973) and by Haimson and Edl (1972). Oriented Brazilian compression tests (Ewy et al., 1988b) determined that the failure location was controlled by rock strength anisotropy, with failure occurring where the tangential stress around the hole was parallel to the bedding plane. These examples are analogous to the situations at the URL described in Chapter 1 of this thesis (Figures 4, 5 and 6), with the foliation and compositional layering in the LDBB granite corresponding to the bedding and schistosity, respectively.

The conclusions by the United States National Research Council (1993) regarding the role of rock mass anisotropy, and their significance to this thesis were as follows:

1. "... The role of anisotropy , discontinuities and imperfections will undoubtedly play an even stronger role in engineering situations outside of a controlled laboratory environment ...",

2. many factors affect the displacements and ultimate stability of both shaft and tunnel wall rock. "... Foremost among these are the magnitude and ratio between the horizontal principal stresses, the extent of rockmass anisotropy and geological

discontinuity, the time lag between excavations and support installation, and the influence of intersections into the primary opening, such as shaft stations and loading pockets".

These factors were considered in the selection of sample locations to assess the role of rockmass anisotropy for this thesis. All samples are from intact rock and are confined to a single in-situ stress domain. All samples are from the portions of tunnels remote from intersections with adjoining excavations, from the ends of tunnel, and from the ends of blast rounds.

3. "...that there are no strict lithology rules..." .. their synopsis emphasizing the importance of the in-situ stress field in combination with the materials strength characteristics, and highlighting the risk of arbitrarily correlating excavation stability with lithology. This may be re-phrased as the risk of assuming that there is a typical behaviour from any given rock type.

This last statement is especially noteworthy, as will be demonstrated in this thesis, where statements such as the following from the literature are shown to be oversimplifications.

1. The LDBB is a type example of a homogeneous granite (Hoek et al., 1995) where the authors noted that there was "no influence of geology" to be seen in the damage zones about the URL excavations.

2. The fine grained phase of the LDBB granite is stronger and less susceptible to damage than the medium grained granite (Martin, 1990; Martin, 1993; Lau et al., 1991 a, b, c).

As was noted earlier in Chapter 1 of this thesis, and as will be examined in the chapters following, the extent of excavation damage within a particular variety of the LDBB granite depends upon the orientation of its fabric relative to the orientations of the excavation and the in-situ stresses.

2.2. The Experimental Determination Of Strength Anisotropies

This section identifies methodologies from the general literature which were used, in circumstances similar to those of this thesis, to define mechanical anisotropy and its relationship to fabric anisotropy. Specific objectives were:

1. to determine if there are naturally occurring directions of preferred fracture in otherwise intact rocks,
2. to correlate these with variations in the tensile strength, and
3. to determine the compressive strength and its variations with orientation.

2.2.1. Determination of Tensile Strength

Tensile fracture is a ubiquitous feature of rock failure ranging in size from micro-fractures to the large-scale explosive failure accompanying rock bursts. Hence the resistance of rock to failure in tension, the tensile strength, is one of the fundamental parameters of rock strength.

Although the measurement of tensile strength is performed in many projects in a routine manner, little attention has been paid to possible variation in tensile strength with the direction of loading (Lajtai, 1980; Duncan, 1987).

Methods to determine the tensile strength, and its variation with direction, include the point loading and line-loading (Brazilian) tests.

In the point-loading method, core discs are loaded axially between a pair of indentors while in line-loading method; the disc is placed on edge and loaded in the direction of its diameter between two flat platens.

In the line-load or Brazilian method, the diametral fracture plane is constrained by the position of the loading indentors, while in the point-load test, the diametral fracture plane is free to take any orientation. In practice, failure tends to be controlled by heterogeneities in the rock, such as foliations or microcracks, which are close to or parallel to the plane of failure under this loading geometry. Heterogeneities well outside this plane, such as incipient core discing, do not affect the test.

According to Lajtai (1980) "... The Brazilian test seems to yield a more accurate definition of both the tensile strength and its variation with direction ... (and is the more commonly applied tool for this application in rock mechanics).... The point load test is more suitable for the determination of the minimum value of tensile strength, and ...(in determining if there are preferred directions of fracture)...".

2.2.2. Point Load Test

This method has been used to determine if there are preferred orientations of failure under conditions of tensile fracture, in what may otherwise appear to be intact rock. Testing under controlled conditions has shown that, in artificially produced isotropic materials, such as a concrete aggregate composed of cement and fine grained sand, tensile fractures induced by Point Load testing develop in random orientations (Paulman, 1966). However, the same test method applied to a variety of rock types is consistent in producing one or more preferred orientations of test-induced tensile fractures, whose orientations are, upon inspection, found to be controlled by natural microcracks or others structures which: 1) reflect the rock's deformation history, and 2) which are pervasive at the specimen scale. Examples include:

1. Test-induced fractures correlate with the microscopic fractures in sandstones (Cardium sandstone - Reik and Currie, 1974), (Mispec, Perry and McCoy sandstones - Lajtai and Alison, 1979), and (various Devonian to Carboniferous sandstones from New Brunswick and Prince Edward Island – Lajtai, 1980; Lajtai and Stringer, 1991).

2. Test-induced fractures correlate with the microscopic fractures in granite (Shield Quarry, Manitoba - Duncan, 1987, and the Charcoal granite - Friedman and Bur, 1974). In the latter example, a preferred orientation of residual strain and framework of feldspar grains with approximately the same attitude as the microscopic fractures was considered as contributing to the fracture anisotropy).

More commonly in rock engineering, the Point Load test is used as a relatively simple method to determine a strength index, the Point Load strength index, which is related to the uniaxial compressive strength of rock (Broch and Franklin, 1972; Bieniawski, 1975; Broch, 1983). The Point Load Strength Index" is given by the following (Goodman, 1989):

$$\text{Point Load strength index (MPa)}, I_s = P/D^2 ,$$

where P = the load to break the specimen, and

D = the distance between the platen contacts.

According to Goodman (1993), tests are normally done on pieces of drill core at least 1.4 times as long as the diameter. In practice, there is a size effect so a correction must be made to reduce results to a common size. Point Load strength is found to fall by a factor of 2 to 3 as one proceeds from cores with a diameter of 10 mm to diameters of 70 mm; therefore, size standardization is required. The Point Load index is reported as the Point Load strength of a 50 mm core (size correction charts are given by Broch and Franklin).

2.2.3. Brazilian Tensile Strength Tests

The Brazilian test is a recognized as an indirect but convenient method for estimating the tensile strength (Goodman, 1989). It has been found that a rock core will split along the diameter and parallel to the cylinder axis when line loaded on its side in a compression machine. The reason for this can be demonstrated by examining the stress inside a disk loaded at opposite sides of a diametral plane. In such a configuration the horizontal stresses perpendicular to the loaded diameter are uniform and tensile. At failure their magnitude determines the tensile strength:

$$Brazilian Tensile strength, \sigma_{t_B} = \frac{2P}{\pi Dt}$$

where P = load at failure,

D = diameter of the specimen, and

t = thickness of the specimen.

The "Brazilian tensile strength - σ_{tB}" (in MPa) is estimated from the test result from the applied stress corresponding to the peak compression load. The actual cause of failure may in fact be more complex, reflecting the interaction of small-scale flaws, compression parallel to the eventual rupture plane, and the horizontal tension induced by this loading.

The Brazilian test has been found to give a tensile strength higher than that of the direct tension test, probably owing to the effect of grain-scale (and larger) discontinuities. However, the Brazilian test method is preferred, as it is much easier to perform this test

than to arrange the precise alignment and end preparation required for a direct tensile test (Goodman, 1989).

Jaeger and Cook (1979) compared tensile strengths results as determined by various test procedures. For three different rock types it was found that Brazilian tensile strengths are generally similar in range to direct uniaxial tensile strengths but only half the value of three-point bending tensile rupture strengths. Lajtai (1982) also found that Brazilian tensile strengths of LDBB granite to be approximately half the three-point bending tensile rupture strength. He attributed strength variations to volume differences as specified by Weibull's theory. Based on Jaeger and Cook's (1979) discussion it may be concluded that a higher tensile strength of intact Shield granite determined using the modulus of rupture tests is likely the function of the mechanics of the physical testing procedure: the Brazilian tensile test sets up a uniform tensile stress normal to the diametral plane of compression of a rock disc being loaded uniaxially, whereas the modulus of rupture test is a three-point bending procedure that sets up non-uniform stresses through the sample in the direct plane of loading. This produces a zone of compression in the upper portion of the block, and a zone of tension in the lower portion of the block. The resulting stress gradient leads to higher tensile strengths.

Duncan (1987) noted that the rupture tensile strength data did not corroborate the same tensile strength anisotropy indicated by the Brazilian tensile strength data, which shows a good correspondence with the microscopic fracture anisotropy. He concluded that ..." the Brazilian tensile strength test is very sensitive to the microscopic fracture properties

that exist...", and that the modulus of rupture test method is not as effective a test procedure for determining tenuous differences in tensile strength in granite.

2.2.4. Compressive strength

Methods to investigate the effect of fabric anisotropy on compressive strength and other deformation properties have been described in several references in recent literature. The testing methods are similar, regardless of rock type, and follow the general procedure laid out by the earliest investigations into anisotropy in rocks, such as the by Donath (1964), and for other, less obviously anisotropic rock types as:

- Shale — Mesri and Gibala (1972),
- Metamorphic rocks — Behrestaghi et al. (1996),
- Granite — Feves and Simmons (1976); Duncan (1987); and Kusumi et al. (1997),
- LDBB granite — Duevel and Haimson (1997); Lajtai (1981); Lau and Gorski (1990; 1991a,b,c); and Lau et al. (1994).

The anisotropy or anisotropies in the rockmass are identified prior to testing, using one or more of the following techniques (from Sano et al., 1992; Hoek and Brown, 1980; Goodman, 1993): sample surface mapping, petrographic examination, sonic velocities, variations in tensile strength, or thermal conductivity.

Oriented samples are then taken from the rockmass, with the structural anisotropy (usually slaty cleavage, foliation bedding, or microcracks) inclined at angles from 0° to 90°, usually through increments of 20°-30° to the intended loading axis.

Alternatively, comparatively homogeneous rocks, granites in particular, have been cut to provide cylindrical samples parallel to each of the following: the rift, the grain, and the hardway as defined from the quarrying operations where the samples were collected. In each study, these structures are correlated with sets of natural (ancient) microcrack development. The sample set is therefore intended to investigate the influence of the microcrack sets on compressive strength and other deformational properties (Feves and Simmons, 1976; Duncan, 1987).

Samples are then subject to one or more of the following test procedures: uniaxial or triaxial compression tests, single or cyclic, conducted under saturated or unsaturated conditions (e.g. shale - Mesri and Gibala, 1972; granite - Feves and Simmons, 1976; Duncan, 1987; LDBB granite - Duevel and Haimson, 1997; metamorphic rocks – Behrestaghi et al., 1996).

The data from these tests is then plotted as series of conventional stress-strain diagrams for each sample orientation, or as rose diagrams or x-y plots illustrating the variation in the measured parameter with the (two-dimensional) orientation of one of the structures present. In spite of the fact that most rocks contain more than one fabric element at various angles of intersection, the use of three-dimensional or stereographic projections

to portray such data are rare in the literature, even when the effect of intersecting fabric planes is the topic of discussion (e.g. Figure 77, p. 163 of Hoek and Brown (1980), which shows the variation in rock strength for a rock with multiple discontinuities, by means of a rose diagram of axial strength against discontinuity inclination).

2.2.5. Application to this Thesis

The methods used in this thesis were those outlined in the preceding sections. Point Load tests were employed to determine if there were preferred directions of fracture in the massive rocks of the LDBB, and Brazilian tests to determine if there are variations in the tensile strength with the direction of loading. The Point Load index was calculated for each of the samples tested in this thesis to show strength differences between rock types and from different orientations.

Directional variation in uniaxial compressive strength related to layering and other structures was investigated using a series of samples from an array of boreholes. Oriented samples were then taken from the rockmass, with the structural anisotropy (layering or microcracks) inclined at angles from 00° to 90°, usually through increments of 20°-30°, to the intended loading axis. The data from these tests are plotted as series of conventional stress-strain diagrams for each sample orientation, and then summarized for each rock type using x-y-z diagrams depicting various measures of compressive and tensile strength versus orientation (Chapter 9).

2.3. Anisotropy in Granite

2.3.1. Introduction

Although rock fabric is a well recognized factor influencing rock strength and response in metamorphic and sedimentary rocks, plutonic rocks (whether mafic to felsic) are still generally regarded as homogeneous and isotropic, with the LDBB being described as a massive (Martin, 1993), and a type example of an isotropic granite in a recently published general reference text (Hoek et al., 1995). This assumption of granite isotropy has been maintained in spite of:

1. nearly a century of literature on the structural and textural variations within plutons, such as presented in the original work by Balk (1937), Cloos (1946), Mayo (1941),

2. repetition of the conclusions in later compilations such as in Dennis (1972), and Davis (1984), and Bouchez (1997),

3. recent case studies appearing in the published literature and major conference proceedings on the complexities of pluton structure by Bouchez (1997), Cruden (1990), Cruden and Lanueau (1994), and

4. for the LDBB in particular, detailed mapping of pluton structure by McCrank (1985), Brown et al. (1989a), Cerny et al. (1987), Stone et al. (1989), Everitt and Brown (1986), Everitt et al. (1990, 1994, 1996 and 1998).

The inappropriateness of the assumption of granite isotropy as it affects geotechnical investigations, including work for a used fuel disposal facility, has been noted by Goodman et al. (1993). They concluded that in addition to joints, granites also contain a variety of foliation planes and schistose zones. The authors also noted that insufficient attention has been paid:

1. to mapping the structural complexity of granite in site investigation programs, and
2. to incorporating this complexity in the design of sampling programs to define rock properties.

It is suggested here, from the literature reviewed for this thesis, that this tendency to refer to granitic plutons as homogeneous and isotropic may be due to a combination of the following four factors:

1. Inadequate site investigations or imperfect evaluation of geological information, as emphasized by Goodman (1993). Davis (1984, p.255) noted that: "... foliations and lineations in granitic rocks are not always conspicuous. Many granitic rocks display very subtle foliations and/or lineations whose physical reason for existence is not at all obvious. Microscopic study is often required to determine the petrographic basis for the foliations and lineations. Foliation and lineation may reflect any number of textural configurations, including aligned feldspars, elongate or discoidal quartz, and closed-spaced fractures or cleavages ".

2. Scale of Observation: It is inherently difficult to recognize fabrics in coarse grained rocks in general, and especially in core samples whose limited dimensions may obscure structures otherwise readily apparent in outcrop. The latter point is especially problematic when samples are routinely shipped from a remote site to another location for lab analyses, without mention of the core orientation relative to any local fabrics.

3. Limitations to site investigation. Most geotechnical work pertaining to plutonic rock originates with the various international nuclear waste programs. Apart from the Canadian program, which is unique in having large volumes of intact or sparsely fractured rock (Davison and Simmons, 1985; Davison et al., 1989, 1993) the granites investigated by other countries with a similar disposal plan, are all sited in naturally fractured blocky rock (Sweden (Stanfors, 1996; Backblom and Olsson, 1996), Finland (Vira, 1996; Tolppanen et al., 1998), France (Raynal, 1996), Spain (Olmo, 1996), Belarus (Kudelsky, 1996), Ukraine (Khrushchov and Starodumov, 1996).

The high fracture frequency in the waste disposal programs of other countries overshadows any flow and mechanical anisotropy that may be induced by foliation and other fabrics. Accordingly, site characterization and design in these programs has concentrated on modelling rock mass response for a discontinuous medium (e.g. Christiansson, 1989; Christiansson and Hamberger, 1991; Kornfalt et al., 1991; Olsson and Conterra AB, 1991; Ouchterlony et al., 1991; Rawlence, 1990). The

rockmass within the fracture-bound blocks tends to be ignored or is considered isotropic.

4. Sampling bias. The almost universal assumption of granite homogeneity that appears in the literature is perhaps the result of a fundamental sampling bias, inherited from the dimension stone industry (DSI) where homogeneity is the prime basis for selecting a quarry, and for its continued development. Dimension stone is defined as: a natural rock material that has been selected, trimmed, or cut to specified or indicated shapes or sizes with or without one or more mechanically dressed surface" (Taylor, 1992).

In a recent compilation of the DSI in Ontario, Marmont (1993) notes that the geology of a prospective dimensional granite quarry should be as simple as possible. In terms of lithology, this means that the quarry should ideally consist of uniform granite/granite gneiss free from crosscutting veins, dikes and inclusions of other rock types.

The dimension stone industry literature therefore shows a strong bias towards the selection and development of the most homogeneous plutons or parts of plutons (Bergeron, 1991a,b,c; Gerow and Bellinger, 1990; Hill, 1989a,b; Hill, 1990a,b; Hinz et al., 1994; Kennedy and Shelock, 1988; Lacey, 1989; Marmont, 1993; Martinsen et al., 1991; Ontario Ministry of Northern Development and Mines, 1989, 1990, 1992;

Papertzian and Farrow, 1995; Verschuren et al., 1986; Verschuren et al., 1989; Verschuren et al., 1985; and Vos et al., 1981).

This bias has likely suppressed the provision of more representative sampling of granite. Such a bias is especially significant when one considers that the published laboratory work identified in this literature review is largely based on samples provided by quarries. Examples include:

- Westerly Granite - e.g. Kronenberg et al. (1990); Feves and Simmons (1976),
- Oshima Granite from the Yamanashi Quarry, Barre Granite from the Rock of Ages Quarry, and Chelmsford Granites from the Fletcher Quarry - Sano et al.(1992).
- Lac du Bonnet Batholith from Cold Spring Quarry - e.g. Svab and Lajtai (1981); Duevel and Haimson (1997); and Martino J.B. (1994).
- Samples of an unnamed granite pluton from the "Shield Quarries of Canada" near Whitemouth, Manitoba. - Duncan (1987).

In spite of these oversights and sampling biases, review of the recent geotechnical literature indicates progress has been made in a number of areas relating to the recognition of the existence of fabric anisotropy in granites, and the effect of this anisotropy on measured rock properties. (e.g. Kronenberg et al., 1990; Goodman et al., 1993; Goodman ,1993; USNRC, 1993). The next sections review progress made in:

1. the recognition of original and deformation fabrics within plutons,
2. and evidence from the dimension stone industry (DSI) and the general geotechnical literature for the influence of this fabric anisotropy in producing mechanical anisotropy in granite.

2.3.2. Field evidence for primary and secondary fabric anisotropy in granite.

Evidence for significant fabric anisotropy in granites is increasingly apparent in the geological literature. Relatively recent compilation maps of Ontario (e.g. Stockwell, 1970) did not differentiate between the various types and ages of granite within the vast areas between the greenstone belts, nor did the mapping efforts include much work on the internal structure of these plutons. However, the granites within each geologic province of the Canadian Shield have since been subdivided and re-classified on the basis of composition, internal structure and age of intrusion (Thurston et al., 1991; 1992 a,b; and Card and Poulsen, 1998). Some types most usually predate regional deformation, while other types generally postdate it; however, these relationships vary locally. The timing of intrusion relative to orogeny is important as it defines to some extent:

- the style and extent of fractures found within the batholiths,
- the complexity of the pluton's geometry and internal structure,
- the types of faults, fractures, deformation structures and recrystallization present, and from these
- the in-situ stresses and rock properties.

Table 7 provides a highly abbreviated summary of the plutonic rocks of the Superior Province. The "vast pink areas" shown in the geological maps of Canada from the 1970's (Stockwell, 1970) are now recognized as including 5 separate suites of plutons, each with its own range of compositional variation and structures.

Table 7:
Plutons Suites in the Superior Province (Thurston et al., (eds.) 1991, 1992 a,b).

Suites 1,2:	Gneissic Tonalite Suite & Foliated Tonalite Suites: This suite is largely pre-orogenic and as such, is recrystallized and moderately to strongly deformed. It occurs as large complex batholiths to sill-like remnants, which incorporate several compositional varieties. The internal structure of these suites tends to be very complex and heterogeneous with abundant, often kilometre-scale, mafic inclusions and strong compositional layering, and several generations of granitic and mafic dykes. Secondary and relict primary foliations and lineations are widespread.
Suite 3:	Granite-Granodiorite Suite: This suite includes the Lac Du Bonnet Batholith, and is often the most abundant pluton type in any given subprovince. In form, many are generally curved sheet-like crescents that may outcrop over a considerable area but be relatively thin in section (less than 2 km thick). Others may reach considerable depths (10-15 km) and may outcrop over an area of 2000 km^2 (e.g. the Lac du Bonnet Batholith). This suite is generally regarded as syn-tectonic but, in some areas, it includes multi-phase pulses, some syn-, some late- and some post-tectonic. Their intrusion near the end of the Kenoran Orogeny, their size and abundance, and a prolonged cooling history are believed to have contributed to the large areas of sparsely fractured rock reported in some members of this suite (Stone et al., 1989; Beakhouse, 1991; Breaks, 1991; M. Gerow, Ontario Ministry of Northern Development and Mines, pers. comm., 1993; B. Schmidtke, Manitoba Energy and Mines, pers. comm., 1993; F. Beard, Ontario Ministry of Northern Development and Mines, pers. comm., 1994). This suite is homogeneous when compared to the other suites, but mapping of the LDBB (by the author and others) has determined that much of this homogeneity is the result of a sampling bias.
Suite 4:	Muscovite-Bearing Suite: This suite includes syn- or post-tectonic batholiths and stocks of regional extent, as well as numerous pegmatitic dykes. Individual plutons are generally less than a few tens of kilometres in area. The granites are commonly very xenolithic and have irregular interfingering contacts with the surrounding host rock (Everitt et. al., 1998).
Suite 5:	Diorite-monzonite-granodiorite suite: This suite may appear under a variety of names depending on location and the rationale for classification. As defined in Thurston et al., (eds.1991a), it includes a compositionally diverse group of syn- to post-tectonic batholiths. Although widespread throughout the Shield, they are neither abundant nor individually large.

Within any single pluton, recent structural analysis has indicated a wide range of textural and structural variations related to the mode of intrusion, timing of intrusion, and the effects of later deformation. Examples, with the structures listed in their relative order of formation, include:

- sheet-like injections of granite between xenolithic zones are common (e.g. Clarke et al., 1998; Cruden et al., 1997; Cruden, 1998), syn-magmatic folding and a subvertical foliation (Roman-Berdiel et al., 1995),
- the existence of both primary and secondary (deformation) foliations within a single pluton (Benn et al., 1998; Gleizes et al., 1998; Djouadi et al., 1997; Riller et al., 1996),
- Textural variations indicative of the progressive ductile deformation of a pluton (Schulmann and Mlcoch, 1996; Riller et al., 1996),
- several sets of fractures including early brittle structures related to the crystallization and cooling of the pluton (Rousell and Everitt, 1981; Guermani and Pennacchioni, 1998),
- partial erasure of such joints by subsequent localized ductile deformation (Guermani and Pennacchioni, 1998; Rousell and Everitt, 1977; 1981), and finally,
- one or more episodes of brittle deformation and joint formation.

The orientation and density of these fractures is often controlled by compositional and textural anisotropy. Examples of fabric control of joint orientation in granite are

described in Reitan and Murphy (1983), Rousell and Everitt (1981), Guermani and Pennacchioni (1997).

2.3.3. Application to this thesis

As such, there is abundant field evidence supporting the view that homogeneity of granites is more the exception rather than the rule, and that granites are internally complex with structures that influence their mechanical properties.

The need to recognize this heterogeneity when sampling for geotechnical investigations was emphasized by Bouchez and Gleizes (1995). The authors made special mention of the need to create "....a sampling pattern consistent with mapped rock types..." so that measured rock properties are representative.

This precaution has been overlooked in geotechnical studies, such as in dam foundations as noted earlier by Goodman (1993), and in the sampling for previous rock properties testing done for the Canadian Nuclear Fuel Waste Management Program, as discussed in section 2.5.

The next section examines correlations between rock fabric and measured rock properties, as noted by the dimension stone industry (DSI), and in select references from the literature. The former provides field-scale evidence of fabric/ rock properties with some lab analyses, and is useful in indicating how common granite anisotropy actually is.

The role of layering, foliations, texture, and microcracks in rock response is examined through selected investigations from general geotechnical literature.

2.4. Field And Laboratory Evidence For Mechanical Anisotropy In Granite.

This section summarizes the influence of fabric anisotropy, in producing anisotropy in rock properties as determined from select case studies in the literature.

The influence of large-scale layering, grain size, mineral alignment and natural microcracking are presented in turn. However, it is recognized that the effect of each of these fabric anisotropies are interrelated, and in many cases it is not possible to separate out the individual effect caused by (e.g.) the alignment of grain boundaries (foliation) and grain boundary cracks.

2.4.1. Large-scale (e.g. decimetre) compositional layering or heterogeneity

Various texture/rock mass response phenomena have been identified in granite by the DSI and in the general engineering literature. Marmont (1993) and others have made the following observations in recent compilations of the DSI.

The DSI follows the American Society for the Testing of Materials (ASTM) specifications for the standards which building stones should meet, and the test methods to establish them (e.g. ASTM, 1989). The more important tests measure water absorption, modulus of rupture, compressive strength, abrasion resistance and flexural strength. Other tests measure the thermal coefficient of expansion, weather resistance, stain resistance, and indentation under concentrated load as a measure of serviceability

(Marmont, 1993). Significantly, it is noted that "....slabs sawn in different orientations from the same rock may have markedly different strengths, and care must be taken to determine the rock's properties in each direction...". Marmont also notes that "...potential planes of weakness may lie parallel to the layering in some granites...". This statement applies equally to the primary layering observed in true granites, as well as to the more obvious metamorphic layering in gneisses.

2.4.2. Influence of texture

For this discussion, texture is limited to grain size. Efforts to define the influence of foliation and lineation on mechanical properties are described in following section.

Zarifa (1998) acknowledged that: 1) granitic rocks show a variety of engineering properties that may affect quarrying operations, tunneling, mining, slope stability and the use of rock as a construction material, and 2) that the physical and mechanical properties of granite are a function of the mineralogical and textural characteristics of the rock. He applied correlation analysis to investigate the relationships between petrographical and engineering properties of a variety of granitic rocks from different parts of Turkey. These were subjected to petrographic analysis, the samples were then tested to determine specific gravity, dry and saturated unit weight, water absorption, effective and total porosity, sonic velocity, Schmidt hardness, point load strength index, uniaxial compressive strength, tensile strength and modulus of elasticity. The relationships between these properties and the petrographical characteristics were then described by regression analyses. The study revealed that the influence of the textural characteristics

on the engineering properties appears to be more important than the mineralogy. It also determined that the types of contacts, grain shape and size significantly influence the engineering properties of the granitic rocks. These results are consistent with those obtained from similar tests on the LDBB (Svab and Lajtai, 1981).

Marmont (1993) and Stecich et al. (1992) identified potential structural problems in dimension stone quarrying associated with coarse or very coarse grained granite. According to these authors, very coarse-grained granites are not as widely used as finer-grained varieties, and equigranular varieties are preferred over porphyritic. The coarser or more inequigranular rocks are recognized as being susceptible to time-dependent degradation by stress relief cracking along grain boundaries or along the cleavage planes in feldspars. An example of such degradation is especially well developed in a highly stressed intact outcrop exposed at a quarry near Whitemouth, owned by Canital Granite of Manitoba (Schmidtke, 1986; also Everitt et al., 1994). Specimens, cut and polished to serve as floor tiles, will disintegrate after a storage period of as little as a month due to the propagation of grain boundary microcracks.

2.4.3. Mineral alignment and natural microcracking

In addition to the aforementioned responses related to grain size, it has also long been recognized that even the most homogeneous and uniform granites usually possess a microscopic structure which predisposes them to break more easily in one direction than another (Duncan, 1987; Marmont, 1993). This is usually caused by weak alignment of elongate mineral grains, and /or by sets of pervasive natural microcracks, either

intergranular, or transgranular (Richter and Simmons, 1977). The DSI terminology for this mechanical anisotropy is as follows:

rift: the direction along which granite splits most easily is the called rift,

grain: the next easiest direction of splitting,

hard way: the direction along which the rock is hardest to split (also known as the "head").

The rift is commonly horizontal or vertical, the grain is usually perpendicular to the rift, and the head perpendicular to rift and grain. These directions commonly correlate with batholith structure. Stecich et al. (1992) describes the rift in dome-shaped granite intrusions being parallel to the granite's contact with the enclosing rocks. The rift and grain are used to plan the quarrying and processing of stone, with stone cut parallel to the rift being stronger than stone cut across it. Understanding of this is considered critical in large architectural panels (Marmont, 1993).

Many of the granites included in the dimension stone literature are technically gneisses, having undergone one or more episodes of deformation and recrystallization (e.g. Marmont, 1993). Marmont notes that good strength characteristics are associated with the more massive granites with "..complex interlocking grain shapes ...". In gneissic granites a well-developed rift usually accompanies the layering. Many granites also possess a linear structure formed by alignment of mineral grains in the plane of the layering, which frequently determines the orientation of the grain. The hard way cuts

across both layering and lineation. Marmont According to the author "...care must be taken in the retrieval of dimension stone to establish that gneissic layering is not a plane of weakness...".

2.4.4. Foliations and mineralogy

Sano et al. (1992) conducted an experimental determination of the elastic constants for the Oshima, Barre and Chelmsford granites. This study is unique in its examination of the effect of mineral anisotropy and its contribution to anisotropic elasticity in rocks. According to the authors, the major rock forming minerals have anisotropic elasticity, with the crystals of quartz, orthoclase and plagioclase being trigonal, monoclinic, and triclinic, respectively. A preferred alignment or segregation of these minerals within a rockmass should therefore result in an anisotropy of the linear elasticity and the coefficients of thermal expansion for the rockmass. To test this hypothesis, their granite samples were cut into polyhedra. These were then used to measure the longitudinal and shear wave velocities in various directions of propagation and polarization, which they then related to the fabric of the samples. The results showed:

1. that oriented microcracks are mainly responsible for the orthorhombic elasticity of both granites under lower confining pressures up to 120 MPa (6-8 km depth).
2. However, a slight anisotropy, oblique to the microcracks, was found even at 180 MPa. This correlated with the preferred alignment of biotite and chlorite.

2.4.5. Microcracks:

In addition to structures such as bedding or foliation, oriented pores and cracks are also a significant cause of anisotropy in rocks. The role of natural microcracks, specifically their influence on rock mass properties, was summarized in a review by Sano et al. (1992), and by others as follows:

1. In granitic rocks, oriented microcracks are very typical, and these cracks may be associated with either residual or external stresses (Dale ,1923; Nur and Simmons, 1970; Sprunt and Brace, 1974; Plumb et al., 1984; Kudo et al., 1987; Homand-Etienne and Sebaibi, 1996).
2. Natural microcracks include the following types: 1) submagmatic, quartz – mica filled intergranular fractures (Bouchez et al., 1992), 2) planes of aligned fluid inclusions representing re-sealed ancient microcracks (Jang et al., 1989; Rehrig and Heidrick, 1972), 3) oxide-filled ancient microcracks, and 4) open to partially sealed microcracks formed along grain boundary and mineral cleavages (Ren et al., 1989; Richter and Simmons, 1977).
3. The fabric of microcracks in granite rocks shows a correlation with the anisotropy of physical properties: for example, with sound velocity (Simmons et al., 1975), Young's modulus (Douglas and Voight, 1969), compressibility (Tod et al., 1973), uniaxial compressive strength (Douglas and Voight, 1969), tensile strength (Peng and Johnson, 1972), dilatancy anisotropy under compression (Scholz and Koczynski, 1979).

4. Duncan (1987) in a study of a Precambrian granite, found that the presence of microscopic fractures in the intact rock influences the Brazilian tensile strength of intact rock, such that reduced tensile strengths occur across those planes characterized by a higher degrees of subparallel microscopic fracture development.

Peng and Johnson (1972) found similar variations in Brazilian tensile strength for several orientations of Chelmsford granite. They found that the tensile strength was:

- lowest in the direction normal to the plane of the preferred orientation of microcracks.
- second highest normal to a plane characterized as having a preferred orientation of mica cleavages, and
- generally higher along other orientations for which there were no corresponding fabric elements.

Baek (1997) examined the effect of oriented microcracks on acoustic wave velocity and axial Point Load indices. Specimens were cored from blocks of medium grained leucocratic granite, bearing strong anisotropy parallel to the rift plane. The circumferential acoustic wave velocity was measured to determine the direction of the minimum velocity, presumably perpendicular to the dominant microcrack direction. The direction of fractures induced by the axial point loading was found to be closely related to the direction of natural microcracks in the specimen, interpreted from the circumferential velocity anisotropy, and supported by microscopy.

Chen et al. (1997) examined the correlation between microfracture type and physical properties of two granites. The Inada granite is anisotropic in "...dynamic property or permeability" and splitting planes, while the Kurihashi granodiorite is isotropic with no clear splitting planes. Three types of microfractures were distinguished in both specimens: intracrystalline cracks, intercrystalline cracks and grain boundary cracks. The orientations of these were measured and a total length per unit area calculated. It was concluded that:

1. the Inada granite was anisotropic due to a preferred orientation of intercrystalline and intracrystalline cracks, while

2. the Kurihashi granodiorite was isotropic as it contained no preferred orientation of intercrystalline cracks, but there is a strong preferred orientation of grain boundary cracks and intracrystalline cracks, which the authors correlate with indistinct splitting planes.

Similar results linking mechanical anisotropy and preferred orientations of natural microcracks were obtained by Kusumi et al. (1997) (Effect of structural anisotropy on deformation properties of granite under cyclic loading), and Park (1996) (The anisotropy of the granite revealed by tensile tests).

2.4.6. Conclusion — Influence of Fabric Anisotropy in Other Granites

Strong evidence from quarrying operations and from rigorous rock properties testing in granite using a variety of sonic and rock properties testing, has indicated that granites are texturally and mechanically anisotropic. Most often this anisotropy can be linked to preferred orientations of natural microcracks. These tend to be enhanced by sampling and stress relief, with the effect markedly less noticeable at high confining pressures typical of depths of 6-8 km. Mineral alignment or mineral segregations also induce mechanical anisotropy to a somewhat lesser degree, but their influence is not affected by confining pressure.

2.5. Rock Properties Testing in the Lac Du Bonnet Batholith.

This section reviews relevant case studies from the published literature, which examined the deformational properties of the LDB granite and, where data was available, their variations with direction. Comments on the results of these studies and their significance to this investigation are provided.

Svab and Lajtai (1981) examined the effects of variable mineralogy and mineral habits on tensile fracture paths through LDBB granite. They noted that the most obvious indicator of anisotropy within the LDBB granite was a (i.e. single) foliation, marked by subvertical quartz-biotite lenses and mineral alignment striking 075°. To test for strength anisotropy related to either foliation or to microstructural control of fracture, they used: 1) biaxial tension tests to define the orientation of preferred fracture, and then 2) Brazilian tests to evaluate the strength of the anisotropy. The first technique is sensitive to weakness

directions in the rock, while the second provides more accurate values of the tensile strength associated with these weakness directions.

The samples used by Svab and Lajtai (1981) were from the Cold Spring Quarry near Lac Du Bonnet, Manitoba. The background information on the geology for this study was based on initial mapping results of the Lac du Bonnet Batholith published by Tammemagi et al. (1979; 1980; 1982). At that time, the major phase of the batholith was described as: "...a medium to coarse grained (0.5-20 mm), pink, and relatively homogeneous granite. Foliation is limited to several kilometres along the contact, trending approximately 075° with a steep northwesterly dip at the quarry."

The testing (by Svab and Lajtai, 1981) of vertical core revealed that: 1) the subvertical 075° foliation was a plane of preferred fracture, 2) fractures also clustered around 005° and 155°, but there were no recognized foliations for these orientations, and 3) although there was a foliation / fracture correlation at 075°, tensile strength in this plane was only slightly lower than in any other orientation and "... not statistically different to justify the assumption of a multimodal population..." within the horizontal plane.

Subsequent investigations by the author and others (most notably, Brown et al., 1989; and Everitt et al., 1999) have shown that: 1) the sample location used by Svab and Lajtai (1981) is more homogeneous than most other locations in the LDBB and at the URL, and the foliations and microstructures less well developed, 2) the pink colour of the granite is due to hematite from alteration and recrystallization which partially cements grain

boundaries and natural microcracks, 3) that foliation is not limited to the margins of the batholith, 4) that some foliations and natural microcrack sets present in the LDBB have been partially sealed by mineral infilling and alteration (including the 075° foliation), and 5) that there are several foliation and natural microcrack sets aligned with the 005° and 155° preferred fracture directions noted by Svab and Lajtai (1981) (see Figure 16 of Brown et al., 1989). Accordingly, it is not surprising that a greater degree of mechanical anisotropy was not detected. The two preferred directions of fracture in the horizontal core – 029°/65° NW and 029°/75° SE, may correlate with any number of foliation or natural microcrack sets found in the URL and elsewhere in the LDBB.

Duevel and Haimson (1997) conducted a mechanical characterization of pink Lac du Bonnet granite to test for evidence of nonlinearity and anisotropy in samples of the pink granite. It was taken that the pink granite may better represent the in-situ properties of damaged grey granite recovered from highly stressed rock. Samples of grey granite, obtained from depth, exhibit mechanical anisotropy due to sample damage induced by stress-relief (Martin, 1990). This sample damage includes discing in core, and the opening of grain–scale microcracks along mineral cleavages and grain boundaries due to stress relief.

The samples used by Duevel and Haimson (1997) were from the Cold Spring Quarry near Lac Du Bonnet, Manitoba. The background information on the geology for this study was based on original mapping and core logging results for the Lac du Bonnet Batholith and the URL, published by Brown et al. (1989). Additional comments on the

mineralogy, joint orientation and microcracking were based on Martin (1990), and Martin and Stimpson (1994). The batholith was again described as "... medium to coarse grained (0.5-20 mm), and relatively uniform in composition and texture, but varying in colour from grey to pink". The pink granite was described as "... shows no visible microcracking (Martin, 1990), though joints are more prevalent at the surface, with the most prominent set striking at 020° and dipping vertically, with a spacing of 1–2 m".

To test for mechanical anisotropy, a suite of specimens was taken from core oriented in three orthogonal orientations: east-west (E-W), north-south (NS), and vertical (V). These were then subjected to: sonic velocity tests, uniaxial and triaxial compression tests, and Brazilian and Uniaxial tension tests. These results were then correlated with known fracture orientations, but no microstructure of fabric analysis of the specimens was done.

Sonic velocity tests yielded minor directional differences on the order of 10% - with the velocity high in the V (vertical) direction which the authors attributed to the predominant vertical joint set, and to microcracks. The lowest velocity was the E-W direction, approximately normal to the subvertical 020°-striking joint set. Although no microcracks were observed in the test specimens, the authors concluded that the velocity results suggest that they do in fact exist, and are predominantly subparallel to the outcrop-scale surface joint set.

The uniaxial and triaxial compression testing results point to compressive strength isotropy. For the uniaxial compression, the maximum difference between any two

directions was 6 MPa (less than 3%), while the variation within each direction was less than 5%. The overall average uniaxial compressive strength is 219 (±9) MPa. Duevel and Haimson concluded that the preferred microcrack orientation implied from the sonic velocity results does not affect failure in compression.

Unlike the compression tests, the tension tests showed evidence of strength anisotropy. Brazilian and uniaxial tensile strengths were both found to vary up to 25% between orientations. For both measures of tensile strength, the E-W direction was the weakest while the V direction was the strongest. The tensile modulus displayed more anisotropy than any other property measured in this study. The results of the sonic velocity and tensile strength tests suggested the existence of microcracks aligned with the predominant surface joint set. The authors again correlated the directions of the least and largest tensile strengths with the smallest and largest velocities, respectively, and these in turn with the preferred orientation of vertical microcracks.

The elastic parameters in both compression and tension varied continuously with the stress magnitude, indicating nonlinear stress-strain behaviour. The tensile modulus of deformation was substantially lower than that in compression. The authors concluded "...Our work brings into question the use of isotropic models in excavation design, in which compressive material constants determined at one level of loading are employed regardless of the local state of stress... ".

Duevel and Haimson (1997) concluded: 1) that the pink Lac du Bonnet granite is practically isotropic with respect to uniaxial and triaxial compressive strength, compressive elastic parameters, and sonic velocities, but 2) the tensile strength shows a difference of 25% between directions, and the tensile modulus of deformation showed an even stronger anisotropy, with differences of up to 80% between directions, 3) that this anisotropy is due to natural microcracks with the same orientation as outcrop-scale joints, and 4) ".... As the gray Lac du Bonnet granite differs from the pink variety only by possessing stress-induced microcracks created during sampling, it can be deduced that the preceding results describe the in-situ gray granite as well....".

The criticisms made earlier regarding the study by Svab and Lajtai (1981) are also applicable to the study by Duevel and Haimson (1997). These are:

1. That the Cold Spring quarry is not representative of the LDBB, especially as seen in the URL.
2. That Duevel and Haimson may have combined results from dissimilar phases of the LDBB granite,
3. That their study been done without identifying the fabric elements actually present at the site from where the samples were taken, and
4. That the orientations chosen for sampling are oblique to each of the various subvertical and subhorizontal structures known to exist at the batholith-scale. There is also no indication how these orientations relate to any local structures at the quarry.

Detailed geological mapping (Brown et al., 1989; and Everitt et al., 1999) has shown that: 1) the Cold Spring quarry from which the samples were taken is more homogeneous than most other locations in the LDBB and at the URL, and the foliations and microstructures are less well developed. 2) that colour is not a valid basis on which to categorize the mechanical behaviour of the LDBB granite. As is described in Chapter 3, there are several genetically distinct phases of the LDBB, which differ from each other in their average grain size, range of grain sizes, degree of recrystallization, and in the number, type and orientation of foliations and natural microcracks. Pinking is the result of secondary alteration superimposed on these diverse rock types wherever fractures have opened the batholith to groundwater movement.

Svab and Lajtai (1981) identified a subvertical striking - 075° foliation in their samples from the Cold Spring quarry, which biaxial tension tests revealed to be one of several planes of preferred fracture. The study by Duevel and Haimson (1997) makes no mention of any foliation in their samples, or of the results of the earlier work by others. As such it is difficult to determine: 1) what textural / compositional rock type was actually being tested, 2) what structures were present, and 3) how the test results are affected by the orientation of the samples. Accordingly, it is not surprising that a greater degree of mechanical anisotropy was not detected. Also, it is uncertain to what extent the results can be applied to the various types of grey granite at the 420 Level of the URL, which hosts the various geomechancial experiments.

An alternative approach to defining the in-situ properties of highly stressed rock at depth, would be to identify the granite varieties present at the intended test location and depth, and then to obtain samples of these same varieties where they are exposed at or near the surface. In adopting this approach, it would be necessary to determine if the granite at surface and at depth differ substantially in the characteristics of their natural microcracks.

2.6. Conclusions

From the literature - general observations on fabric anisotropy, methodology and earlier site work are as follows:

1. Rock fabric is a recognized factor influencing rock strength and response in metamorphic and sedimentary rocks, but plutonic rocks (mafic to felsic) are generally regarded as homogeneous and isotropic.
2. Most work pertaining to plutonic rock comes from the various international nuclear waste programs. The majority of this is from the Canadian program as Canada is unique in having large volumes of intact or sparsely fractured rock – in other words – the granites of other countries are anisotropic due to their pervasive fracturing.
3. Significant fabric anisotropy has been recognized in other granites.
4. Recent investigations provide evidence that, in other granites, these fabrics, usually foliations or natural microcracks, influence deformational properties,
5. The dimension stone industry (DSI) has long recognized the existence of mechanical anisotropy related to fabric anisotropy in granites, and has utilized these phenomena to facilitate exploration and excavation. In contrast, the inherent anisotropy of granitic rocks has been overlooked by the various radioactive waste disposal

programs, but especially in the Canadian program which is unique in that it is being conducted in large volumes of unfractured and intact rock. Programs in other countries are being conducted in granites which are inherently anisotropic due to abundant joints and other discontinuities.

6. The Lac du Bonnet Batholith is incorrectly referred to as a homogeneous granite in literature as recent as 1998, while Hoek and Brown (1995) incorrectly refer to the Mine-by Experiment at the 420 Level as demonstrating that there is no influence of geology.

The methodologies used in this thesis are based on the findings and recommendations of earlier researchers. An array of oriented samples was obtained. Strength anisotropy and the influence of foliation was then systematically investigated using rock mechanics tests that are sensitive to planar anisotropy (Point Load and Brazilian tests), the former defining planes of naturally preferred fracture. Variations in the compressive strength of the granite related to grain size and fabric was examined through uniaxial compression testing of an array of samples providing a range of angles between the loading axis and the fabric.

Although the material properties of granites (and the LDBB) have been investigated in the literature, these investigations differ from this investigation in the following areas:

1. other studies (e.g. Duevel and Haimson, 1997) have been done without identifying the fabric elements present in the granite tested, or have combined results from

dissimilar phases of the LDBB granite, or have incorrectly identified the orientation of structures present

2. other studies have not identified and classified the foliations and other anisotropies present in granite at a variety of scales,
3. nor have they combined this information with the influence these anisotropies have had on the development of both ancient and excavation-induced fractures.

In these aspects, the present study is unique and original in its approach, scope and application.

Chapter 3

SITE DESCRIPTION

3.1. General Geology of the Lac du Bonnet Batholith

The study location for this investigation into the influence of foliation on rock mass properties is the Lac du Bonnet Batholith (LDBB). Its location and regional setting are shown in Figure 1. The Lac du Bonnet Batholith is one of many late-tectonic granites emplaced in the western Superior Province of the Canadian Shield towards the end of the 2760-2670 Ma Kenoran event (McCrank et al., 1981; Davis et al., 1986; Stone et al., 1989). The presence of very large sparsely fractured volumes within these plutons is characteristic of this suite, and is attributed at least in part to:

1. their intrusion at or near the end of regional deformation (Brown et al., 1989),
2. to prolonged cooling, which delayed the onset of brittle deformation, due to the size of the bodies and their proximity to each other, and
3. to the distance separating the intrusions regionally from later tectonic events in the Superior Province (Everitt et al., 1990).

To the north, the batholith is in sharp contact with a narrow belt of metavolcanic rocks in the Bird River Greenstone Belt, and to the south it is in gradational contact with gneisses and migmatites of the Winnipeg River Subprovince (Beakhouse, 1977). From a tapered eastern margin, surface exposures of the batholith extend westward 85 km. West of the Winnipeg River, the batholith is largely concealed by glacio-lacustrine sediments and by

Paleozoic carbonate rocks; however, geophysical data indicate that the granitic rocks extend westward at least another 20 km (McRitchie, 1971).

3.2. Underground Research Laboratory

The Lac du Bonnet Batholith was selected for investigations by Atomic Energy of Canada Limited (AECL) as part of a program to assess the concept of nuclear waste disposal in plutonic rocks of the Canadian Shield (Whitaker, 1987). The geology of the batholith was defined through surface and airborne studies and by 130 boreholes, some reaching depths of 1100 m. The subsurface structure has been further characterized in detail by the author through geologic mapping of the shafts and galleries of AECL's Underground Research Laboratory (URL).

The URL (Figure 1) includes a vertical access shaft that extends to a depth of 443 metres and several hundred metres of tunnels at depths of 240 and 420 metres (240 and 420 Levels, respectively). Additional exposure is provided by raise-bored ventilation shafts, a timber-framed raise at the 420 Level, and small shaft stations in the main access shaft at depths of 130 m and 300 m. Boreholes from the base of the shaft and lowest level provide an additional 600 m of vertical exposure. These excavations and the boreholes provide an 1100 m cross section of the roof zone of the Lac du Bonnet Batholith, two low-dipping thrust faults and associated splays, and the subvertical intrablock fractures that flank the major faults. The roof zone is marked by deuteric alteration and by shallow-dipping compositional layering. Low-dipping fractures, including thrust faults, parallel the large-scale compositional layering, and are generally confined to the contacts

between massive leucocratic and foliated xenolithic litho-structural domains. The geology of the URL is representative of the batholith.

3.3. Batholith Structure

The many late to post-tectonic granites in the western Superior Province, and the LDBB in particular, are noted for their structural and compositional homogeneity over extensive surface areas (Beakhouse, 1991; Cerny et al., 1987; MacLeod, 1980; McCrank, 1985), and have been described as type examples of "massive homogeneous plutons" in the literature. However, mapping in the 443 m deep access shaft at the Underground Research Laboratory (URL), borehole logs, and detailed surface mapping clearly demonstrate that dekametre-scale layering and smaller scale structures are widespread in the LDBB. Simplified geological maps of the upper and lower portions of the URL access shaft are shown in Figure 10 a and b, respectively. The upper shaft (0 to 257 m depth) has a rectangular cross section. From left to right are shown the north, east, south, and west shaft walls. The main unit of the granite is shown in white, while the metavolcanic xenoliths and the three generations of slightly younger dykes, sills and masses are shown in other colours. The shaft between 257 m and 442 m has a circular cross-section. The numerals on the left side of each shaft segment are the lithostructural domain reference numbers, and the depth (in metres) from the shaft collar. To the right side of each segment are short descriptions of the domains or of other distinctive features. Block diagrams summarizing the structures in the Lac du Bonnet Batholith as seen at AECL's URL are shown in Figure 11.

Individual layers or litho-structural domains are distinguished by the type and abundance of xenoliths and late residual or metasomatic segregations, by auto-intrusive contacts, and by variations in style and orientation of mesoscopic foliations (Note: the term auto-intrusive refers to late residual segregations, coming from the same magma as that comprising the bulk of the batholith, and it specifically excludes other dykes or veins related to younger plutons and tectonic events). The litho-structural domains are inconspicuous at surface due to their low dip and the flat topography; however, detailed mapping in the central part of the URL has identified their surface expression as a series of broad and open antiforms and synforms. The textural and compositional layering is clearly delineated in the URL shaft (Everitt and Brown, 1986), where it has been shown to exert a strong control on the localization of low-dip thrust faulting, and on the frequency and properties of the subvertical fractures.

The litho-structural domains host three systems of auto-intrusive dykes, sills, and recrystallized zones whose abundance and mode of occurrence change with depth. Late magmatic granodioritic dykes are the predominant rock type below 300 m depth at the URL, but the swarm narrows rapidly up-dip, and at surface is represented only by narrow zones of alteration and ductile deformation. Late pegmatite-aplite dykes are pervasive across all rock types at surface, but are limited to the larger fine grained granite dykes at 420 m depth at the URL. The distribution of inclusions, alteration and fractures in the LDBB suggest the present topographic surface is close to the original roof zone of the batholith.

Table 8.
Comparison of Petrological Units from surface and subsurface mapping of the Lac du Bonnet Batholith.

Occurrence	Unit #	Reference Cerny et al.(1987)	McCrank (1985), Stone et al. (1984)	Everitt et al. (1998)
xenoliths	1,2	Predominantly tonalites and amphibolites but also some granitoids	Same	Same
main unit	3	Biotite granite	Biotite granite, and textural variants.	Same *
auto-intrusive dykes	4		Irregular pegmatitc masses and porphyroblastic schlieren	Granite to pegmatitc sills, and lesser masses, dykes and porphyroblastic schlieren *
auto-intrusive dykes	5	Late-tectonic biotite granodiorite dykes		Granite-granodiorite dykes*
auto-intrusive dykes	6	Pegmatite dykes	Pegmatite - aplite dykes, and quartz veins	Same

* Note: For the sake of convenience, units 3,4 and 5 are referred to in this report as the medium, fine and coarse grained granites, respectively.

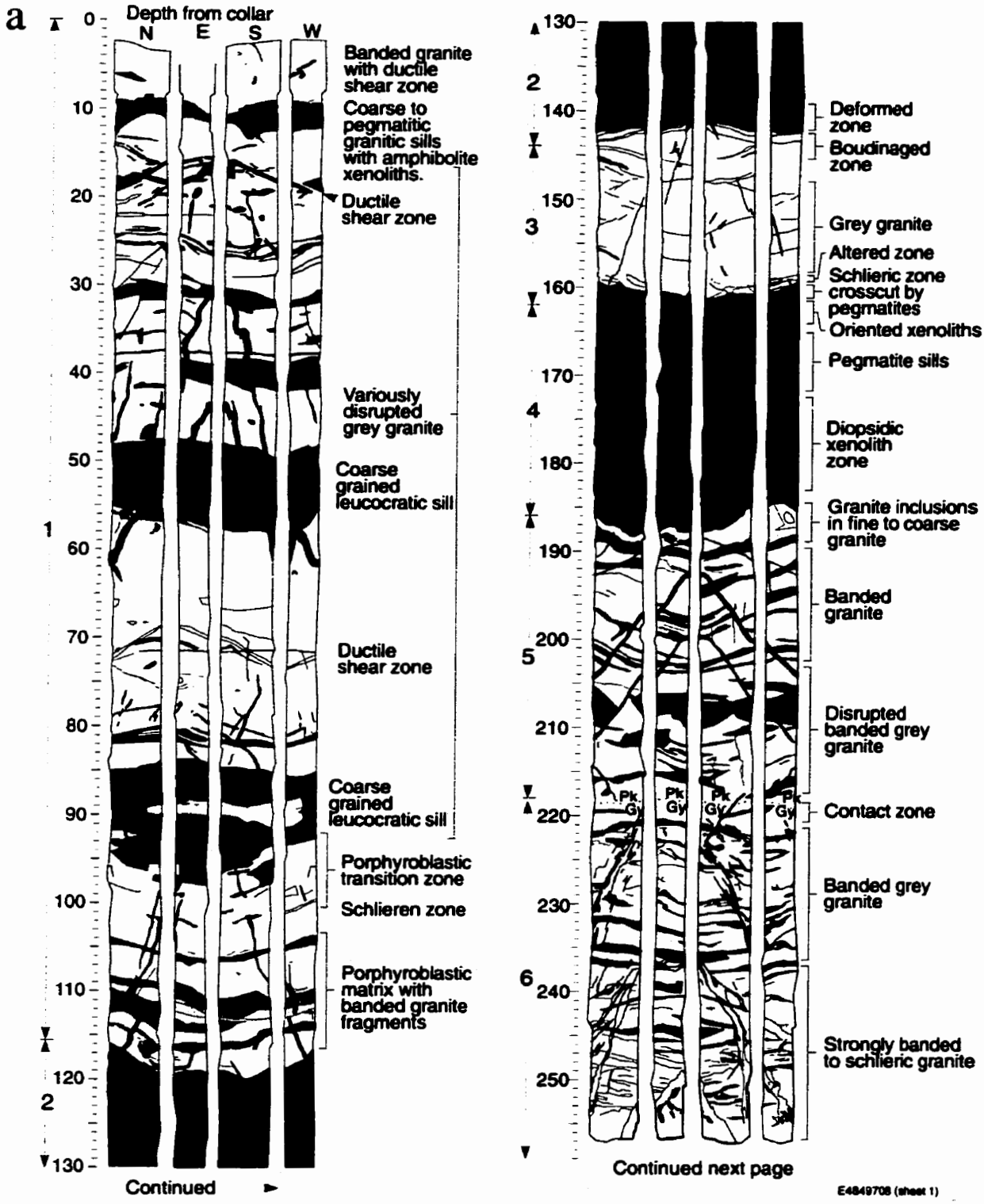

Figure 10a. Simplified geological map of the upper portion of the URL access shaft (continued next page, refer to text for explanation).

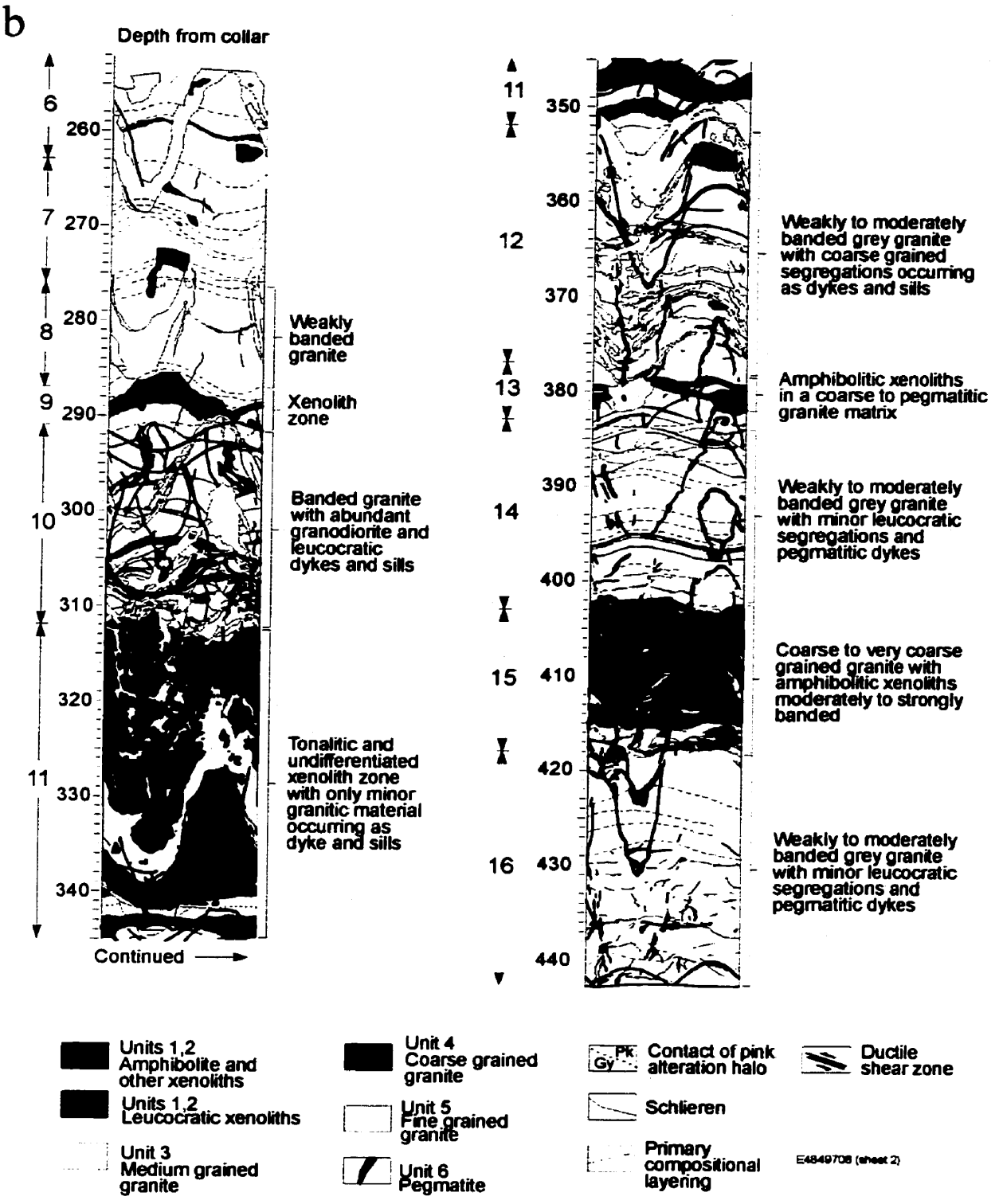

Figure 10b. Simplified geological map of the lower portion of the URL access shaft (refer to text for explanation).

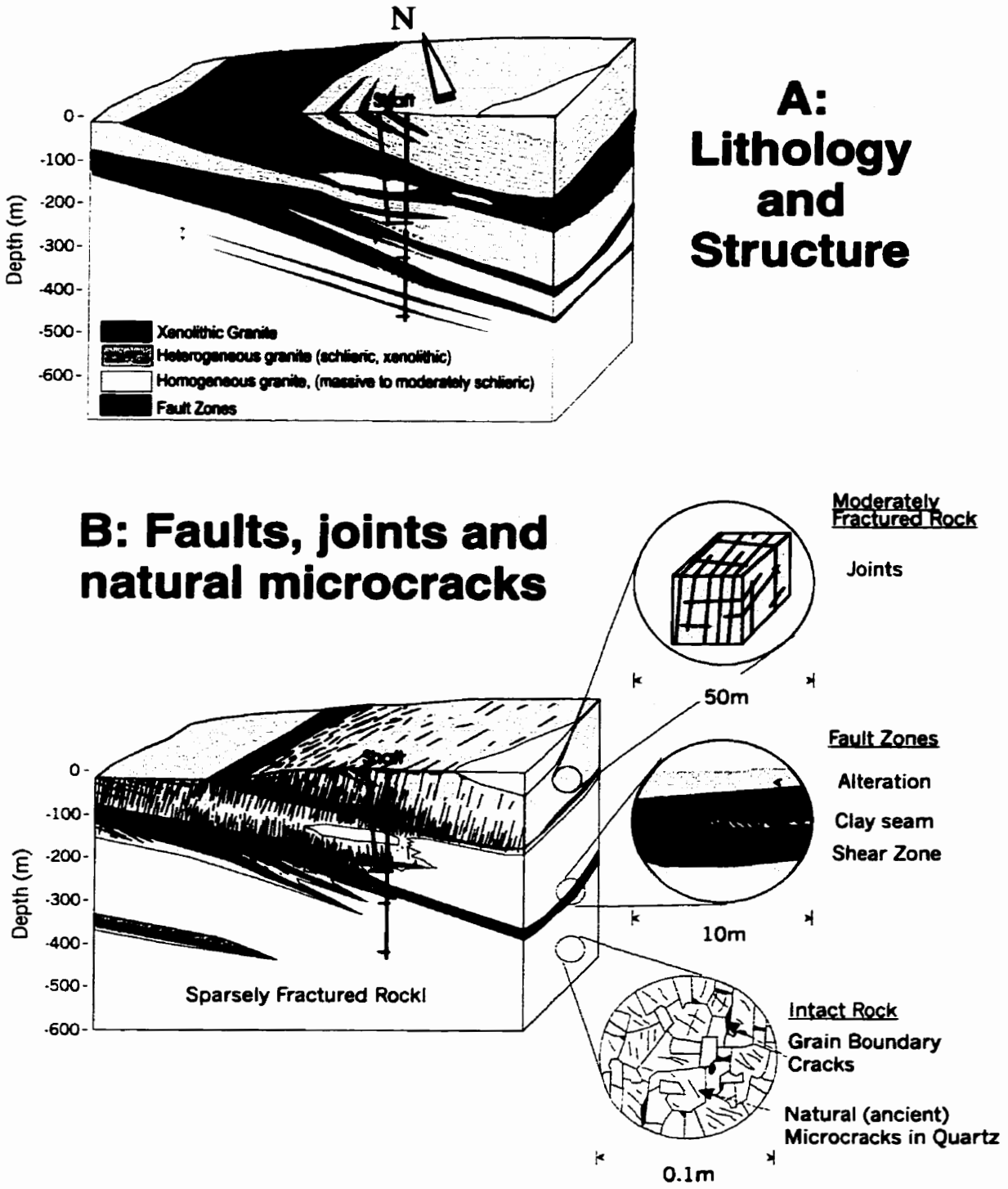

Figure 11. Block diagrams summarizing the structures in the Lac du Bonnet Batholith as seen at AECL's URL. A: Large-scale compositional layering and the low-dipping thrust faults, which are concordant with the layering. B: Faults, joints and natural microcracks within the same area.

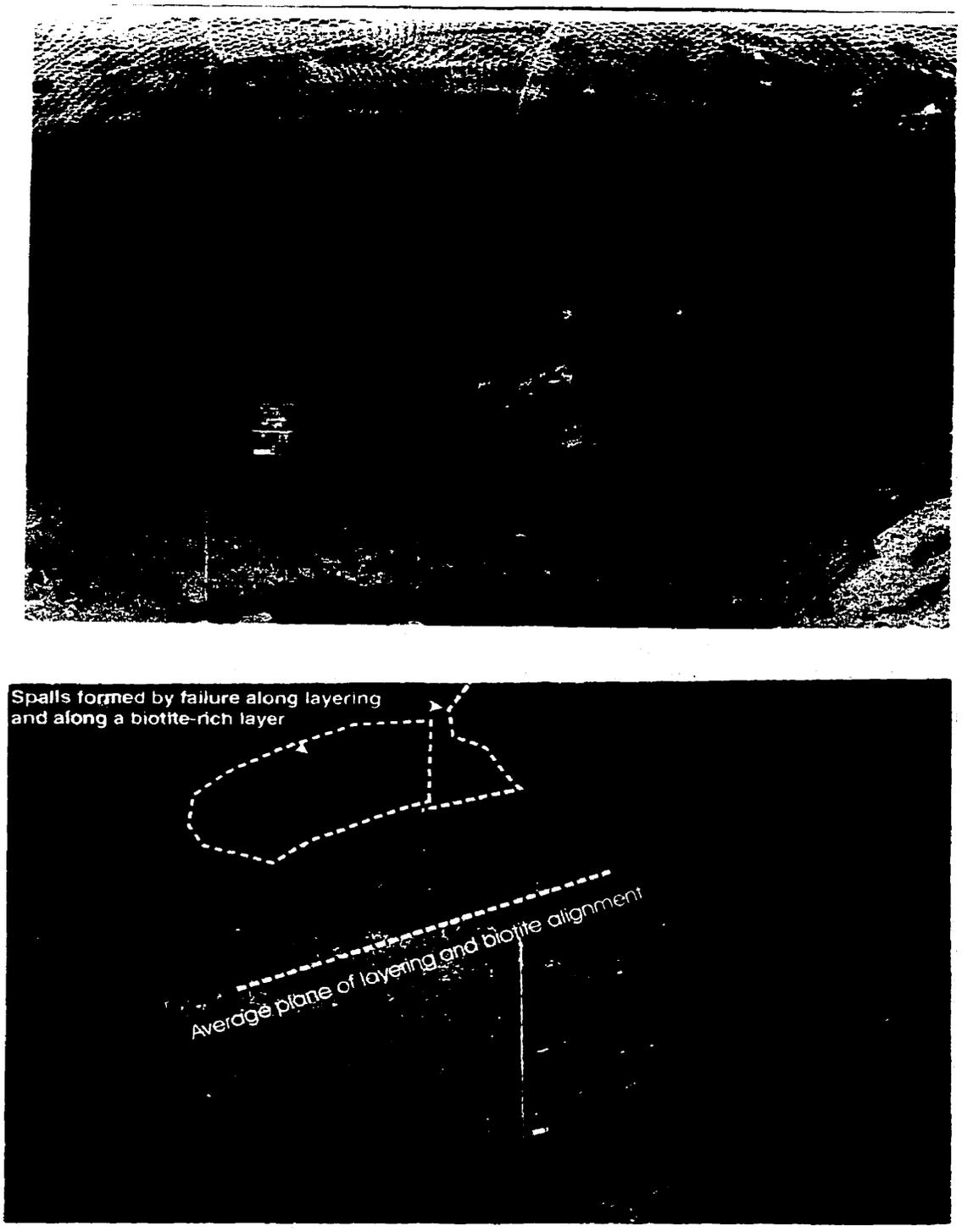

Figure 12. Rock units and structures recognized at depth in the URL, and selected for rock properties testing in this study. Each photograph is of a vertical tunnel face. The scales are approximately the same, each photo showing an area of approximately 3.5 m by 2.5 m. The measuring stick is 1m long. The fine and medium grained granites are shown in the upper photograph (A). The coarse grained and (locally xenolithic) granite is shown in the lower photograph (B).

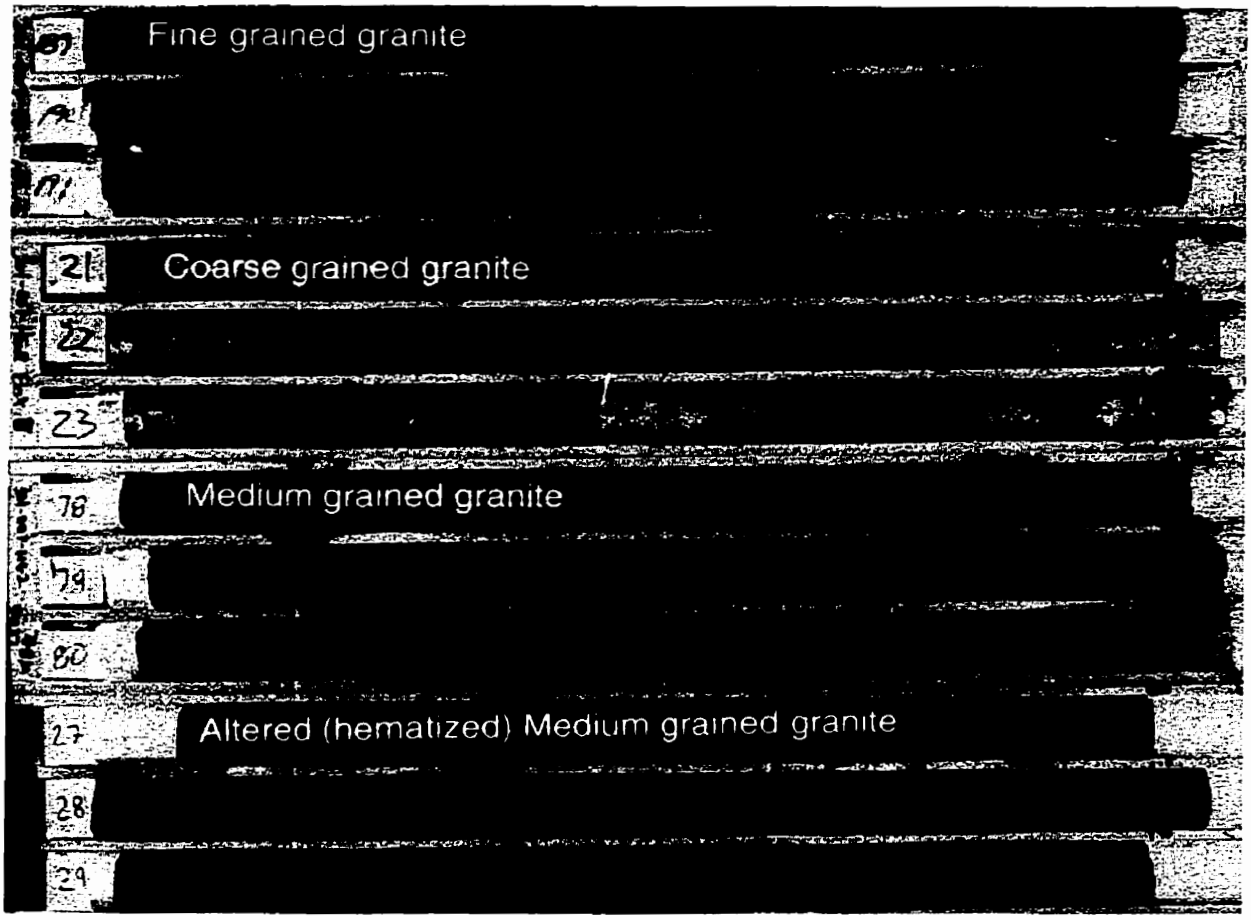

Figure 13. Typical appearance in core, of the granite types selected for rock properties testing in this investigation. From top to bottom are the fine-, coarse-, and medium-grained granites, respectively, and the pink (altered) equivalent of the coarse granite.

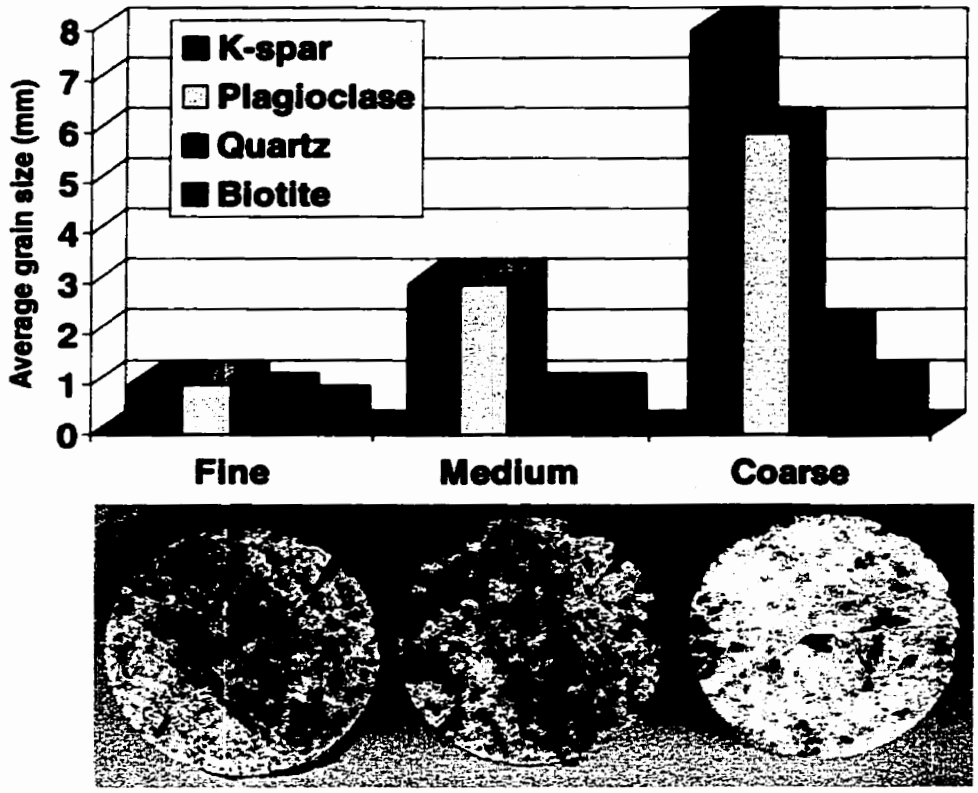

Figure 14. Grain sizes and variation with mineralogy, of the three rock types selected for rock properties testing.

3.4. Outcrop-scale Rock Units

On the basis of mineralogy, texture, intrusive relationships, and geochemistry seen from surface exposures, various authors have identified up to six units, with additional textural variants (Table 8). These may be broadly grouped as follows:

- meta-volcanic xenoliths and earlier granites (units 1 and 2 in Table 8),
- the main unit of the granite (unit 3 in Table 8).
- several sets of auto-intrusive dykes (units 4,5 and 6 in Table 8), which range from fine- to very coarse-grained.

Photographs of these units as they appear at the tunnel- and borehole-scales are shown in and Figure 12 and Figure 13, respectively. Colour is not a distinguishing characteristic of the rock units nor is it a guide to compare rock mass response, although it has been used frequently as such in the literature (e.g. Lau and Gorski, 1991a,b). Each of the rock units listed ranges from a uniform grey, to a red or pink where altered. Most reddening is associated with fractures, where the rock has been subject to long-term exposure to groundwater, and cuts across rock unit boundaries (Brown et al., 1989; Stone et al., 1989). Low temperature alteration overprints the higher temperature forms in the area of the major low-dipping fracture zones. Illite replaces epidote and biotite and Fe-oxides are removed, leaving the rock bleached in appearance.

Three distinct textural varieties of the Lac Du Bonnet granite, differing in type and orientation of foliation were identified and selected for testing. These are: 1) fine grained granite dykes with subvertical flow banding, 2) medium grained and weakly to moderately layered granite forming the main mass of the batholith, and 3) a generally coarse grained and leucocratic unit that occurs as sills and recrystallized zones in the main unit. For the sake of convenience, these are referred to as the fine, medium and coarse grained granites, respectively. The grain sizes for each of these units are illustrated in Figure 14.

3.4.1. Fine Grained Granite

This rock unit (unit 5 in Table 8) occurs as a dyke swarm, which increases in both size and complexity with depth. A typical exposure of the contact between a fine grained

granite dyke as seen at the 420 Level, and the medium grained granite is shown in Figure 12A. The location selected for sampling was similar to this exposure.

Initial petrographic analyses of samples from the 240 Level confirmed Cerny's (1987) granodiorite classification for this unit, but subsequent analysis of additional samples from the 420 Level indicate this unit straddles the granite-granodiorite boundary of the IUGS classification, with substantial overlap into the (biotite) granite field (IUGS, 1973). At the 240 Level, these dykes comprise up to 10% of the rockmass, and are up to 5 m thick with well-developed chilled margins and flow banding. Flow banding is defined by a preferred alignment of biotite crystals, biotitic aggregates and inclusion trains. At the 300 and 420 Levels of the URL, granodiorite occurs as a stockwork of large dykes and minor interconnecting sills and is the most abundant rock type. The largest dykes at and below the 420 Level are medium grained and, apart from the orientation of the foliation, are indistinguishable in hand specimen from the biotite granite they intrude.

3.4.2. Medium Grained Granite

This rock type comprises the main unit of the granite (unit 3 in Table 8, the unshaded area in the shaft geology maps (Figures 10a and b, and Figure 11). Its description matches that of Cerny et al. (1987) and McCrank (1985) from surface mapping, but in the subsurface, its fabric ranges from massive to schlieric, its texture from equigranular to porphyritic. The area selected for sampling of this rock type was similar to the exposure but was free of inclusions and schlieren, and the layering was weakly developed.

3.4.3. Coarse Grained Granite

This rock type (unit 4 in Table 8 and shown in Figures 10a and b, and Figure 11) comprises a heterogeneous assemblage of residual leucocratic segregations and porphyroblastic zones. Textures range from aplitic to pegmatitic, and porphyritic to equigranular. The contacts of this unit range from sharp to gradational, and are generally parallel to the layering of the main unit granite. The largest zones (up to 30 m thick) occur in association with xenolithic horizons, and have complex margins and internal fabrics. The photograph shows the actual area where the samples for this rock type were taken. Note the well developed layering. The dark area on the left hand side of the crown is the scar left by the spalling of a slab along a plane of biotite-rich band.

3.5. Rock Fabric

A summary of fabric elements present at the (420 Level) level of the case studies is given in Figure 15. The structures are listed in order of relative age. The orientations of each structure are summarized on the stereographic projections, and in the accompanying conceptual block models which also summarize the age relationships. Poles to the gneissosity and larger scale layering cluster about a pole with a strike (dip direction) dip of 032°(122°)/22°. The basic geometries of the fine grained granite and pegmatite dyke systems are similar but are differently oriented. For each system:

- poles plot along great circles but several sets are recognized;
- the subvertical set is dominant;
- the subsidiary sets fall into two groups, those inclined about 45° to 60° from the subvertical set and those whose orientations indicate local control by older fabric

elements (e.g. the southeast dipping fine grained granite sills follow the gneissosity and the subvertical pegmatites follow some of the fine grained granites).

Points to note from the block models include the normal offset of the layering by the subvertical fine grained granite, the orientation of the subsidiary fine grained granite dykes relative to the layering, and the location and pattern of the pegmatites and the minor joints relative to fine grained granite. The pegmatites and joints at the 420 Level are largely confined to the fine grained granite.

The litho-structural domain boundaries and the small scale gneissic layering are thought to represent primary compositional layering in the batholith. The fine grained granite dykes are considered to be auto-intrusive (Everitt and Brown, 1986). Their orientation and general pattern of offset suggest at least local extension of the batholith roof. This may have been initiated by subsidence of the roof zone of the batholith, or by variations in the relative rate of intrusion. The subsidiary, low-dipping sets are thought to represent secondary shear fractures developed to accommodate differential movement within the dyke swarm.

The pegmatite dykes, the quartz veins and the minor joints intersected in some boreholes are largely confined to the fine grained granite dykes, and are interpreted as successive generations of cooling fractures. For the joints, this interpretation is based on their parallelism to the fine grained granite dyke swarm in which they occur, the infilling assemblage of lineated quartz-chlorite-sericite-sulphide, and on the similarity of these fractures to other late- to post-magmatic fractures found elsewhere within the URL. The

unoxidized sulphides on the fracture surface and the absence of wall rock alteration and detectable seepage support the conclusion that these fractures are closed.

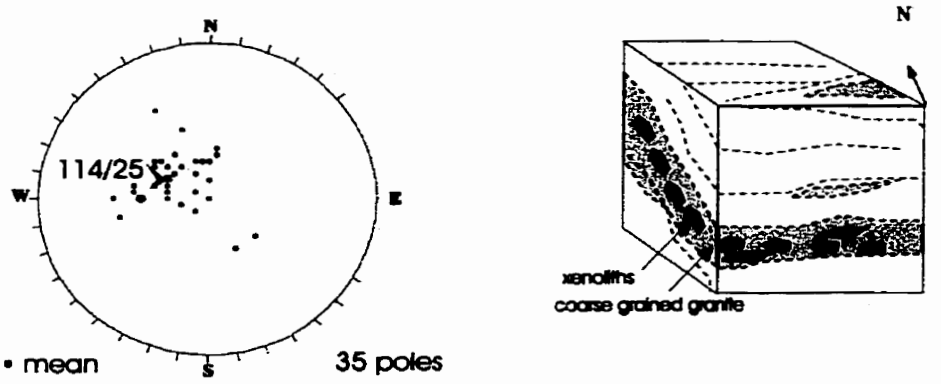

A. Compositional and Textural (Gneissic) Layering

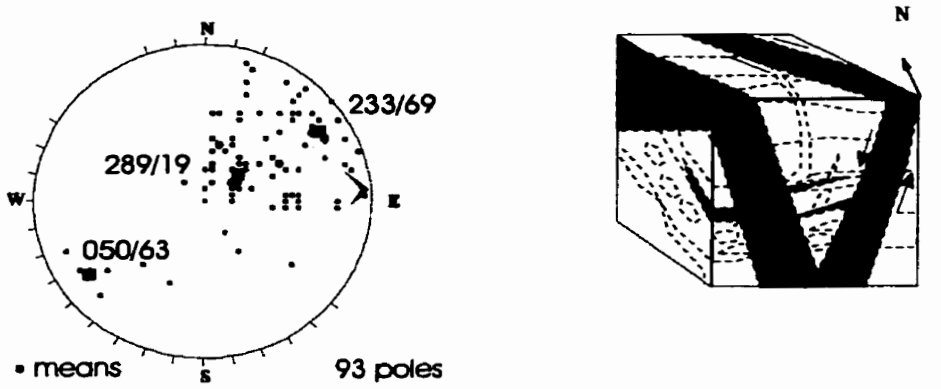

B. Fine Grained Granite Dykes

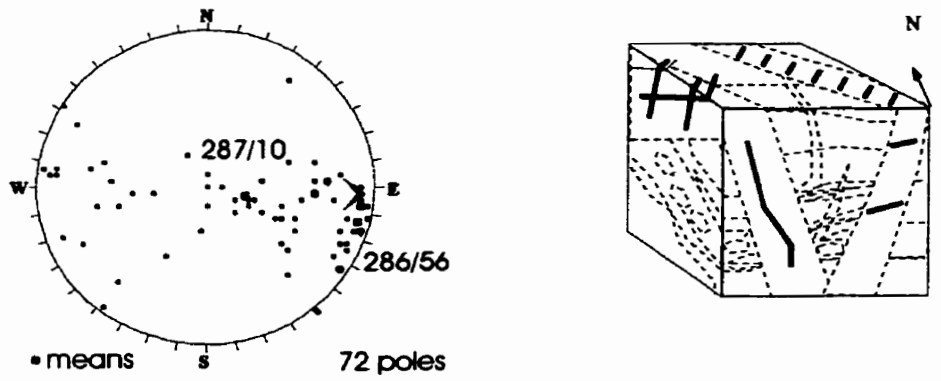

C. Pegmatite Dykes and Quartz Veins

Figure 15. A summary of fabric elements present at the 420 Level, listed in order of relative age. The orientations of each structure are summarized on the stereographic projections, and in the accompanying conceptual block models which also summarize the age relationships.

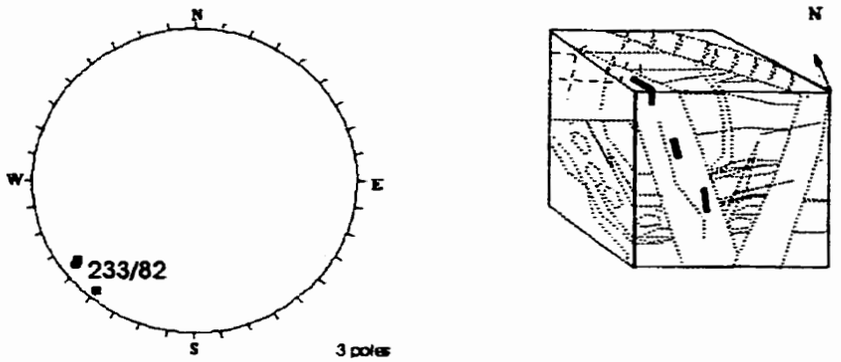

D. Quartz- Chlorite-filled fractures in the fine grained granite dykes

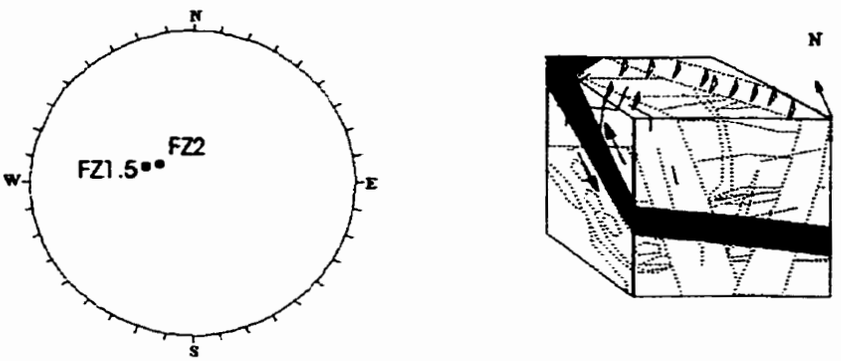

E. Low-dipping thrust faults (Fracture Zones 1.5 and 2)

Figure 15 (continued). A summary of fabric elements present at the 420 Level, listed in order of relative age. The orientations of each structure are summarized on the stereographic projections, and in the accompanying conceptual block models which also summarize the age relationships.

3.6. Faults and Fractures

The URL access shafts provide a cross section of the roof zone of the batholith, and of two low dipping thrust faults and associated splays. In terms of scale, fractures at the URL include:

1) kilometre-scale low-dipping thrust faults (Figures 16a and b),
2) subvertical joints, (Figure 16), and
3) natural (i.e. ancient) microcracks.

The natural microcracks are described separately in Chapter 4.

Shaft mapping has shown that the thrust faults are low-dipping, variously permeable horizons that contain both low-dipping and steeply dipping fractures. The thrust faults have chloritic slip surfaces which grade into complex cataclasite zones where fault movement has been significant (on the order of metres). The cataclasites consist of recrystallized fault rubble cemented by a fine grained chlorite-carbonate matrix, and they are crosscut by chloritic slip surfaces, minor fractures, and seams of soft clay - goethite gouge. This assemblage is in varying stages of groundwater-induced decomposition.

The thrust faults and splays follow the large scale compositional layering, and divide the rockmass into a number of tabular to wedge-shaped blocks. These blocks are crosscut by one or more sets of subvertical joints, the pattern and frequency of which varies from one block (fracture domain) to the next (Figure 16). The factors influencing the pattern of intrablock joints include:

1) the overall distance from the surface,
2) the proximity to the bounding faults, and

3) the local rock type.

With increasing depth, the subvertical joints become less frequent, less continuous, and with fewer preferred orientations. They also become increasingly confined to the immediate margins of the fault zones or to lithological heterogeneities such as dykes. These trends may reflect a general change from three-dimensional, to predominantly two dimensional, strain in the lowermost thrust sheets at the base of the sequence. The subvertical joints were interpreted as extensional intrablock fracturing generated during and after faulting (Everitt and Brown, 1986). Flexing of the fault blocks during thrusting is the most likely mechanism for their initiation. Reactivation may have occurred as a result of regional extension associated with subsequent cycles of uplift and erosion, and likely resulted in continued flexing of the thrust plates, reactivation of existing fractures, and the formation of new fractures.

Samples for this study were taken from intact rock below the lowest thrust fault, at the 420 Level (420 m depth from surface). Drilling and excavation at the 420 Level have exposed six quartz-chlorite filled fractures. All were dry and tight. They appear to be smaller-scale (and lower temperature) equivalents of the pegmatite-aplite dykes, formed by parting along the flow banding during cooling and contraction of the dykes. None were observed in the areas of the 420 Level selected for sampling.

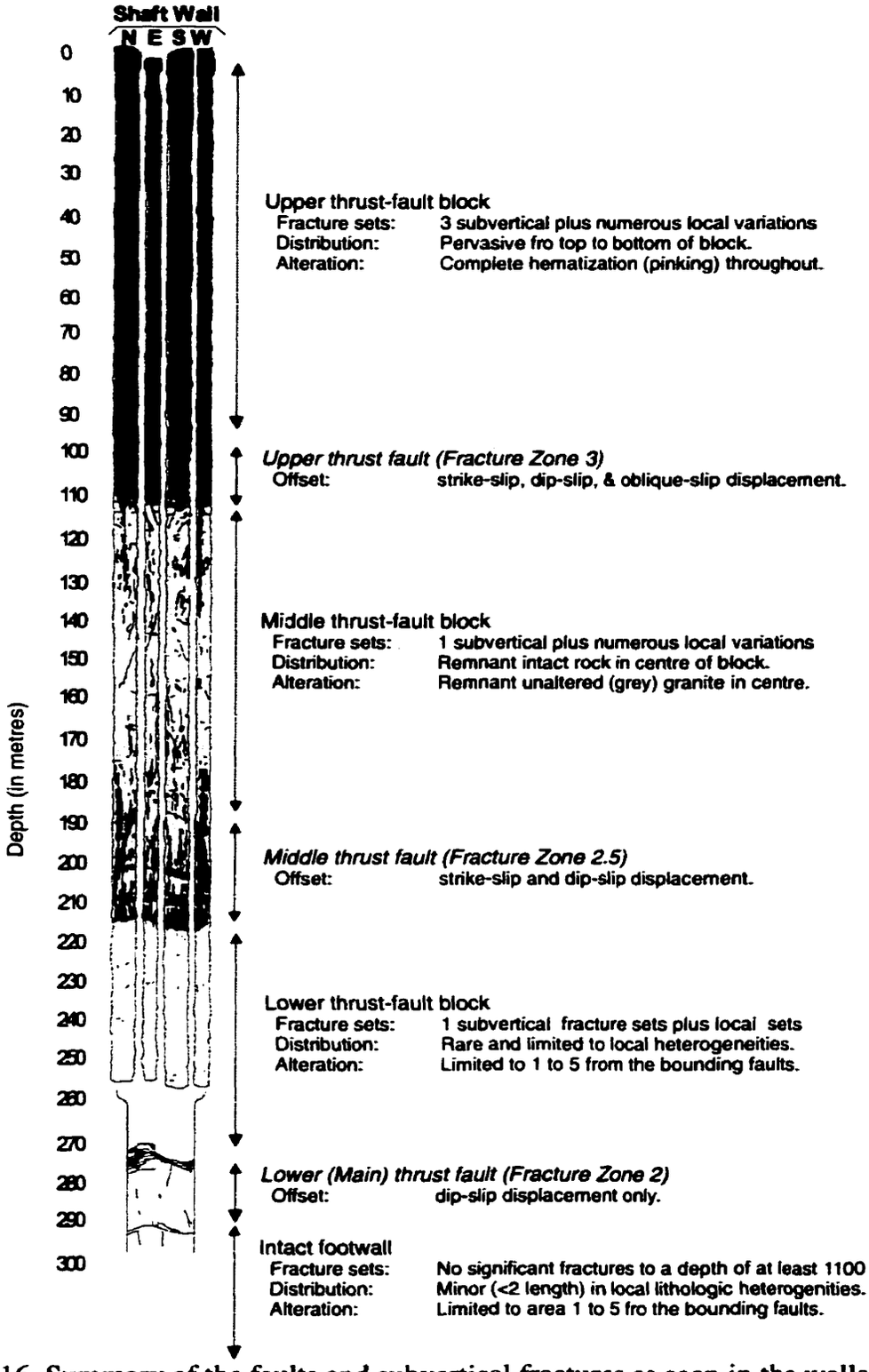

Figure 16. Summary of the faults and subvertical fractures as seen in the walls of the access shaft (the shaft from surface to 255m has a rectangular cross section, which changes to a circular cross section below this depth). The shaft below 290m is unfractured, and for this reason is not shown. Fracture Zone 2 is shown in greater detail in Figure 16 b following.

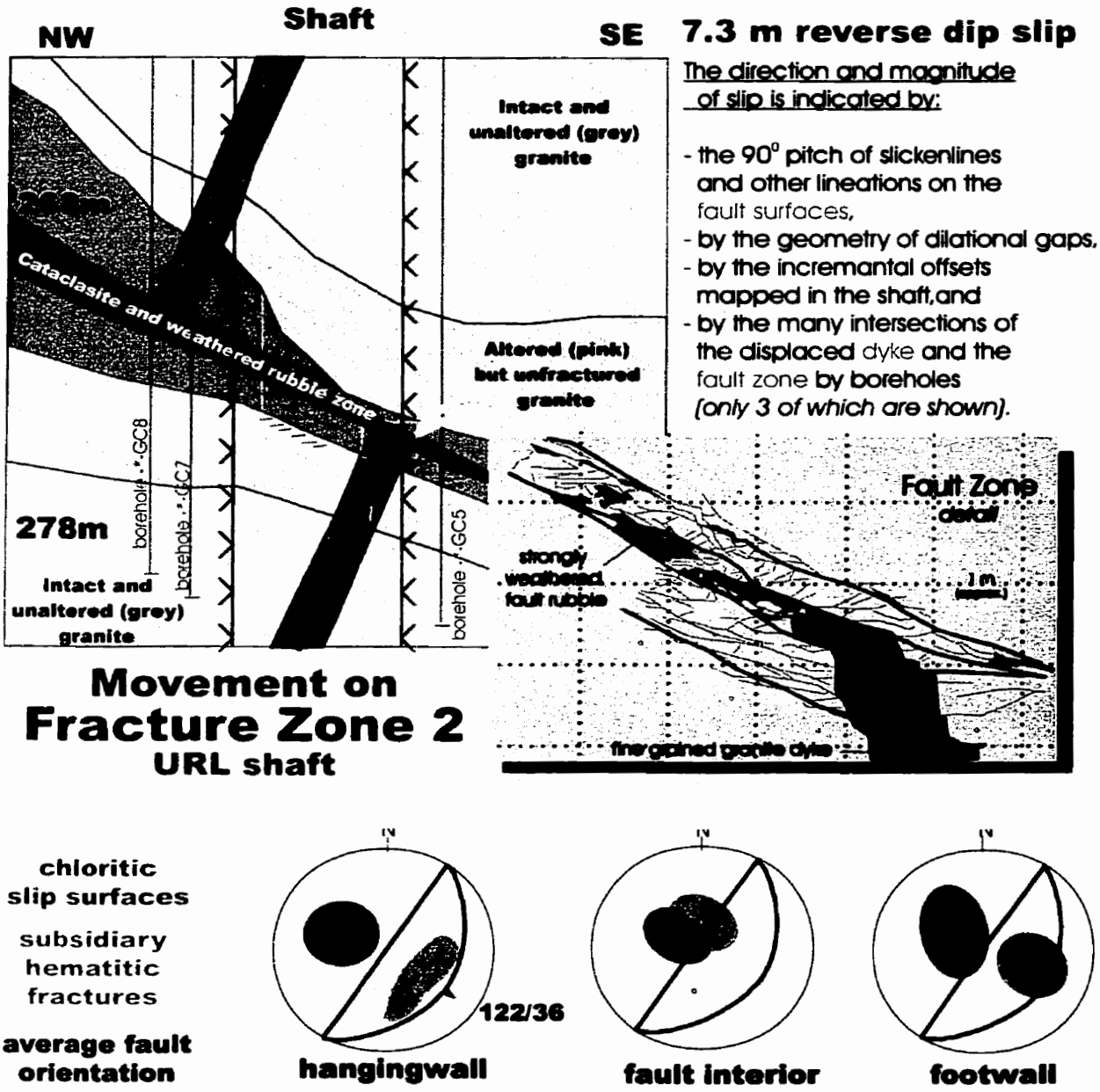

Figure 16b. Fracture Zone 2 as seen in the access shaft and its environs. The vertical section shows the offset determined from multiple borehole intersections and shaft mapping. The incremental nature of offset and the sense of movement is indicated in the inset (a portion of the shaft wall). Fracture orientations and the average fault orientation in the hangingwall, fault interior and footwall are shown in the stereographic projections. (modified from Everitt and Brown, 1996).

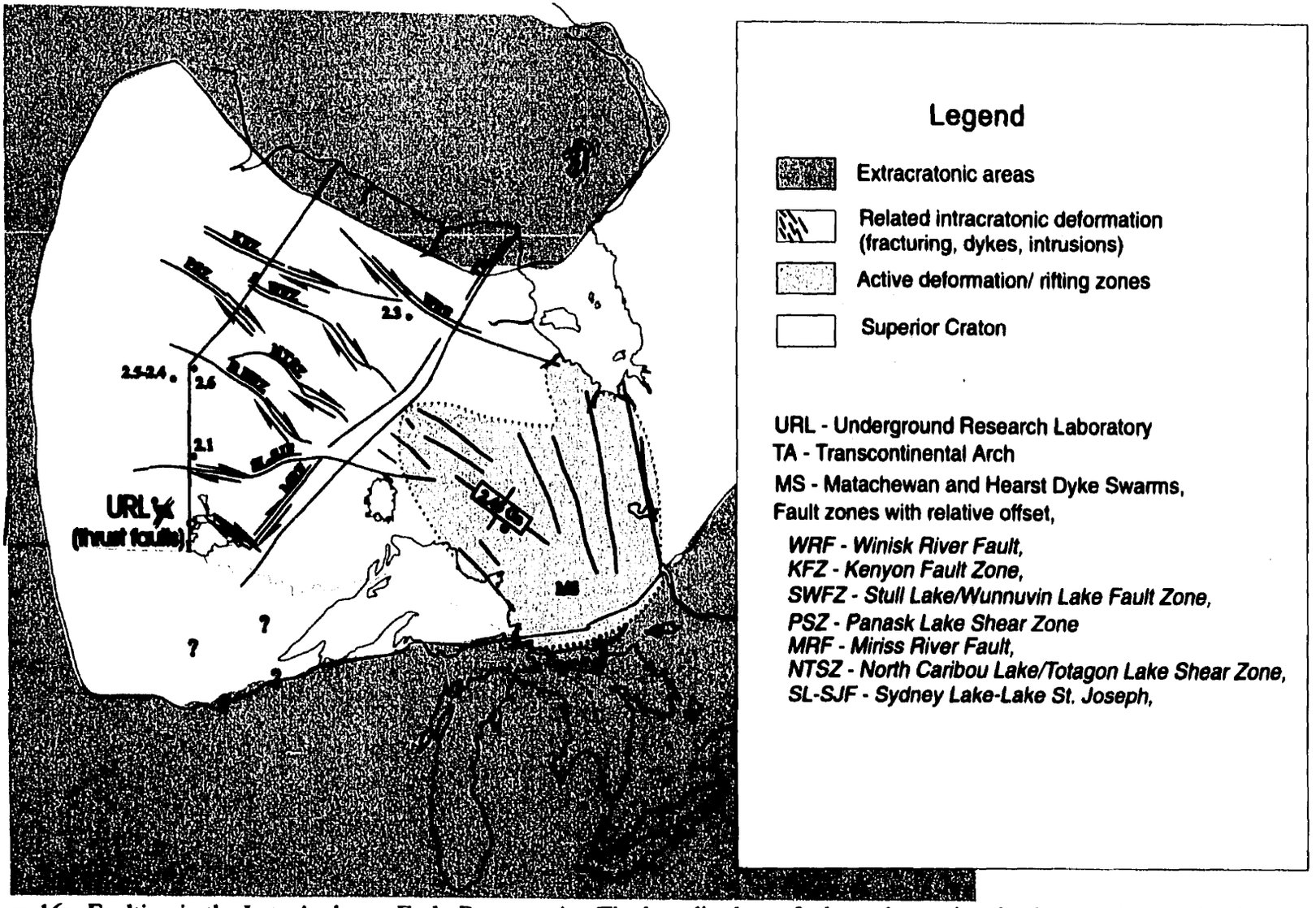

Figure 16c. Faulting in the Late Archean -Early Proterozoic. The low dip thrust faults and associated splays are believed to be associated with the craton-scale faulting shown (modified from Osmani 1991).

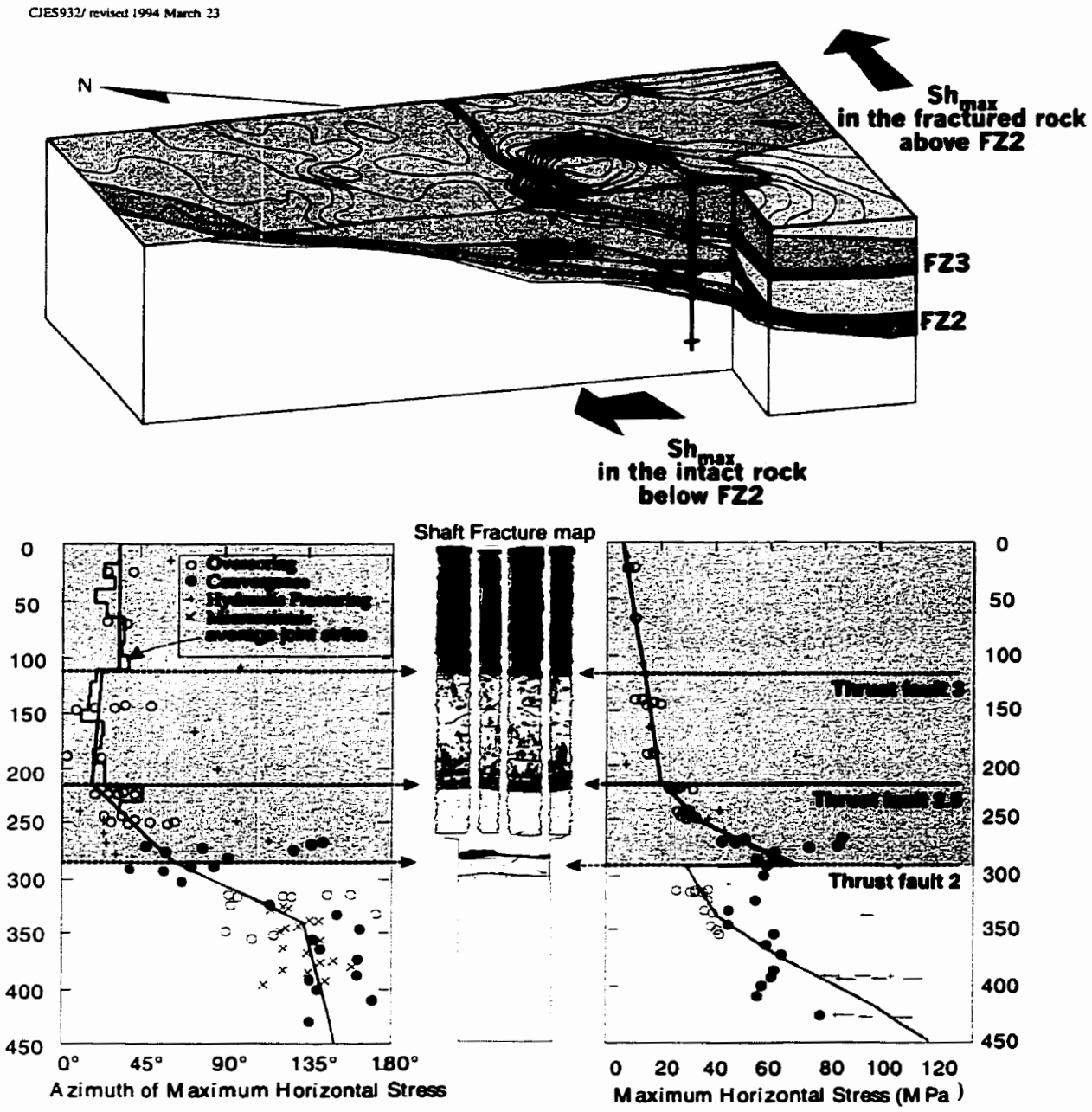

Figure 17. In-situ stress domains in the URL in relation to the fracture domains (stress data from Martin, 1989). The variations in average stress orientation and magnitude with depth are indicated by the dark green lines. For explanation refer to text.

3.7. In-situ Stresses

Figure 17 and Table 9 summarize the general orientation of principal stresses at the URL and their geometric relationships with the rock structure. The figure includes the following components:

A. a block model of the URL showing the thrust faults, the jointed rock between them and the intact rock below the main thrust fault (FZ2).

B. two charts depicting the variation in stress orientation and stress magnitude with depth, and

C. the shaft fracture map with the locations of the thrust faults, jointed rock, and intact rock highlighted.

The thrust faults, Fracture Zone 2 (FZ2) in particular, act as stress domain boundaries (Everitt et al., 1990; Martin, 1989b; 1990; 1993). Intact rock below the fault preserves high in-situ stresses, but these have been relieved above the fault by movement and fracture formation. The large arrows on the block model represent the average orientation of the maximum horizontal stress above and below the main thrust fault (FZ2). In the sparsely fractured rock below Fracture Zone 2, the maximum horizontal stress is oriented NW-SE, perpendicular to the strike of the thrust fault. In the fault block above Fracture Zone 2, the maximum principal stress is considerably lower and is oriented NE-SW, parallel to the dominant fracture set and the strike of Fracture Zone 2. This presumably represents a reduction and re-orientation of stresses through the formation of fractures in the hangingwall block. The footwall, including the area of the 420 Level has not been affected by the reorientation and reduction of stresses associated with the formation of the subvertical joints above Fracture Zone 2.

The thrust faults are believed to have formed during the late Archean - early Proterozoic in response to tectonism in the orogenic belt to the south (Figure 16c, also Everitt et al., 1990). Based on the geometry of the fault system, the intermediate and maximum principal stresses were subhorizontal and directed northeast-southwest and northwest-southeast, respectively. The present in-situ stresses at this level in the URL (i.e. in the intact rock beneath FZ2) retain this geometry, which supports the suggestion by Haimson (1990) for a domain within the mid-continent region in which the maximum horizontal principal stress is directed northwest-southeast. Whether this is a remnant stress field or a fortuitous alignment of recent and ancient stresses is unknown.

The in-situ stress measurements shown in this figure are a compilation of results obtained over the duration of the facility (Martin, 1989b; 1990; 1993). The measurement techniques have included:

1. convergence measurements
2. overcoring
3. hydraulic fracturing, and
4. microseismic monitoring

A brief explanation of these techniques, based on Chandler et al. (1996) and other unpublished material provided by Paul Thompson and Jason Martino of AECL follows.

3.7.1. Convergence Measurements

Convergence measurements are traditionally taken to obtain information related to the performance of underground support systems, especially in rock masses where the convergence is expected to be several centimetres or more. Convergence measurements in stiff rock masses are more difficult to accurately determine however, with the appropriate instrumentation and an understanding of the time dependent nature of the deformation, it is possible to measure convergence in unsupported rock mass, and to back calculate the horizontal in-situ stresses from the measured convergence. Martin et al. (1996) presents the analytical solution used to calculate the in-situ stresses from convergence measurements and also illustrates the role convergence measurements played in establishing the in-situ stress state at the URL when traditional testing methods, such as overcoring, were not fully successful.

The convergence of the circular shaft was measured at 26 locations between 267 and 430 m depths (Martino, 1989). Convergence pins were installed within 300 mm of the shaft floor at eight locations around the circumference of the shaft, facilitating convergence measurements across four diameters. The Kern Distometer used for taking convergence measurements had a repeatability of $\pm$ 0.1 mm, sufficient for the back analysis of in-situ stresses. The total convergence measured in the shaft typically varied between 1 and 3 mm, and was generally attained once the excavation face had advanced two or three shaft diameters (10 to 15 m) below the elevation of the convergence array.

The circular shaft geometry facilitated the calculation of in-situ stresses from the measured convergence values using a formulation proposed by Goodman (1989) based on the Kirsch equations for stresses and displacements around a circular opening (this was explained in detail in Martin et al., 1996). In-situ measurements of the displacements ahead of an advancing face suggest that 50-60% of the total displacement had already occurred ahead of the advancing excavation. These observations and numerical modelling supported a 60% correction factor for convergence measured in the shaft. Horizontal in-situ stresses calculated from shaft convergence measurements are shown in Figure 17.

3.7.2. Overcoring

Overcoring involves installing a strain-measuring instrument either at the flattened bottom of a borehole, or in a small-diameter pilot borehole drilled concentrically at the base of a larger hole then extending the original borehole past the instrument location (i.e. overcoring the instrument) usually by using a special thin-walled bit. For typical overcore tests at the URL, the large hole size is HQ (96-mm-diameter) and the pilot hole, if used, is EWG (38.7 mm diameter). Overcoring relieves the stresses acting on the cylinder of rock containing the instrument, thus inducing strains. The induced strains can then be used to back-calculate the stresses acting on the cylinder prior to overcoring if the stress-strain behaviour and properties of the rock are known. Depending on the strain measuring instrument, either the stresses in the two-dimensional plane orthogonal to the borehole, or the complete three-dimensional stress tensor, can be determined.

The overcore technique of stress measurement using borehole deformation or USBM (United States Bureau of Mines) gauges (Hooker and Bickel, 1974), triaxial strain cells (Leeman, 1967) or doorstopper gauges (Leeman, 1971) is well documented and thoroughly tested. Overcoring is used to determine the stresses in either the two-dimensional plane perpendicular to the borehole using USBM and doorstopper gauges, or the complete three-dimensional stress tensor using CSIR (Council for Scientific and Industrial Research) and SSPB (Swedish State Power Board) cells. All of these instruments have been used at the URL in the determination of in-situ stresses. The CSIR triaxial strain cell, in particular, provides consistent three dimensional stress information. In total, approximately 1000 overcore tests have been conducted at the URL, 350 of which are far-field triaxial stress measurements.

The greatest limitation to conducting overcore stress measurements at the URL is the high horizontal stress below Fracture Zone 2 which frequently induces discing of the core, making elastic interpretation of the results inappropriate.

The doorstopper (Leeman, 1971) is the name given to strain gauge rosettes that can be attached to the flattened end of a borehole and subsequently overcored. Doorstopper gauges have been used on the 420 Level of the URL when core discing makes it impossible to conduct USBM and triaxial cell tests. In theory, doorstopper strain measurements are unaffected by discing of the core. At the URL, the method of Corthesy et al., (1993) was used to determine non-linear and anisotropic elastic constants from doorstopper biaxial tests, and of applying these constants to the results from

overcoring in order to determine the in-situ stresses. This method has been applied to 13 doorstopper tests conducted in four boreholes on the 420 Level.

3.7.3. Hydraulic Fracturing

Hydraulic fracturing (hydrofracing) involves isolating a section of a borehole with a straddle packer system and creating fractures by injecting fluid into the zone at a pressure high enough to fracture the rock (Wijesinghe, 1987). The pressure required to fracture the rock (i.e., the breakdown pressure) and the "shut in" pressure or pressure required to re-open the fracture are used to calculate the rock stresses in the plane orthogonal to the borehole axis. The initial breakdown pressure is theoretically a function of the tensile strength, and the near-field tangential stress acting around the borehole.

In hydraulic fracturing, the straddle packer is lowered to the testing location and the packers inflated. Packer pressures are maintained slightly above the pressure in the zone isolated between the tow packers. The zone pressure is increased until the measured pressure drops suddenly indicating that the fluid is lost into a newly created pressure (P_b). A break in the plot of pressure versus time is often referred to as the "shut in pressure" (P_{si}). The shut-in pressure is often determined using a variety of graphical techniques and is believed to correspond to closure of the fracture. More recently, a slow repressurization test has been used to determine at what pressure the fracture reopens. In most cases, the reopening pressure is very nearly the same as the shut-in pressure but is generally more accurately determined.

The equations for maximum and minimum stress in the plane perpendicular to the borehole (σ_H and σ_h) are as follows:

$$\sigma_H = 3\,\sigma_h + T - P_b - P_0$$

and

$$\sigma_h = P_{si}$$

where T is the tensile strength of the rock and P_0 is the ambient pore pressure. The rock pore pressure is often taken to be the water pressure in the fluid filled borehole at the test location, since the borehole provides drainage to the rock where the fracture will initiate.

It is important to note that these equations assume:

1. that one of the principal stresses acts parallel with the axis of the borehole,
2. that the plane of the induced fracture is parallel with the axis of the borehole and propagates in the direction of the maximum principal stress,
3. That the rock mass tested is mechanically isotropic.

As is shown in this thesis, the last assumption does not correlate with either the mapping results done during excavation (this chapter), or with the results of the rock properties testing program presented in the following chapters.

Six series of hydrofrac test have been conducted at the URL in twelve different boreholes. Hydraulic fracturing was conducted in 1981 and 1982 prior to shaft sinking and was the first stress determination used at the URL. Nine tests were conducted in the

borehole URL-1 from 50 to 600 m depth (Haimson, 1982) and a second series of twelve tests was conducted in borehole URL-6 (Bawden, 1982). A third series of fifteen tests was done from the 240 Level in a subvertical probe hole (206-020-PH1) drilled down form the 240 Level (Doe, 1987). A fourth series of tests was conducted in three horizontal boreholes drilled form the 240 Level and two horizontal boreholes drilled from the 420 Level (Doe, 1989). A fifth series of fourteen test was done in borehole 401-009-HF1 drilled downwards form the 420 Level of the URL (Haimson, 1991) and a sixth series was conducted in three holes oriented in three different direction on the 420 Level (Haimson, 1992).

The tests produced consistent results at depths less than 300m, the depth corresponding to the predominant fracture zone (FZ2). Although tests were conducted both above and below FZ2, the induced hydraulic fractures below the fracture zone were either subhorizontal or could not be induced within the limits of the testing equipment. Evidence from the shut-in pressures was sufficient to conclude that the fracture zone acted as a stress domain boundary (i.e. a sharp transition from moderate to high in-situ stress magnitudes). The horizontal stress magnitudes from the hydraulic fracture tests conducted above FZ2 were later confirmed by overcoring stress measurements. The two stress determination methods provided very similar results for stress magnitudes (Figure 17). However, there is a 30° to 60° discrepancy in the azimuth of the major horizontal stress between the two methods. This difference has been attributed to either the natural variation of preferred joint directions in the rock leading to variation in the direction of induced hydraulic fractures, or to the existence of magnetite in the granite at

the URL which may affect the compass directions recorded on impression packers. The data and observations presented in this thesis support the first interpretation – that is, control of fracture orientation by the rock fabric. Evidence of this was first obtained in the first application of hydrofracing at the URL in 1983. Hydrofracing was conducted from a pilot hole centered on the axis of the shaft prior to excavation. The hydrofrac was stained by a dye. Careful mapping of the shaft floor and walls was then done, as the excavation of the shaft provided a rare opportunity to observe the detailed geometry of a hydrofracture (unpublished mapping by the author and A. Brown, 1984). The exposures provided clear and conclusive evidence that the rockmass was not isotropic and that the orientation of the hydrofracture was not determined solely by the in-situ stress orientations. Instead, the hydrofracture followed narrow (<10 cm) pegmatite veins, alternating between vertical and horizontal whenever the veins changed orientation. It should be added, that these veins were tightly sealed and closed surfaces before the hydrofracing.

The presence of these veins and their structural control was not realized at the time of the hydrofrac tests. The evidence for fabric control invalidates several assumptions under which the test is based – namely – the fracture orientation is controlled by the in-situ stress, and that the rock mass is isotropic.

3.7.4. Microseismic Monitoring

Microseismic monitoring requires the use of arrays of triaxial accelerometers and / or geophones to record the low energy seismic waves from small scale cracking and microcracking around tunnels. The system is used to identify damage as it occurs during

excavation. This damage is related to stress redistribution around the excavations (Read and Martino, 1996). AE/MS systems have been used at the URL during shaft extension and Mine-by Experiment.

Accelerometers were installed in boreholes collared from the 300 Level and inclined downwards 45° around the shaft extension Young and Talebi (1989). The system was used to monitor events during shaft excavation between 324 and 443 m. In a horizontal plane, most of the microseismic activity was located within 1 to 2 m of the shaft walls and in some cases showed a preferred orientation similar to the zones of microcracking mapped at the 300 Level (Everitt et al., 1988). The events are concentrated in the zone of maximum compression, and indicate a northwest-southeast maximum horizontal stress orientation. This orientation agrees with observations of shaft wall notching, core discing and with results from convergence measurements.

Another array of sixteen accelerometers was installed around the Mine-by tunnel (Talebi and Young, 1990) also showed a concentration of events (Figure 46) in the orientation perpendicular to the maximum stress direction Talebi and Young (1992). The AE/MS system has been shown to provide valuable information regarding the orientation of in-situ stresses in a moderate to high stress environment.

In summary, the convergence measurements provide information on the deformation resulting from excavation, from which the orientation and approximate magnitude of the in situ stresses can be inferred. The microseismic monitoring during excavation identifies regions of high compressive stress concentrations which, in turn, can be used to

infer in situ stress directions. The hydrofracing method provides both the stress orientations and magnitudes, but is susceptible to spurious results resulting from fabric control of hydrofrac development. The overcoring methods have provided the best estimates of in-situ stress orientation and magnitude, however only in intermediate to low stress rock not affected by core discing.

Table 9

In-situ stresses measured at the 240 Level.

(Martin and Kozak, 1992)

	Magnitude	trend	plunge
σ_1	25.5 MPa	228°	8°
σ_2	16.8 MPa	135°	23°
σ_3	12.8 MPa	335°	65°

In-situ stresses measured at the 420 Level.

(Martin, 1993)

	Magnitude	trend	plunge
σ_1	55± 3 MPa	135°	14°
σ_2	48± 3 MPa	47°	8°
σ_3	14± 2 MPa	73°	74°

Chapter 4

NATURAL MICROCRACKS

Natural microfractures in quartz and other minerals are visible on close inspection of the coarser grained phases of the Lac du Bonnet granite (Figure 18), and are common in thin section. This chapter provides a compilation of the author's work on natural microfractures in quartz at the URL. The objectives of this work were as follows:

1. Are there preferred orientations or patterns of development for the natural microfractures?
2. Does their frequency and development vary with depth and in a manner consistent with the domains of large-scale fractures and the in-situ stresses?
3. Can microfracture orientations be used to infer the orientations of the larger scale fractures in areas of sparsely fractured rock? This application is considered to be most valuable during the initial stages of site investigation, as it would provide information on which to base the planning of exploration drilling and in the placement of in-situ stress measurements.
4. Are the natural microcracks responsible for the certain phenomena at the tunnel scale, such as the preferred development of excavation-induced fractures in certain orientations?

5. Can natural microcracks be responsible for strength anisotropies identified by rock properties testing (Point Load, Brazilian and uniaxial compression tests)?

This chapter presents the variations in microfracture orientation with depth at the URL, and their spatial relationship to the domains of macroscopic fractures and in-situ stresses. This study was undertaken in three stages: 1) an initial reconnaissance survey, 2) a more detailed reconnaissance survey, and 3) a study of samples from the 420 Level only to correlate with the samples taken for geomechanical testing. The data is presented in Everitt (2000).

Table 10

Microfracture types

1)	Natural microfractures which are dependent on some pre-existing fabric anisotropy, which includes:
	a) microfractures developed along grain boundaries, or
	b) microfractures formed by parting along crystallographic directions such as the cleavages in feldspars or biotite, and
2)	Natural microfractures that are independent of some pre-existing fabric anisotropy, the most significant of which are those developed in isotropic minerals such as quartz.

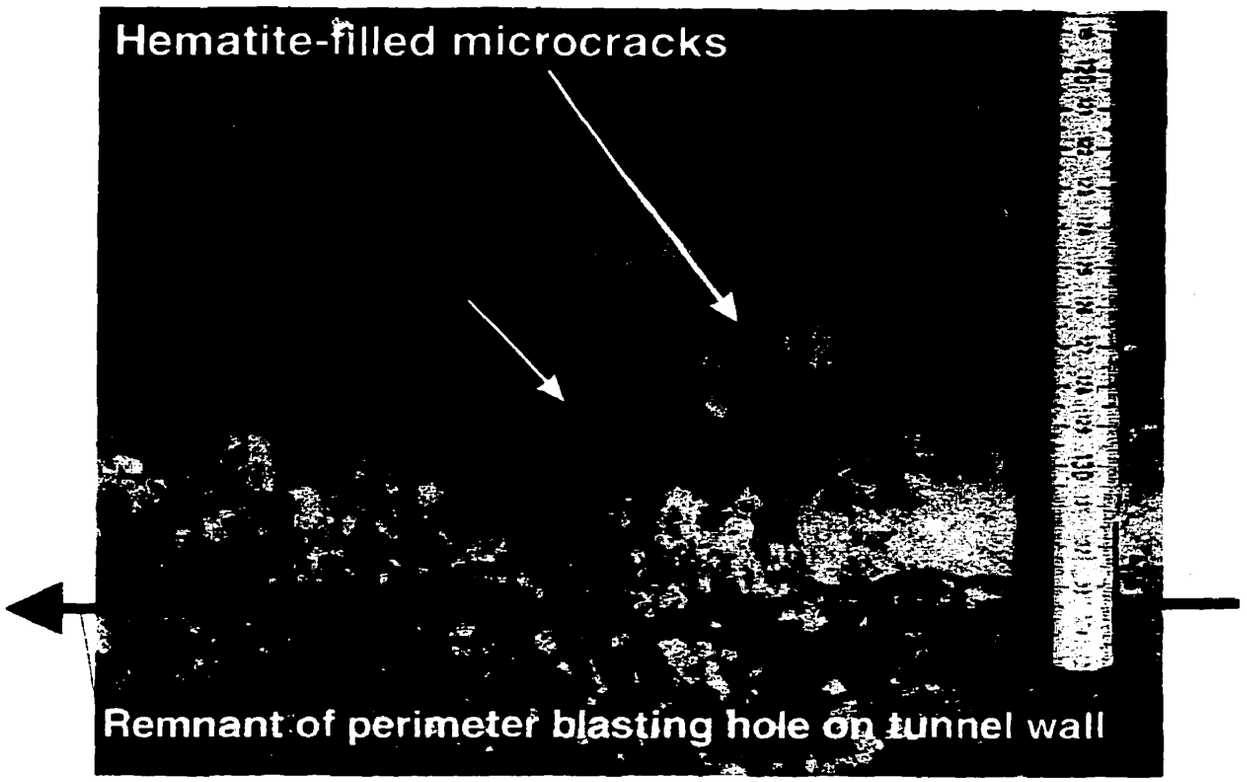

Figure 18. Examples of microcrack varieties as seen in a coarse grained phase of the Lac Du Bonnet Batholith, exposed on a tunnel wall at the 240 Level of the URL. The whitish linear groove running the length of the photograph is the remnant of a percussion-drilled perimeter blasthole as seen on the tunnel wall. The rock immediately adjacent to the hole appears whiter than the rock surrounding it due to abundant blast-induced microfractures. A much larger but related (20 cm long) excavation induced "microfracture" runs parallel to the blasthole. These are easily distinguished from natural microcracks by the presence of mineral infilling or alteration, as in the prominent hematite -stained microcrack in the large microcline crystal near the centre of the photograph.

4.1. Terminology

For the purposes of this report, microfractures are defined as grain scale discontinuities. Their importance lies in their influence on rock mass response, whether in the lab during testing, or in the excavations themselves. Preferred directions of natural microcracking have long been recognized and utilized in the quarrying industry. Two general types of natural microfractures can be distinguished, based on their mode of occurrence. These are listed in Table 10.

It is not uncommon for each of these microfracture types to exist together in any given sample, and each or all may be the result of both ancient and recent processes (Figure 18). Stress relief and blast damage in the proximity of an excavation, drilling, and sample preparation tends to accentuate the fabric-related fractures, but can also lead to the formation of new transgranular or intragranular microfractures (including both types 1 and 2). These induced microfractures, along with any changes to the type 1 microfractures, are considered sample damage.

Ancient or natural microfractures are related to geologic events, including the development of the larger scale faults and fractures, and tend to be penetrative (pervasive or statistically homogeneous) through large portions of the rock volume. As such, they are associated with consistent patterns of rock mass response, such as the rift, grain and hardway described in the dimension stone industry.

In a report on exploration targets for the dimension stone industry in Ontario, Marmont (1993) noted that even the most homogeneous and uniform granites usually possess a

microscopic structure that predisposes them to break more easily in one direction than another. This is usually caused by weak alignment of elongate mineral grains, and/or by sets of pervasive natural microcracks, either intergranular, or transgranular (Richter and Simmons, 1977). The direction along which a granite splits most easily is the rift, the next easiest in the grain, while the direction along which the rock is hardest to split is the hard way. The rift is commonly horizontal or vertical, the grain is usually perpendicular to the rift, and the hard way perpendicular to rift and grain (Marmont, 1993). These directions commonly correlate with batholith structure, with the rift in dome-shaped granite intrusions being parallel to the granite's contact with the enclosing rocks.

Experienced stone workers can see or feel the rift and grain, and plan their quarrying and processing accordingly. Stone cut parallel to the rift will be stronger than stone cut across it. Determining the existence and orientation of these natural anisotropies is considered critical in large architectural panels (Marmont, 1993; Stecich et al., 1992).

Of the natural microfractures types recognized, those developed in quartz are the most widely recognized and studied (Richter and Simmons, 1977). They are thought to have originated during cooling (or heating) in the presence of fluids and a deviatoric stress field (Jang et al., 1989). Their development in an isotropic mineral, their pervasiveness on the hand- specimen- scale, and their tendency to occur as sets related geometrically to the causative stresses, make microfractures in quartz useful fabric elements with which to interpret the stress and fracture history of their host. Their use in determining regional

stress orientations related to specific orogenic events have been described by Jang et al. (1989), and Ren et al. (1989).

The natural microfractures in quartz are also the type most easily distinguished from sample damage. In this study (and in general), natural microfractures were distinguished from induced microfractures by the presence of mineral filling or alteration, or by trains of fluid and mineral inclusions. The predominant filling mineral in the URL samples appears to be hematite, but in most instances the filling and fluid inclusion compositions were not optically determinable. Open (i.e. induced microcracks) were abundant in the URL samples. They were usually curviplanar to conchoidal, transgranular, and had no obvious pattern. The filled microfractures in contrast, were usually intragranular, planar and generally displayed some type of repeating pattern on the thin section scale.

4.2. Scope of Work

This study of natural microfractures in the Lac Du Bonnet granite at the URL was done in three stages to accommodate funding and construction schedules, and included:

1. an initial reconnaissance survey;
2. a more detailed reconnaissance survey,
3. a study of samples from the 420 Level only, to correlate with the samples taken for geomechanical testing.

In stages 1 and 2, the purpose of sampling was to identify the variation in microfracture pattern, with depth and location relative to the major faults and the large-scale fracture domains. Samples were obtained from each of the following structurally-defined blocks

(as shown previously in Figures 18 and 19, Chapter 3), each of which is bound by a thrust fault, and is represented by considerable differences in the number, size and spatial distribution of outcrop-scale fractures).

- Fracture Domain A: (the pervasively fractured rock between the ground surface and extending to the base of the uppermost thrust fault - Fracture Zone 3).
- Fracture Domains B and C: (the moderately to sparsely fractured rock between Fracture Zones 3, 2.5 and 2), and
- Fracture Domain D: the sparsely fractured rock below FZ2.

The results of the three stages of microcrack study are presented in Everitt (2000). The methodology used and an overview of the results are presented in the following sections.

4.3. Sampling

All samples were taken from oriented core, in areas of homogeneous granite away from the low-dipping thrust faults and their alteration halo, and any subvertical fracture zones. Three mutually perpendicular, polished thick sections (100 μm) were made from each specimen, one perpendicular and two parallel to the core axis.

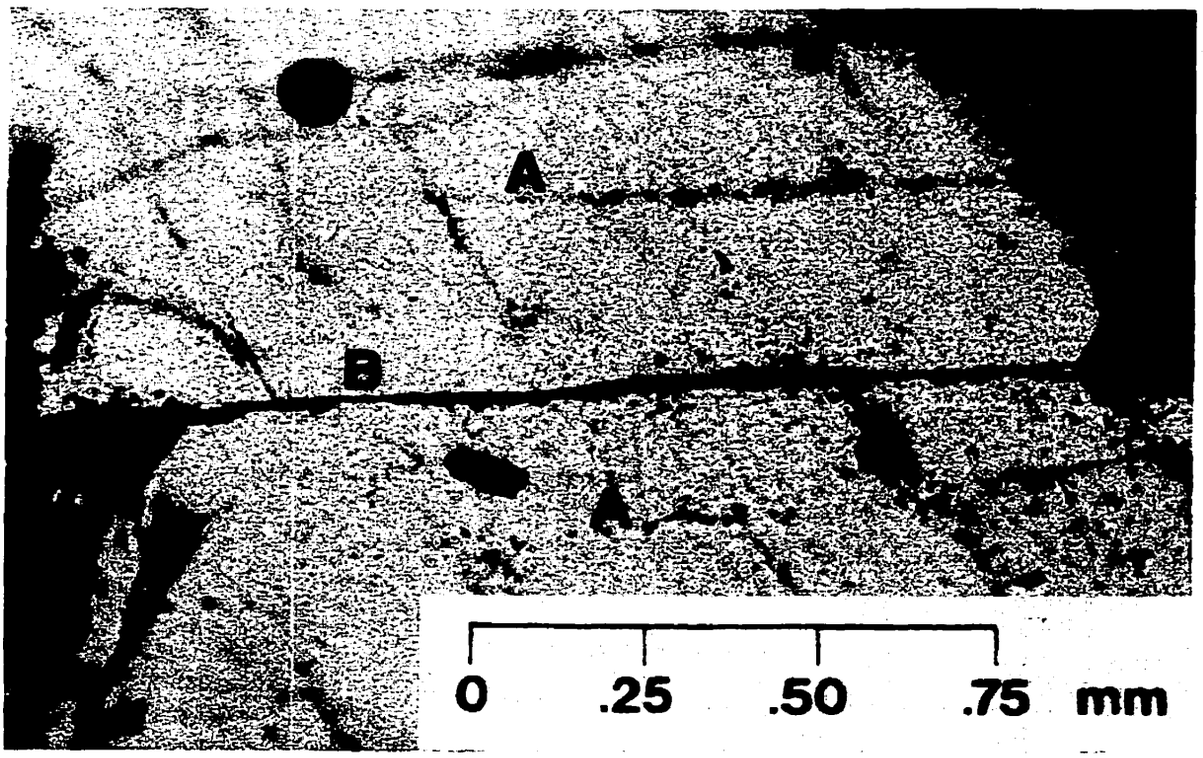

Figure 19. Photomicrograph of a single hematite-filled natural microcrack in quartz. Photograph by C. McGregor. A – Sealed microcrack with fluid and mineral inclusions. B – open microcrack with hematite infilling.

4.4. Natural vs. induced microcracks

Natural microcracks were distinguished from induced microcracks by the presence of mineral filling or alteration, or by trains of fluid and mineral inclusions. A single, hematite filled natural microcrack in quartz is shown in Figure 19. The predominant filling mineral appeared to be hematite, but in most instances the filling and fluid inclusion compositions were not optically determinable.

Open cracks with no visible wall rock alteration or filling were abundant, but were not measured to avoid grouping natural microcracks related to the stress relief history of the

rock, with others probably induced by excavation, drilling or sample preparation. Open (i.e. induced microcracks) were usually curviplanar to conchoidal, transgranular, and had no obvious pattern. The filled microcracks in contrast, were usually planar and generally displayed some type of repeating pattern on the thin section scale.

4.5. Microcrack Distribution

Microfracture homogeneity on the sample-scale was investigated by systematic mapping of three mutually perpendicular thin sections (Figure 20). Photomicrographs, taken at low magnification were used as a base on which were plotted the grain boundaries, and the location and identifying letter of each measured microcrack.

The mapping was undertaken to determine if there was any indication that the pattern of natural microcracks in quartz was spatially and geometrically related to any textural heterogeneity at the specimen-scale (such as a radial pattern around feldspar phenocrysts or xenoliths). No such evidence was found, and it is concluded that the natural microcracks are pervasive, reflecting the site-scale paleo-strain, and not local-scale textural anomalies.

Quartz is typically interstitial and allotriomorphic in all thin sections. Most of the quartz shows undulose extinction (i.e., the crystal lattice of the quartz is strained). If this strain is due to one or more episodes of cooling and/ or tectonic stresses as described by West (1991), it has not been relieved by recrystallization. This undoubtedly contributes to the

strains measured in rock properties testing at the URL, but the relative magnitude of this influence is not known.

Microfractures were present in both strained and unstrained grains at all levels, and crossed the partially recrystallized margins (sub-grain fabric) of some strongly undulose quartz. This superficially resembled transgranular cracking, but the microfractures are limited by the original grain boundaries.

Figure 20. Map of natural microcracks (hematite or fluid inclusion-filled planes) within a sample from the 420 Level.

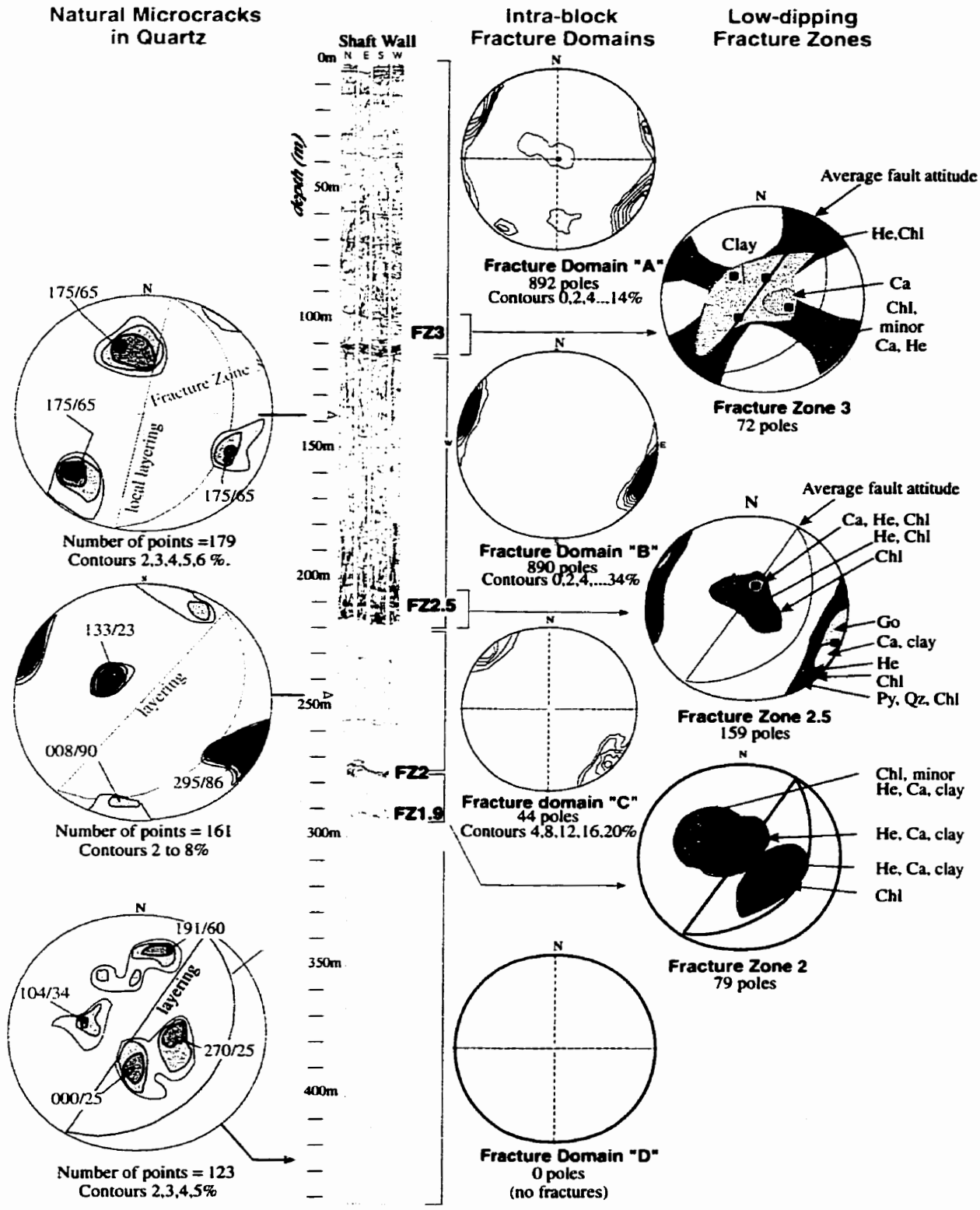

Figure 21. Summary stereographic projections of poles to fracture and microcracks sets from the 130, 240 and 420 Levels. ● - average pole to local fracture set in low-dipping fracture zones. Infilling types: He –hematite, Chl – chlorite, Go – goethite, Ca – carbonate.

4.6. Natural Microcrack Sets

The orientations of the natural microfractures were then determined along with the orientations of quartz c-axes using a 5 - axis Universal stage, mounted on a petrographic microscope, at a magnification of 10x as described by Jang et al.(1989), and Rousell (1981). The relative orientations measured in each section were converted to true orientations, and these were plotted on summary stereographic projections for each sample.

The results of this study indicate that the pattern and domains of microcracking are consistent with the patterns and domains previously defined for the macro-scale fractures at this site (Figure 21). The microcrack sets at each level correlate well with the sets of macro-scale fractures. This includes a well developed microcrack pattern above Fracture Zone 2, and a weak and predominantly low-dipping pattern below (Figure 22).

Microcracks in the samples from the 420 Level are weakly developed. They are predominantly low dipping, and very similar in orientation to the major low-dipping fault zones. Microfractures are more abundant above Fracture Zone 2 (e.g. from the 240 and 130 Levels), with a well defined low dipping set and two subvertical sets.

The low-dipping set in the sample from the 240 Level parallels the average orientation for Fracture Zone 2, as well as the compositional layering, which this fault follows. The low dipping set in the sample from the 130 Level parallels the orientation for Fracture Zone 3 (based on an average taken over a 500 m^2 area), but not the local compositional layering, which deviates here from the regional norm. This is consistent with other URL

surface work, which showed that the low-dipping fracture zones are fabric-controlled where the layering is near the theoretical failure plane, but not where the layering varies substantially in orientation (Brown et al., 1989a).

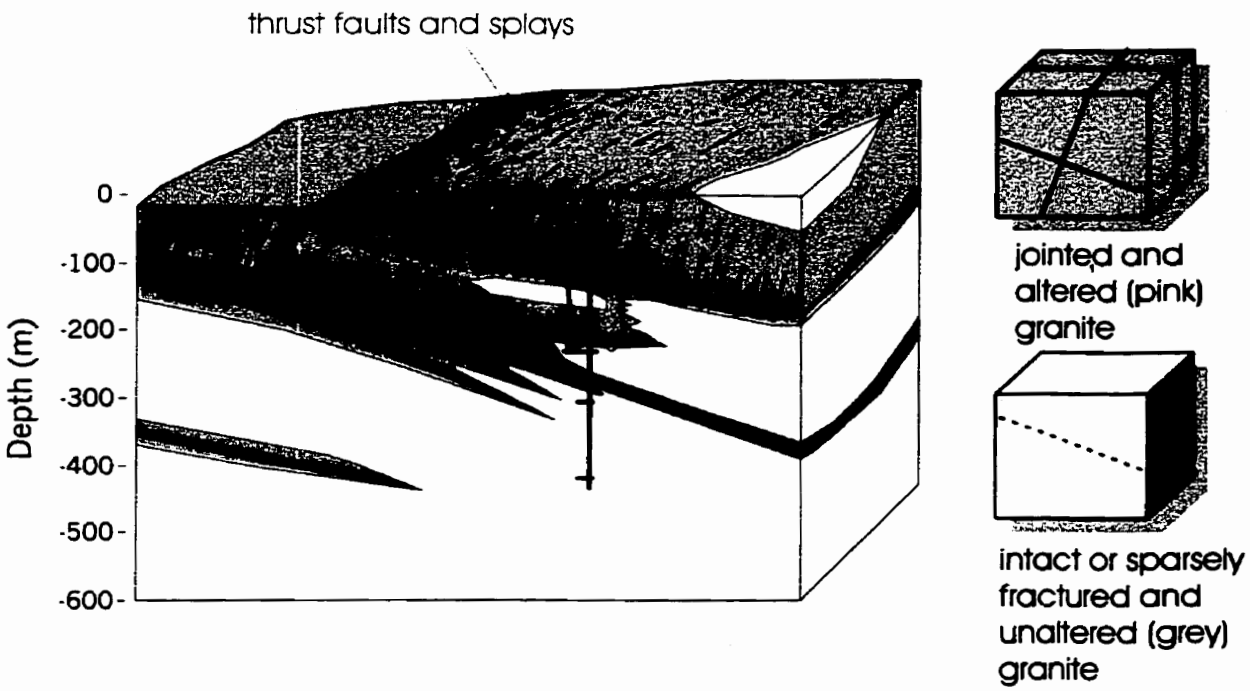

Figure 22. Schematic illustration of the sets of natural microcracks in quartz at the URL.

4.7. Natural Microcrack Length

Average microcrack lengths are dependent on depth from surface and average grain size. A summary of natural microcrack lengths for samples ranging from surface to the 420 Level is shown in Figure 23. Mean crack length decreases noticeably with increasing depth from surface. In the moderately fractured rock above Fracture Zone 2, microcracks equal or exceed the grain size, while in the sparsely fractured rock at and below the 240 Level, the microcracks are usually less than the grain size. Microcrack apertures are also dependent on depth and sample disturbance (stress relief) (Chernis, 1981; 1984).

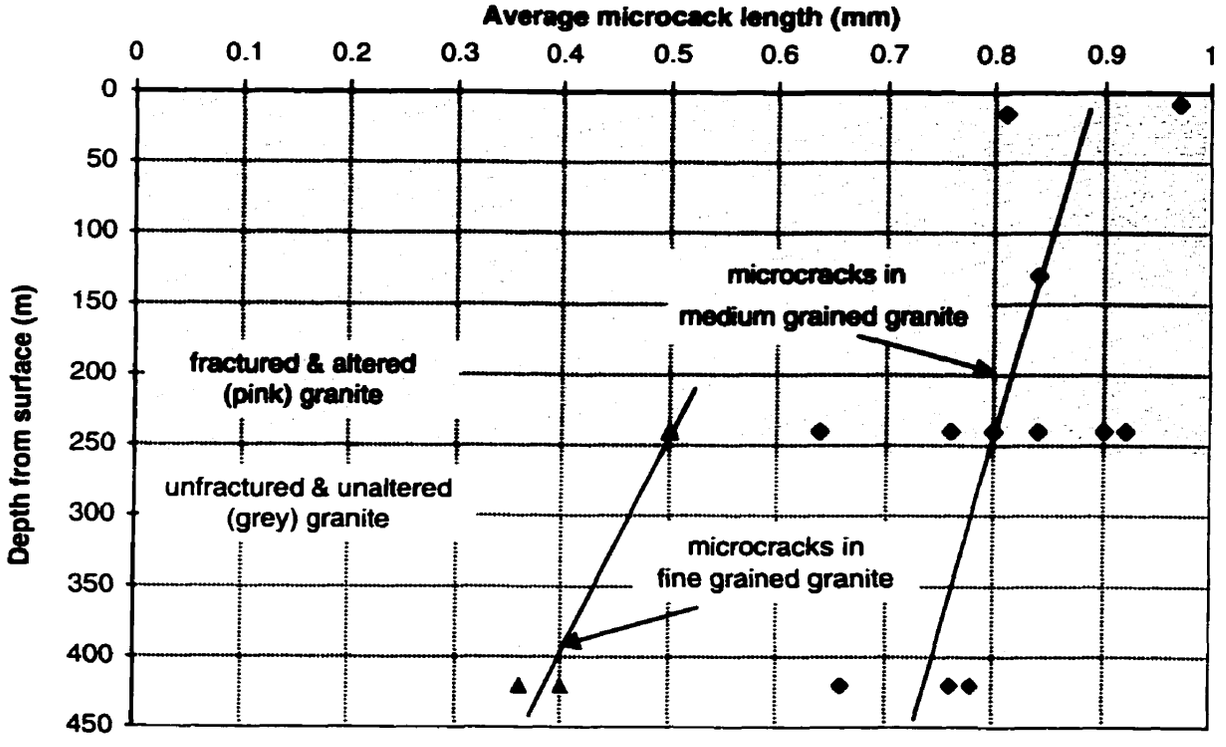

Figure 23. Variation with depth of the average length of natural microfractures in quartz.

4.8. Conclusions of Microfracture Study

There are preferred orientations for the ancient natural microfractures at the URL, which are consistent with the patterns and domains previously defined for the macroscopic-scale fractures at this site. This suggests that the microfracture orientations could have been used to provide estimates of the likely orientations of larger scale fractures, not intersected by boreholes, in the sparsely fractured rock at this site. Changes in the overall geometry of microcracks, such as exists on opposite sides of Fracture Zone 2, indicate the existence of different fracture domains.

Natural microfractures in quartz are pervasive at the sample scale, even in areas of sparsely fractured rock, and as such must be considered in assessing sample response to testing. Correlations between microcrack orientation, sample response to testing, and excavation damage at the tunnel-scale exist, and are described in the following chapters.

Chapter 5

FIELD OBSERVATIONS ON THE INFLUENCE OF GEOLOGY ON FRACTURE DEVELOPMENT

5.1. Evidence of Fabric Control of Natural and Induced Fractures at the URL

The present-day response of an intact rockmass to stress can be gauged by its history of deformation. Fabric control of fractures, for example, is an indication that the rockmass has reacted as an anisotropic medium when previously subjected to brittle deformation. Fabric control refers to the preferential development of fractures, in certain locations and (or) directions, due to the presence of mechanical anisotropy in the rockmass. This anisotropy may be induced by the presence of compositional and textural layering, and by the development of secondary structures such as foliations and lineations. This phenomenon is widely recognized and anticipated in sediments and metamorphic rocks with obvious structure (e.g. Reitan and Murphy, 1983), but is often overlooked in rocks such as granite where the fabric is far more subtle.

The rock mass response in "apparently homogeneous" rocks can be defined thorough a (costly) program of drilling, mechanical testing, and modelling. However, before this is undertaken, physical evidence of a mechanical anisotropy in a rockmass and of its

geometry, can be obtained from an examination of the distribution of the ancient, natural fractures and natural microfractures.

Detailed mapping of the URL excavations, the shaft in particular, and borehole data have clearly indicated that textural and compositional heterogeneities control:

1) the location of large-scale fault zones,
2) the extent, distribution and infilling characteristics of lesser-scale fractures between the fault zones, and
3) the extent and density of excavation-induced fractures (Everitt and Brown, 1986; Everitt et al., 1996).

It has also been demonstrated, in a qualitative manner, that crack initiation and propagation stresses are influenced by rock fabric and grain size. Breakout development for example has been observed to vary in response to textural and structural variations in the granite present at the tunnel- and site-scales (Everitt et al., 1996, and in the sections following). In particular, at compressive stress concentrations the breakout is far more extensive in the coarser grained variants, especially where the foliation coincides with the direction of expected slabbing.

The following sections describe examples where even subtle fabric in the "homogeneous" granite of the LDBB has influenced both natural and excavation-induced fractures at a variety of scales and excavation orientations.

5.2. Fabric Control of Large Subhorizontal Faults

The URL access shafts provide a cross section of the roof zone of the Lac Du Bonnet Batholith, and of a system of low dipping thrust faults and associated splays, each extending more than a kilometre along strike, and spaced in the order of 50 to 200 m apart. Detailed mapping by the author has revealed that:

- these faults follow the large scale compositional layering in the roof zone of the batholith, which in turn is defined by the batholith shape. The similarity between the orientation of the fault, and of the floor of the batholith, is obvious (Figure 24).
- that each of the three faults and lesser splays are confined to the more heterogeneous layers (e.g. as shown in Figure 25, Fracture Zone 2 (a low-dipping thrust fault), has developed within a one to two metre thick "plane" of amphibolitic inclusions and biotitic schlieren. The surrounding granite is more weakly layered or massive, and is not fractured. Site drilling has determined that this fault continues to follow this layer over a kilometre from the shaft, along both the dip and strike directions.

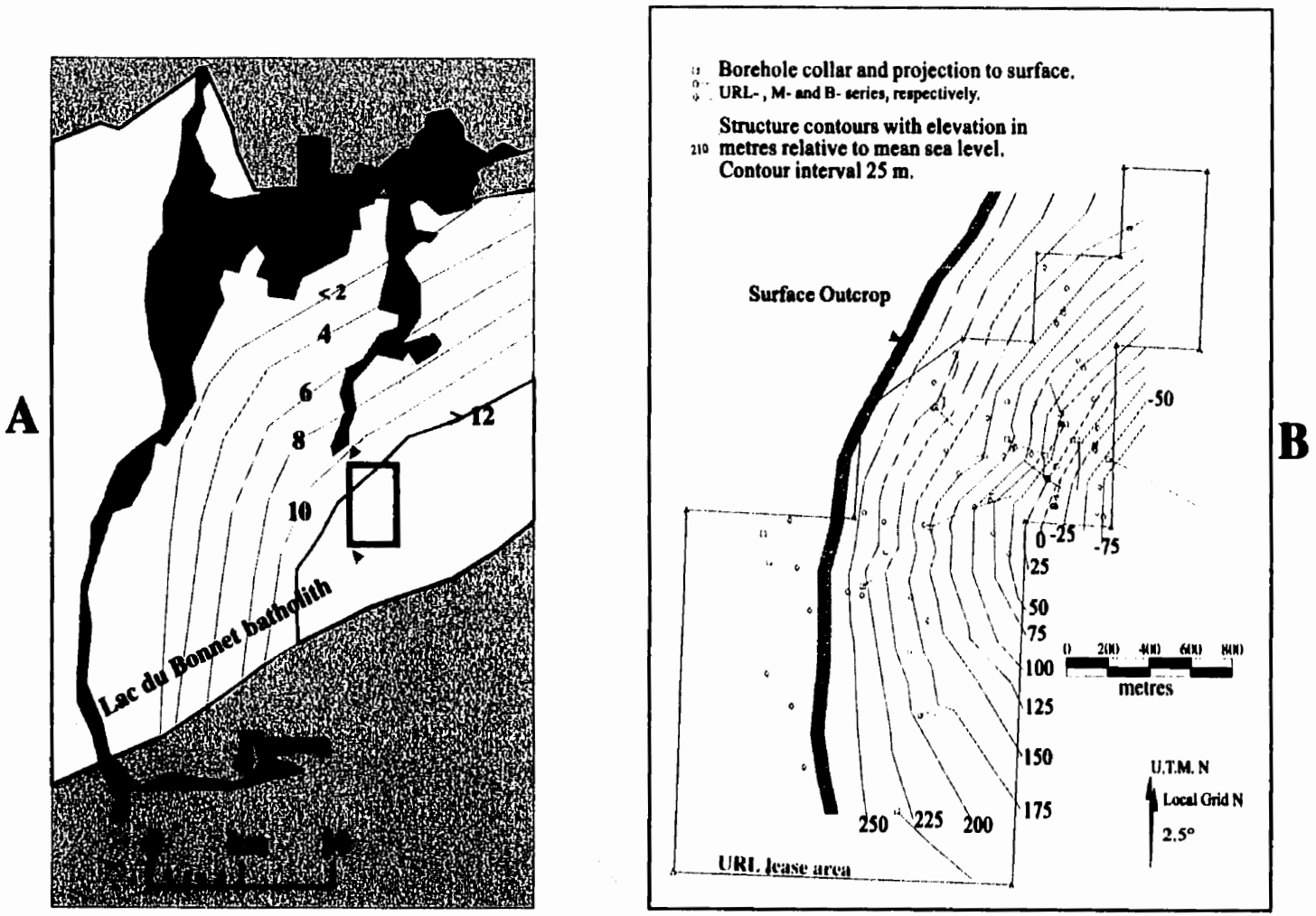

Figure 24. Influence of batholith contacts and internal structure on fault orientation. Structure contours showing the depth (in km) to the base of the Lac du Bonnet Batholith are shown in (A) (as interpreted from profiles appearing in Tomsons et al. (1995) based in turn on gravity and magnetic data). Dekametre-scale layering within the pluton varies locally in orientation, but is broadly parallel to the lower contact. The low-dipping fault zones (e.g. Fracture Zone 2) are controlled in location and orientation by the layering. Structure contours on the lower contact of Fracture Zone 2 are shown in B.

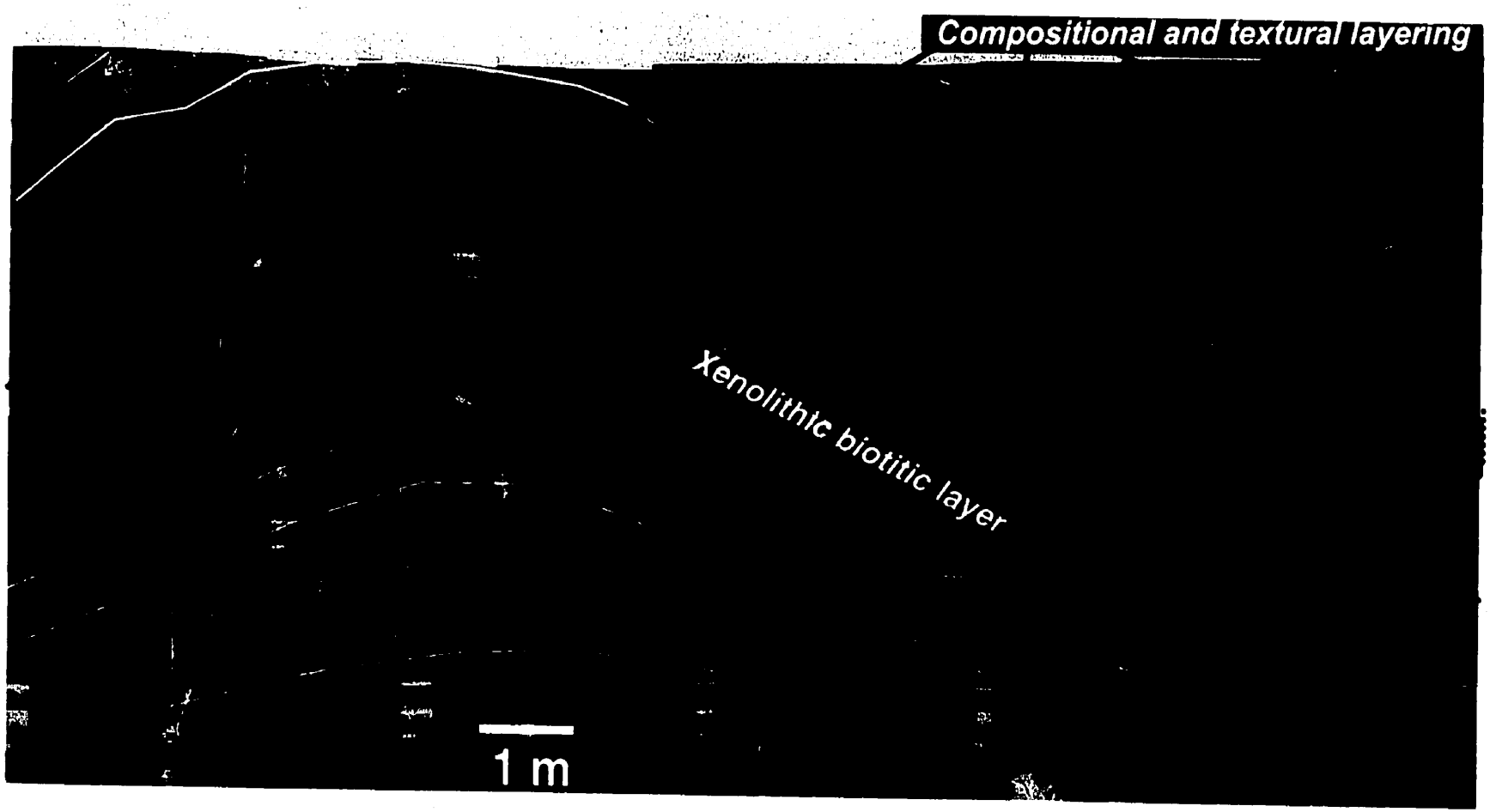

Figure 25. Fracture Zone 2 as seen in the URL shaft. An example of fabric control of fracture orientation and location on the dekametre-scale. This photomosaic presents an unrolled 360° view of the walls of the access shaft over a vertical distance of about 8 m. The squares of the metal grid visible at the bottom of the mosaic are each 40 by 40 cm. The apparent sinusoidal trace of the fault is an artifact formed by the intersection of a plane (the fault) with an unrolled cylinder (the shaft wall).

5.3. Fabric Control of Subvertical Natural Joints

The rockmass between the fault zones is host to one or more sets of subvertical fractures, the pattern and frequency of which is affected by variations in the room-scale fabric. This influence is summarized in Figure 26, with the horizontal axis representing the full range of fabric variations, and the vertical axis representing the frequency of several classes of natural fractures (faults and joints) for each of the ten fabric types. The frequency curves are based on a continuous 240-m long scan-line down the URL upper vent raise. It is apparent that fractures, both subvertical and subhorizontal, are most frequent where the granite is mostly strongly layered. This situation is analogous to the situation in sedimentary strata, where frequency for a given lithology varies in a direct linear relationship with bed thickness (Price and Cosgrove, 1994).

Fracture frequency and extent are also affected by local heterogeneities. As shown in Figure 27, natural hematite -filled microfractures have been preferentially developed within a zone of very coarse microcline crystals. At any given depth and distance from faults, the subvertical fractures at the URL are generally more frequent in structural / textural variants of the host granite, such as the aplitic, granitic and pegmatitic dykes or sills (e.g. Figure 28). Apart from grain size and homogeneity of grain size, these rock units differ from the surrounding host granite in that they contain a variety of internal contacts, schlieren, vein-filled fractures, and foliations. As will be discussed in this work, these structures contribute to strength anisotropy, and promote the formation of both natural and excavation-induced fractures.

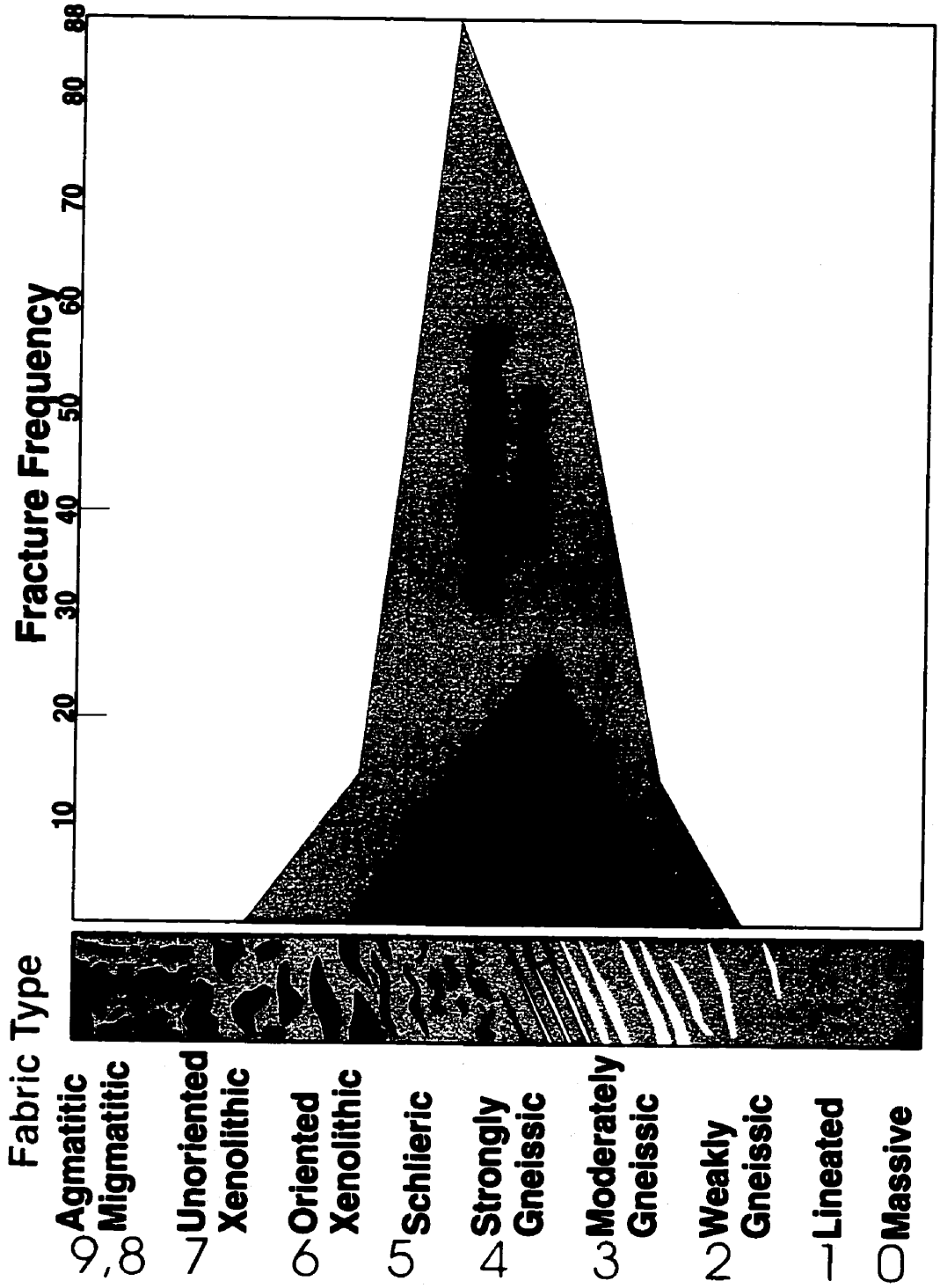

Figure 26. The Influence of Rock Fabric on Natural Fractures in the Lac du Bonnet Granite. Histogram depicting the frequency of several classes of natural fractures (faults and joints) as a function of the dekametre-scale fabric of the Lac du Bonnet Batholith. Variation in fracture frequency with granite fabric type, based on data from a 240-m scan-line down the URL upper vent raise.

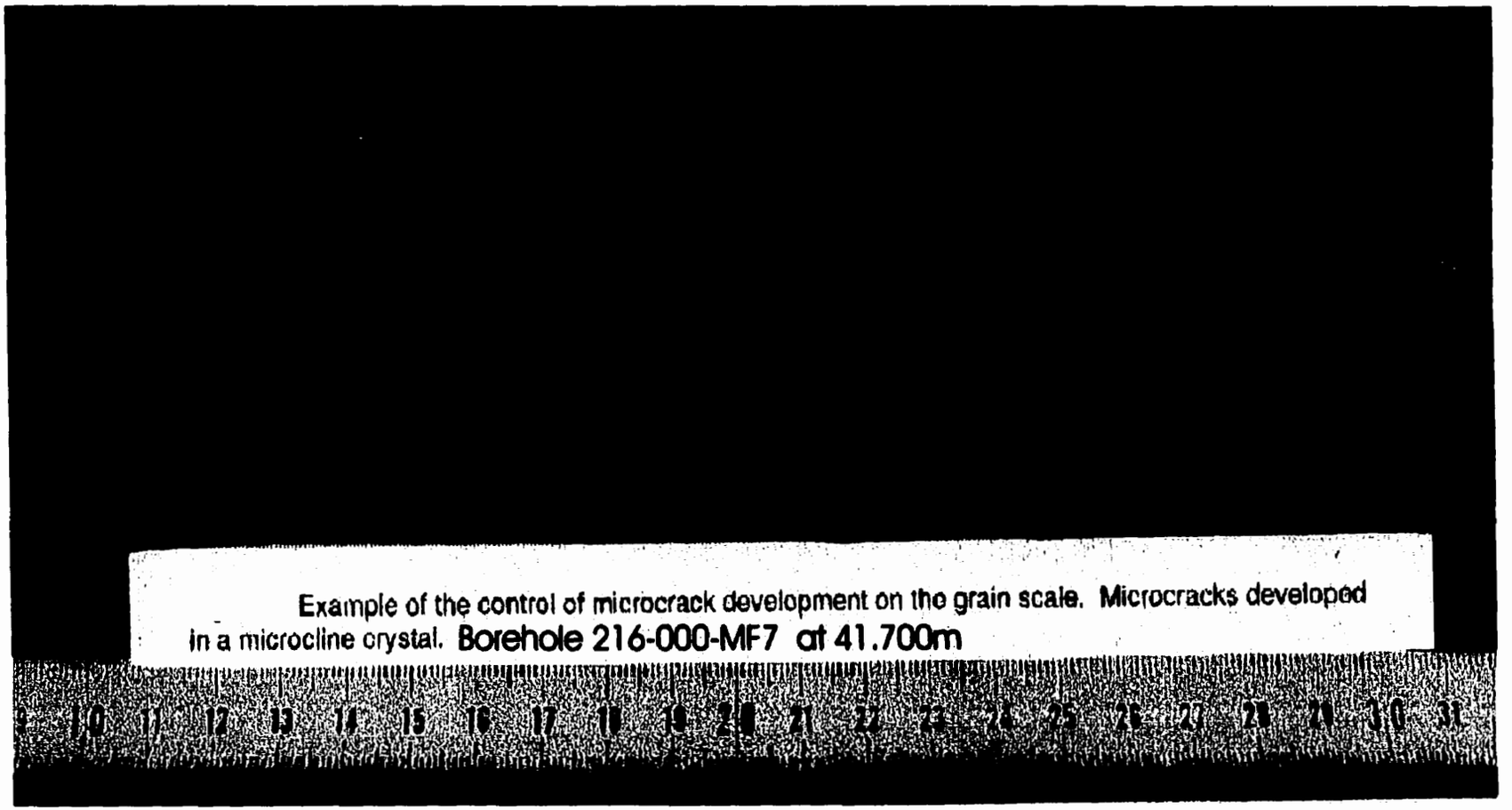

Figure 27. The Influence of Rock Fabric on Natural Fractures in the Lac du Bonnet Granite - An example of fabric control of fracture orientation and location on the grain scale - natural microcracks developed in a zone of coarse microcline crystals.

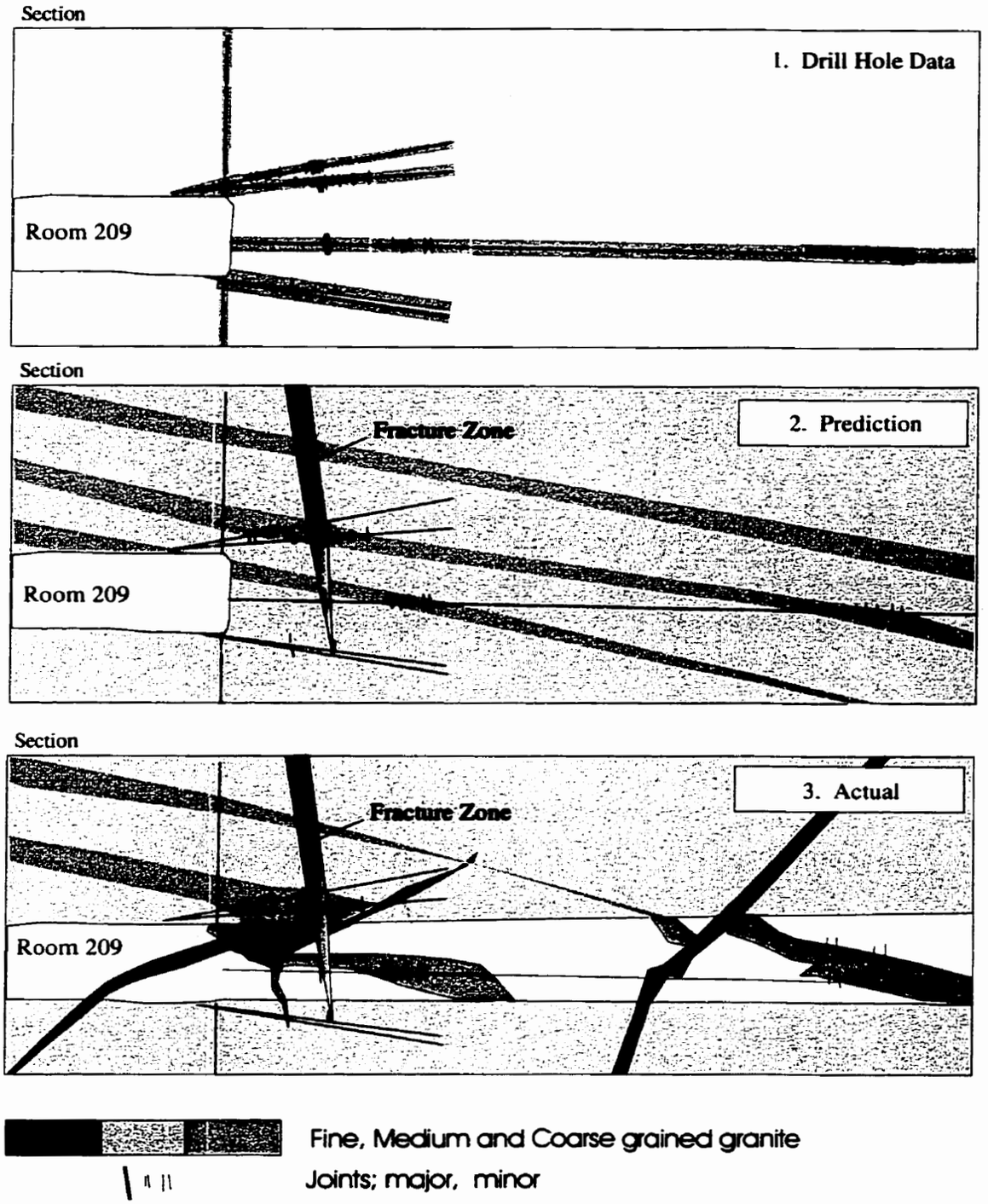

Figure 28. Control of fracture location and extent due to variations in granite at the 240 Level. Fractures are most frequent in the coarse grained granite sills, and in the fine grained granite dyke, while the main phase medium grained granite is largely unfractured. Note: these are all phases of the Lac du Bonnet Batholith, and not separate unrelated rock units.

5.4. Fabric Control of Excavation - Induced Fractures

Mapping of the shafts and the various tunnels at the 240 Level indicated that excavation-induced fractures were far more numerous than natural fractures except within the fault zones. In the shaft below Fracture Zone 2, in most of the 240 Level, and in all of the 420 Level, natural fractures (e.g. shear zones and joints, whether open or sealed) are absent, and the only fractures present are those induced by excavation. This result, based on mapping, is supported by the detailed logging of several kilometres of boreholes. An 1100 m long steeply-dipping borehole collared at the 420 Level intersected only one fracture (Everitt and Woodcock, 1999).

Excavation-induced fractures are distinguished from natural fractures by the absence of mineral infilling or wall rock alteration, by their position and geometry relative to blasthole remnants, and by their position and geometry relative to the tunnel profiles or tunnel face. In general, they form an onion-skin pattern of surfaces, similar to the exfoliation fractures seen in surface outcrops, but in the subsurface their orientation and size is dependent on their location relative to the tunnel perimeter, and to the location of tunnel faces during excavation.

Evidence that rock structure was contributing to excavation damage development was first obtained during routine mapping of tunnels during the construction of the 240 Level (Everitt and Read, 1989), and was confirmed by subsequent observations during: 1) the extension of the URL shaft (Everitt and Passmore, 1993; Everitt et al., 1993), and 2) during level development at the 420 Level (Everitt et al., 1993). Damage development has been observed to vary in response to textural and structural variations in the granite in

both the vertical and horizontal planes (Everitt et al., 1996). In particular, at compressive stress concentrations damage is far more extensive where the foliation coincides with the direction of expected slabbing.

In areas where the rock fabric is truly massive (i.e., homogeneous, as in the strict sense of this term), or where the fabric is normal to the excavation axis, the geometry of the excavation damage tends to be symmetrical about the tunnel or shaft profile. This symmetry tends to be lost however; in areas where the excavation axis runs along the "grain" in the rock. This is demonstrated in the following examples from the tunnels at the 240 and 420 Levels, and from the shaft at the 300 Level.

5.5. Fabric Control of Excavation - Induced Fractures in Horizontal Tunnels at the 240 Level

The tunnels at the 240 Level demonstrate the influence of subtle fabric on excavation damage development (Figure 29). The axis of tunnel (Room) 207 is parallel to the maximum principal stress and to the strike of the gneissosity, while Room 209 is oriented perpendicular to them. The tunnel profile of Room 207 is asymmetric, with induced fractures paralleling the gneissosity being not only more frequent, but also larger than those in other directions. In Room 209, the layering is not favourably oriented to serve as exfoliation planes, and - the damage profile is symmetrical. In this example, it is also noteworthy that the greatest damage developed not in the tunnel subject to the higher stresses, but in the tunnel subject to the lower stresses. Clearly, while the damage is initiated by stress release about the tunnel profile, the geometry and extent of this damage is very dependent upon the presence of the low-dipping layering.

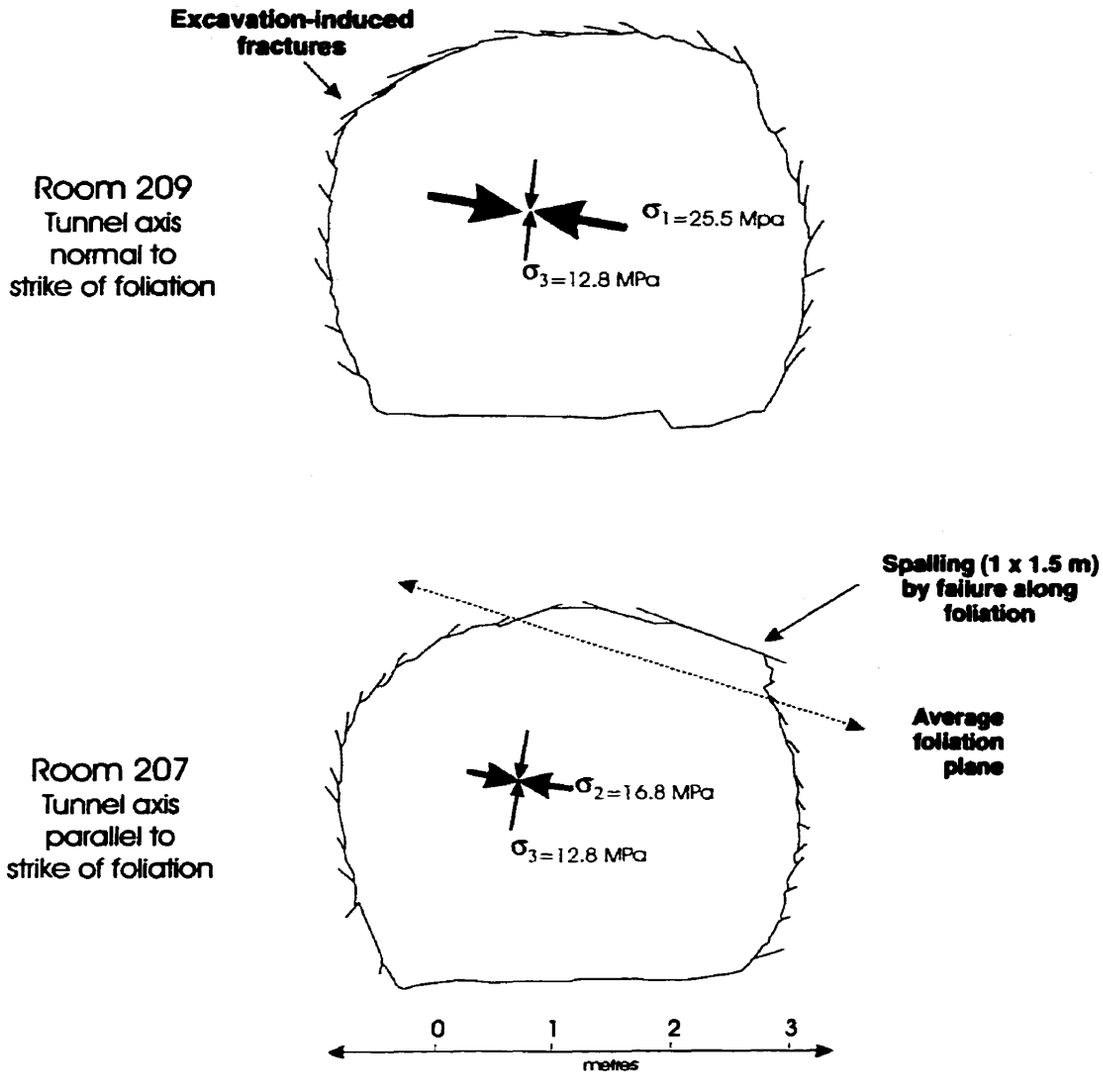

Figure 29. Influence of rock fabric on excavation damage - example from the 240 Level. This figure depicts the damage associated with different tunnel orientations in the same rock type – a medium grained granite. While apparently massive in hand specimen, more careful inspection reveals that the granite possesses both a weak mineral alignment (foliation) and a decimetre-scale layering. These apparently weak structures nevertheless impart a mechanical anisotropy to the rockmass, which is evident in the differences in excavation damage between these two profiles. The tunnel profile of Room 207 is asymmetric, with induced fractures paralleling the gneissosity being not only more frequent, but also larger than those in other directions, with spalling developing in the upper right corner (also shown in Figure 30). In Room 209, the layering is not favourably oriented to serve as exfoliation planes, and - the damage profile is symmetrical.

The excavation damage is also influenced by other fabric elements present. In addition to the layering and foliation shown in the medium grained granite, it is also host to steeply dipping fine-grained granite dykes. Where present, these inhibit the spalling developed in the tunnels parallel to the foliation (Room 207 of Figure 29), as is shown in Figure 30. As will be shown in the section 5.6 following, similar rock type-dependent damage relationships exist at the 420 Level (e.g. cf. Figure 30 with Figure 32) where the development of a breakout notch in the medium grained granite, is arrested wherever the fine grained granite occurs.

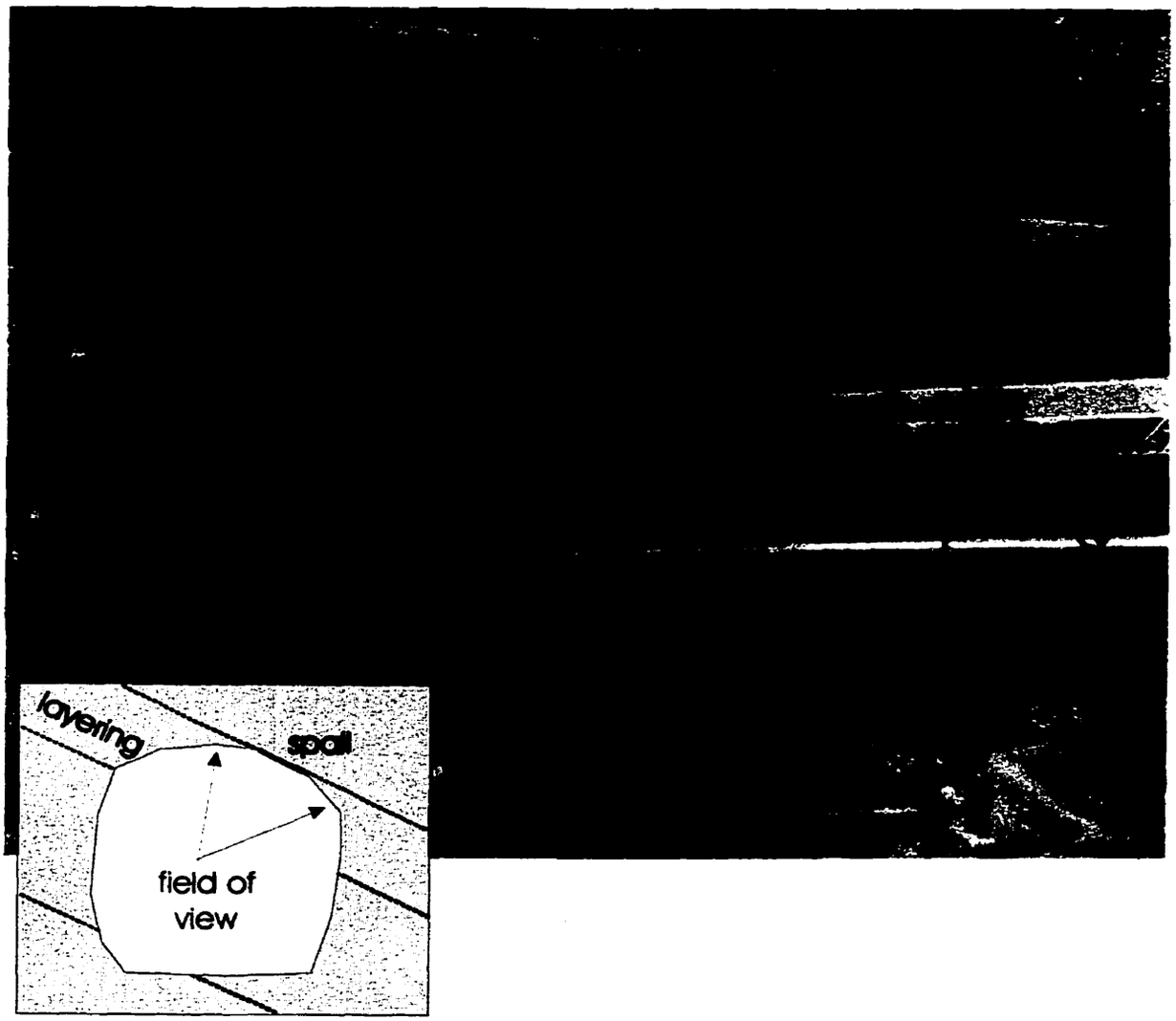

Figure 30. Influence of Rock Fabric on Excavation Damage - example from the 240 Level. This photograph shows the surface of the large spall formed by separation along the plane of layering and parallel biotite alignment in the granite in Room 207 (shown in Figure 29). The inset shows the field of view and the relationship between the tunnel profile, layering and the spall. This type of damage is not present in the tunnels, which are normal, or near normal to the strike of the layering. Spalling along the layering is arrested wherever the layering is absent or recrystallized - as in this case – by intrusion of fine grained granite dykes on the right and left sides of the field of view.

5.6. Fabric Control of Excavation - Induced Fractures in Horizontal Tunnels at the 420 Level

Excavation damage characteristic of the 420 Level is shown in Figure 31, and includes:

1. Stress-induced subhorizontal fractures which have propagated from pilot boreholes, along the plane of gneissosity, prior to excavation,
2. Excavation induced fractures of uncertain origin (i.e. blasting and/ or stress redistribution) on the tunnel surface, and
3. Breakout notches in the crown and floor of the tunnel. These notches comprise; (1) a broad zone where the reaming hole half barrels have spalled off, and (2), a central "V shaped" crush zone where the rock disintegrates into slabs and chips by a process of grain-scale fracturing.

The stress-induced subhorizontal fractures that have propagated from pilot boreholes or bootleg remnants (damage types 1 and 2 in Figure 31) can be large and pervasive at the scale of a tunnel face. In the medium and coarse grained granites, they are clearly developed along the plane of gneissosity, but they also occur in the fine grained granite, where they are discordant to the steeply-dipping flow banding, but parallel to the preferred orientation of natural microcracks at this level (as noted in the preceding chapter, and in Chapter 7, Figure 52). The subhorizontal induced fractures are interpreted as propagating from stress concentrations such as boreholes, their orientation controlled by the ambient stress field (i.e. normal to σ_3), with their development aided by the presence by of favourably oriented foliations and natural microcracks.

The rate of development, location and extent of the breakout notches (damage type 4 in Figure 31) appears to result from a combination of factors, including the sequence of excavation, the angularities in the room geometry, and the variations in local geology. In

excavation, the angularities in the room geometry, and the variations in local geology. In particular, at compressive stress concentrations the breakout is far more extensive where the foliation coincides with the direction of expected slabbing. Subsequent extensional failure (buckling) and spalling along these surfaces led to the development of breakout notches in the crown and floor. Where the layering was reoriented or absent (due to the presence of either fine grained dykes or xenoliths), notch development was much slower to develop (time-dependent, with time varying by rock type), and reduced in size.

The influence of geology on excavation response is illustrated using two examples from the 420 Level. In the first example, (Figure 32) excavation was by carefully controlled line-drilling and mechanical excavation – blasting was avoided so the purely stress—related effects of excavation could be assessed. Damage was allowed to progress to a stable state by careful scaling and limited (temporary) screening. In the second example (Figure 33), excavation was by conventional drill-and-blast methods. The tunnels are parallel to each other, approximately 50 m apart, with the same geology and stress environment. The tunnel axes parallel σ_2 at this level, with their transverse sections in the σ_1 σ_3 plane. In both examples, the tunnels were designed with circular cross-sections.

In both examples, spalling and notch development began almost immediately in areas of medium to coarse grained granite, and progressed rapidly (within a week) to their final form. The rate of notch development in the fine grained granite was much slower, regardless of excavation method, and in some areas never developed at all. For the area within the medium grained granite (in Figure 32), the ceiling and floor notches kept pace

development fell one or more rounds behind the advancing face and was much reduced in depth.

It should be noted however, that all the previous examples were conducted in areas where the tunnel axis was normal to the subvertical foliation in the fine grained granite. In this orientation, the presence of the foliation does not influence breakout development. This situation changes in those few tunnels where the tunnel axis is parallel to the strike of the foliation. As shown in Figure 35, spalling is now preferentially develop along this structure. As will be described in the following section, a similar damage / fabric relationships was observed in the 300 Level shaft and station, with damage being most prevalent in the "generally stronger" fine grained granite.

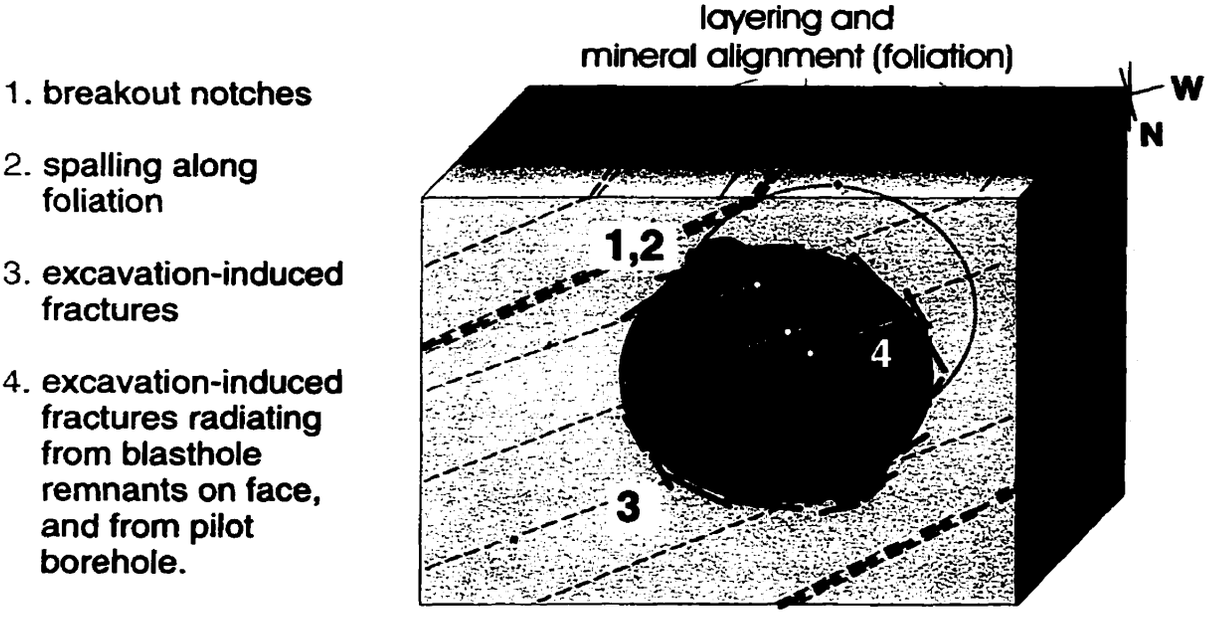

Figure 31. Influence of rock fabric on Excavation Damage - example from the 420 Level.

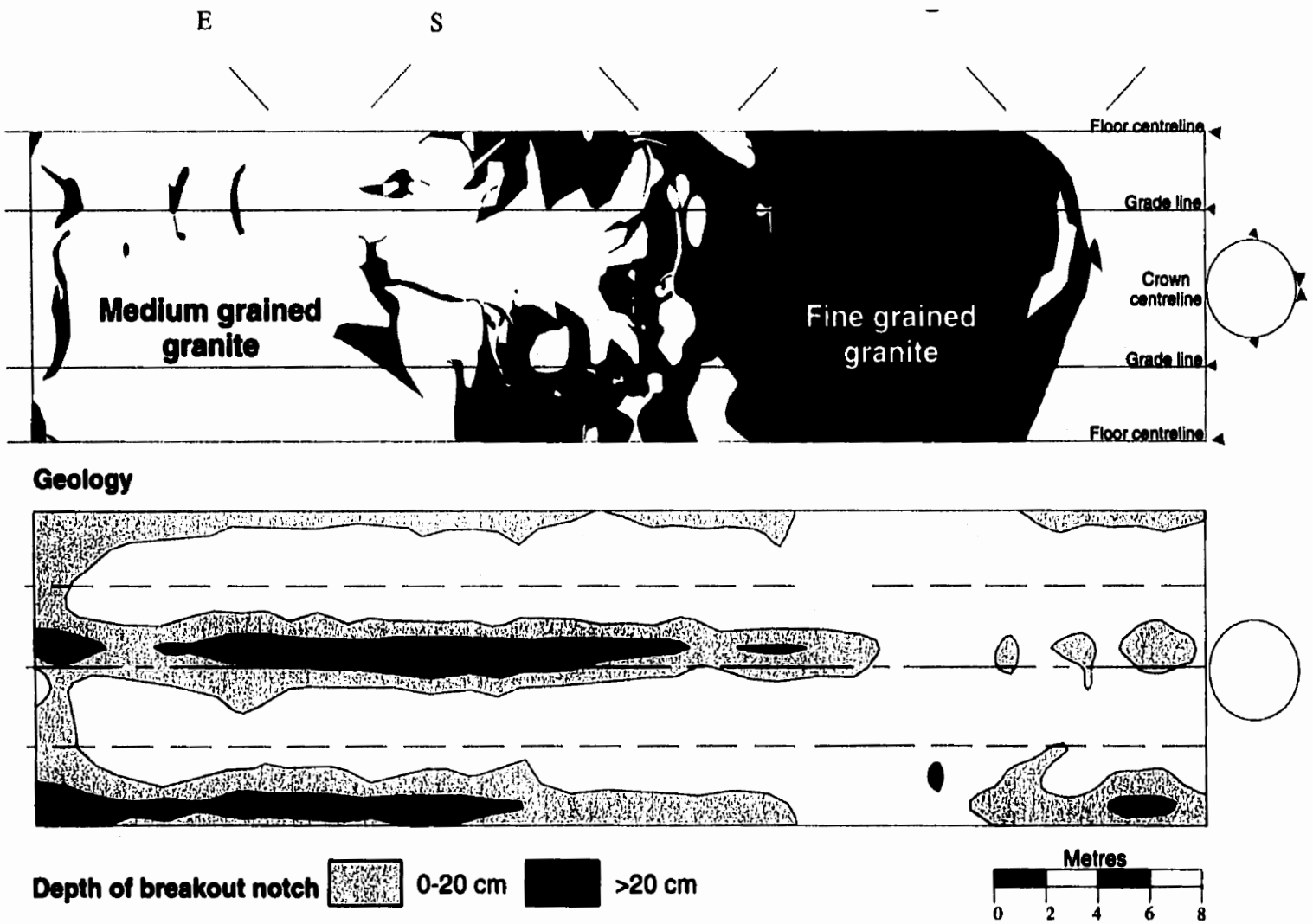

Figure 32. Influence of geology on breakout development within a single line-drilled tunnel (the Mine-by Experiment). Room 415 at the 420 Level of the URL provides an example of the influence of subtle differences in geology on breakout development in granite. The geology, notch depth and construction are shown.

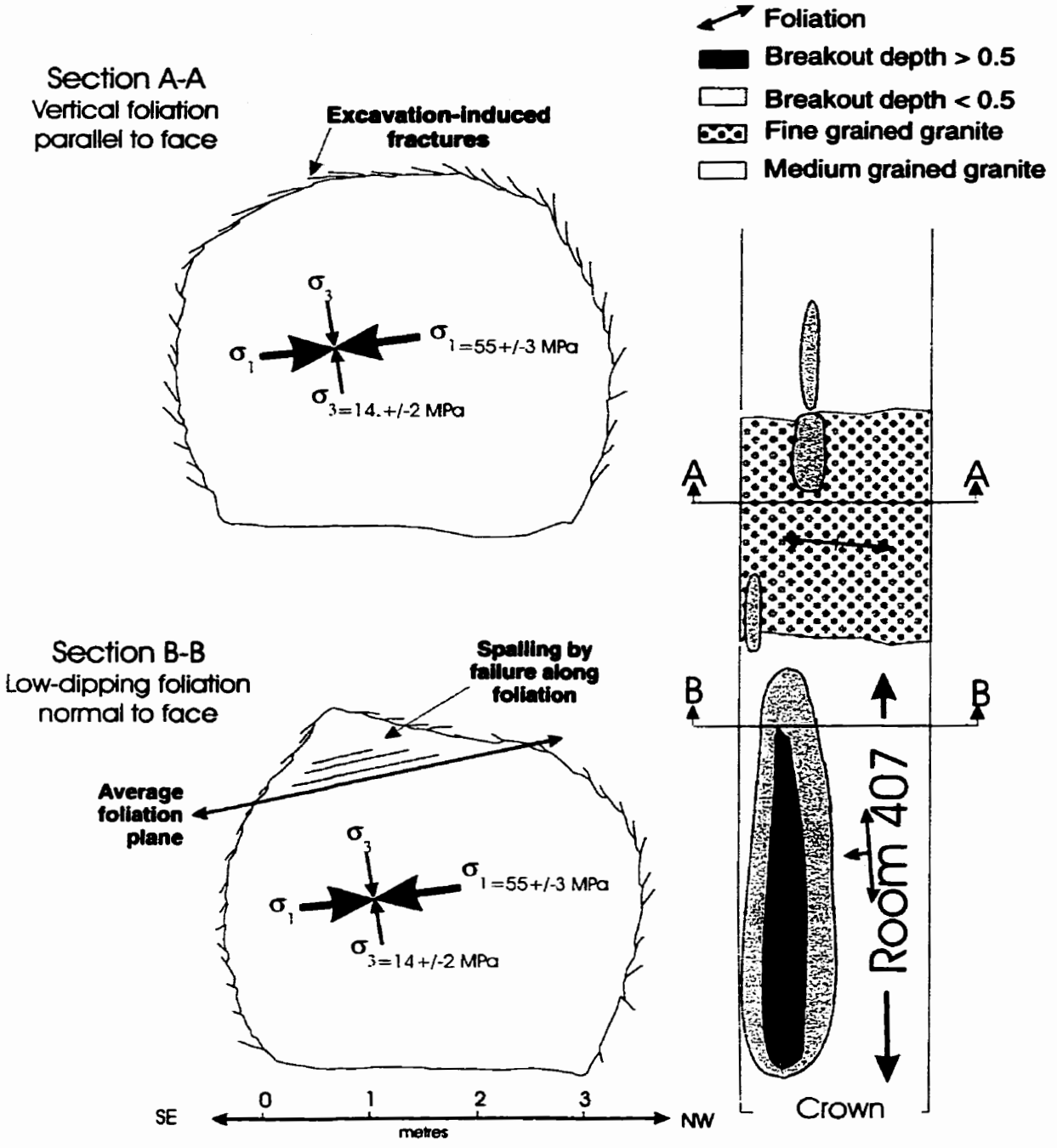

Figure 33. Influence of geology on breakout development within a single drill-and-blast tunnel. Room 407 at the 420 Level of the URL provides an example of the influence of subtle differences in geology on breakout development in granite where conventional excavation is used. The tunnel profiles developed in the fine grained and medium grained granites are shown in A and B, respectively.

Figure 34. Influence of geology on breakout development within a single drill-and-blast tunnel. Room 421 at the 420 Level of the URL provides an example of the influence of subtle differences in geology on breakout development in the fine grained granite where conventional excavation is used. In the previous figure it was noted that a biotite foliation also exists in the fine grained granite, but it is subvertical and normal to the tunnel axis. As such, its presence does not influence breakout development for this excavation orientation and geometry". In Room 421 however, the tunnel axis is parallel to the strike of the foliation, and spalling now occurs along this structure. A similar situation occurred in the shaft at the 300 Level, with spalling developed along this foliation where it paralleled the shaft wall (see Figure 35 and section 5.7 following).

5.7. Fabric Control of Excavation - Induced Fractures about the Vertical Shaft at the 300 Level

The 300 Level Shaft Station (Figure 35) is located in unfractured grey granite below Fracture Zone 2. The grey granite here is cut by three generations of auto-intrusive dykes, the most noteworthy of which, a granodiorite swarm, is the predominant lithology at this stop. The host phase of the batholith is represented by angular inclusions of granite and by variously disrupted blocks between the dykes.

Special efforts were made during the excavation of the 300 Level Shaft Station to optimize the amount and quality of exposure available in order to characterize the damage zone around the circular access shaft. Prior to construction of the 300 Level Shaft Station, the shaft was excavated to a depth of about 15 m, or 3 shaft diameters below the floor of the station to accommodate any time-dependent behaviour in the formation and propagation of the excavation damage, and to avoid the effect of stress concentration. The 300 Level Shaft Station access station was then excavated using controlled pilot and slash techniques for the walls, floor, and crown. This was done to duplicate the quality of excavation characteristic of the shaft, and to avoid inadvertent excavation of damaged rock. Two surfaces were then made available for observation of the excavation damage zone about the shaft perimeter. These were: 1) a temporary 90° brow formed by the intersection of the shaft walls, 2) the station crown (once photographed, this was trimmed to a more stable 45° slope), and 3) the station floor. A third area, referred to as the station lip and lip pocket, provided a sample of the damage zone beneath the floor of the station as seen from the shaft walls.

The results of the excavation damage zone mapping are shown in Figure 35. Although it may be possible to distinguish in outcrop certain specific fractures that originated either through excavation-induced stress or through blasting (chiefly on the basis of location and pattern), most fractures are likely to be the result of a combination of processes.

Damage distribution may be correlated with rock fabric and with the principal stress orientations. In Figure 35, note the preferential development of induced fractures in the fine grained granite, on the east side of the shaft. As was the situation in Figure 34, the fine grained granite contains a subvertical foliation which, where parallel to the excavation surface, facilitates spalling. This does not occur in the medium grained granite, where the foliation is subhorizontal and therefore not favourably oriented with respect to the local stresses to induce spalling.

Clearly, while the damage is initiated by stress release about the shaft profile, the geometry and extent of this damage is again, very dependent upon the presence of a suitably oriented fabric such as layering or foliation.

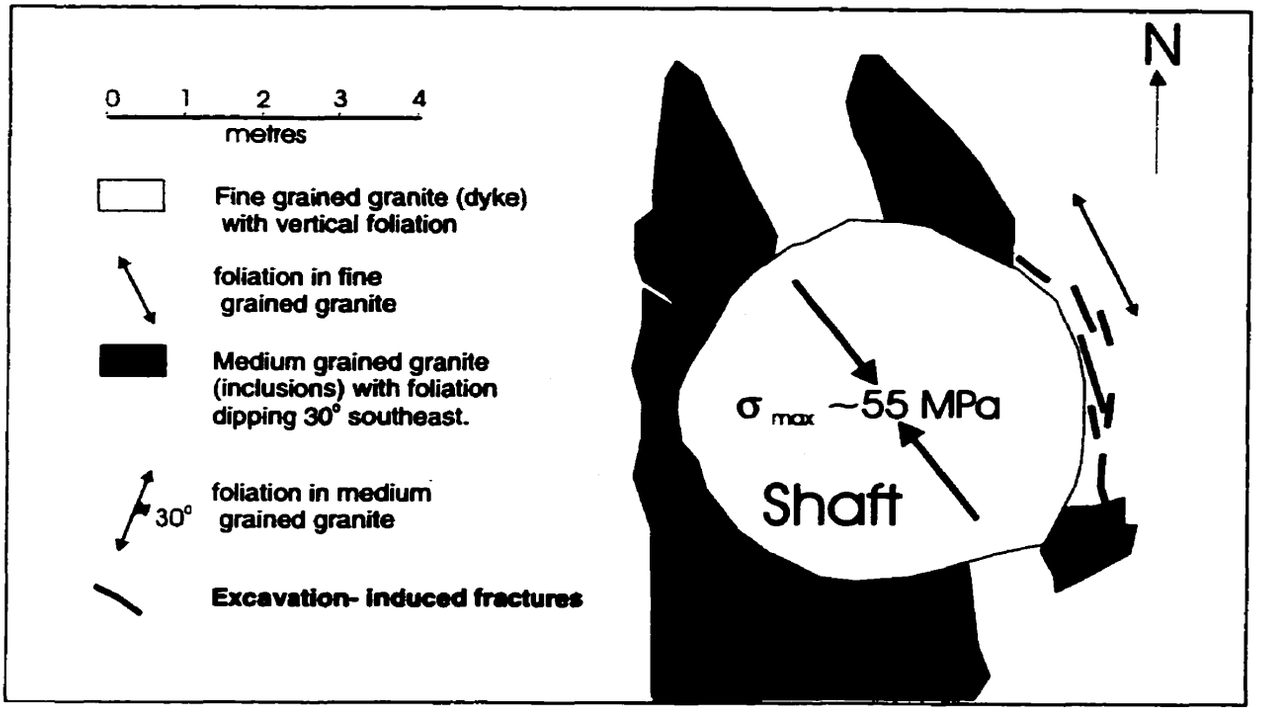

Figure 35. Simplified geological map showing the excavation damage at the 300 Level station.

5.8. Conclusion of Field Investigations into Fabric Control of Excavation - Induced Fractures

Within the allegedly homogeneous Lac du Bonnet Batholith, there is ample evidence at all scales, that even subtle variations in rock type, and in the degree and orientation of foliations and other fabrics have clearly influenced subsequent brittle deformation, whether this was natural or induced by excavations. This influence is present in excavations with vertical or horizontal axes, and in tunnels excavated by different methods. At compressive stress concentrations around excavations, breakout is far more extensive where the foliation coincides with the direction of expected slabbing. Rock fabric and its influence on rock strength are therefore significant to the testing and interpretation of rock mass response, and to experiment and excavation design.

Chapter 6

SAMPLE COLLECTION FOR ROCK PROPERTIES TESTING

Three locations (sample areas) were chosen to further examine the interaction between rock fabric and excavation damage, through the collection of a suite of samples for rock properties testing. The three locations selected provide a representative sample of the range of the compositional and textural heterogeneity present in the Lac du Bonnet granite, and their affect on rock strength and rock mass response. These are:

1. a fine grained granite dyke with subvertical flow banding,
2. a medium grained and weakly to moderately layered granite forming the main mass of the batholith, and
3. a generally coarse grained and leucocratic unit that occurs as sills and recrystallized zones in the main phase.

For the sake of convenience, these are referred to as the fine, medium and coarse grained granites, respectively.

The three case studies were sited in newly excavated tunnels at the 420 Level (420 m depth of the URL) where the damage due to stress relief can be observed in the process of developing. The sites are in close proximity to each other. They are distant from faults or major fractures, and are in the same in-situ stress-domain. As such, they are subject to the same stress magnitudes and orientations.

The general location of the 420 Level, and the names of the various horizontal tunnels and inclined ramps referred to in this text are shown in Figure 36. The location of the samples, and the local geology at each sample location are shown in Figures 37, 38 and 39.

At each site, oriented core has been obtained from an array of boreholes. The arrays were designed to intersect the most prominent foliation / microcrack set at 90°, and then at 20°-30° increments until the core axis was parallel to the foliation (as noted earlier in Table 5 and 6, p. 24 and p. 27). The core was logged for foliations and microcracks, and then cut to provide oriented samples for uniaxial compression tests. Strength anisotropy and the influence of foliation were then systematically investigated using rock mechanics tests that are sensitive to planar anisotropy (Point Load and Brazilian tests).

6.1. Coarse Grained Granite

The geology, tunnel profile, excavation damage, and sampling array at the coarse grained granite study location in Room 418 is shown in Figure 40. This tunnel (Room 418) trends 055°, plunges at 15% (06°), and is parallel to σ_2. The tunnel section is oval, with

its major axis rotated 11° from horizontal to align with the σ_1 direction. The rockmass here contains a variety of pervasive and non-pervasive foliations including decimetre to dekametre-scale layering, and a parallel mineral foliation (chiefly biotite). These are deformed or crosscut by boudinage structure and ductile faults, and by fine grained granite dykes, semi-ductile faults, and mineral alignments. Spalling along compositional layering and biotitic schlieren, was well developed in the area of the floor and crown. Compositional heterogeneity also appears to be responsible for a pop-up developed at the floor at the array location. This pop-up (1.95 x 0.3 x 0.03 m) between two drill traces popped up (i.e. buckled) at the array. Unlike similar pop-ups at this level, (e.g. Figure 32, p. 144) this one was oriented such that the long axis of the buckled slab was aligned with the tunnel axis rather than tangential to the tunnel.

6.2. Medium Grained Granite

The geology, tunnel profile, excavation damage, and sampling array at the medium grained granite study location in Room 417 is shown in Figure 41. This tunnel trends 235°, plunges 00°, and is parallel to σ_2. Half barrels, an indication of controlled quality blasting, were evident in the sidewalls following blasting, but were lost by spalling over a 2 to 3 m section of the roof where notch development occurred. Blast-induced fractures radiate away from blastholes on the tunnel face, but those dipping 10°-40° to the southeast are much larger and more frequent than other directions. Tensile fractures oriented radial to the tunnel periphery in the tensile sidewall region are also present. This orientation is coincident with the σ_1 / σ_2 plane (or the normal to σ_3), and as noted in Chapter 4, is coincident with the preferred orientation of natural microcracks.

6.3. Fine Grained Granite

The geology, tunnel profile, excavation damage, and sampling array at the fine grained granite study location in Room 421 is shown in Figure 42. Room 421 trends 235°, plunges at (07°), and is parallel to σ_2. The tunnel section is oval, with its major axis horizontal. At this location, the fine grained granite has a tendency to break in a blocky fashion, with block surfaces being defined by a well-developed subvertical flow banding, and by low-dipping excavation-induced fractures. No natural fractures were encountered. Blast-induced fractures on the tunnel face radiate away from blastholes but those dipping 10°-40° to the southeast are much larger and more frequent than other directions. This orientation is coincident with the σ_1 - σ_2 plane (or normal to σ_3). It is also parallel to the average orientation of the thrust faults above this level, and to one of the microcrack sets developed at this level. Half-barrels were evident in the sidewalls following blasting, but were removed by spalling from a 2.5 to 3 m section of the roof in each round.

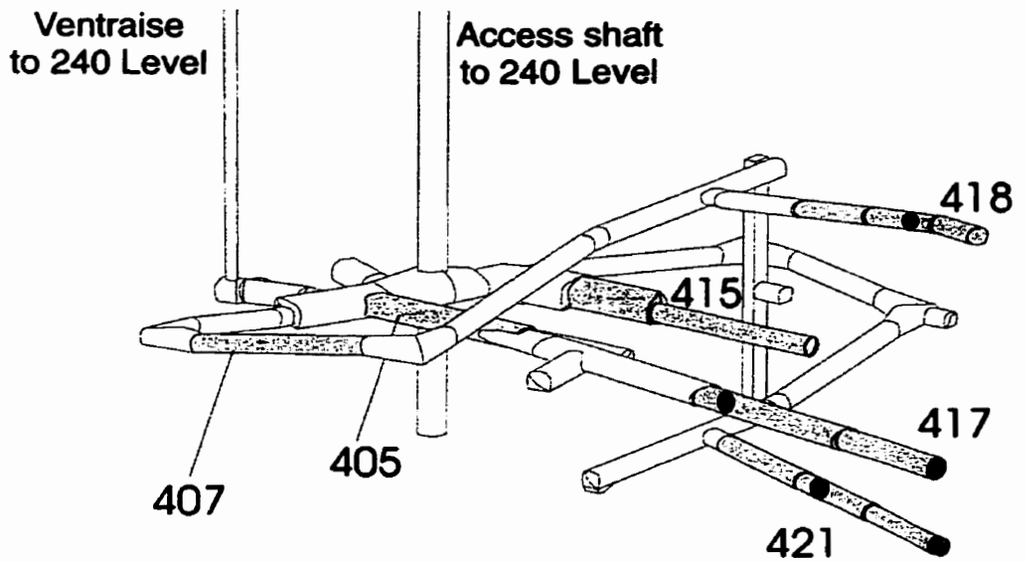

Figure 36. General location of the 420 Level, and the names of rooms referred to in this text. The black ellipses represent the sample locations.

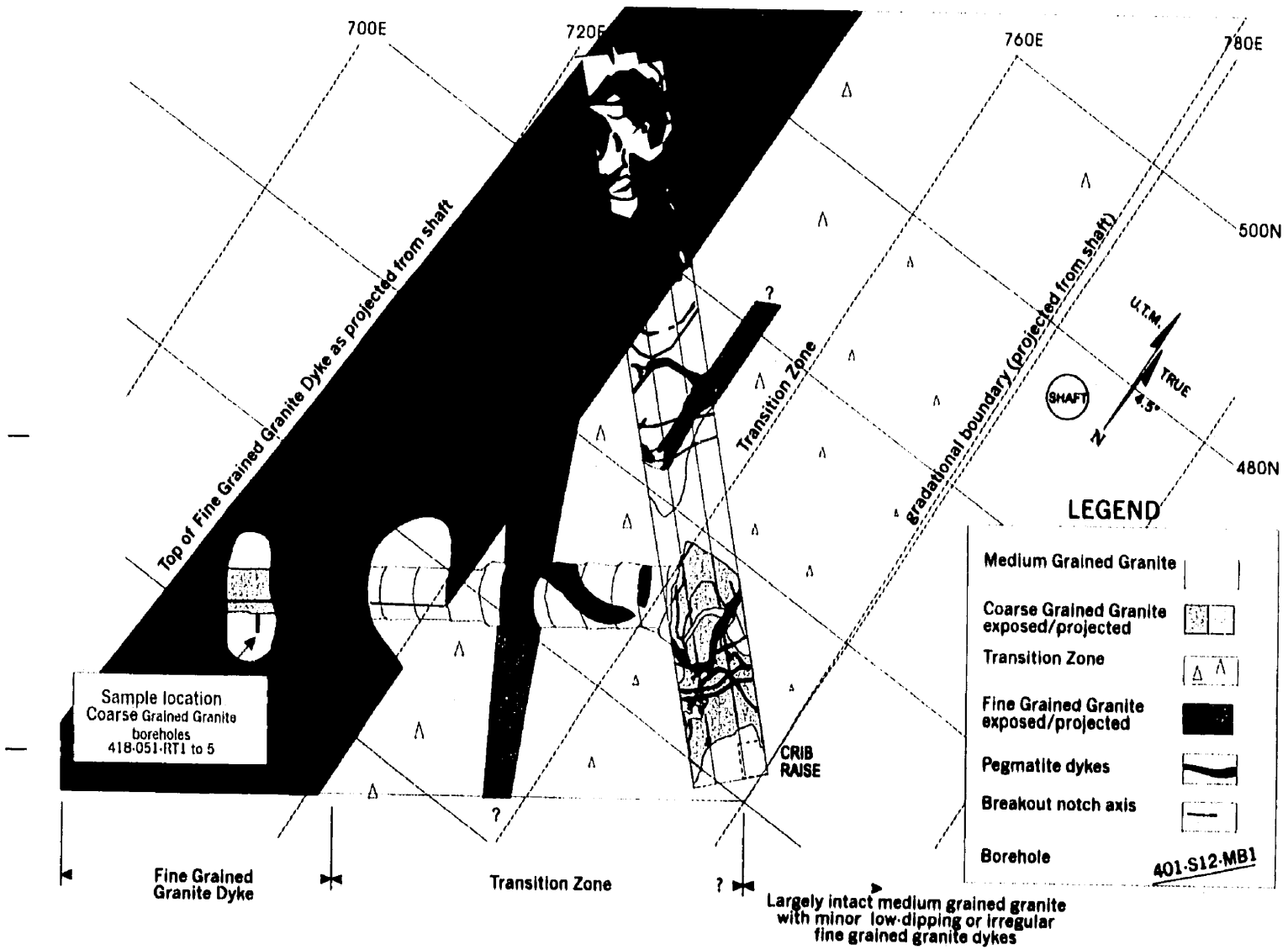

Figure 37. 420 Level geology, upper ramp level (depth 354 m).

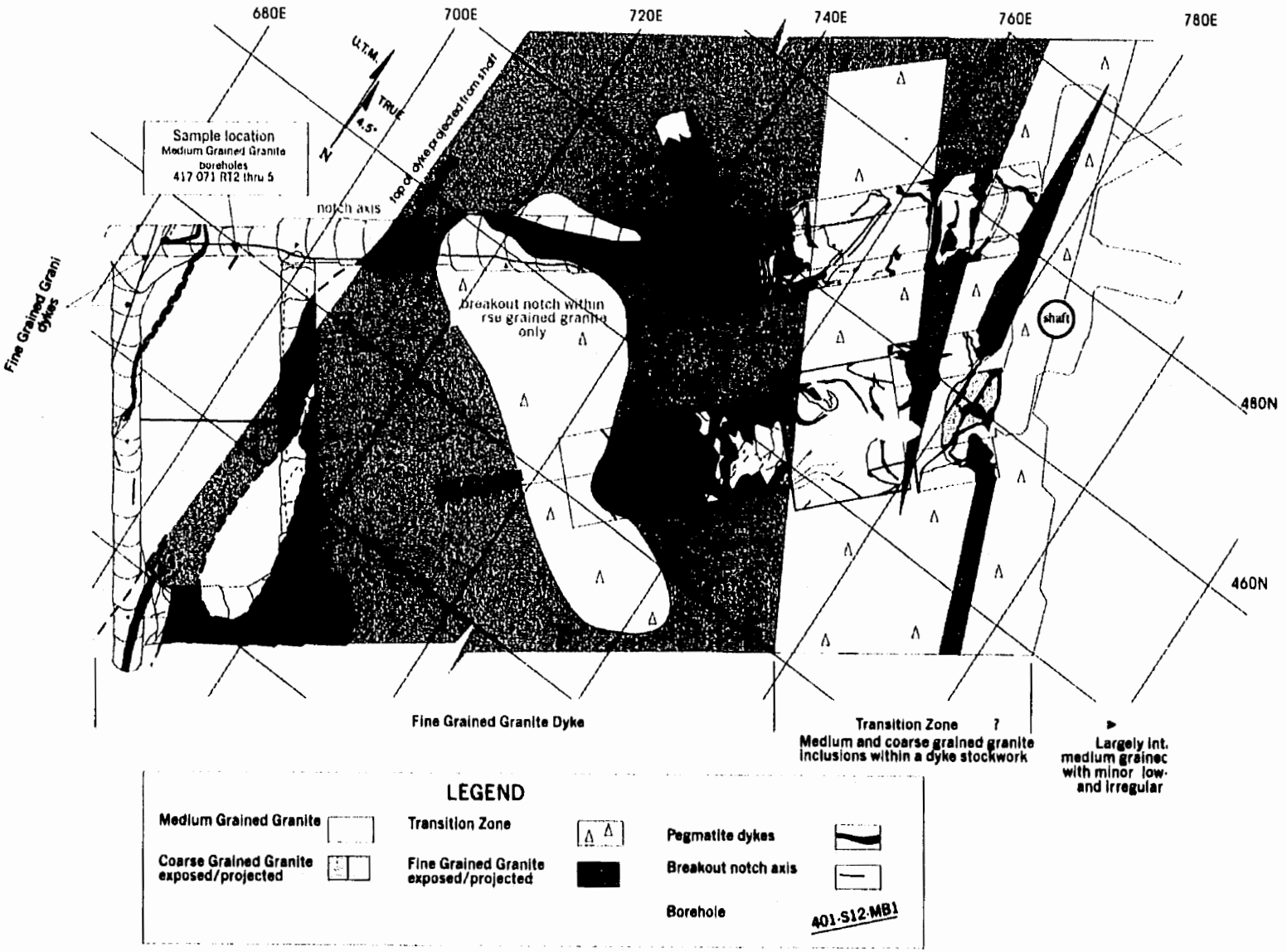

Figure 38. 420 Level geology, main level (depth 415 m).

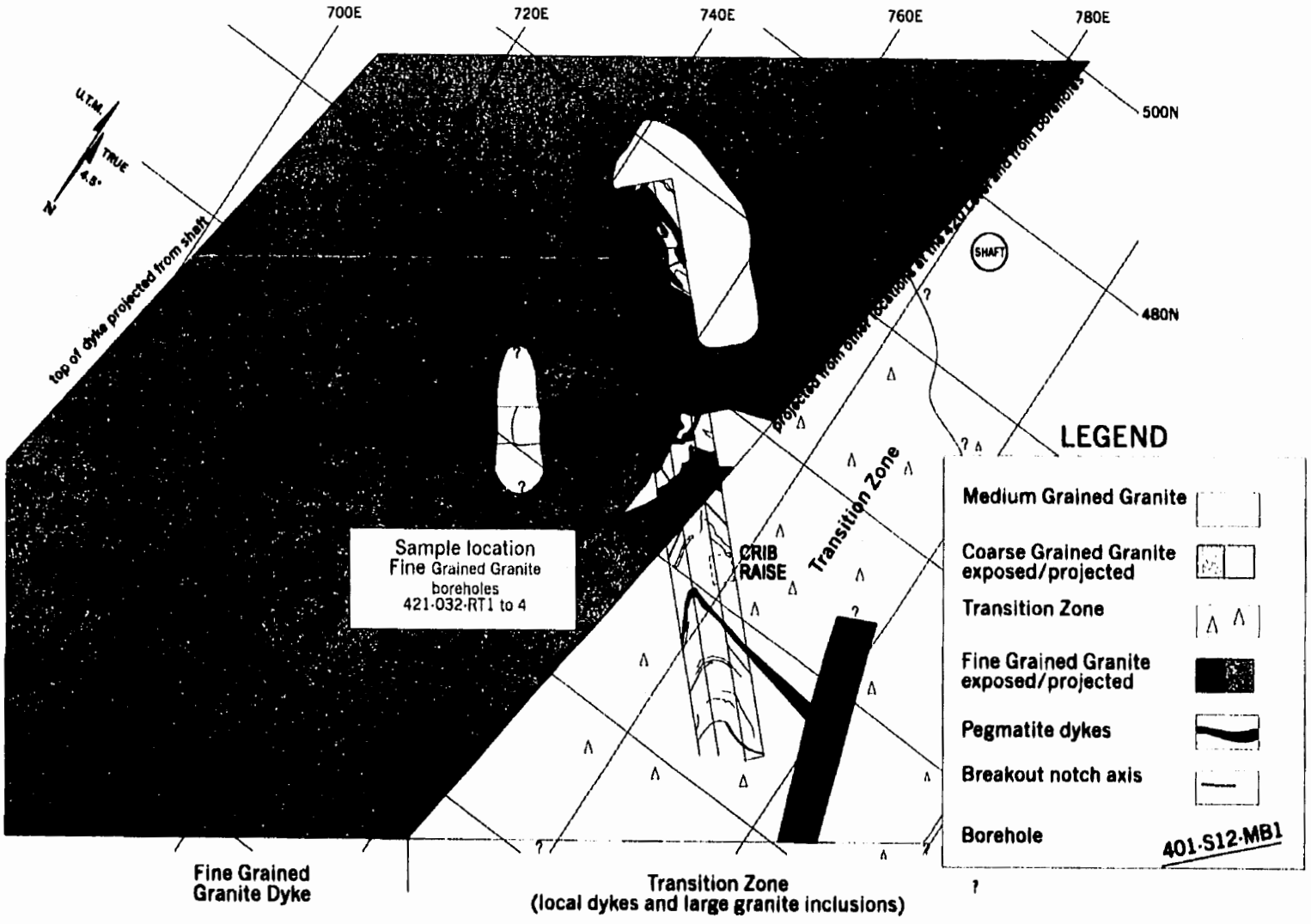

Figure 39. 420 Level geology, lower level, (depth 437 m).

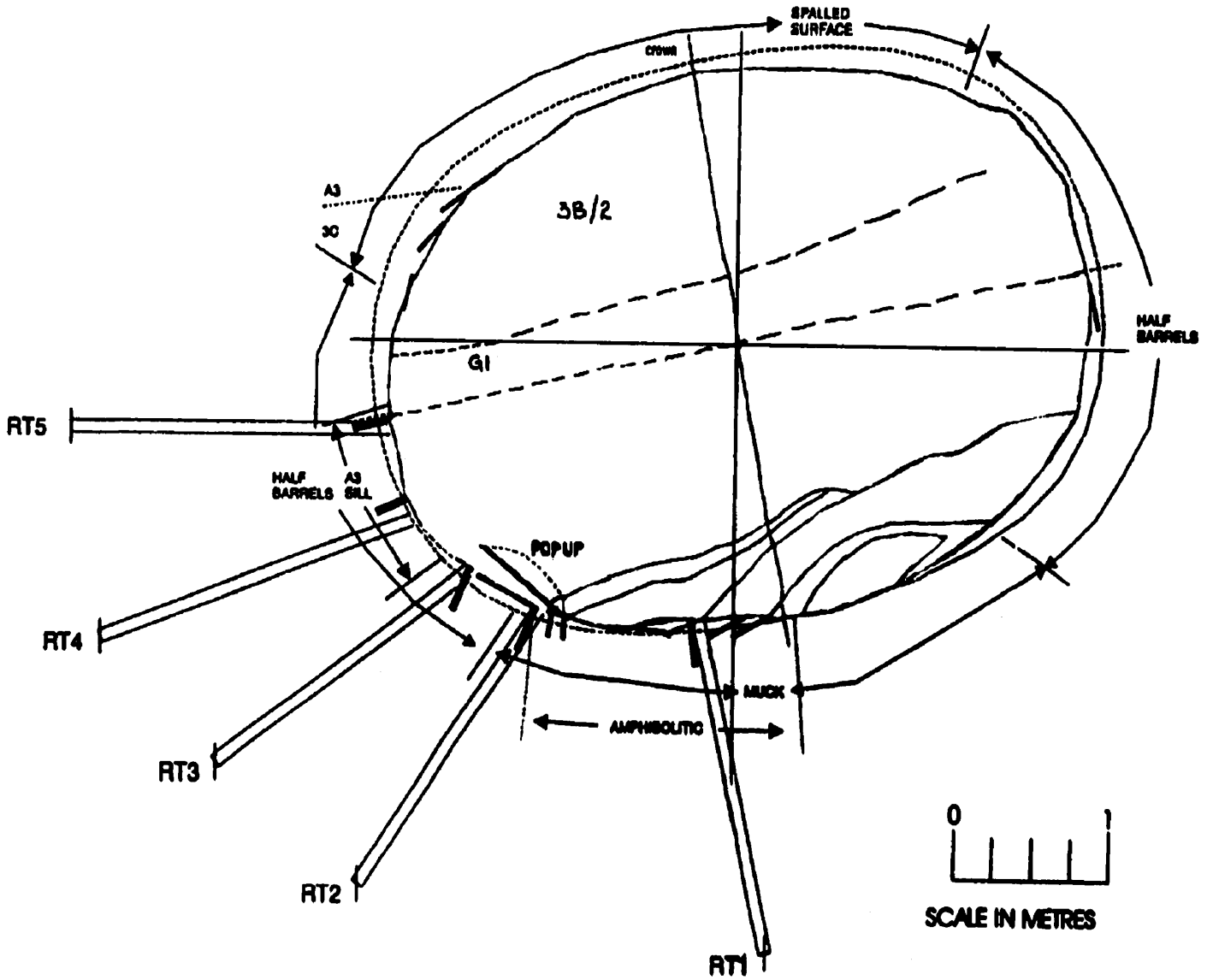

Figure 40. The geology, tunnel profile, excavation damage, and sampling array at the coarse grained granite location in Room 418.

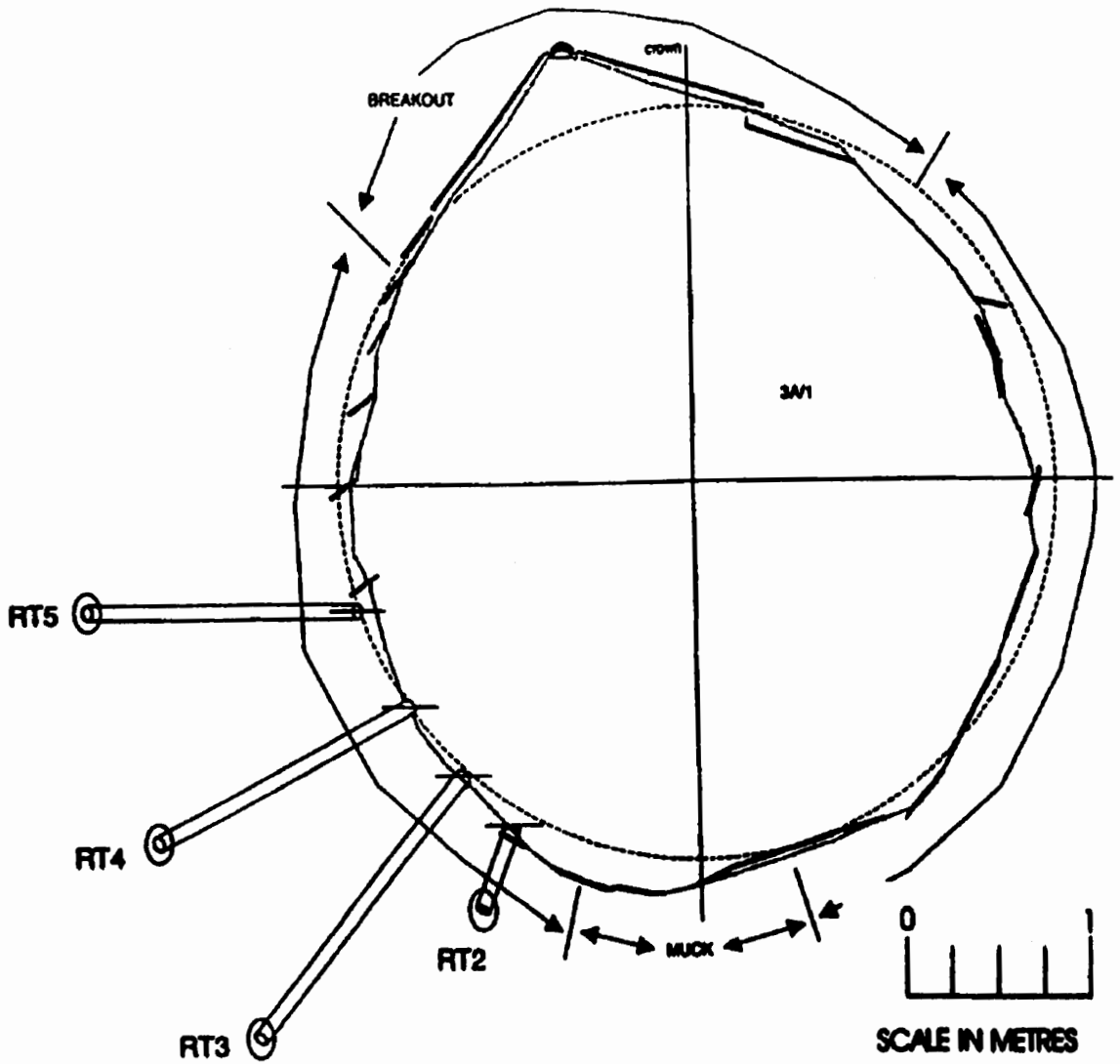

Figure 41. The geology, tunnel profile, excavation damage, and sampling array at the medium grained granite location in Room 417.

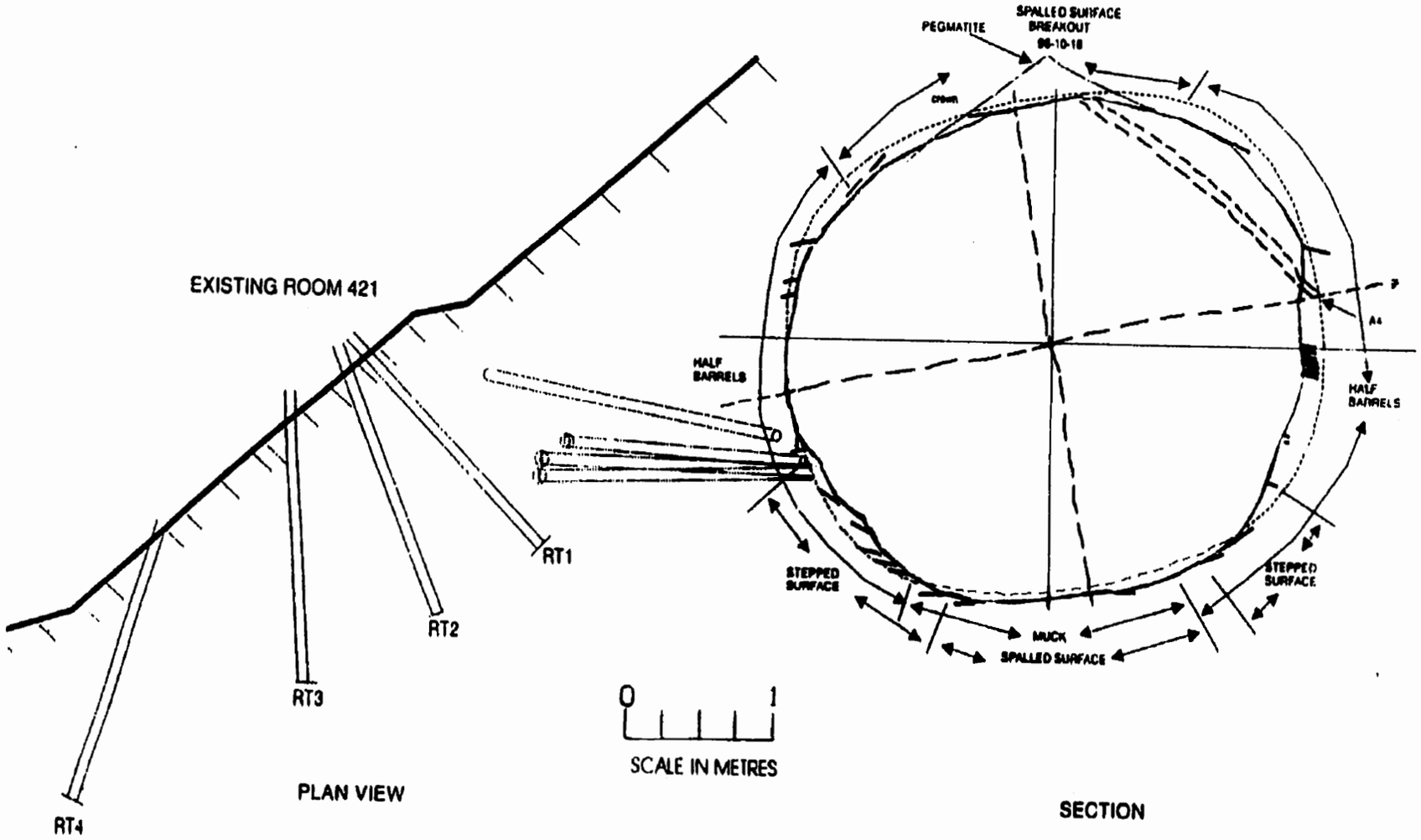

Figure 42. The geology, tunnel profile, excavation damage, and sampling array at the medium grained granite sample site, Room 421.

Chapter 7

POINT LOAD TESTING

7.1. Introduction

This section summarizes Point Load testing conducted to identify variation in tensile strength with the direction of loading, and its relationship to rock fabric within the granite of the Lac Du Bonnet Batholith. Three texturally distinct end-members of the granite of the Lac Du Bonnet Batholith were tested: 1) fine grained granite dykes with subvertical flow banding, 2) a medium grained and weakly to moderately layered granite forming the main mass of the batholith, and 3) a generally coarse grained and leucocratic unit that occurs as sills and recrystallized zones in the main phase. For the sake of convenience, these are referred to as the fine, medium and coarse grained granites, respectively.

7.2. Specimen Preparation

Samples used in these tests were obtained from the boreholes listed in Table 11. All samples are segments of HQ- sized core (46 mm diameter), the choice of specimen diameter being largely dictated by budget constraints. Specimens were prepared in accordance with the procedure described in (Coates and Gyenge, 1966; Gyenge, 1980), and by the International Society for Rock Mechanics (Brown, 1981). The end surfaces of each of the specimens were ground flat to ensure that they were parallel to each other and perpendicular to the axis of the specimen.

A total of 105 oriented specimens were selected as summarized in Table 11. Their size and density statistics are summarized in Table 12. The mean bulk density ranged from 2.54 to 2.72 gm/cm^3; these corresponding to the leucocratic and melanocratic layers in the coarse grained granite. Density variations showed no correlation with distance from the excavation.

Each specimen was retained after loading to failure for detailed mapping of their fabric and the test-induced fractures formed. The orientations of foliations, natural microcracks and the test-induced fractures, all relative to the core reference line, were recorded and these were then converted to true orientations. The fabric / fracture maps for each specimen and data tables for each specimen are provided in Appendix A.

The orientation of all fabric elements and test-induced fractures in the samples were required so that the compressive and tensile strength results could be compared to the results from tunnel mapping of rock structure, to the natural microcrack investigations, and to the in-situ stress data and rock structure. Accordingly, each specimen was retained after loading to failure for detailed mapping of their fabric and the test-induced fractures. The orientations of foliations, natural microcracks and the test-induced fractures, relative to the core reference line, were recorded and these were then converted to true orientations. The angles necessary to convert relative orientations to true orientations, given the trend and plunge of the borehole are shown in Figures 43 to 45.

Table 11.
Sample and testing summary

Rock Type	Borehole	Orientation		test type and number		
		trend	Plunge	Uniaxial compression	Brazilian	Axial Point Load
Coarse grained granite	418-051-RT1	324.90	77.10		*Discing*	
	418-051-RT2	143.61	54.76	1	8	15
	418-051-RT3	143.40	35.40	1	8	6
	418-051-RT4	143.56	19.70	1	7	6
	418-051-RT5	143.38	0.40	1	4	12
Medium grained granite	403-014-MB2			1		
	417-071-RT1	Not drilled				
	417-071-RT2	190.43	59.44		*Discing*	
	417-071-RT3	190.20	39.48		*Discing*	
	417-071-RT4	189.10	19.50	1	6	6
	417-071-RT5	189.70	-0.20	1	4	8
Fine grained granite	421-032-RT1	133.99	0.23	1	4	10
	421-032-RT2	157.61	0.46	1	6	7
	421-032-RT3	175.81	0.80	1	5	10
	421-034-RT4	199.05	0.00	1	6	13

Table 12.
Sample Properties

Granite type [1]	Number of samples	Diameter (mm)			Thickness (mm)			Average T/D Ratio	Density gm/cm^3			Point Load Strength Index (MPa) [2]		
		min.	-mean-	max	min.	-mean-	max		min.	-mean-	max	min.	-mean-	max
Fine	43	44.75	44.87	44.96	18.30	20.37	23.34	0.55	2.61	2.64	2.67	16.20	21.32	27.00
Medium	16	44.68	44.73	44.80	19.40	20.73	22.45	0.46	2.60	2.62	2.63	12.90	16.32	22.58
Coarse	41	44.50	44.80	45.10	18.60	20.50	22.80	0.45	2.54	2.65	2.72	13.20	15.00	18.00

[1] Listed by average grain size, these are the abbreviated names. The full rock names are: 1) fine grained and flow banded granodiorite dykes, 2) the homogeneous to weakly banded main phase granite, and 3) the coarse grained xenolithic leucocratic granite.

[2] These are averages based on all boreholes. The Point Load Index (and the tensile strength) is in fact anisotropic, and varies with respect to the orientation of the loading axis relative to one or more fabric elements within each rock type.

7.3. Methodology

The most commonly used laboratory methods to study tensile strength, are the point-loading and the line-loading (or Brazilian) methods. In the point-loading method, core discs are loaded axially between a pair of indentors while in line-loading method; the disc is placed on edge and loaded in the direction of its diameter between two flat platens. In the line-load method, the diametral fracture plane is constrained by the position of the loading indentors, while in the point-load test, the diametral fracture plane is free to take any orientation. In practice, failure tends to be controlled by heterogeneities in the rock, such as foliations or microcracks, which are close to or parallel to the plane of failure under this loading geometry. Heterogeneities well outside this plane, such as incipient core discing, do not affect the test.

According to Lajtai (1980) "... The Brazilian test seems to yield a more accurate definition of both the tensile strength and its variation with direction ... (and is the more commonly applied tool for this application in rock mechanics).... The point load test is more suitable for the determination of the minimum value of tensile strength, and ...(in determining if there are preferred directions of fracture)...".

The same approach was applied in this study: with Point Load tests to determine if there are preferred directions of fracture in the massive rocks of the LDBB, and Brazilian tests to determine if there are variations in tensile strength with the direction of loading.

The Point Load test was also used to provide a relative ranking of the tensile strength of the various rock types, although this was a secondary objective of this experiment. This ranking is based on calculation of the "Point Load Strength Index" (Goodman, 1989). The "point load index" is given by the following:

$$\text{Point Load strength index, } I_s = P/D^2 ,$$

where P = *the load to break the specimen, and*

D = *the distance between the platen contacts.*

The methodology used in this study followed the recommendations laid out in Brown (1981), Goodman (1989), and Gyenge (1980). The tests were performed in the CANMET Bell's Corner's Laboratory. The testing machine incorporated a loading system, a system for measuring the load required to break the specimen and a system for measuring the distance between the two platen contact points. Two spherically truncated conical platens (an upper and lower), transmitted the load to the specimen. The load measuring system incorporated a maximum-indicating device so that the reading was retained in the case of sudden specimen failure.

There are two variants of the Point Load Test: the diametral test and the axial test. In the diametral test, the specimen is inserted in the test machine and the conical platens advanced to make contact along a core diameter, ensuring that the distance, L, between the contact point and the nearest free end is at least 0.7 D. In the axial test, the specimens

are loaded parallel to the core axis. In both cases, the inclination of layering, foliation or other plane of weakness is recorded with respect to the line of loading.

For this project only axial loading was conducted, as the length of core available was insufficient to allow for multiple samples for both diametral and axial loading, as well as Brazilian and uniaxial compression tests. Sampling was also limited by the fact that there is sufficient fabric heterogeneity at the core-scale to make it difficult to limit samples (for a given test type) to a single texture/ composition / fabric domain.

7.4. Determination of Orientation

The orientation of all fabric elements and test-induced fractures in the samples were recorded so that the compressive and tensile strength results could be compared to the results from tunnel mapping of rock structure, to the natural microcrack investigations, and to the in-situ stress data. and rock structure.

The upper figure shows the angles necessary to convert relative orientations to true orientations, given the trend and plunge of the borehole

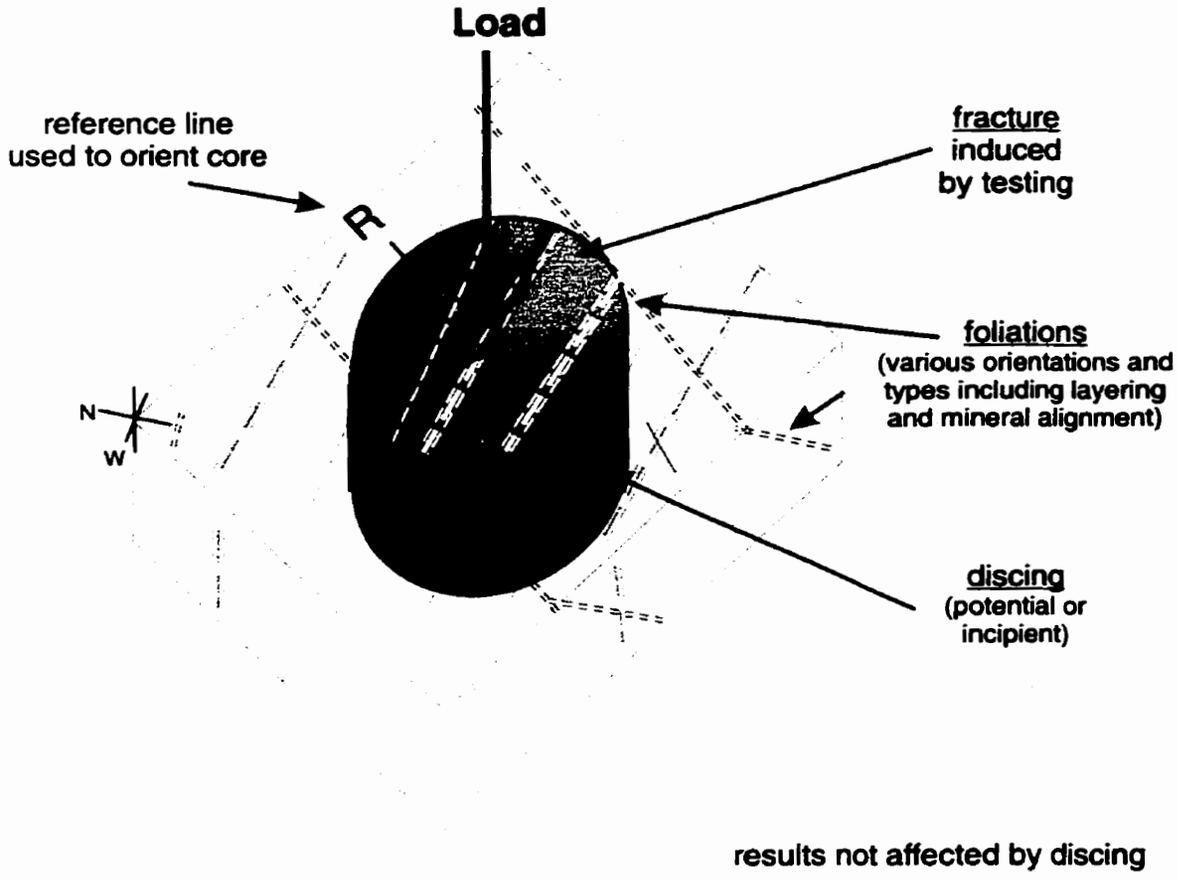

Figure 43. Point Load testing, rotation of loading direction relative to foliation. Rock cylinders were placed vertically in a loading frame and subjected to axial point loading as shown. The orientation of the test-induced fracture, and the fabrics present were recorded, and converted to give the true orientation.

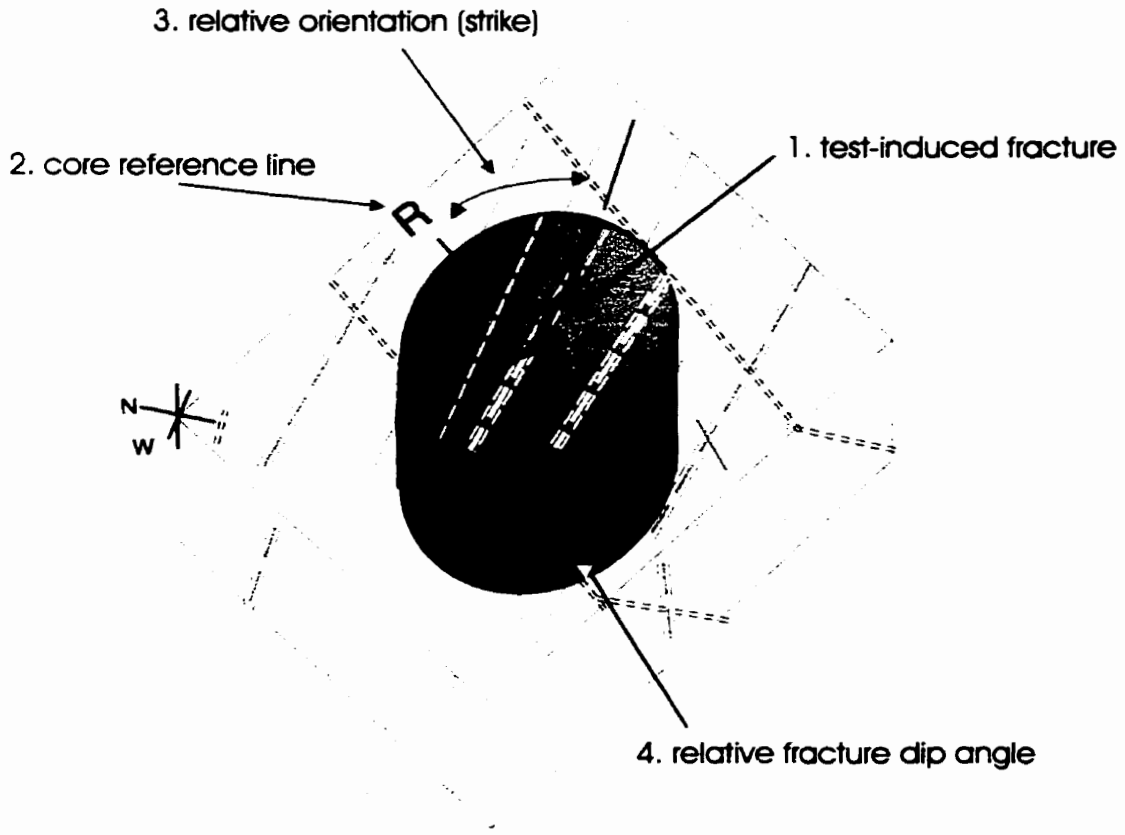

Figure 44. Method for recording orientation of test-induced fracture.

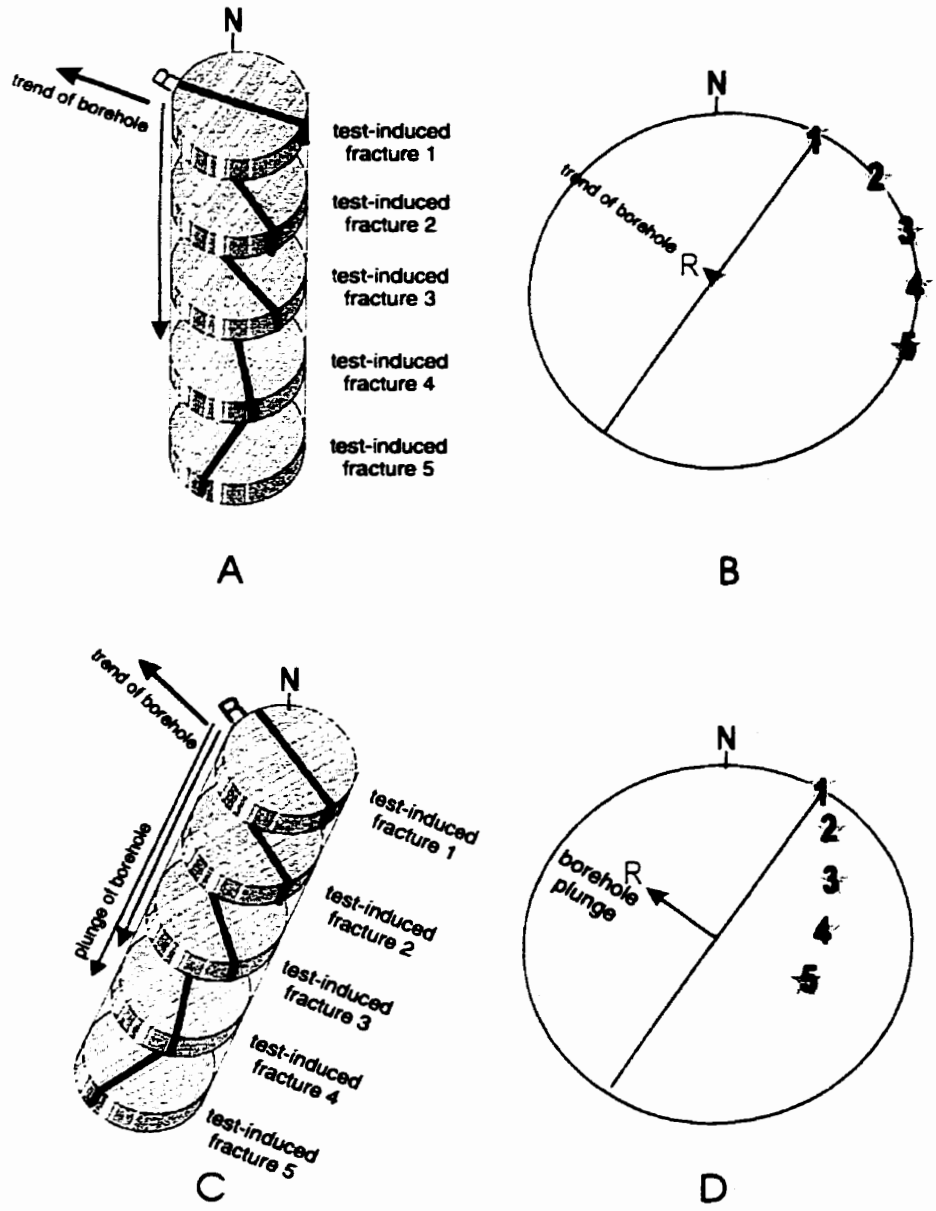

Figure 45. Conversion of relative orientations to true orientations. In each case, the "R" and red arrow represent the reference line painted on the up-dip side of the core, and oriented to show the trend and plunge directions. A: A series of samples with test-induced fractures. In this view, the core is aligned along the trend of the borehole, but "held" in a vertical orientation so that it plunges 90°. The strike of each fracture is recorded relative to the reference line. B: The data from A plotted on a lower hemisphere equal area projection, with the reference line and the poles to the induced fractures indicated. C: As A, but with the core rotated to the correct plunge for this borehole. D: Lower hemisphere equal area projection of the data in C. The reference line "R" rotates from its position in B, to the location shown here. The poles to each fracture rotate in the same direction and orientation.

Table 13.
Average Point Load Strength Index by Rock Type and Borehole.

	Fine Granite				Medium		Coarse Granite			
	RT1	RT2	RT3	RT4	RT4	RT5	RT2	RT3	RT4	RT5
Count	10.0	10.0	10.0	13.0	6.0	14.0	15.0	6.0	6.0	11.0
Mean	21.8	19.9	23.3	20.5	16.4	16.2	15.0	14.4	15.3	15.1
Median	21.3	20.3	23.4	20.6	15.7	16.1	15.3	14.3	15.2	14.1
Maximum	24.8	22.2	27.0	23.2	21.0	19.7	16.8	15.9	17.5	18.0
Minimum	19.9	16.2	19.3	17.3	13.9	13.8	13.4	13.4	13.4	13.2
Skewness	0.9	-0.9	-0.2	-0.2	1.7	0.7	0.0	1.0	0.3	0.7
Kurtosis	-0.5	0.0	-1.2	-0.1	3.5	0.6	-1.4	1.5	-1.1	-1.1
Std. dev.	1.7	1.9	2.8	1.6	2.4	1.5	1.2	0.9	1.5	1.8

Table 14.
Average Point Load Strength Index by Rock Type and Borehole.

	Fine Granite	Medium	Coarse Granite
Maximum	27.0	21.0	18.0
+ *1 std.dev*	23.4	18.3	16.3
Mean	**21.4**	**16.3**	**15.0**
- *1 std.dev*	19.4	14.3	13.6
Minimum	16.2	13.8	13.2
Skewness	-0.1	1.2	0.5
Kurtosis	-0.4	2.0	-0.5
Std. dev.	2.0	2.0	1.3

7.5. Summary of Point Load Testing Results

7.5.1. Presentation

The data from each rock type are presented in the following format and order:

1. summary tables for each rock type, which lists the boreholes, the samples from each borehole, the sample densities, and the tensile strengths recorded (Table 13 and 14).
2. a summary figure of the average point load indices grouped by grain size to indicate the relative strength of each rock type (Figure 46). The resultant ranking is consistent with that determined from the uniaxial compression test data, but much of the variability shown is in fact direction dependent.
3. For each rock type and borehole, a pair of histograms which show the strike of the test-induced fractures, and the strike of the foliations in the same samples (Figures 47 to 51).

Additional information is provided in Appendix A. Drawings of the foliations and test-induced fractures in each of the samples. The axial point load testing results, including the sample dimensions, load at failure, the index and the index normalized to the average sample size are also included.

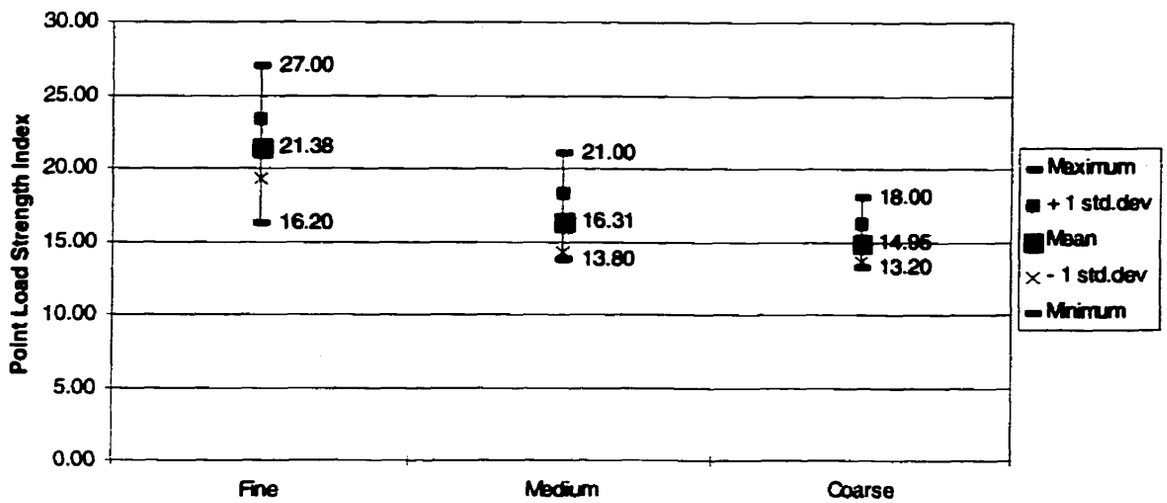

Figure 46. Comparison of Point Load Strength Indices by rock type (relative average grain size).

7.5.2. General Observations.

The Point Load testing indicated that failure was controlled by heterogeneities in the rock, such as foliations or the preferred orientation of natural microcracks, which are close to or parallel to the plane of failure under the various loading geometries tested. This affect was present to some degree in all three of the rock types tested, but varies systematically with the rock heterogeneity, and with the relative orientation of the loading direction. The Coarse Grained Granite has the most repeated tendency to split along dominant (low-dipping) fabric elements, with the lowest average tensile strength and Point Load strength index. The Medium Grained granite has a lesser tendency to split along dominant (and other) fabric elements, but with a comparable average tensile strength and Point Load strength index. The Fine Grained Granite has the least repeated tendency to split along any fabric, which in this case alternated between the steeply-dipping flow banding and the plane correlating with the preferred orientation of natural microfractures, and with the highest average tensile strength and Point Load strength index.

This systematic variation reflects the relative strength of the low-dipping fabric, which comprises a mixture of coplanar compositional layering, mineral alignment, and natural microcracks. All of these elements are present and well developed in the coarse granite, the weakest and most mechanically anisotropic of the group. Where this fabric is less well developed or absent, as in the medium and fine grained granites, this is reflected by an increase in rock strength and isotropy.

7.5.3. Influence of Grain Size on Tensile Strength

As noted earlier in this presentation, the Point Load test provides a relative index of the tensile strength of the various rock types (the Point Load Index, Goodman, 1989), although this was a secondary objective of this experiment. The result, shown in Figure 46 and in Tables 13 and 14, is consistent with the uniaxial compression testing described in Chapter 9, in that relative strength decreases with increasing grain size.

7.5.4. Influence of Fabric on Tensile Strength

The principal objective of applying the Axial Point Load Test in this study was to determine if there were preferred orientations of failure, and if these existed, their correlation with rock fabric. In the axial point configuration, the fracture is free to form in any orientation. If however, the rock is anisotropic, there is a tendency for failure to follow one or more preferred orientations that generally correspond with some fabric element such as natural microfractures, mineral alignment, etc. The results of this testing for the coarse, medium and fine grained granites are presented for each rock type in the following sections.

7.5.5. Coarse Grained Granite, Borehole 418-051-RT 2, 3, 4, 5.

The results of point load testing in each of the 4 boreholes from the coarse grained granite are shown in Figure 47, and in Tables 13 and 14. A pair of histograms for each borehole shows the strike of test-induced fractures, and the strike of the foliations in the same samples. This granite is marked by a well developed low dipping foliation referred to for convenience as the large scale layering, but in fact a mixture of metre to millimetre scale compositional layering, mineral alignment, schlieren (in some cases showing evidence of slip) and natural microfractures in quartz.

In this rock type, there is a very clear tendency for the tensile failure to be localized by the foliations present in each sample. Which foliation is responsible is dependent upon the orientation of the borehole (and sample) axis. In shallow dipping boreholes (< 45 °), axial point loading of the core produces fractures following the strongest fabric. In steeply dipping boreholes, the layering is not favourably oriented with respect to axial loading, and the plane of failure then "jumps" to other, steeper dipping foliations (this transition is reflected in the values of the average tensile strength), and is shown schematically in Figure 48.

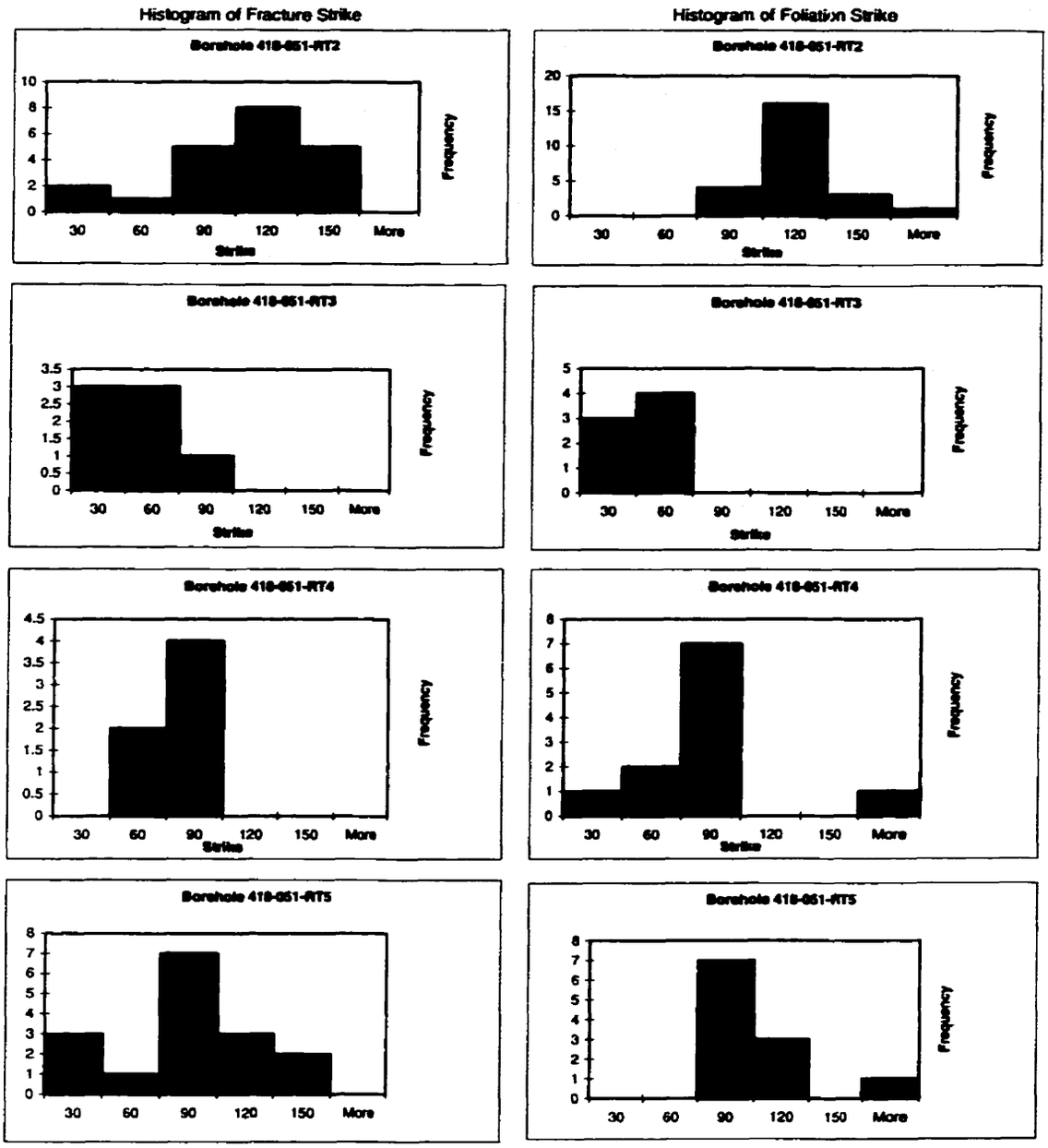

Figure 47. Point Load test results from the coarse grained granite. For each borehole, a pair of histograms shows the strike of test-induced fractures and the strike of the foliations in the same samples.

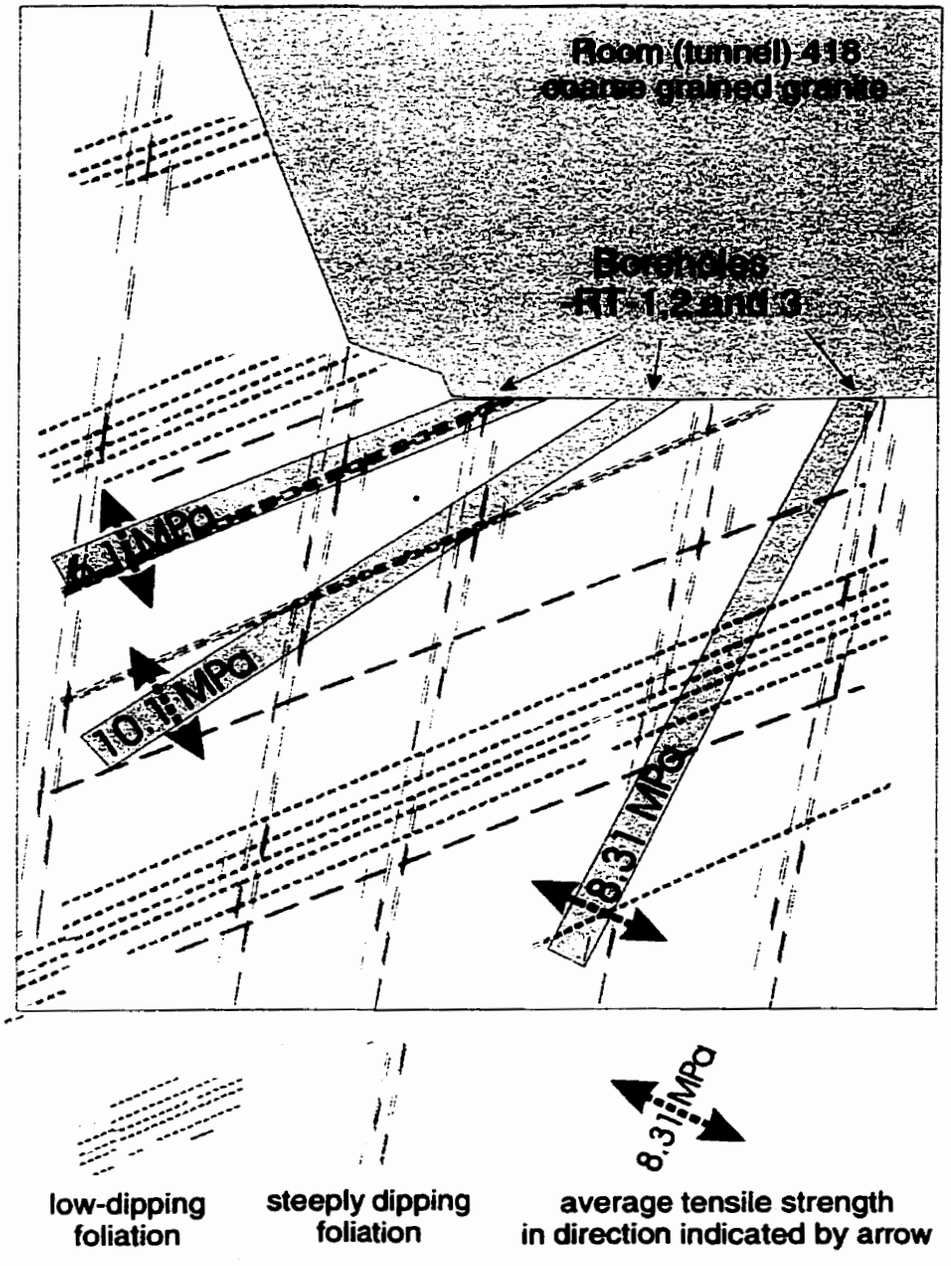

Figure 48. Schematic representation of the variation in tensile strength in the coarse grained granite and its correlation with the fabrics present. In shallow dipping boreholes (< 45 °), axial point loading of the core produces fractures following the strongest fabric (referred to for convenience as the large scale layering, but in fact a mixture of metre to millimetre scale compositional layering, mineral alignment, schlieren (in some cases showing evidence of slip) and natural microfractures in quartz). In steeply dipping boreholes, the layering is not favourably oriented with respect to axial loading, and the plane of failure then "jumps" to other, steeper dipping foliations (this transition is reflected in the values of the average tensile strength). These relationships are shown schematically above.

7.5.6. Medium Grained Granite, Borehole 417-071-RT 4, 5.

The results of point load testing in each of the 2 boreholes from the medium grained granite are shown in Figure 49, and in Tables 13 and 14. A pair of histograms for each borehole shows the strike of test-induced fractures, and the strike of the foliations in the same samples. This granite is marked by a weakly developed low dipping foliation referred to for convenience as the large scale layering, but which is in fact a mixture of metre - scale compositional layering, mineral alignment, and natural microfractures in quartz.

In this rock type, there is also a tendency for the tensile failure to follow the direction of the large scale layering, but the correlation is not as strong as in the coarse grained, well-foliated granite, and the load required to break the rock along this plane is, on average, greater.

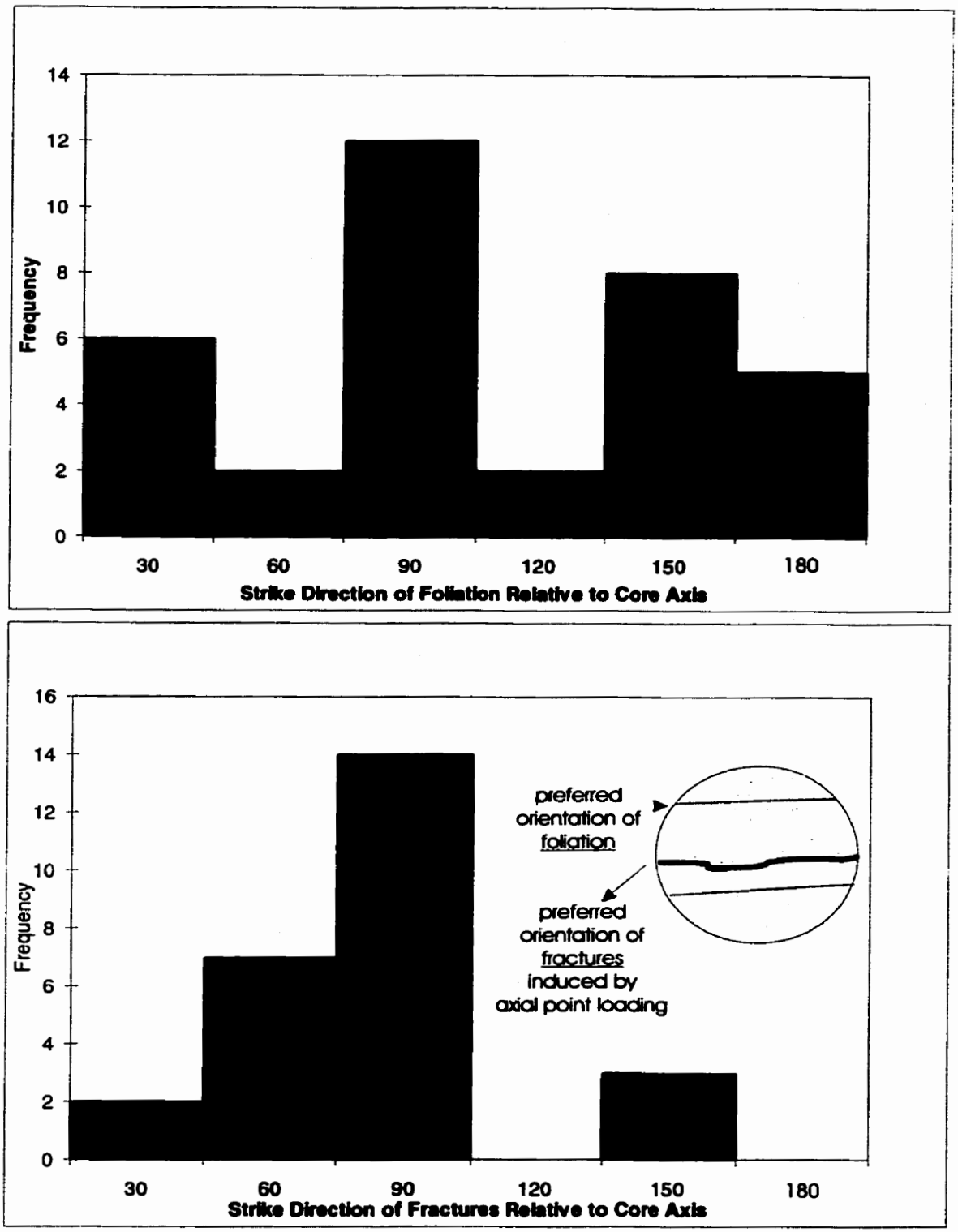

Figure 49. Point Load test results from the medium grained granite. This pair of histograms shows the strike of the foliations (upper) and the strike of the test-induced fractures (lower) from the same samples.

7.5.7. Fine Grained Granite, Borehole 421-032-RT1, 2, 3, 4.

The results of point load testing in each of the 4 boreholes from the fine grained granite are shown in Figure 50, and in Tables 13 and 14. A pair of histograms for each borehole shows the strike of test-induced fractures, and the strike of the foliations in the same samples. This granite is marked by a well developed subvertical flow banding, and a low-dipping natural microcrack set.

In this rock, the tendency is for splitting to occur in the plane of the natural microcracks, and to a lesser extent, along the subvertical layering. This is consistent with the Brazilian tests.

The links between rock structure and the preferred orientations of the fractures induced by the point load tests are also shown in Figures 51 and 52. The former is a summary plot of poles to fractures induced by axial point loading in each of the specimens taken from the 4 boreholes, each oriented at different angles to the foliation. The latter is a lower hemisphere equal area plot of poles to natural fractures (fluid inclusion or alteration-filled planes in quartz) obtained by universal stage mapping of thin section from the granodiorite. The correlation between the test-induced fractures (Figure 51) and the natural microcracks (Figure 52) is obvious.

The pattern of point load induced fractures is dominated by the low-dipping to subhorizontal fractures (the vertical sets are quantitatively minor in both outcrop and in specimens). The orientation of the low-dipping fractures is consistent with that of the natural microcracks (Figure 52).

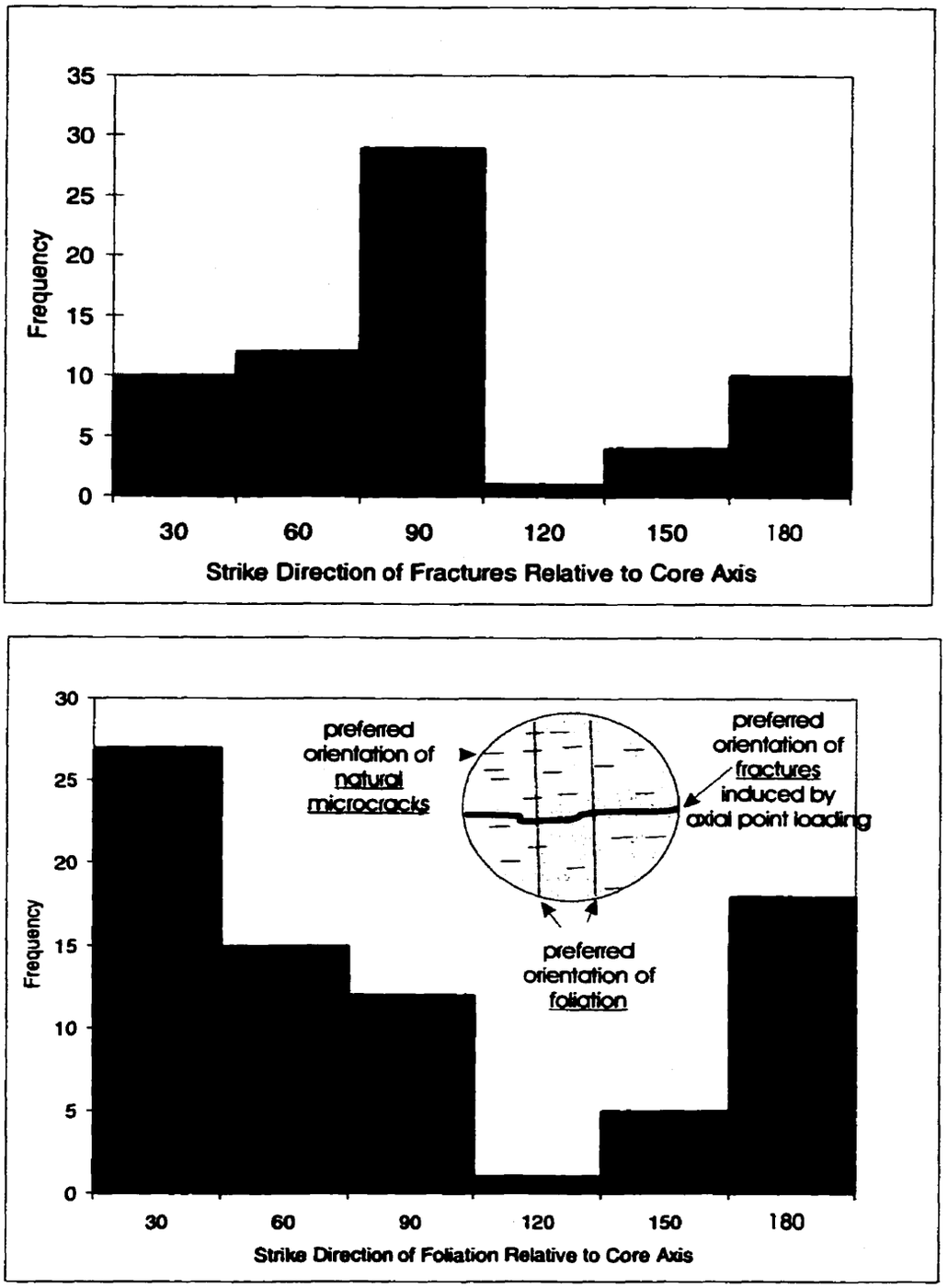

Figure 50. Point Load test results from the fine grained granite. The histograms show the strike of the test-induced fractures (upper), and the strike of the foliations (lower) from the same samples. This granite hosts a well developed subvertical flow banding and a low-dipping natural microcrack set. Fractures induced by axial point loading preferentially follow the (low-dipping) plane of the natural microcracks (which strike ~90° in this 2-D view), the subvertical foliation being ignored. This relationship between the natural microcrack set and the point-load induced fractures is displayed to better effect in Figure 51 following.

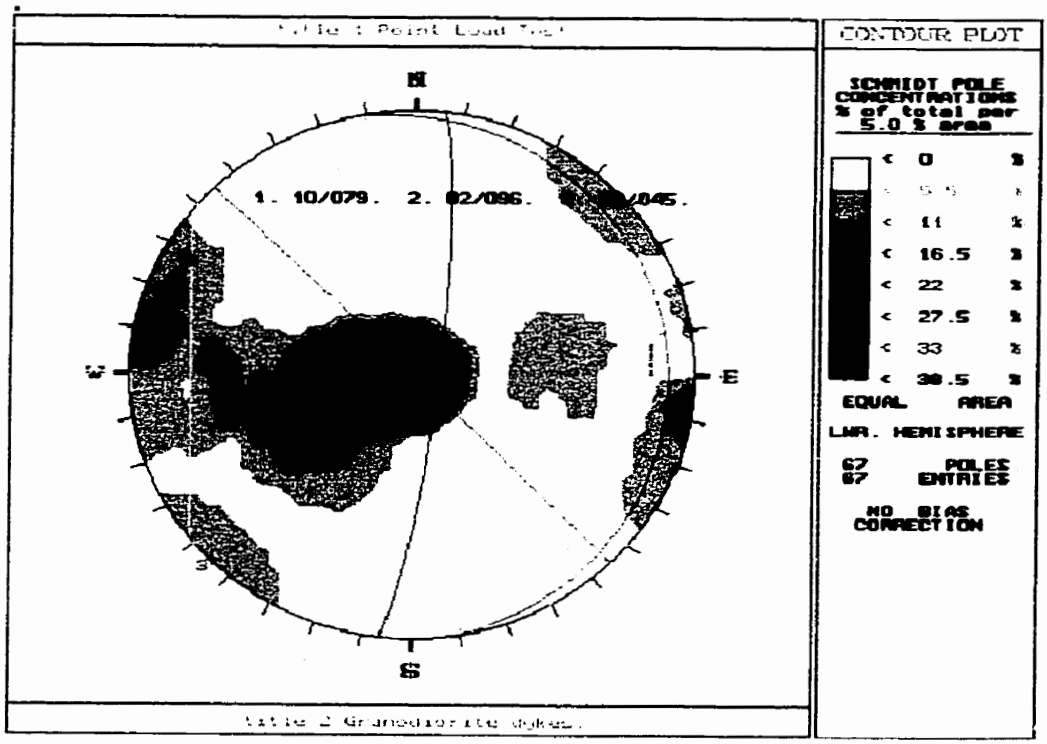

Figure 51. Lower hemisphere equal area plot of poles to fractures induced by axial point loading, in fine grained granite from boreholes 421-032-RT1,2,3 and 4.

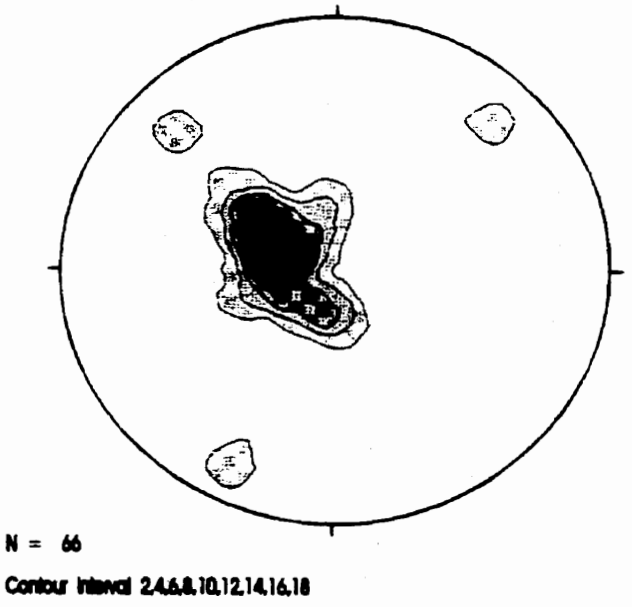

Figure 52. Lower hemisphere equal area plot of poles to natural fractures (fluid inclusion or alteration-filled planes in quartz) obtained by universal stage mapping of thin section from the granodiorite. The induced fractures in Figure 51 share the same general orientation as the natural fractures shown here.

Chapter 8

BRAZILIAN TESTS

The Brazilian test method is a convenient but indirect method for estimating the tensile strength (Goodman, 1989). It has been found that a rock core will split along the diameter and parallel to the cylinder axis when line loaded on its side in a compression machine. The reason for this can be demonstrated by examining the stress inside a disk loaded at opposite sides of a diametral plane. In such a configuration the tensile strength is calculated from:

$$Brazilian Tensile\ strength,\ \sigma_{tB} = \frac{2P}{\pi D t} \qquad \text{Equation 1}$$

where P = load at failure, D = diameter of the specimen, and t = thickness of the specimen

The "Brazilian tensile strength - σ_{tB}" is estimated from the peak compression load. The actual cause of failure may in fact be more complex, reflecting the interaction of small-scale flaws, compression parallel to the eventual rupture plane, and the horizontal tension induced by this loading.

The Brazilian test is an indirect but popular method, as it is much easier to perform this test than to arrange the precise alignment and end preparation required for a direct tensile test (Goodman, 1989). According to Goodman (1989), the estimates it provides are

generally higher than those produced by direct tension tests, and the difference between estimates increases with increasing grain size and heterogeneity. This is attributed to the effect of grain-scale (and larger) discontinuities, in which "...*larger fissures in the coarse rocks weaken a direct tension-specimen more severely than they weaken a splitting tension specimen* .... , The ratio of Brazilian to direct tensile strength has been found to vary from one to more than ten as the length of preexisting fissures grows larger.

In this study, values for tensile strength were also calculated using the modification suggested by Chen (1993), which includes a correction needed for modulus values owing to the presence of microcracks. The correct tensile strength can be approximated by the following function:

$$\sigma_t = 1.023k^{0.252}\left(\frac{P}{\pi R}\right) \qquad \text{Equation 2}$$

where k = ratio of Young's moduli in tension and compression

(the value used was that of the Westerly granite (0.24) given on p. 79 of Chen, 1993)

A comparison of values calculated using both equations is given in Table 15. The results are consistent with the general observation, with the coarser rocks being most strongly affected.

Table 15.
Comparison of Calculated Brazilian Tensile Strengths

Average tensile strength	Fine	Medium	Coarse
From equation 1	7.0 MPa	5.0 MPa	6.0 MPa
From equation 2	2.4 MPa	1.25 MPa	1.5 MPa
Ratio (2/1%)	34%	25%	25%

The testing methodology used in this study followed the recommendations laid out in Brown (1981); Goodman (1989); Gyenge (1980), and in the Pit Slope Manual Supplement 3-5 (Gyenge and Ladanyi, 1977). All specimens were prepared in accordance with the procedure described in the Pit Slope Manual Supplement 3-5 (Gyenge and Ladanyi, 1977) and the method suggested by the International Society for Rock Mechanics (Brown, 1981).

Rock cylinders were placed vertically in a loading frame and subjected to line-loading in compression along a preset diameter at a known angle to some reference line or foliation (Figure 53), and then repeated through a series of angles (Figure 54). These angles were recorded, and converted to give the true orientation of the tensile strength vector so determined (Figure 55). The tests were performed by the author, at the CANMET Laboratories at Bells Corners, Ottawa. The compression machine used included a load measuring system for indicating the failure load, and a maximum-load indicating device, i.e. one which retains the maximum load so that the latter can be recorded after specimen failure loading platens.

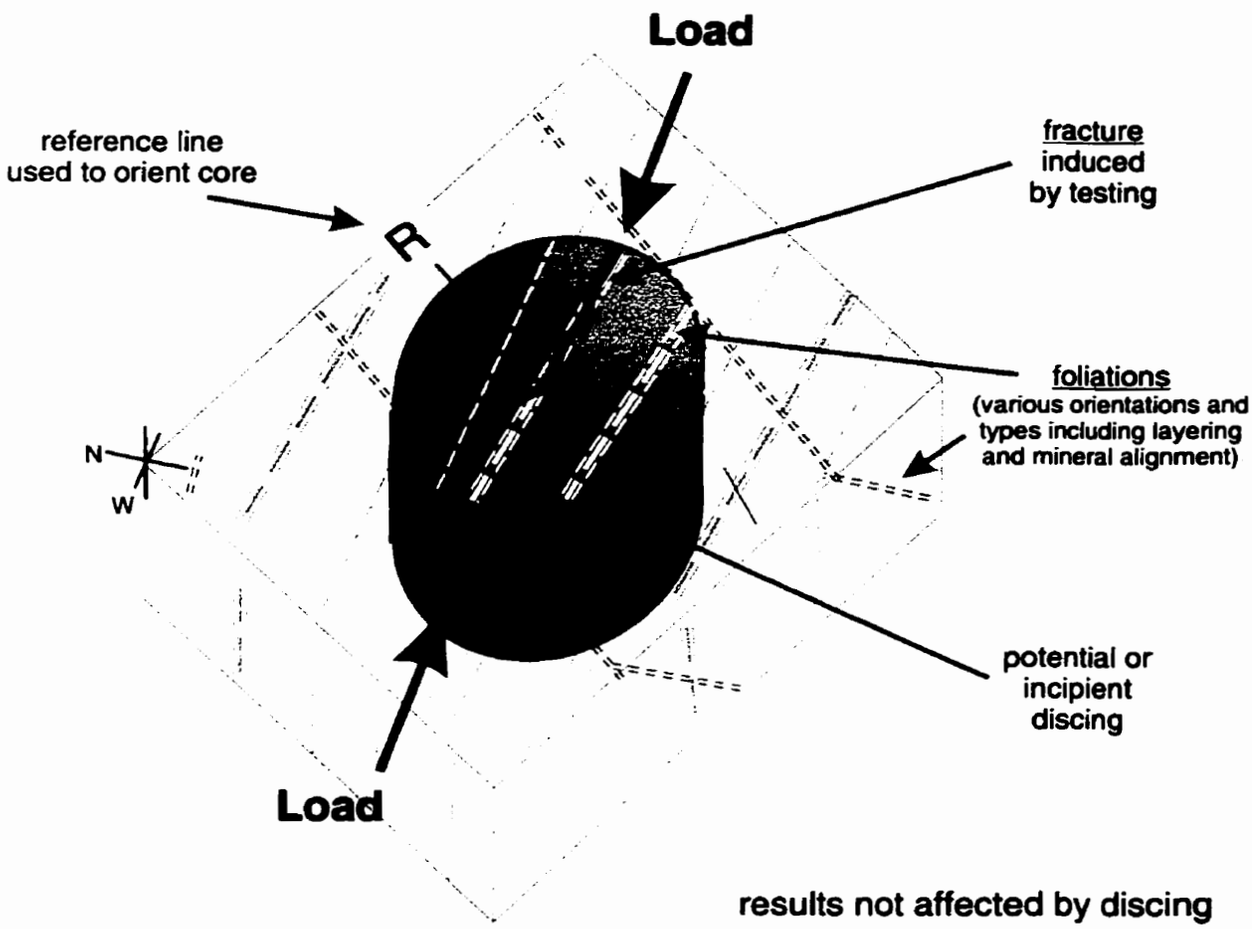

Figure 53. Configuration of loading for the Brazilian test as seen on a single specimen.

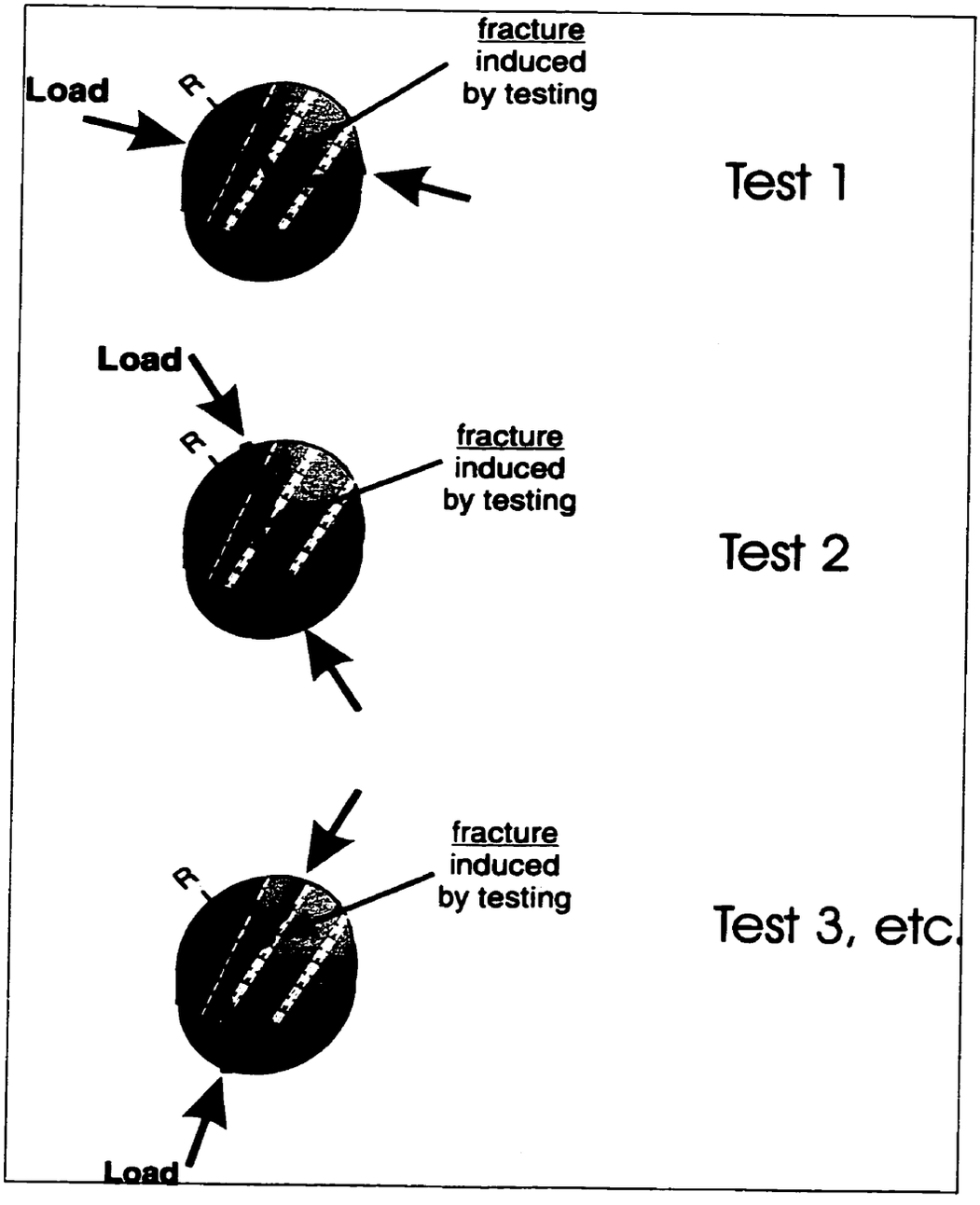

Figure 54. Brazilian tests, rotation of loading direction relative to foliation.

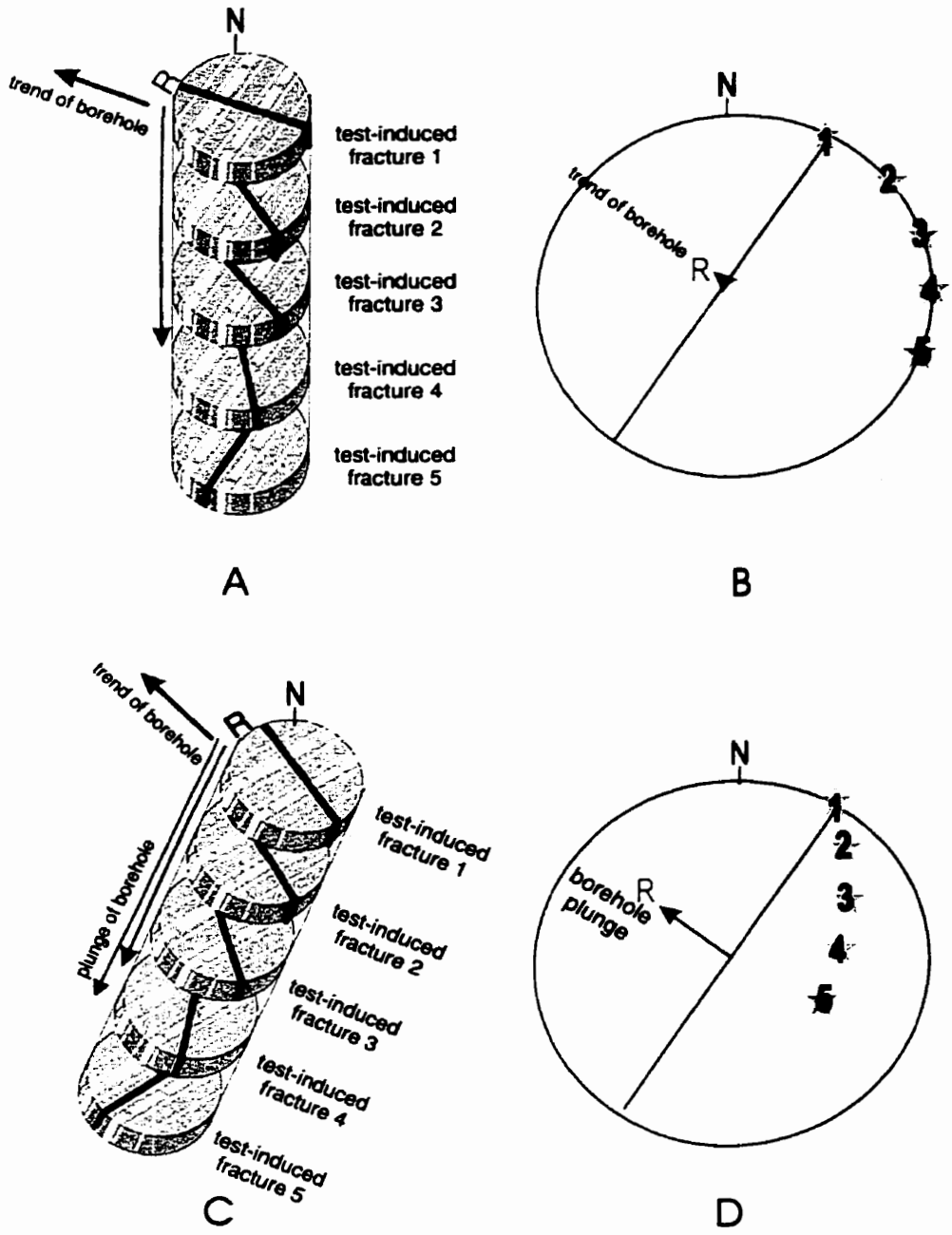

Figure 55. Conversion of relative orientations to true orientations. In each case, the "R" and red arrow represent the reference line painted on the up-dip side of the core, and oriented to show the trend and plunge directions. A: A series of samples with test-induced fractures. In this view, the core is aligned along the trend of the borehole, but "held" in a vertical orientation so that it plunges 90°. The strike of each fracture is recorded relative to the reference line. B: The data from A plotted on a lower hemisphere equal area projection, with the reference line and the poles to the induced fractures indicated. C: As A, but with the core rotated to the correct plunge for this borehole. D: Lower hemisphere equal area projection of the data in C. The reference line "R" rotates from its position in B, to the location shown here. The poles to each fracture rotate in the same direction and orientation.

8.1. Rock Type and Specimen Preparation

Samples used in these tests were obtained from the boreholes listed in Table 16. All samples are segments of HQ- sized core (46 mm diameter), the choice of specimen diameter being largely dictated by budget constraints. Specimens were prepared in accordance with the procedure described in the Pit Slope Manual Supplement 3-5 (Gyenge and Ladanyi, 1977) and the method suggested by the International Society for Rock Mechanics (Brown, 1981). The end surfaces of each of the specimens were ground flat to 0.015 mm to ensure that they were parallel to each other and perpendicular to the axis of the specimen.

The average dimensions and bulk densities of samples from each of the three rock types are listed in Table 17. The mean bulk density ranged from 2.54 to 2.72 gm/cm^3; these corresponding to the leucocratic and melanocratic layers in the coarse grained granite. Specimen lengths varied from 22.03 to 28.36 mm and diameters varied from 44.43 to 44.91 mm, with length to diameter ratios ranging from 0.56 to 0.58.

Table 16
Sample and testing summary

Granite Type	Borehole	Orientation		test type and number		
		trend	Plunge	uniaxial compression	Brazilian	Axial point load
Coarse grained	418-051-RT1	324.90°	77.10°		*Discing*	
	418-051-RT2	143.61°	54.76°	1	**8**	15
	418-051-RT3	143.40°	35.40°	1	**8**	6
	418-051-RT4	143.56°	19.70°	1	**7**	6
	418-051-RT5	143.38°	0.40°	1	**4**	12
Medium grained	403-014-MB2	225°	00°	1		
	417-071-RT1	not drilled				
	417-071-RT2	190.43°	59.44°		*Discing*	
	417-071-RT3	190.20°	39.48°		*Discing*	
	417-071-RT4	189.10°	19.50°	1	**6**	6
	417-071-RT5	189.70°	-0.20°	1	**4**	8
Fine grained	421-032-RT1	133.99°	0.23°	1	**4**	10
	421-032-RT2	157.61°	0.46°	1	**6**	7
	421-032-RT3	175.81°	0.80°	1	**5**	10
	421-034-RT4	199.05°	0.00°	1	**6**	13

Table 17.
Sample Properties

Granite type	Number of samples	Diameter mm $_{min.}$ -mean- ^{max}	Thickness Mm $_{min.}$ –mean- ^{max}	Average T/D ratio	Density gm/cm^3 $_{min.}$ –mean- ^{max}	Tensile Strength (MPa) [1] $_{min.}$ –mean- ^{max}
Fine grained	21	44.82 44.86 44.91	22.24 24.93 28.36	0.56	2.61 2.64 2.67	4.62 2.4 9.14
Medium grained	10	44.73 44.77 44.80	22.56 25.86 28.06	0.58	2.60 2.62 2.63	3.47 1.25 7.15
Coarse grained	27	44.43 44.60 44.81	22.03 25.05 27.55	0.56	2.54 2.65 2.72	3.71 1.5 10.12

[1] These are averages based on all boreholes. Tensile strength is in fact anisotropic, and varies with respect to the orientation of the loading axis relative to one or more fabric elements within each rock type.

8.2. Brazilian Test Results

The data for each rock type are presented in the following format and order:

- a summary table that lists the boreholes, the samples from each borehole, the sample densities, and the tensile strengths recorded (Tables 18 to 20).
- a summary figure that depicts the variation in average tensile strength between boreholes (Figure 56, 60, 63). This was done to look for directional anisotropy that might not be obvious at the hand-specimen scale of testing.
- an x-y plot of sample density versus their respective tensile strengths (Figures 57, 61, and 64). This was done to see if any variations in tensile strength could be due to sample damage. If the damage zone around the excavation affected the samples, it would be expected that such damage would lower both the rock density and the tensile strength, and that the specimens affected would be closest to the excavation (or to the known stress concentrations about the excavation).
- an x-y plot of the Brazilian tensile strengths of each sample against the inclination of the loading axis relative to the preferred orientation of the dominant fabric element(s) (Figures 58,62,65). Insets on these plots graphically illustrate the orientation of the loading axis (arrows) relative to the flow banding as seen in a cross section of the core. The best-fit linear regression curve, the equation for the curve, and the R^2 correlation coefficient are included.

8.3. General Observations.

The following observations, though qualitative, illustrate the differences in response to loading which correlate with rock fabric.

1. 23% of the coarse grained granite samples displayed audible cracking well before failure. When loaded parallel to the foliation / mineral banding, failure was often marked by a simple weak "pop", with the sample splitting into two pieces along the foliation plane. In contrast, failure in the medium and fine grained granites was sudden and sharp. These observations are consistent with those from tunnel mapping, and highlight the importance of the foliations as weakness planes.
2. The load rate to failure increased much more slowly in the coarse (and heterogeneous) granite than in the medium and fine grained granites. It is suspected that this behaviour is attributable to a greater degree of crack closure under loading in the coarse grained granite, than occurred in the other finer grained rock types.

8.4. Fine Grained Granite, Borehole 421-032-RT1, 2, 3, 4.

Brazilian test results for the Fine Grained Granite from boreholes 421-032-RT1, 2, 3, 4 are summarized in Table 18. This summary includes, for each sample, the loading axis angles relative to structure, and two calculated tensile strengths for each sample. The first strength (max) represents the value at failure. The second strength (min.) includes values in which audible cracking (fracture initiation) preceded failure. As this occurred in only one sample for this rock type, this data set is nearly identical to the first, and is not further discussed.

Summary statistics for the Brazilian tests from the entire borehole array within the Fine Grained Granite are shown in Figure 56. The array of boreholes was arranged in a horizontal plane, and oriented to intersect the subvertical flow banding at angles of approximately 60°, 45°, 10°, and 00°, respectively. The data from each borehole includes loading orientations ranging from 00° to 90° to the foliation, but have been averaged together to look for directional anisotropy at the metre-scale. This was done to test for systematic variation within the horizontal plane, or put in another way - to examine the affect of borehole orientation when sampling for rock properties testing.

The results indicate that there is significant direction -dependent anisotropy.
To determine if this trend is a function of varying degrees of sample damage, the tensile strength for each sample was plotted against its density (Figure 57). The tensile strength of the sample suite decreases with increasing density, which is the opposite of what would be expected if the sample was damaged by discing and enhanced microcracking. This result indicates that the direction anisotropy seen is not due to damage.

The influence of the subvertical flow banding on tensile strength is examined in Figure 58. The tensile strength is somewhat lower when the loading axis is parallel to the flow banding, but the tendency for this is weak, and the data curve could be subdivided into linear segments. This is believed to reflect the influence of additional fabric elements in the rock, most notably the natural microcracks. At this location in the URL, these microcracks are subhorizontal or have a shallow (<30°) southeast dip. Variation in the tensile strength relative to the preferred orientation of the microcracks is shown in

Figure 59. In this case, the data spread is much less, and the anisotropy is much greater - i.e. the tensile strength parallel to the natural microcrack set is ~ 65% of that measured perpendicular to the microcracks.

- This space intentionally left blank for effective pagination -

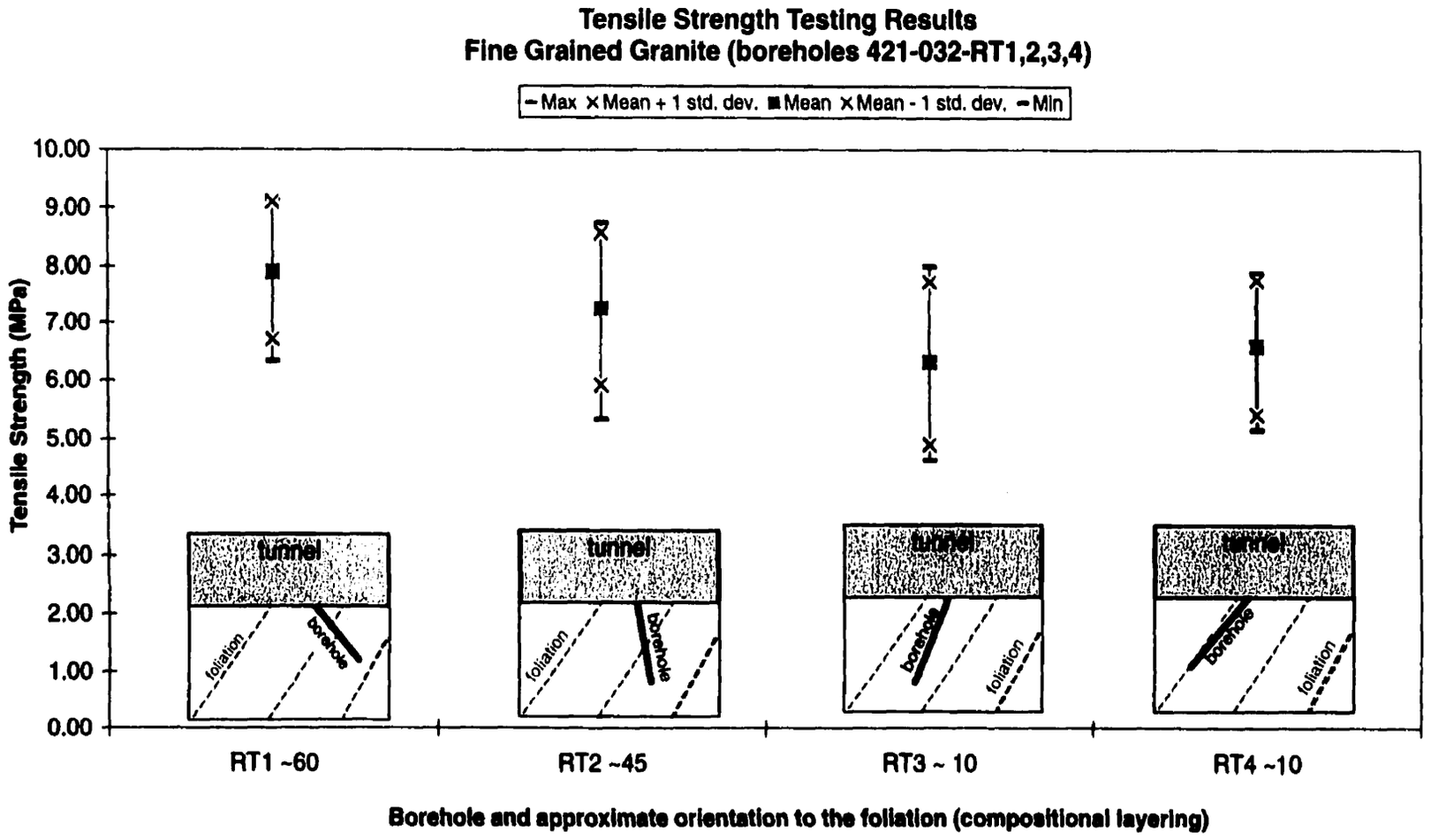

Figure 56. Summary statistics for the Brazilian tests from the entire borehole array within the Fine Grained Granite. The array includes boreholes 421-032-RT1, 2, 3, 4. These were arranged in a horizontal plane, and oriented to intersect the subvertical flow banding at angles of ~60°, ~45°, ~ 10°, and ~00°, respectively. The data from each borehole includes loading orientations ranging from 0° to 90° to the foliation in each borehole. This was done to test for systematic variation within the horizontal plane, or put in another way - to examine the affect of borehole orientation when sampling for rock properties testing. The results indicate that there is significant direction -dependent anisotropy.

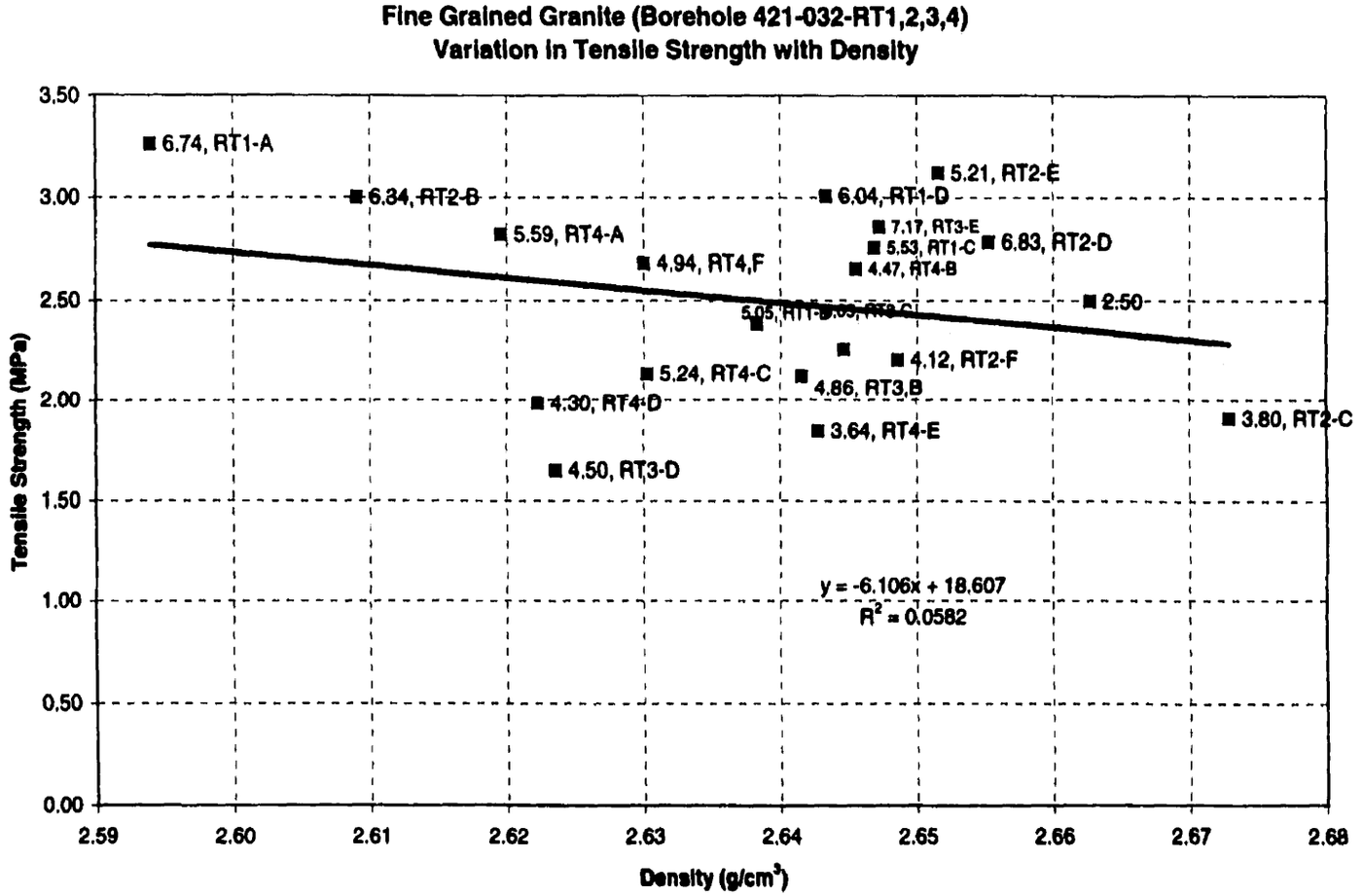

Figure 57. Brazilian test results for the Fine Grained Granite from boreholes 421-032-RT1, 2, 3, and 4, showing the variation in the estimated tensile strengths of each sample plotted against the corresponding sample density. If the damage zone around the excavation affected the samples, it would be expected that such damage would lower both the rock density and the tensile strength, and that the specimens affected would be closest to the excavation. Instead, there is no correlation between density and location (as given by the sample numbers). Tensile strength actually decreases with increasing sample density, which is the opposite of what would be expected if damage was present.

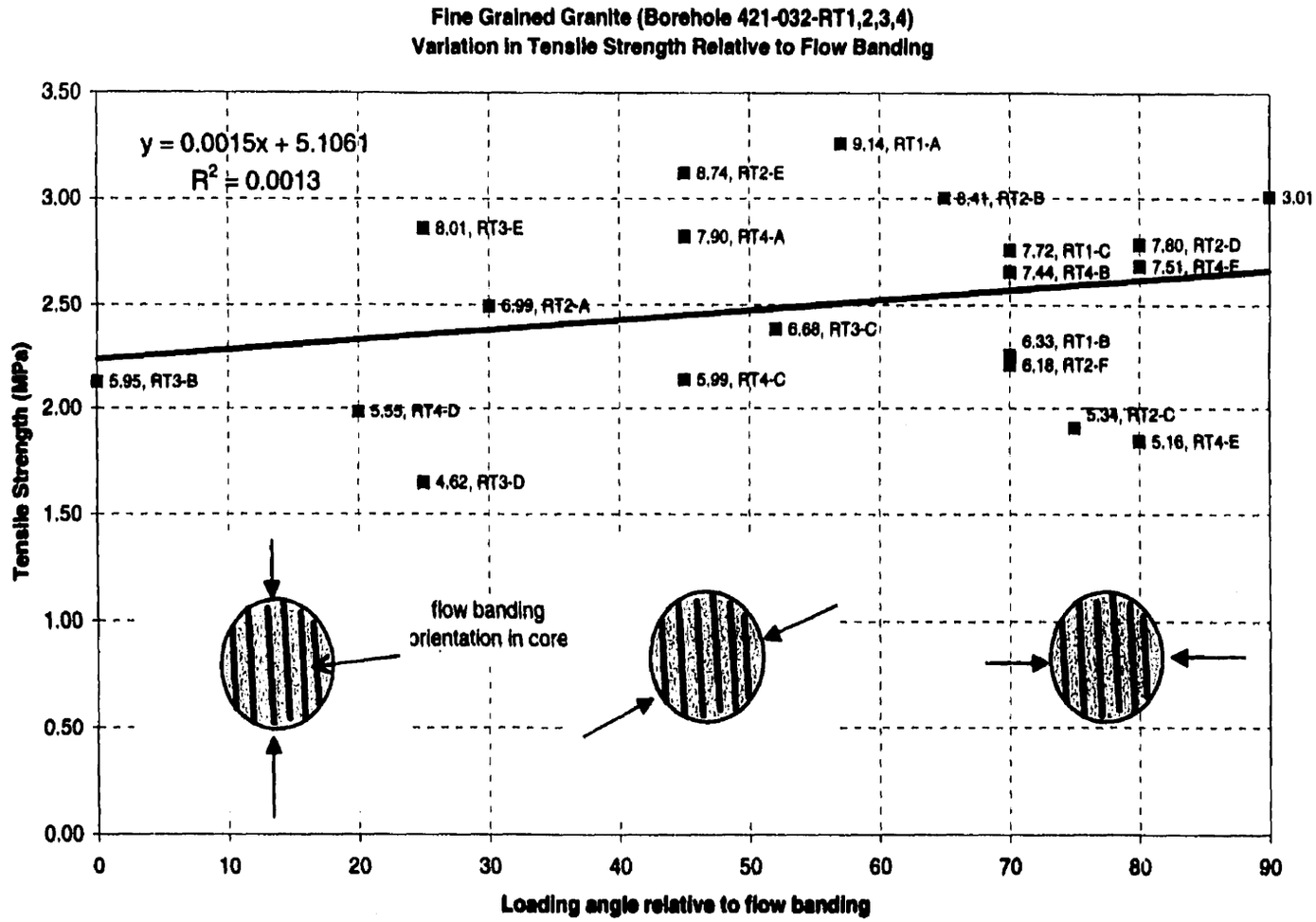

Figure 58. Brazilian test results for the Fine Grained Granite from boreholes 421-032-RT1, 2, 3, and 4. Variation in the estimated tensile strengths of each sample against the inclination of the loading axis relative to the flow banding. The three insets show the orientation of the loading axis (arrows) relative to the flow banding as seen in a cross section of the core. The best-fit linear regression curve, the equation for the curve, and the R^2 correlation coefficient are included. In this example, the tensile strength is somewhat lower when loading is done parallel to the flow banding, but the trend is dispersed.

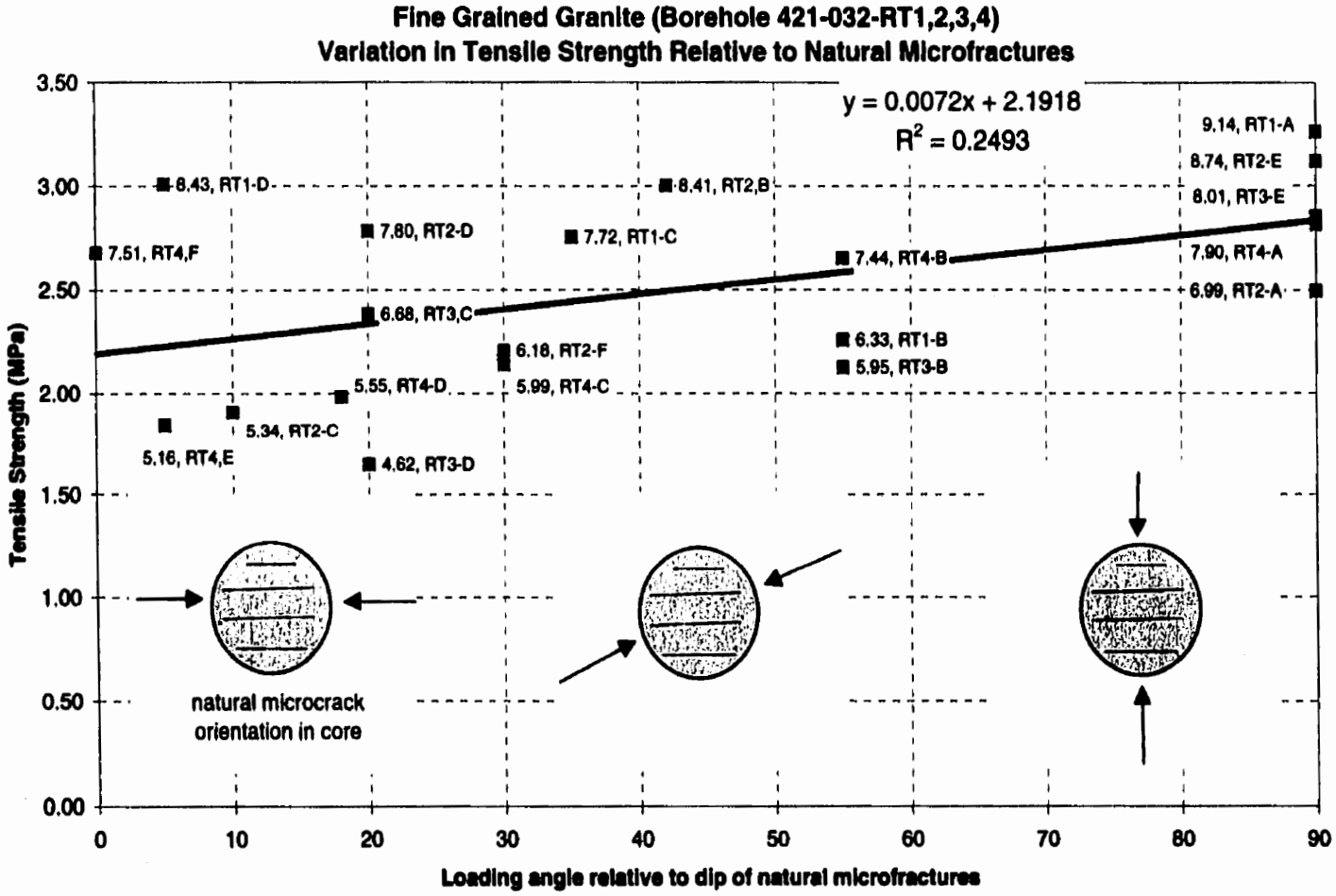

Figure 59. Brazilian test results for the Fine Grained Granite from boreholes 421-032-RT1, 2, 3, and 4. Variation in the estimated tensile strengths of each sample against the inclination of the loading axis relative to the preferred orientation of natural microcracks. The three insets show the orientation of the loading axis (arrows) relative to the microcracks as seen in a cross section of the core. The best-fit linear regression curve, the equation for the curve, and the R^2 correlation coefficient are included. In this example, the tensile strength parallel to the natural microcracks is ~ 65% of that perpendicular to the microcracks.

8.5. Medium Grained Granite, Borehole 417-071-RT 4, 5.

Brazilian test results for the Medium Grained Granite from boreholes 417-071-RT 4, 5 are summarized in Table 19. This summary includes, for each sample, the loading axis angles relative to structure, and two calculated tensile strengths for each sample. The first strength (min.) includes values in which audible cracking (fracture initiation) preceded failure, while the second strength (max) represents the value at failure. Three samples were affected by this phenomenon. These samples do not appear to be anomalous in shape (finishing), texture or in terms of their orientation and location. Summary statistics for the Brazilian tests from the entire borehole array within the Medium Grained Granite are shown in Figure 60. The array of boreholes was arranged in a vertical plane, and oriented so as to intersect the very inconspicuous low-dipping layering at angles of ~45°, and ~00°. The data from each borehole includes loading orientations ranging from 00° to 90° to the foliation in each borehole, and have been averaged together as if the rockmass was massive. This was done to test for systematic variation within the horizontal plane, or put in another way - to examine the effect of borehole orientation when sampling for rock properties testing. Although this array was less extensive than the arrays in the fine grained and coarse grained granites, the results confirm a similarly oriented direction -dependent anisotropy.

To determine if this trend is a function of varying degrees of sample damage, the tensile strength for each sample was plotted against its density (Figure 61). The tensile strength of the sample suite decreases with increasing density, which suggests that the direction anisotropy seen is not due to damage. There is no correlation between density and

location (as given by the sample numbers). Further, tensile strength decreases with increasing sample density, which is the opposite of what would be expected if damage was present. This evidence suggests that the observed variations in tensile strength with orientation are not the result of sample damage.

The influence of the low-dipping fabrics (an inseparable combination of compositional layering, mineral alignment and natural microcracks) on tensile strength is examined in Figure 62. Tensile strength parallel to the preferred orientation of these structures is up to 70% of that measured perpendicular to these structures.

Table 18.
Brazilian test results
Fine Grained Granite from boreholes 421-032-RT1, 2, 3, 4.

Borehole	Sample	Density	Loading angle relative to low-dipping compositional layering	Minimum Tensile Strength (Crack Initiation) (MPa)	Maximum Tensile Strength (Failure) (MPa)
RT1	D	2.64	90		3.01
	A	2.59	57		3.26
	B	2.64	70		2.26
	C	2.65	70		2.76
RT2	A	2.66	30		2.50
	B	2.61	65		3.00
	C	2.67	75		1.91
	D	2.66	80	1.34	2.79
	F	2.65	70		2.21
	E	2.65	45		3.12
RT3	A	2.64	0		
	B	2.64	0		2.12
	C	2.64	52		2.38
	D	2.62	25		1.65
	E	2.65	25		2.86
RT4	A	2.62	45		2.82
	B	2.65	70		2.66
	C	2.63	45		2.14
	D	2.62	20		1.98
	E	2.64	80		1.84
	F	2.63	80		2.68

Figure 08-08.cdr

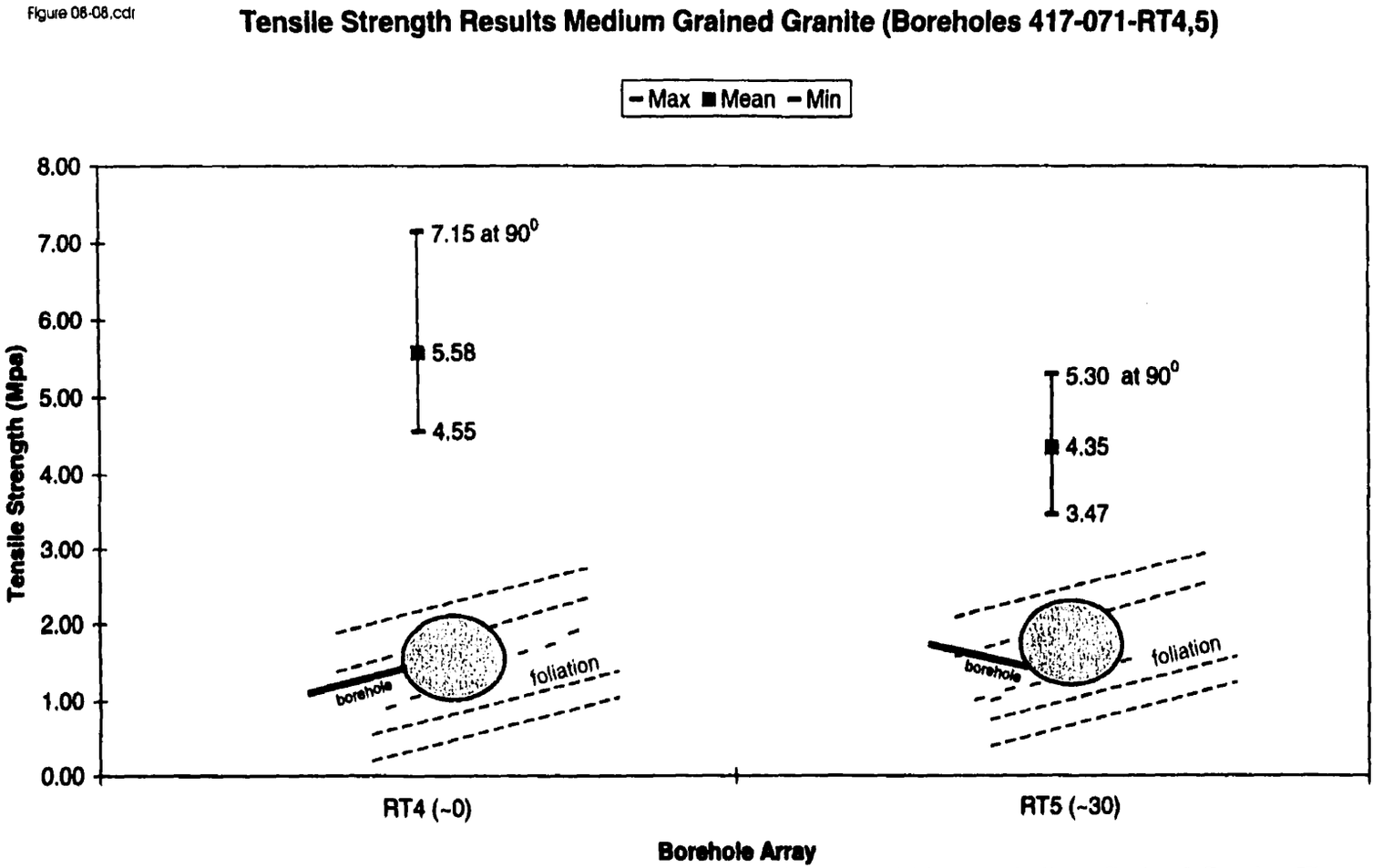

Figure 60. Summary statistics for the Brazilian tests from the entire borehole array within the Medium Grained Granite. The array includes boreholes 417-071-RT4 and 5. These were arranged in a vertical plane, and oriented to intersect the subvertical flow banding at angles of ~45°, and ~00°, respectively. The data from each borehole includes loading orientations ranging from 0° to 90° to the foliation in each borehole. This was done to test for systematic variation within the horizontal plane, or put in another way - to examine the affect of borehole orientation when sampling for rock properties testing. The results indicate that there is significant direction -dependent anisotropy.

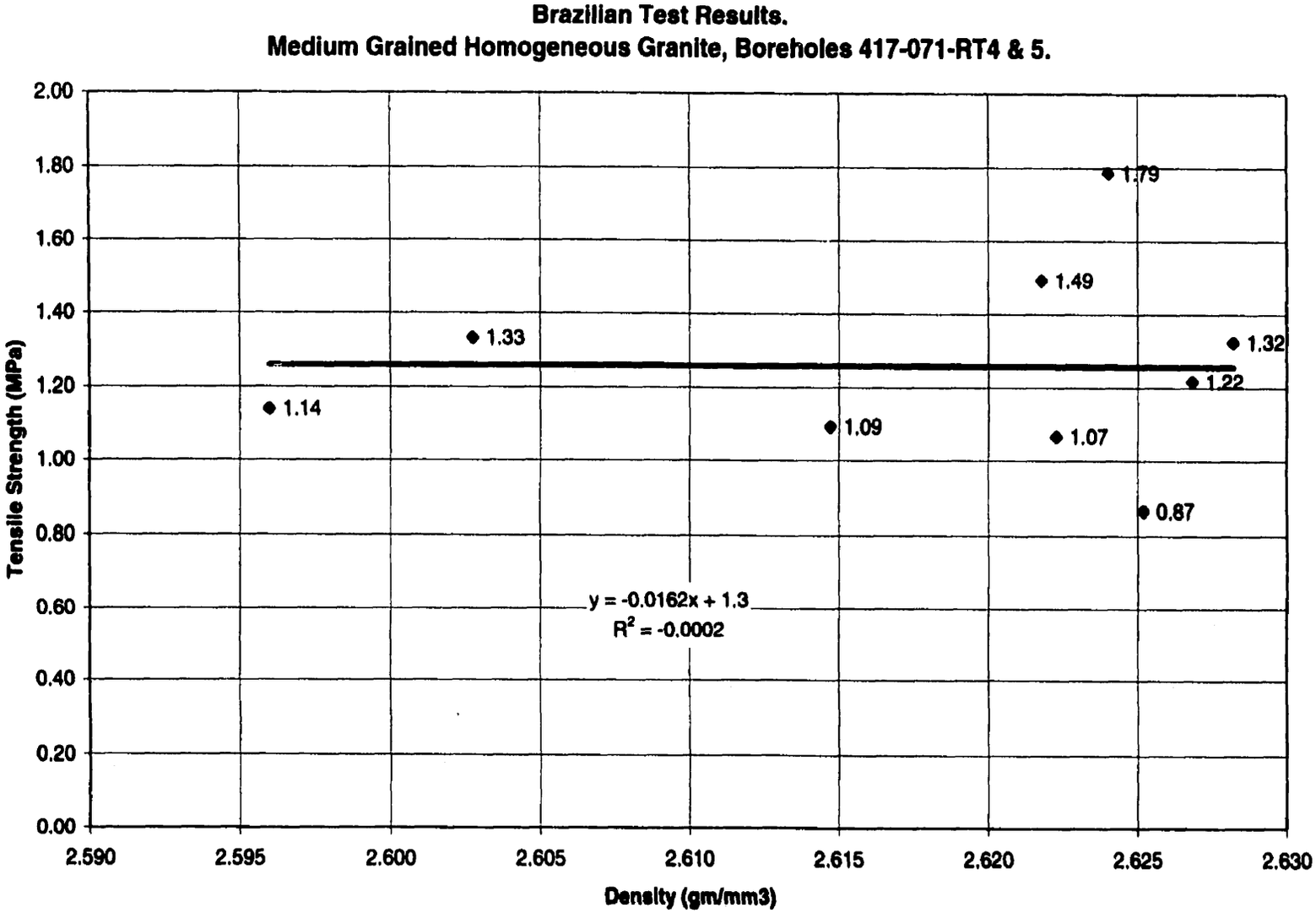

Figure 61. Brazilian test results for the Medium Grained Granite from boreholes 417-071-RT4 and 5. Variation in the estimated tensile strengths of each sample against the corresponding sample density. There is no correlation between density and location (as given by the sample numbers). Tensile strength decreases with increasing sample density, which is the opposite of what would be expected if damage was present.

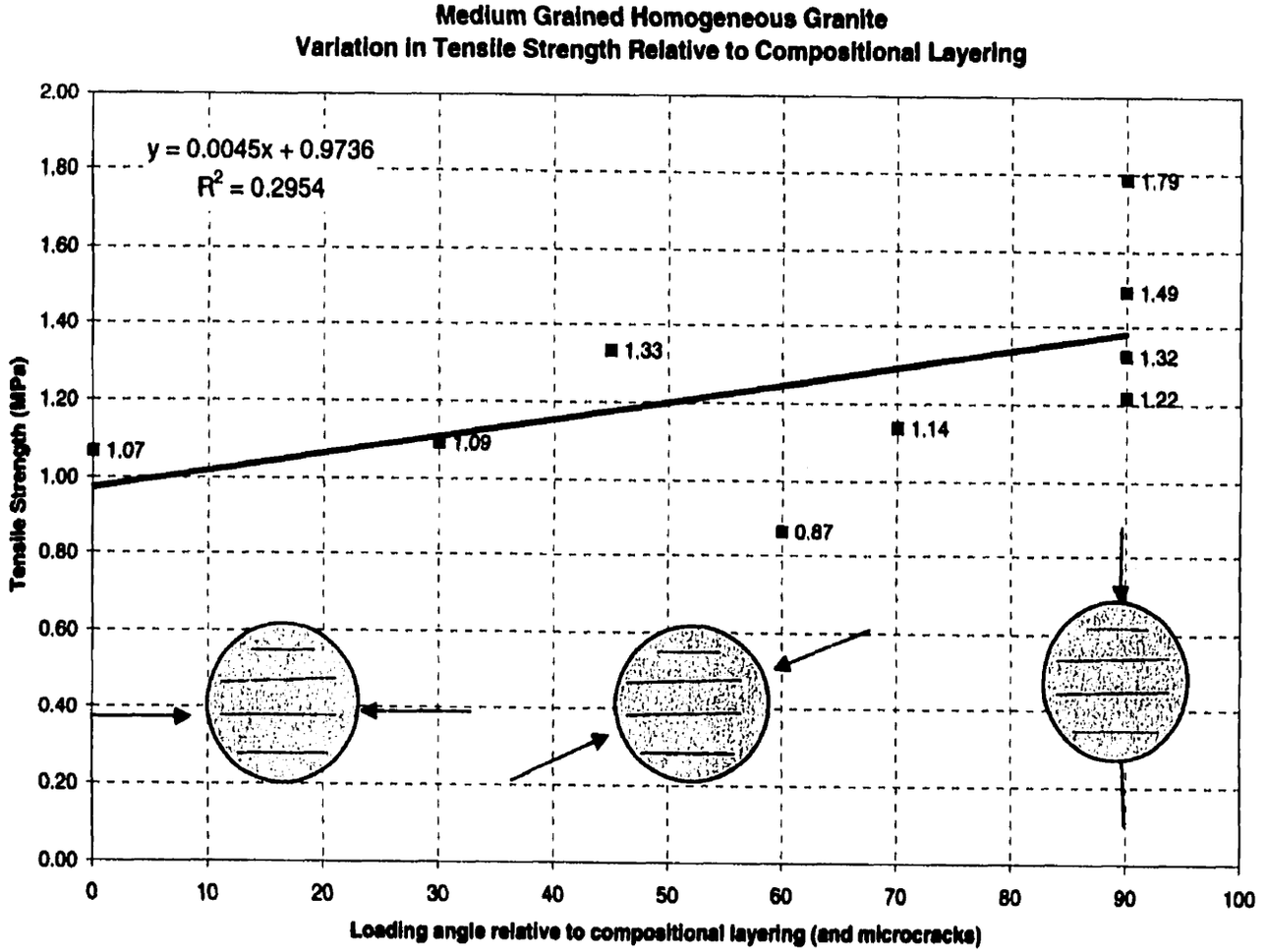

Figure 62. Brazilian test results for the Medium Grained Granite from boreholes 417-071-RT4, and 5. Variation in the estimated tensile strengths of each sample against the inclination of the loading axis relative to the compositional layering. The three insets show the relative orientation of the loading axis (arrows) relative to the flow banding as seen in a cross section of the core. The best-fit linear regression curve, the equation for the curve, and the R^2 correlation coefficient are included.

8.6. Coarse Grained Granite, Borehole 418-051-RT 2, 3, 4, 5.

Brazilian test results for the Coarse Grained Granite from boreholes 417-071-RT 2, 3, 4, 5 are summarized in Table 20. This summary includes, for each sample, the loading axis angles relative to structure, and two calculated tensile strengths for each sample. The first strength (min.) includes values in which audible cracking (fracture initiation) preceded failure. Six samples were effected. These samples do not appear to be anomalous in shape (finishing), texture or in terms of their orientation and location.

Summary statistics for the Brazilian tests from the entire borehole array within the Medium Grained Granite are shown in Figure 63. The array of boreholes was arranged in a vertical plane, and oriented so as to intersect the low-dipping fabric elements, an inseparable mixture of compositional layering, mineral foliation, and natural microcrack, at angles of ~90°, ~30°, ~ 15°, and ~00°, respectively. The data from each borehole includes loading orientations ranging from 0° to 90° to the foliation in each borehole, but have been averaged together here as if the rockmass was massive. This was done to test for systematic variation at the metre-scale, or put in another way - to examine the affect of borehole orientation when sampling for rock properties testing. The results indicate that there is significant direction -dependent anisotropy.

To determine if this trend is a function of varying degrees of sample damage, the tensile strength for each sample was plotted against its density (Figure 64). The tensile strength of the sample suite increases with increasing density, which is the opposite of what is seen in the other rock types. However, this does not appear to be attributable to damage,

but rather to the marked differences in composition and degree of banding/ foliation that occur at the array scale. This conclusion is supported by the fact that there is no decline in sample density and strength with proximity to either the borehole collar, or to areas of known stress concentration.

The influence of the low-dipping compositional layering on tensile strength is presented in Figure 65. The tensile strength is lower when the loading axis is parallel to the low-dipping fabric. The scatter in the data reflects the compositional heterogeneity noted earlier, and is indicated in this figure by the symbols used for each data point. Strength anisotropy in this rock type is marked. The tensile strength varies from a low of approximately 1 MPa in the plane of the layering, to approximately 2 MPa normal to this plane. (4 and 10 MPa, respectively using Equation 1 from p. 180).

Audible crack initiation was heard more frequently in this rock type than in the others types combined. The samples affected do not have any obvious characteristic in common. The phenomena occurred over the whole range of borehole orientations, loading angles. There does not appear to be any correlation with distance from the excavation, and any stress release phenomena that would be associated with proximity. Incipient discing is not a factor as any discing fractures would be unfavorably oriented for propagation under the diametric line loading of Brazilian tests.

Table 19.
Brazilian Test Data
Medium Grained Granite (Borehole 417-071-RT4, 5)

Borehole	Sample	Density	Loading angle relative to low-dipping compositional layering	Minimum Tensile Strength (Crack Initiation) (MPa)	Maximum Tensile Strength (Failure) (MPa)
RT1, 2,3	- not suitable due to core discing -				
RT4	A	2.62	90°		1.49
RT4	B	2.60	90°		1.79
RT4	C	2.60	70°	0.91	1.14
RT4	D	2.63	45°		1.33
RT4	A'	2.62	90°	1.03	1.22
RT5	A	2.63	90°		1.32
RT5	B	2.61	30°		1.09
RT5	C	2.62	0°	0.87	1.07
RT5	D	2.63	60°		0.87

Table 20.
Brazilian Test Data.
Coarse Grained Granite (Borehole 418-051-RT2,3,4,5)

Borehole	Sample	Density	Loading angle relative to low-dipping compositional layering	Minimum Tensile Strength (Crack Initiation) (MPa)	Maximum Tensile Strength (Failure) (MPa)
RT1	- not suitable due to core discing -				
RT2	A	2.67	90°		1.70
	B	2.70	75°		1.75
	C	2.68	90°		2.07
	D	2.67	0°		1.49
	E	2.66	45°		1.69
	F	2.68	0°		1.11
	G	2.63	10°		1.17
	H	2.67	0°	0.60	1.39
RT3	B	2.70	45°		1.45
	C	2.69	75°	0.67	2.01
	D	2.67	90°		2.53
	E	2.70	85°		2.49
	F	2.71	0°		1.88
	A'	2.68	55°		1.56
	G	2.65	60°	0.60	1.65
RT4	A	2.61	50°		0.96
	B	2.59	45°		1.21
	C	2.60	45°		1.04
	D	2.56	15°		1.33
	E	2.60	20°		1.53
	F	2.60	38°	0.62	0.88
	G	2.61	52°	0.54	1.42
RT5	A	2.62	0°		0.93
	B	2.54	25°	0.52	1.18
	C	2.65	45°		1.52
	D	2.64	85°		1.65

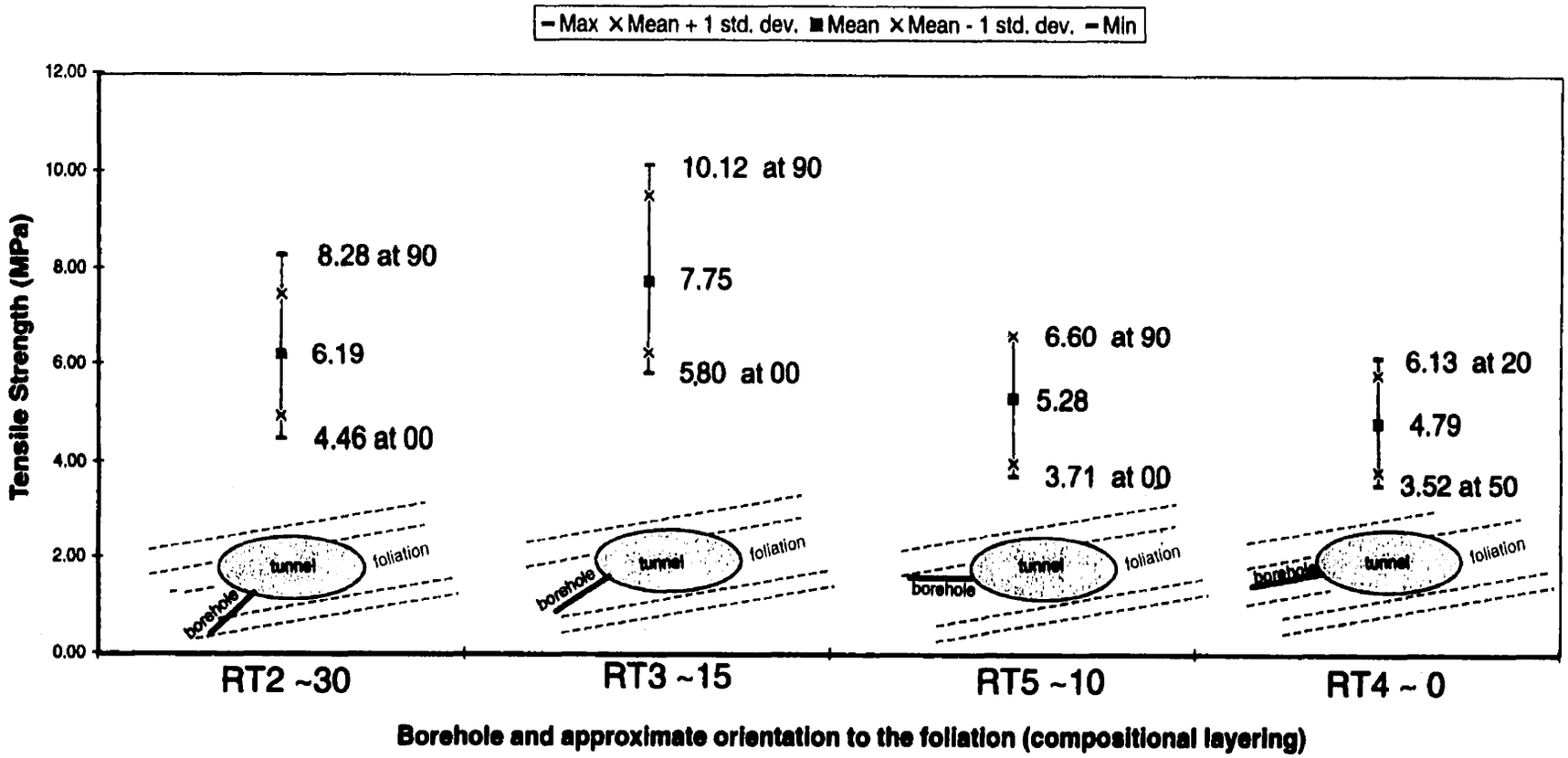

Figure 63. Summary statistics for the Brazilian tests from the entire borehole array within the Coarse Grained Granite. The array includes boreholes 418-051-RT1, 2, 3, 4. These were arranged in a vertical plane, and oriented so as to intersect the compositional layering at angles of ~90°, ~30°, ~15°, ~ 0°, and ~10°, respectively as shown by the schematic illustrations - (the tunnel profile is represented by the ellipse, a xenolithic zone by the grey shading, the layering by the light grey dashed lines, and the boreholes by the solid lines Note: the near-vertical borehole RT1 was not useable due to discing). The data from each borehole includes loading orientations ranging from 0° to 90° to the foliation in each borehole. This was done to test for systematic variation within the vertical plane, or put in another way - to examine the affect of borehole orientation when sampling for rock properties testing. The results indicate that there is significant direction -dependent anisotropy in tensile strength.

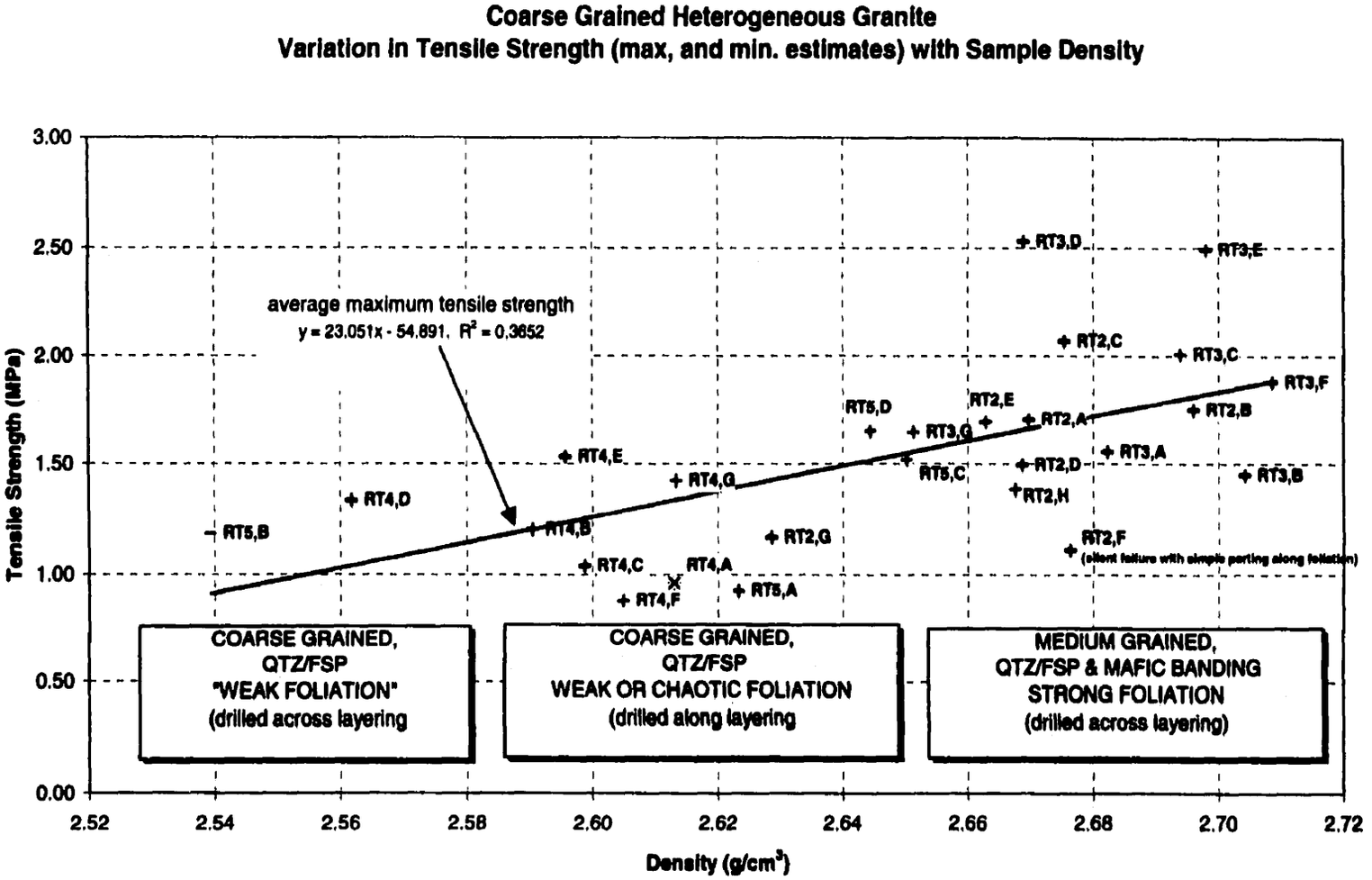

Figure 64. Brazilian test results for the Coarse Grained Granite from boreholes 418-051-RT2, 3, 4, and 5. Variation in the estimated tensile strengths of each sample against the corresponding sample density. This suite differs from the fine and medium grained granites in that tensile strength increases with increasing density. This does not however, suggest sample damage, as there is no correlation between strength and the depth of the sample from the borehole collars. Instead, this relationship appears to be due to a combination of factors, including the orientation of the borehole relative to the layering, and to differences in rock composition and degree of fabric development as indicated in the boxes above.

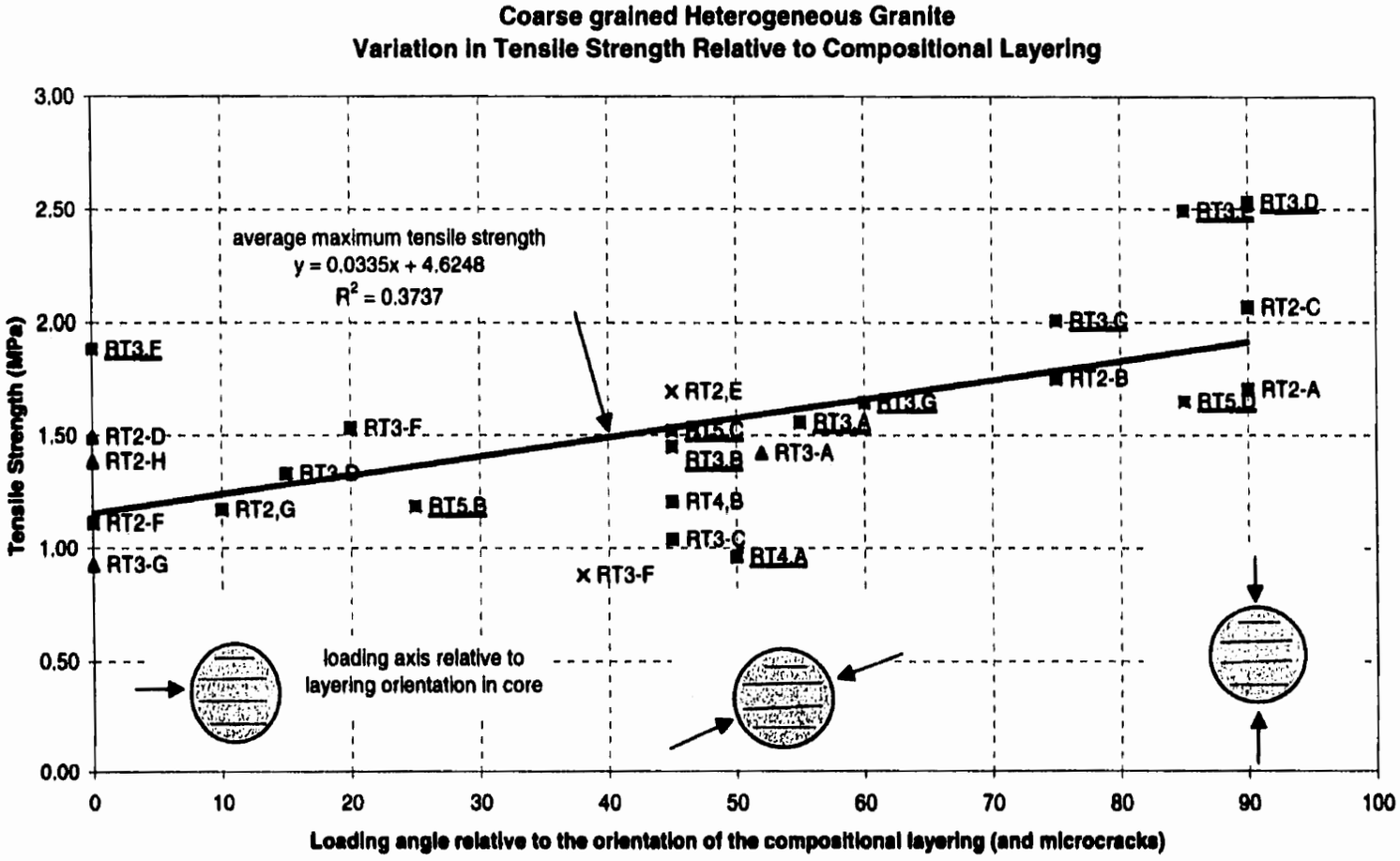

Figure 65. Brazilian test results for the Coarse Grained Granite from boreholes 417-071-RT2, 3, 4, and 5. Variation in the estimated tensile strengths of each sample against the inclination of the loading axis relative to the low-dipping compositional layering. The three insets show the relative orientation of the loading axis (arrows) relative to the flow banding as seen in a cross section of the core. The best-fit linear regression curve, the equation for the curve, and the R^2 correlation coefficient are included. Tensile strength is lowest when splitting occurs along the plane of the foliation. The scatter in the data reflects the compositional heterogeneity noted earlier, and is indicated in this figure by the following symbols (■- sample has obvious compositional banding and mineral foliation, ▲ - sample has mineral alignment only, X - sample appears nearly massive or has a chaotic or folded foliation).

8.7. Summary and Conclusions from the Brazilian Tests

The Brazilian tests reveal that tensile strength varies with average grain size, and is also anisotropic, being dependent upon the orientation of loading relative to the fabrics in each granite.

The tensile strength in the fine grained granite varies with the orientation of the sampling borehole, and on the orientation of loading relative to the fabric in each sample. Directional anisotropy in strength is most noticeable in the vertical plane. In this case, the tensile strength measured in the plane of natural microcracks is approximately 65% of that measured normal to the microcracks. In the horizontal plane, the tensile strength is lowest when loading is parallel to the flow banding, and greatest when normal to this structure.

The medium grained granite shows directional anisotropy in tensile strength, which may be correlated with the rock mass fabric. Tensile strength parallel to the preferred orientation of the low-dipping layering and natural microcracks is ~ 70% of that measured perpendicular to these structures.

The coarse grained granite is the most heterogeneous of the rock types tested. A low-dipping fabric dominates its structure at the tunnel and the hand specimen scales. This fabric includes a largely concordant assemblage of compositional and textural layering, an alignment of biotite and feldspar laths, and a preferred orientation of natural microcracks in quartz. This fabric induces a marked directional anisotropy, with the

Brazilian tensile strength parallel to the layering being ~ 40% of that measured normal to this plane.

The correction for calculation of the Brazilian test recommended by Chen (1993) reduces the calculated strengths by approximately 50%, but does not affect the presence of directional anisotropy in tensile strength, or their correlations with rock fabric.

Chapter 9

UNIAXIAL COMPRESSION TESTS

9.1. Introduction

This chapter summarizes the uniaxial compression testing conducted to define strength anisotropy related to the textural and structural variations in the Lac Du Bonnet Batholith. The purpose of this test is to measure the ultimate compressive strength of a cylindrical rock sample loaded axially. The axial deformation of the specimen is also measured to obtain information on the deformation and failure characteristics of the rock substance to its ultimate strength.

9.2. Rock Type and Specimen Preparation

As noted earlier, three distinct textural varieties of the Lac Du Bonnet granite, differing in type and orientation of foliation were identified and selected for testing. Eleven samples were obtained from the boreholes listed in Chapter 1. All samples are segments of HQ-sized core (46 mm diameter), the choice of specimen diameter being largely dictated by budget constraints. Specimens were prepared in accordance with the procedure described in the Pit Slope Manual Supplement 3-5 (Gyenge and Ladanyi, 1977; and Gyenge, 1980) and the method suggested by the International Society for Rock Mechanics (Brown, 1981). The end surfaces of each of the specimens were ground flat to 0.015 mm to ensure that they were parallel to each other and perpendicular to the axis of the specimen.

9.3. Test and Apparatus And Procedure

For each sample, axial and lateral strains induced during compression were provided by the attached strain gauges. All samples were loaded, parallel to their long axis, in the testing apparatus at the Canadian Mine Technology Laboratory, Mining Research Laboratories, CANMET, Energy, Mines and Resources Canada in Ottawa. For a detailed description of the testing apparatus and its operation, the reader is referred to Gorski (1987). The data records for each specimen were saved as ASCII text files, and included the time (sec), load (MPa), and corresponding axial and lateral strains. Loading was continuous rather than cycled. As the peak strength of the specimen was approached, loading was closely monitored to prevent rapid failure.

9.4. Presentation Of Results

The data obtained in this experiment were compiled as follows:

1. Stress-strain data tables for each sample, which list the axial, lateral and volumetric strains recorded for each strain gauge by the data acquisition system, under accumulating load. Volumetric strain was computed by using the following equation:

$$\varepsilon_v = \varepsilon_a + 2\varepsilon_c$$

where ε_v = volumetric strain, ε_a = axial strain, and ε_c = circumferential strain.

2. Stress-strain diagrams for each sample, showing the axial, lateral and volumetric strains under accumulating loads.
3. Summary tables listing the tensile strength (from the Brazilian tests), and the values for crack closure, the onset of dilatancy (yield stress), and the peak load failure

obtained by inspection of the stress-strain curves, as described in the following section.

4. Summary charts depicting the tensile strength (from the Brazilian tests), and the values for crack closure, the onset of dilatancy (yield stress), and the peak load failure obtained by inspection of the stress-strain curves, as described in the following section.

The data readings (1) and stress-strain diagrams (2) are provided in Appendix C, while the summary tables (3) and summary charts (4) are presented in this Chapter.

9.5. Interpretation of Stress-strain Curves

Figure 66 illustrates the general stress-strain characteristics for the Lac du Bonnet granite under uniaxial compression. When an applied load exceeds the rock strength, bonds break and separate and a fracture (or microcrack) is formed with an attendant release of energy. For brittle rocks, under tensile conditions, the initiation of cracking coincides with failure. However, under compressive loading, crack initiation occurs well before failure. Bieniawski (1967a,b) identified five stages of crack development on brittle rock (also Goodman, 1989).

1. Crack closure: Grain boundaries act as, or may contain, microcracks. Microcracks can also exist within grains especially if stress-relief or previous loading has occurred. This first stage of loading involves the closure of microcracks which are not parallel to the applied stress. This increases the modulus of elasticity of the rock and produces a non-linear stress-strain curve. This region is more prominent for tests performed at low confining pressures than those performed at high confining

pressures, typical for rock samples obtained from the 420 Level of the URL, due to the presence of stress-induced microcracks in those samples.

2. Linear elastic deformation: This stage follows crack closure, and is noted by a linear "straight line segment of both the axial and lateral strain curves, the sample approximating linear elastic behavior.

3. Crack initiation: During the active loading of each specimen, "... a change from a deformation that is elastic and therefore recoverable to one that involves permanent deformation occurs at a point where the initially linear stress versus lateral strain, or stress versus volumetric strain curve deflects from its initial, linear trend ..... From this point on, the rate of lateral strain increases above what can be attributed to purely elastic deformation. The point of deflection is the "crack initiation point". More than one crack initiation point can occur in a given specimen, due to the contribution of different mineral phases, or to grain or sub-grain scale heterogeneities..." (Lajtai, 1982).

4. Stable crack propagation: Existing cracks extend and new cracks can nucleate. As the cracks develop parallel to the major principal stress, the strain gauges oriented along the specimen axis (axial) still produce a linear response while those oriented laterally produce a non-linear response. The volumetric strains also become non-linear at this time. The point of crack initiation varies with rock type ad structure, but a range of 40-50% of the peak strength is common for brittle rock.

5. Unstable crack growth: Also referred to as the onset of dilatancy, this point in the loading curve, occurs at approximately 80% of the peak strength. It is marked by a relatively sudden change in the pattern of propagating cracks, by reversal of the sign

of volumetric strain, with a rapid increase in volume. There is permanent lateral (circumferential) and volumetric strain on loading.

6. Failure: In this region, crack formation, crack growth and sliding on existing crack interfaces results in a decrease of the slope of each of the strain curves. Failure of the specimen is the peak stress achieved which is easily noted by a decrease in axial strain on the stress-strain curve. The final post-peak stage is denoted by decreasing stress (i.e. not load-bearing).

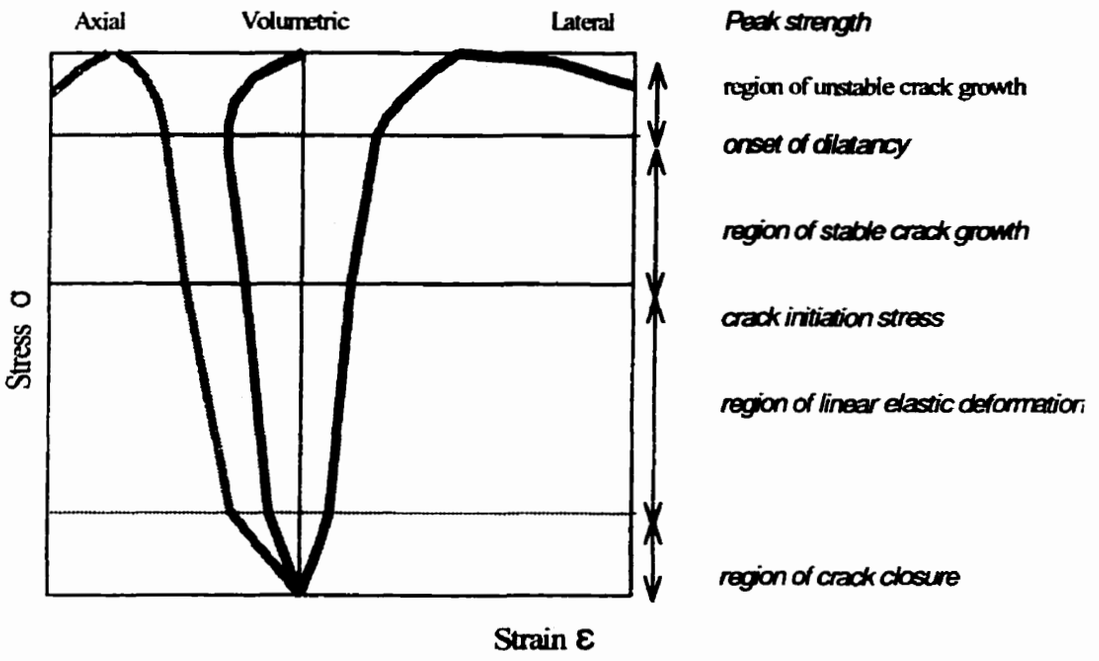

Figure 66. Idealized stress-strain diagram for a brittle rock with the stages of brittle deformation as represented by the axial, volumetric and lateral stress-strain curves.

9.6. Summary of Observations

The results of the uniaxial compression tests are presented in the summary charts which show: 1) the influence of grain size, and 2) the influence of loading angle relative to the dominant fabric element. Crack closure, the onset of stable crack growth (also referred to as the onset of dilatancy), and the peak load at failure all vary in a systematic manner with the average grain size of the rock, and with rock mass fabric.

9.6.1. Influence of Grain Size

The relative minimum rock strength data are listed in Table 21, and are shown in Figures 67, 68 and 69 for each of the fine, medium and coarse grained granites. The stresses corresponding with crack closure, the onset of dilatancy and the peak load failure were determined from the stress / strain curves in Appendix C. The data for the very coarse granite is from Everitt (1995).

Strength decreases as the grain size and heterogeneity of the granite increases (Figure 67). This trend is shown best by the minimum estimates for each of the various measures of strength. This trend is obscured by the specimen-scale heterogeneity in the coarser granites, where the mean and maximum strengths are more variable (Figures 68 and 69). In other words, depending on the location and orientation of the borehole, the coarsest granite can be either weaker than, or stronger than, the medium grained granite.

9.6.2. Influence of Rock Fabric

Anisotropy of the various measures of compressive strength as a function of rock fabric is presented in Table 22 and in Figures 70, 71 and 72. The "measures" referred to here include: the peak load at failure, the onset of dilatancy, the crack initiation point, the

crack closure stress, and the average tensile strength. The average tensile strength was obtained from the Brazilian tests. The values for crack closure, crack initiation, the onset of dilatancy and the peak load failure were determined from inspection of the individual stress / strain curves in Appendix C. There is insufficient data to review the influence of fabric in the medium grained granite on compressive strength.

Anisotropy of compressive strength related to rock fabric, is most strikingly displayed by the fine grained granite (Figure 70). In this rock, each of the various measures of rock strength decrease together in a systematic manner as the orientation of the sampling borehole, (and therefore the axis of the test specimen) rotates towards parallelism with the strike of the rock unit contact. The weakest direction correlates with the strike of the dykes and of rare subvertical fractures found at this level.

Directional anisotropy is also evident in the coarse grained granite, although its relationship to the rock fabric requires more explanation. The variation, with orientation, of the compressive (and tensile) strengths for the coarse grained granite is shown in Figure 71. Inspection of this figure indicates that samples are weakest in compression when the centimetre- to decimetre –scale layering intersects the sample axis at an angle between 20° and 40°. The rock is stronger (at the specimen scale) when the sample is within the plane of layering, or sharply inclined to it. This interpretation is consistent with field observations and with the Point Load and Brazilian tests, in that the contacts between layers provide more clearly defined and continuous weakness planes, than those structures that would promote axial splitting of the specimens (i.e. grain alignment or

natural microcracks) at the test-specimen scale. Similar results were obtained from the tests for the medium-grained granite (Figure 72).

For this coarsely layered medium grained granite, the various measures of strength were lowest when the layering, and the subparallel natural microcracks, were inclined 30 degrees to the loading axis.

9.6.3. Summary and Conclusions from Uniaxial Compression Tests

The uniaxial compression tests conducted in this study reveal that the compressive strength varies with average grain size, and with the direction of loading relative to the dominant fabric present in each sample. Directional anisotropy, related to different types of fabric elements, exists to a significant degree in each of the three rock types. The minimum estimates for peak load strength for the fine, medium, coarse, and very coarse grained granites are 168, 155, 125, and 120 MPa, respectively.

Table 21
Summary tables of peak load failure and other strength measures (in MPa) as determined by manual inspection of the stress-strain curves. (tensile strength data from Brazilian tests).

Minimums

	Very coarse granite	Coarse granite	Medium granite	Fine granite
Peak load failure	120	125	155	168
Onset of dilatancy	80	92	96	100
Microcrack closure	20	16	22	40
Tensile strength	3.5	3.7	3.5	4.6

Means

	Very coarse granite	Coarse granite	Medium granite	Fine granite
Peak load failure		158	161	193
Onset of dilatancy		110	100	128
Microcrack closure		18	23	40
Tensile strength		6.8	5	6.3

Maximums

	Very coarse granite	Coarse granite	Medium granite	Fine granite
Peak load failure		183	166	210
Onset of dilatancy		128	104	150
Microcrack closure		20	24	40
Tensile strength		10.1	7.1	9.1

Table 22
Uniaxial Compression Testing Summary by Rock Type and Borehole (in MPa)
(tensile strength data from Brazilian tests)

Fine grained granite

Minimums	421-032-RT1	421-032-RT2	421-032-RT3	421-032-RT4
	*75**	*50**	*35**	*10**
Peak load failure	210	196	168	120
Onset of dilatancy	150	136	108	*88*
Crack initiation	130	120	82	60
Microcrack closure	40	40	40	28
Average tensile strength	9.1	8.7	8	7.9

Medium grained granite

Minimums	403-014-MB2	417-071-RT4	417-071-RT5
	*53**	*0**	*30**
Peak load failure	166	163	155
Onset of Dilatancy	92	104	95
Crack initiation	75	90	60
Microcrack closure	23	32	24
Average Tensile strength	5	5	5

Coarse grained granite

Minimums	418-051-RT2	418-051-RT3	418-051-RT4	418-051-RT5
	*40**	*20**	*0**	*15**
Peak load failure	140	125	183	183
Onset of Dilatancy	92	96	128	126
Crack initiation	72	84	96	100
Microcrack closure	16	16	20	20
Tensile strength	4	4	4	4

Note: The angle between the borehole and the dominant rock structure is indicated in italics below each borehole name.

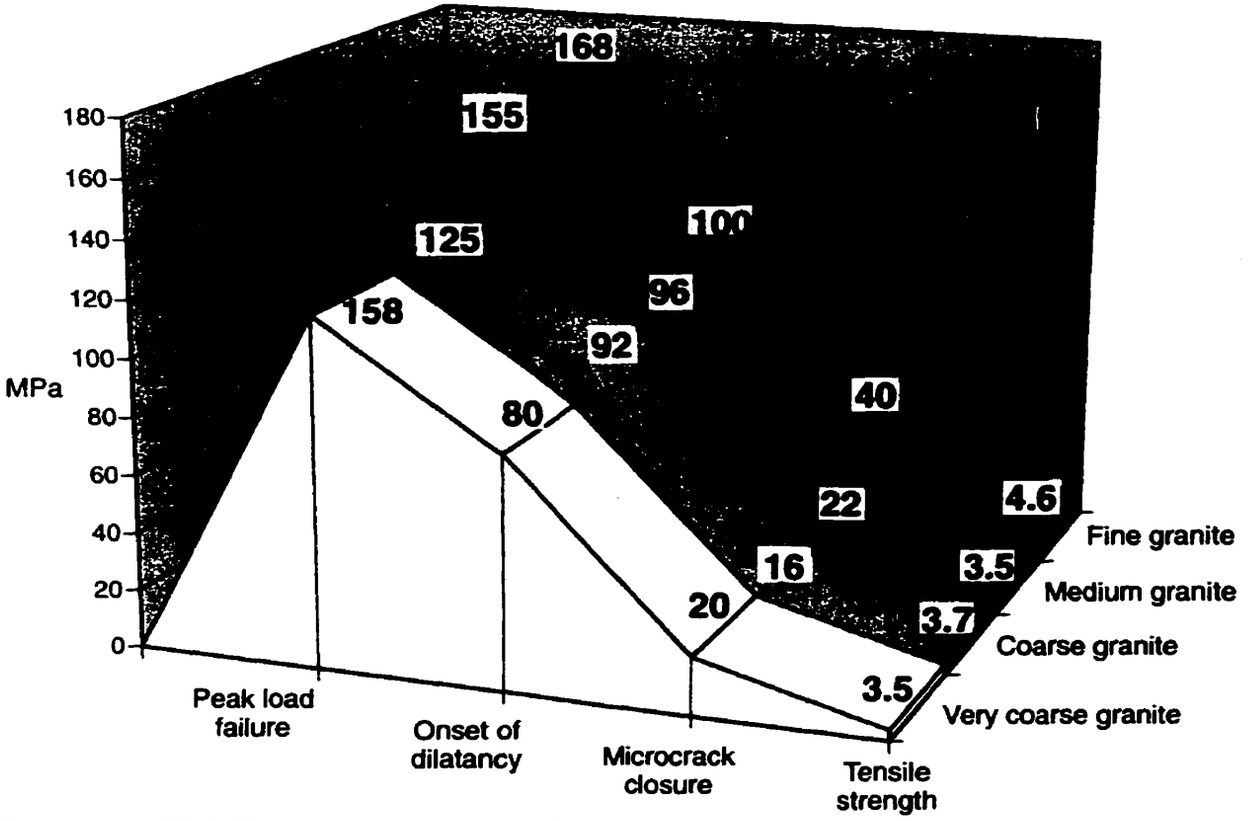

Figure 67. X-Y-Z comparison chart of the minimum uniaxial compression and (Brazilian) tensile strengths of the 3 rock types. The stresses corresponding with crack closure, the onset of dilatancy and the peak load failure were determined from the stress / strain curves in Appendix C. The data for the very coarse granite is from Everitt (1995). The figure clearly indicates that the various measures of strength decrease as the grain size and heterogeneity of the granite increase. Compare with Figures 68 and 69 showing the mean and maximum Uniaxial Compression and (Brazilian) Tensile Strengths, respectively.

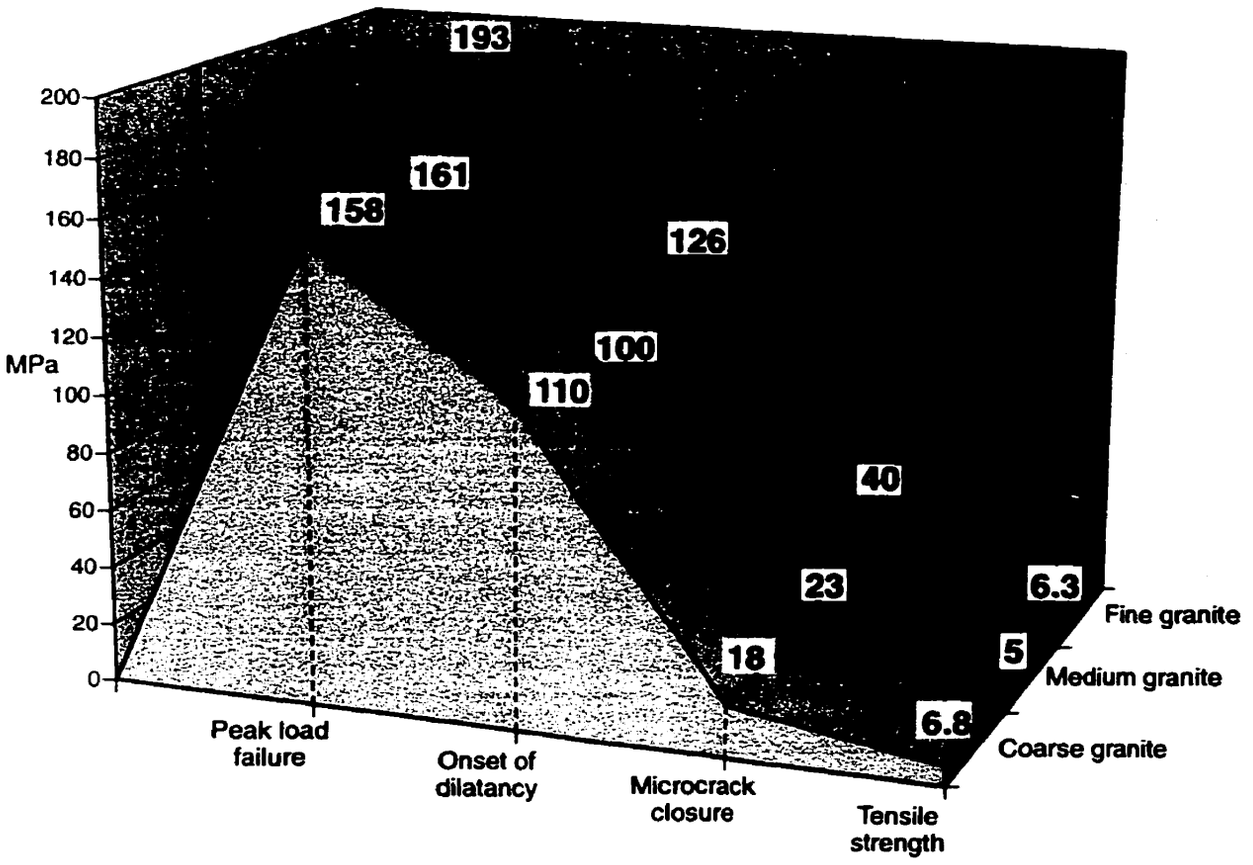

Figure 68. X-Y-Z comparison chart of the mean uniaxial compression and (Brazilian) tensile strengths of the 3 rock types. The stresses corresponding with crack closure, the onset of dilatancy and the peak load failure were determined from the stress / strain curves in Appendix C. The data for the very coarse granite is from Everitt (1995). The figure clearly indicates that the various measures of strength decrease as the grain size and heterogeneity of the granite increase. Compare with Figures 67 and 69 showing the minimum and maximum Uniaxial Compression and (Brazilian) Tensile Strengths, respectively.

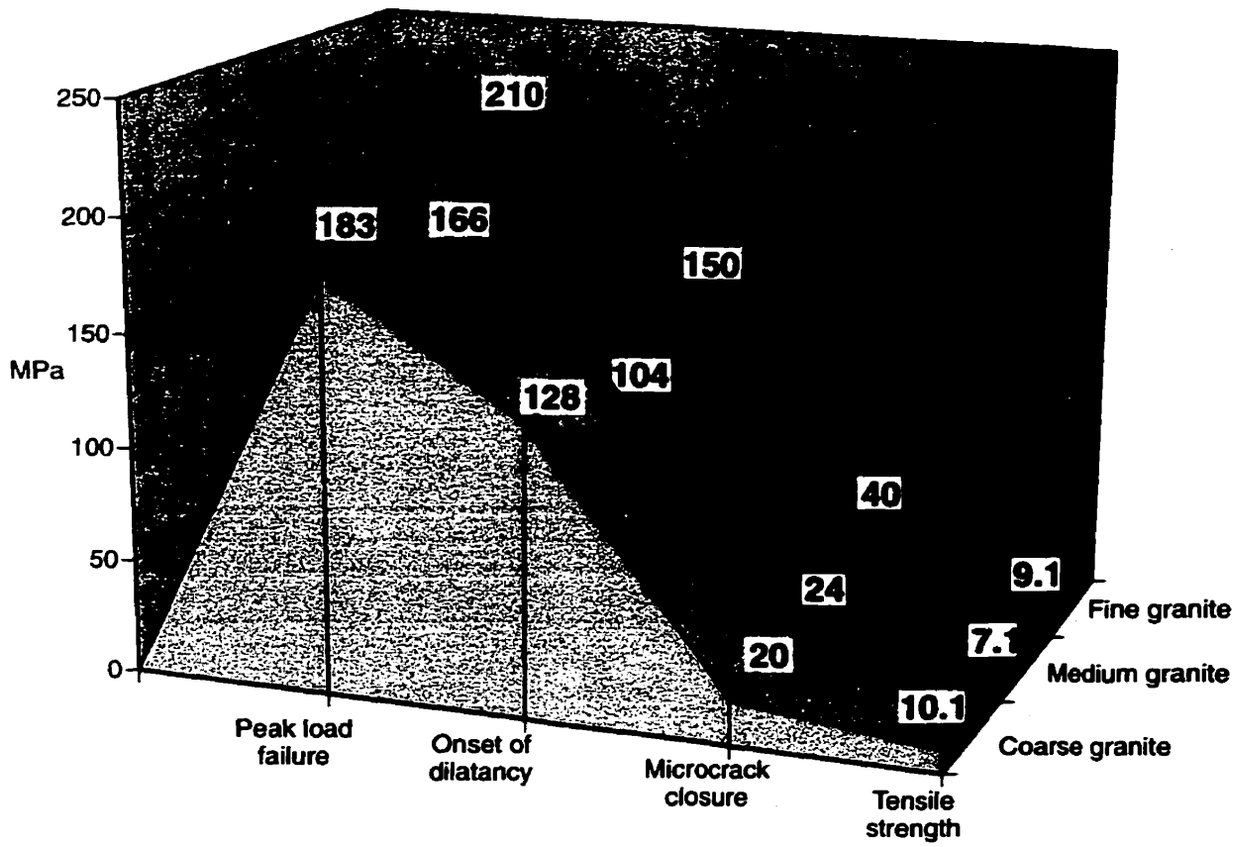

Figure 69. X-Y-Z comparison chart of the maximum uniaxial compression and (Brazilian) tensile strengths of the 3 rock types. The stresses corresponding with crack closure, the onset of dilatancy and the peak load failure were determined from the stress / strain curves in Appendix C. The data for the very coarse granite is from Everitt (1995). As was shown in Figure 67 (minimum values), the various measures of strength decrease as the grain size and heterogeneity of the granite increase. This trend is obscured by the specimen-scale heterogeneity in the coarser granites, where the mean and maximum strengths are more variable (Figure 68 and 69). In other words, depending on the location and orientation of the borehole, the coarsest granite can be either weaker than, or stronger than, the medium grained granite.

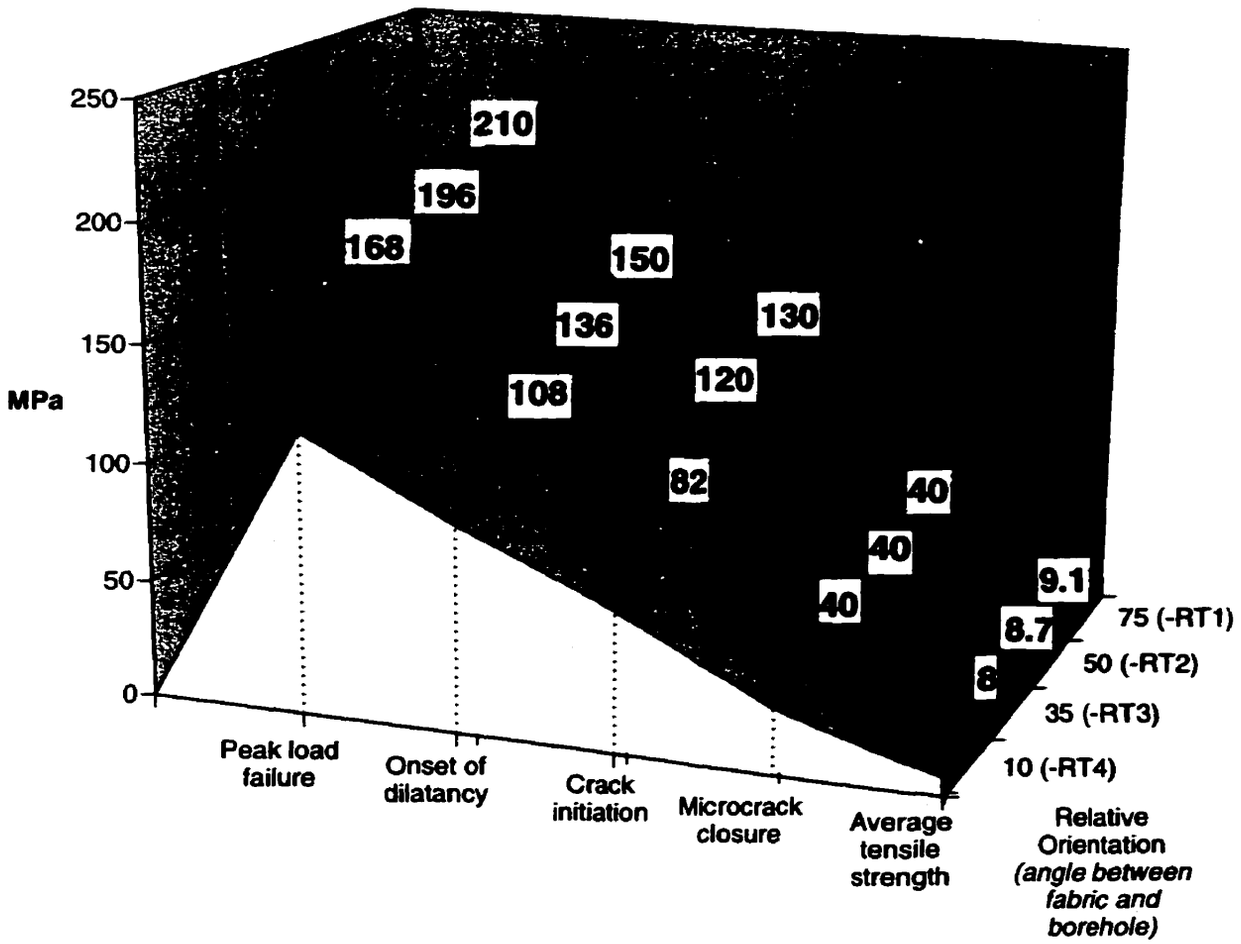

Figure 70. Anisotropy of compressive strength related to rock fabric, is most strikingly displayed by the fine grained granite. This figure compares the variation in the various strength estimates with orientation. Orientation refers to the angle between the strike of the dyke and the sampling boreholes, which ranges from 10°, 35°, 50°, and 75° in boreholes –RT4, - RT3, - RT2 and - RT1, respectively. The values for the peak load failure, onset of dilatancy, crack initiation, and microcrack closure are derived from the uniaxial compression data (stress /strain curves) in Appendix C. The tensile strength is from the Brazilian tests. In this rock, each of the various measures of rock strength decrease together in a systematic manner as the orientation of the sampling borehole rotates towards parallelism with the strike of the rock unit contact. The weakest direction correlates with the strike of the dykes and of rare subvertical fractures found at this level.

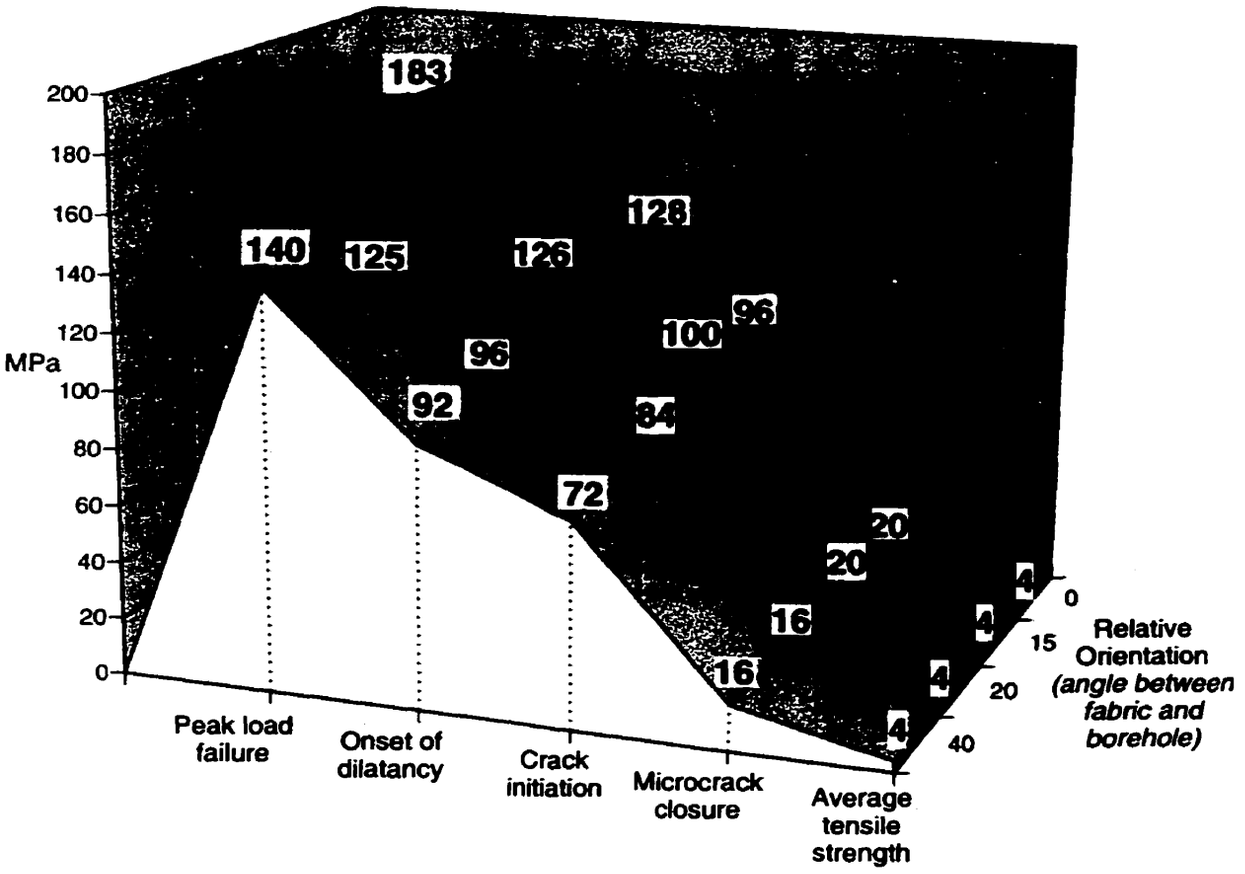

Figure 71. Influence of low-dipping fabric on rock strength for the coarse grained granite. This figure compares the variation in the various strength estimates with orientation. The values for the peak load failure, onset of dilatancy, crack initiation, and microcrack closure are derived from the uniaxial compression data (stress /strain curves) in Appendix C. The tensile strength is from the Brazilian tests.

The data presented in this figure clearly indicate that directional anisotropy is also evident in the coarse grained granite. In the coarse grained granite, samples are weakest in compression when the centimetre- to decimetre –scale layering intersects the sample axis at an angle between 20° and 40°. The rock is stronger (at the specimen scale) when the sample is within the plane of layering, or sharply inclined to it.

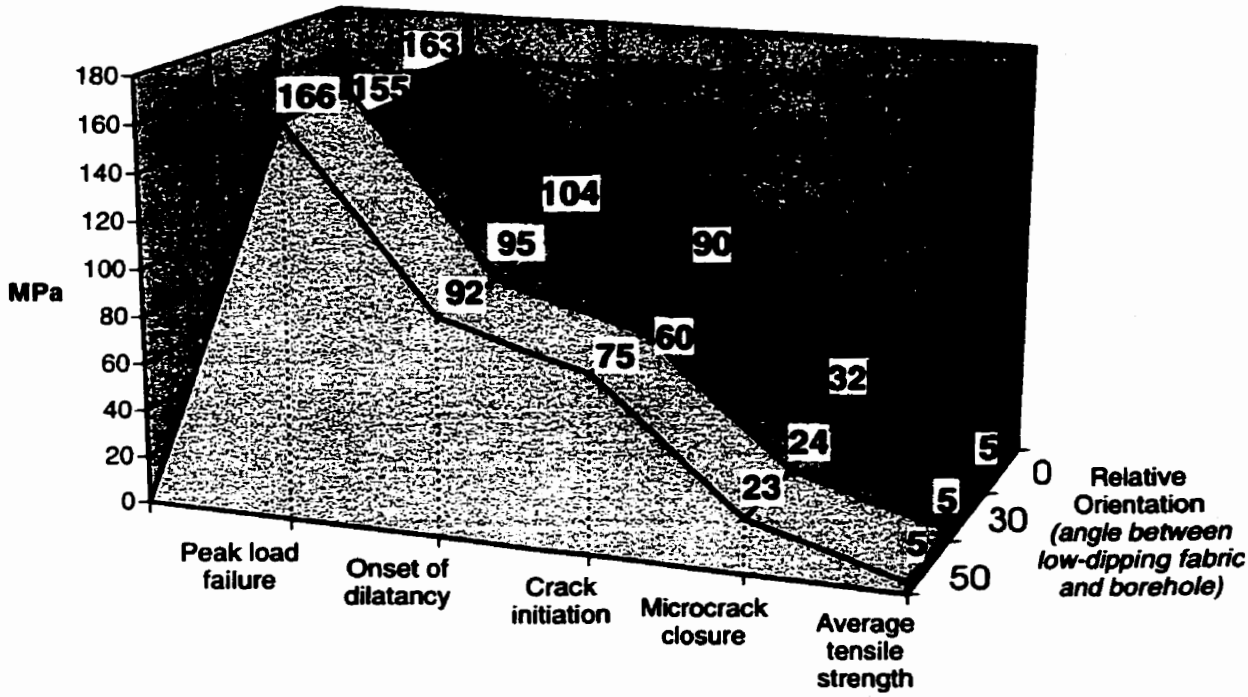

Figure 72. Influence of low-dipping fabric on rock strength in the medium grained granite. X-Y-Z comparison chart of the variation, with orientation, of the estimated average strengths for the medium grained granite. The values for the peak load failure, onset of dilatancy, crack initiation, and microcrack closure are derived from the uniaxial compression data (stress /strain curves) in Appendix C. The tensile strength is from the Brazilian tests. Samples are weakest in compression when the centimetre- to decimetre – scale layering intersects the sample axis at 30°. The rock is stronger (at the specimen scale) when the sample is within the plane of layering, or sharply inclined to it.

Chapter 10

SUMMARY AND CONCLUSIONS

The purpose of this thesis was to investigate and document the contribution of rock fabric on excavation damage development. The hypothesis, based on observation of failure in a variety of rocks at the URL, was that failure occurred at strengths lower than expected, because of fabric-induced strength anisotropy. The hypothesis was tested by undertaking a combined laboratory and field investigation. Although the different excavation response of texturally distinct granite varieties at the URL has been noted, previous investigations assumed that granite (at the URL site and elsewhere) could be treated as a continuous intact (unfractured) mass that is homogenous and isotropic in strength.

The conclusion from this investigation is that the Lac du Bonnet Batholith is not, in fact homogeneous, but contains structural elements and distinct textural varieties which differ significantly in their response to rock properties testing and to excavation.

Data collected in this study demonstrates unequivocally, and for the first time, the highly heterogeneous internal structure characteristic of allegedly homogenous batholiths, and the influence of this heterogeneity on rock mass response. Evidence for anisotropic behaviour of the rockmass is demonstrated to:

1. have occurred on the geological time-scale, and its influence is still present in recent excavations, and
2. at a wide range of scales, from the localization of fault zones along low-dipping layering at the kilometre-scale, to the localization of failure around tunnels by separation along this and other weakness directions.

10.1. Outline of Investigation

The hypothesis was tested through a detailed and combined program of mapping and rock properties testing. The geological setting and the general geology of the study site were described, with emphasis on the factors affecting the development of the ancient (natural) fractures. This description includes a synopsis of the site-scale patterns of natural microfractures, an extensive effort conducted as part of this investigation. To investigate the role of rock fabric on rock strength and damage development, three case studies were selected in the intact rock at the 420 Level of the Underground Research Laboratory (URL). The case studies included fine, medium and coarse grained varieties of the LDBB granite. Foliations of various types and orientations are present at each sample site, and borehole arrays were designed at each of the three locations to provide a wide range of intersection angles for rock properties testing.

The rock properties testing conducted was intended to define the influence of foliation and preferred microcrack orientations in creating strength anisotropies, which in turn influence excavation damage development. Techniques sensitive to planar anisotropy in rock were identified from the literature. It is recognized that fabric is just one of the factors contributing to lowering strength from what is seen under lab conditions. This report summarizes:

1) what was learned from the URL that is useful in future site characterization,
2) how geological features in granite influence excavation damage (link between geology and engineering), and
3) the role of rock fabric on rock mass response (including rock properties testing and in-situ stress measurement).

A relative ranking of rock strength correlating with average grain size is presented. The results are compared with field observations of excavation damage development. Directional anisotropy in rock strength is compared to the orientation of known fabric elements such as natural microcracks directions and some foliations. The results are consistent with tunnel mapping observations regarding preferential development of excavation damage in some rock types and in certain directions.

10.2. Identification of Anisotropy in the "Homogeneous" Lac du Bonnet Batholith

This investigation has revealed two basic errors in the literature regarding the structure of the LDBB and its influence on excavation response:

1. The Lac du Bonnet Batholith is a type example of a homogeneous granite pluton in the Canadian Shield (e.g. Beakhouse, 1991; Card and Poulsen, 1998).
2. With regard to excavation damage development, the LDBB has been used as textbook example of a homogeneous and isotropic granite (e.g. Hoek E., Kaiser P.K. and Bawden W.F., 1995. Support of Underground Excavations in Hard Rock).

Neither of these assumption is correct. At the URL, textural and compositional heterogeneities control: 1) the location of large-scale fault zones, 2) the extent, distribution and infilling characteristics of lesser-scale fractures between the fault zones, and 3) the extent and density of excavation-induced fractures. It has also been demonstrated by the testing program conducted here, that crack initiation and propagation are influenced by rock fabric and grain structure. Finally, breakout development and other types of excavation damage for example vary in response to textural and structural variations in the granite present at the tunnel- and site-scales.

10.3. Natural Microcracks

The site characterization included a compilation and synopsis of the studies of natural (i.e. ancient) microfracturing in quartz at the URL. This study was undertaken in three stages: 1) an initial reconnaissance survey, 2) a more detailed reconnaissance survey, and 3) a study of samples from the 420 Level only to correlate with the samples taken for geomechanical testing.

The results of this study indicate that the orientations and domains of ancient (natural) microcracking are consistent with the patterns and domains defined for the macro-scale fractures at this site. Microfractures are more abundant, more strongly oriented with more sets above the basal thrust fault (Fracture Zone 2), than in the sparsely fractured rock below the fault. Natural microfractures in the sparsely fractured rock below FZ2 are low dipping. In the moderately fractured rock above the fault, the microfracture pattern comprises a low dipping set and two subvertical sets. The low-dipping set in the sample from the 240 Level parallels the average orientation for Fracture Zone 2, as well as the compositional layering, which this fault follows. The low dipping set in the sample from the 130 Level parallels the orientation for Fracture Zone 3 (based on an average taken over a 500 m^2 area), but not the local compositional layering, which deviates here from the regional norm. This is consistent with other URL and surface work, which showed that the low-dipping fracture zones are fabric-controlled where the layering is near the theoretical failure plane, but not where the layering varies substantially in orientation.

Average microfracture lengths are dependent on depth from surface and grain size. The mean crack length decreases with depth from surface. In the moderately fractured rock above Fracture Zone 2, microfractures equal or exceed the grain size, while in the sparsely fractured rock at and below the 240 Level, the microfractures are usually less than the grain size.

The rock properties testing results indicate that the various foliations, compositional layering and natural microfractures influence rock properties, in particular inducing anisotropy to tensile and compressive strength.

10.4. Influence of Grain Size on Rock Strength

Strength, (whether expressed as tensile strength, crack closure strength, crack initiation stress etc.) decreases as the average grain size and heterogeneity of the granite increase. This trend is shown best by the minimum estimates for each type of strength. The mean and maximum strengths are much more variable, being affected by the relative size and orientation of specimen-scale heterogeneities. These influences are most pronounced in the coarser granites.

10.5. Influence of Rock Fabric on Compressive Strength

The testing program has also demonstrated that there is a directional anisotropy to the compressive and tensile strengths in each of the three phases of the LDBB granite, and that this anisotropy is controlled by the different fabrics present in each case. Directional anisotropy of strength and the influence of subvertical fabric on the compressive strength was noted in the fine grained granite. The compressive strength of the fine grained granite is dependent upon the orientation of the sampling borehole relative to the strike of the dyke. Its strength parallel to the dyke contact is 40% less than that measured (near-) normal to this direction.

Directional anisotropy is also evident in the medium and coarse grained granites, although its relationship to the rock fabric is more complex. Samples are weakest in compression when the centimetre- to decimetre– scale layering intersects the sample axis at an angle between 20° and 40°. The rock is stronger (at the specimen scale) when the sample is within the plane of layering, or sharply inclined to it. This interpretation is consistent with field observations and with the Point Load and Brazilian tests, in that the

contacts between layers provide more clearly defined and continuous weakness planes, than those structures that would promote axial splitting of the specimens (i.e. grain alignment or natural microcracks).

10.6. Influence of Grain Size on Tensile Strength

The Point Load test provides a relative index of the strength of the various rock types (the Point Load Index, Goodman, 1989), although this was a secondary objective of this experiment. The "point load strength index" is defined as follows:

$$\textit{Point Load strength index, } I_s = P/D^2$$

$$\textit{where } P = \textit{the load to break the specimen,}$$

$$\textit{and } D = \textit{the distance between the platen contacts.}$$

The test results are consistent with the uniaxial compression testing, in that relative strength decreases with increasing grain size. However, the principal objective of the Point Load Test was to identify weakness planes and their relative strengths. The result of this application is summarized in the following section.

10.7. Fabric-induced Anisotropy of Tensile Strength

In the Point Load test configuration, the fracture is free to form in any orientation parallel to the load. If however, the rock is anisotropic, there is a tendency for failure to follow one or more preferred orientations which generally correspond with some fabric element such as natural microfractures, mineral alignment, etc. In the case of the URL granite, there is a very clear tendency for the tensile failure to be localized by the foliations present in each sample. Which foliation is responsible varies with the sample, being dependent upon the orientation of the sampling borehole relative to the local fabric or fabrics.

In shallow dipping boreholes (< 45°), axial point loading of the core produces fractures following the strongest fabric (referred to for convenience as the large scale layering, but which is in fact a mixture of metre- to millimetre-scale compositional layering, mineral alignment, schlieren (in some cases showing evidence of slip) and natural microfractures in quartz. In steeply dipping boreholes, the layering is no longer favourably oriented with respect to axial loading, and the plane of failure then "jumps" to other, steeper dipping foliations. The presence of "preferred failure planes" is marked by significant directional variations in the average tensile strength (as defined by the Brazilian tests). In the coarse grained granite for example, the tensile strength can be 60% and 80% of the strength obtained when the sample is forced to break oblique to the primary and secondary foliations, respectively.

10.8. Influence of Natural Microcracks on Tensile Strength

In the case of the fine grained granite there are two distinct fabric elements to consider - a subvertical flow banding, and a low-dipping microcrack set. While the microcrack set is also present in the medium and coarse granite, it and its effects are easily masked by the subparallel foliation. In the fine grained granite, the two structures are nearly perpendicular to each other, and their affect on rock strength can be examined separately. The Brazilian tests indicate the tensile strength within the horizontal plane is somewhat lower when the loading axis is parallel to the flow banding, but the tendency for this is weak, and the scatter in the data is considerable. For testing done for the vertical plane, the data spread is much less, and the anisotropy is greater - with the tensile strength parallel to the natural microcrack set being approximately 65% of that normal to this

direction. In this rock unit, it appears that the natural microcracks in quartz have a greater influence on the tensile strength than the centimetre-scale compositional layering.

10.9. Summary of Variations by Rock Type

The coarse grained granite is the most heterogeneous of the types tested. A low-dipping fabric dominates its structure at the tunnel and the hand specimen scales. This fabric includes a largely concordant assemblage of compositional and textural layering, an alignment of biotite and feldspar laths, and a preferred orientation of natural microcracks in quartz. Point Load and Brazilian tests indicate that this fabric imparts a mechanical anisotropy, with the tensile strength in the plane of the fabric being about 40% of that determined for the normal to this plane. This anisotropy is obvious underground, where it facilitates scaling, and the development of excavation-induced fractures where these are developed in an orientation comparable to the predominant foliation. There is also a very clear tendency for the tensile failure to be localized by other foliations. Which foliation is responsible is dependent upon the orientation of the sampling borehole.

In shallow dipping boreholes (< 45°), axial point loading of the core produces fractures following the strongest fabric (the large scale layering as defined above). In steeply dipping boreholes, the layering is not favourably oriented with respect to axial loading, and the plane of failure then "jumps" to other, more steeply dipping foliations. The transition from one foliation plane to another is reflected by fluctuations in the tensile strength as noted in the preceding section.

The properties of the fine grained granite are influenced by two distinct fabric elements - a subvertical flow banding, and a low-dipping microcrack set. While the microcrack set is also present in the medium and coarse granite, it and its effects are easily masked by the subparallel foliation. In the fine grained granite, the two structures are nearly perpendicular to each other, and their influence on rock mass response can be examined separately. Brazilian tests indicate that the tensile strength is somewhat lower when the loading axis is parallel to the subvertical flow banding, but the tendency for this is weak, and the scatter in the data is considerable. A stronger correlation is shown by the influence of the low-dipping natural microcrack set, with the tensile strength parallel to the natural microcrack set being approximately 65% of that normal to this direction. In this rock type, it appears that natural microcracks in quartz have a greater influence on the tensile strength than centimetre -scale compositional layering.

The Point Load testing indicated that failure was controlled by heterogeneities in the rock, such as foliations or the preferred orientation of natural microcracks, which are close to or parallel to the plane of failure under this loading geometry. This tendency was present to some degree in all three of the rock types tested, but varies systematically with the degree of heterogeneity. The coarse grained granite has the most repeated tendency to split along dominant (low-dipping) fabric elements, with the lowest average tensile strength and Point Load strength index. The medium grained granite has a lesser tendency to split along dominant (and other) fabric elements, but with a comparable average tensile strength and Point Load strength index. The fine grained granite has the least repeated tendency to split along any fabric, which in this case alternated between the

steeply-dipping flow banding and the plane correlating with the preferred orientation of natural microfractures, and with the highest average tensile strength and Point Load strength index.

This systematic variation reflects the relative strength of the low-dipping fabric, which comprises a mixture of co-planar compositional layering, mineral alignment, and natural microcracks. All of these elements are present and well developed in the coarse granite, the weakest and most mechanically anisotropic of the group. Where this fabric is less well developed or absent, as in the medium and fine grained granites, this is reflected by an increase in rock strength and isotropy at the specimen –scale.

At the tunnel-scale, these differences in mechanical properties result in a differences in excavation damage including: whether breakouts develop or not, and the rate at which they develop, varying from hours in the case of the coarse grained granite, to days or weeks in fine and more homogeneous granites.

10.10. Application of Results

The geological investigations described in this thesis have the following significance with respect to the selection of a site for a disposal facility.

1. It must be recognized that even "simple" batholiths such as the Lac du Bonnet Batholith have complex internal structure. This structure is a product of the mode of intrusion, cooling history, and later deformation.
2. The rock fabric produced by these events exerts a significant control on the location, extent and orientation of natural (i.e. ancient) fractures. This association therefore

provides a guide to predicting fracture occurrence in the rock mass. It also provides an indication of the potential rock mass response to excavation.

3. Subtle variations in granite fabric can lead to significant differences in the rock mass response to excavation. Foliations and preferred orientations of natural microcracks may reduce strength, and act as weakness planes, in one or more directions. This anisotropy will influence the development and propagation of excavation induced fractures and breakouts.
4. The results presented in this thesis highlight the risk of arbitrarily correlating excavation stability with lithology, or in assuming that there is a typical behaviour from any given rock type. The Lac du Bonnet Batholith granite is not isotropic, and excavation response was shown to vary with the orientation and shape of the excavation relative to the rock structure. Granite types that resisted damage development, including breakout, in the vertical shaft, were more susceptible to damage in the horizontal tunnels. It is to be expected that similar results will occur in other granites.

Based on these findings, the following recommendations are made with regard to the site characterization program required to design, construct and monitor a disposal facility:

1) The geology program for site characterization in granites must include a single program of mapping, core logging and the compilation of the results through the construction of geological models.
2) This effort must be done in a comprehensive and consistent manner rather than as a series of separate follow-on investigations funded by individual experiments. The

latter may produce spurious results or overlook significant geological influences, and in the process, be more expensive over the duration of the facility.

3) The geology program should define the lithology and fabric of the rockmass as well as the natural fractures and types of excavation damage.

4) The effort on lithology should focus on identifying the litho-structural domains that correlate with the intrusion history of the pluton, and which influence the ancient and recent rock mass response (i.e. the natural and induced fractures, respectively). These litho-structural domains vary in texture and composition (as in a dyke which changes from fine to coarse grained as its dimensions increase). Characteristic rock units should then be identified, and subjected to standard petrography, as well as the analysis of fabric and natural microcracks.

5) This effort should only then be followed by the selection of a suite of representative rock types for rock properties testing. As this study has shown, colour is not an appropriate criterion on which to base a program of geotechnical investigation and facility design.

6) There should be a proper core logging program, not just of the current borehole, but of the entire array of boreholes in view of the decametre-scale layering and directional sampling biases identified in this study. Each borehole should be logged according to a standard procedure, which should include a complete analysis of the rock structure.

7) An alternative approach to defining the in-situ properties of highly stressed rock at depth, would be to identify the granite varieties present at the intended test location and depth, and then to obtain samples of these same varieties where they are exposed

at or near the surface. In adopting this approach, it would be necessary to determine if the granites at surface and at depth differ substantially in the characteristics of their natural microcracks.

8) Efforts to determine the in-situ stresses by overcoring or hydrofracing, and to interpret the results of ground penetrating seismic and radar surveys must incorporate the structural and mechanical anisotropy of the granites.

a) Overcore results are dependent upon orientation of a borehole relative to foliations and natural microcrack sets. In the sample itself, strain cells can be adversely affected by their positioning with respect to textural heterogeneities such as coarsely crystalline feldspars. As such, instrumentation placement should be based on a thorough logging, not just of a single borehole, but of the entire array of boreholes which have been designed to provide a range of samples with which to test for directional anisotropy.

b) Determination of in-situ stress by the hydrofracturing method assumes that the rockmass is isotropic, that the tensile fracture created by the test is normal to the least principal stress direction, and that this fracture is not deflected by fabric anisotropy. However, careful excavation at the URL through fractures formed by hydrofracture tests revealed that hydrofracture orientations were nearly always following either the low-dipping compositional layering or the steeply dipping pegmatite dykes (an incipient fracture direction in much of the URL). As such the results from these and similar hydrofracture tests at this site are suspect. Local-scale structures must be considered in the siting of hydrofrac tests and in their interpretation.

9) Ground penetrating radar and portable seismic surveys have been used in attempts to quantify excavation damage about a tunnel. Hayles et al. (1991) found that the pattern of anomalies could not be interpreted without some knowledge of the variations in rock composition and rock fabric. It is recommended that applications of ground penetrating radar and portable seismic be done in an area of a tunnel selected for optimum geology, and that the structure and microstructure be understood prior to running an experiment. Attempts to fill in the geology later to address difficulties in interpretation may not be successful.

These efforts will provide:

- more realistic models of batholith shape, internal structure, and the distribution of both natural and induced fractures,
- better (i.e. more representative) sampling for rock properties testing.
- better understanding of in-situ rock strength, and
- a better understanding of the rock mass response to different excavation geometries and methods.

REFERENCES

ASTM. 1974. Annual Book of ASTM Standards "Standard method of test for direct tensile strength of rock core specimens"; Designation: D2936-71; American Society for Testing and Materials.

ASTM. 1989. Annual book of ASTM Standards, Section 4: Construction, Volume 04.08: Soil and Rock; Building Stones; Geotextiles. American Society for Testing and Materials, 1916 Race Street, Philadelphia, PA 19103-1187, USA.

Baek, H. 1997. Effect of the rock fabrics on the physical properties of a granite. Geological Society of America (GSA), Abstracts with Programs - Geological Society of America vol. 29 no. 6; p. 447.

Balk, R. 1937. Structural behaviour of igneous rocks: Geological Survey of America, Memoir 5, 177 pages.

Bawden, W.F. 1982. In situ stress determination by hydraulic fracturing in well bore URL-6. A report prepared by Geotechnical Resources Ltd. for Atomic Energy of Canada Limited.

Beakhouse, G.P. 1977. A subdivision of the western English River Subprovince. Canadian Journal of Earth Sciences 14: 1481-1489.

Beakhouse, G.P. 1991. Winnipeg River Subprovince. In: Geology of Ontario, (eds. P.C. Thurston, H.R. Williams, R.H. Sutcliffe and G.M. Stott). Ontario Geological Survey, Special Volume 4, Part 1, 279-302.

Behrestaghi, M.H.N., Rao, K.S., and Ramamurthy, T. 1996. Engineering geological and geotechnical responses of schistose rocks from dam project areas in India, Engineering Geology 44(1-4) 183-201.

Benn, K., Ham, N.H., Pignotta, G.F., and Bleeker, W. 1998. Emplacement and deformation of granites during transpression: magnetic fabrics of the Archean Sparrow pluton, Slave Province, Canada. In: Special Issue: Extraction, Transport and Emplacement of Granitic Magmas, edited by K. Benn, A.R. Cruden and E.W. Sawyer, Journal Of Structural Geology Vol. 20 (9-10), 1247-1259.

Bergeron, M. 1991a. Granite Industry in Canada, 1990 Summary Industrial Minerals Division, Mineral Policy Sector of Energy Mines and Resources Canada.

Bergeron, M. 1991b. Granite Industry in Canada, Directory. Mineral Policy Sector, Industrial Minerals Division, MP-4825-2.

Bergeron, M. 1991c. Granite industry in Canada. 1991 Directory. Energy Mines and Resources, Mineral Policy Sector, Industrial Minerals Division, MP4825-2.

Bieniawski, Z.T. 1967a. Stability concept of brittle fracture propagation in rock, Eng. Geol. Vol. 2, p. 149-162.

Bieniawski, Z.T. 1967b. Mechanism of brittle fracture of rock, Int. J. Rock Mech. Min. Sci. Vol. 4. p. 395-430.

Bieniawski, Z.T. 1972. Propagation of brittle fracture in rock. Proceedings, 10th Symposium Rock Mechanics, AIME, New York, 409-427.

Bieniawski, Z.T. 1975. The Point Load test in geotechnical practice. Engineering Geology 9, 1-11.

Bouchez, J.L. 1997. Granite is never Isotropic: An introduction to AMS studies of granitic rocks. In: Granite: From segregation of melt to emplacement fabrics, eds. J.L Bouchez, D.H.W. Hutton, and W. E. Stephens, p. 95-112. Kluwer Academic, Dordrecht.

Breaks, F.W. 1991. English River subprovince. In Geology of Ontario, Thurston, P.C., Williams, H.R., Sutcliffe, R.H., and Stott, G.M. (eds.). Ontario Geological Survey Special Volume 4, Part 1, 239-278.

Broch, E. 1974. The influence of water on some rock properties. In: Advances in Rock mechanics, Proc. 3rd Congress, International Society of Rock Mechanics. Denver, 1974, Part A, pages 33-38.

Broch, E. 1983. Estimation of Strength Anisotropy Using the Point-Load Test. International Journal of Rock Mechanics, Min. Sci. & Geomech. Abstr. Vol. 20, No. 4, 181-187.

Broch, E. and Franklin, J.F. 1972. The Point Load Test. International Journal of Rock Mechanics, Min. Sci. 9, 669-697.

Brown, A. and Everitt, R.A. 1984. Hydrofracing experiment in shaft. 2 p. plus 1 map. Memo #URL-GEN-M007 (URL-GEN-M00 Series).

Brown, A., Soonawala, N.M., Everitt, R.A., and Kamineni, D.C. 1989a. Geology and geophysics of Underground Research Laboratory site, Lac du Bonnet batholith, Manitoba. Canadian Journal of Earth Sciences, 26, 404-425.

Brown, A., Kamineni, D. C., and Everitt, R.A. 1989b. Deformation in the Lac du Bonnet Batholith, Man., Canada. In: Geological Association of Canada/Mineralogical Association of Canada Annual Meeting, Montreal, PQ, Canada, May 15-17, 1989, Program with Abstracts, vol. 14, p. 54.

Brown, E.T. 1981. Rock Characterization testing and monitoring. ISRM Suggested methods for determining the uniaxial compressive strength of rock materials and the point load strength index"; International Society for Rock Mechanics; Commission on Standardization of Laboratory and Field Tests; Committee on Laboratory Tests; Document no. 1; October 1972.

Card, K.D. and Poulsen, K.H. 1998. Geology and Mineral Deposits of the Superior province of the Canadian Shield. Chapter 2 In: Geology of the Superior province of the Canadian Superior and grenville Provinces and Precambrian Fossils in north America, (co-ord) S. Lucas; Geological Survey of Canada, no. 7, p.13-194. (also Geological Survey of America, The Geology of North America, v. C-1).

Carter, B.J. 1992. Size and Stress gradient effects on fracture around cavities. Rock Mechanics and Rock Engineering, 25, (3), 167-186.

Cerny, P., Fryer, B.J., Longstaffe, F.J., and Tammemagi, H.Y. 1987. The Archean Lac du Bonnet Batholith, Manitoba: Igneous history, metamorphic effects, and fluid overprinting. Geochimica et Cosmochimica Acta, 51: 421-438.

Chandler, N.A., Read, R.S., and Martin C.D. 1996. In situ stress measurement for nuclear fuel waste repository design. In: proceedings of the 2nd North American Rock mechanics Symposium: NARMS'96. A regional conference of ISRM/ Montreal/ Quebec/ Canada. 19-21 June 1996. 929-936.

Chen, R. 1993. In situ and laboratory study of potash deformation, with reference to Saskatchewan potash. University of Manitoba, Winnipeg, MB, Canada. Doctoral Thesis. 280p.

Chen, Y., Nishiyama, T., Kita, H., and Sato, T. 1997. Correlation between microfracture type and splitting planes of Inada granite and Kurihashi granodiorite. Journal of the Japan Society of Engineering Geology. v. 38:4. p. 196-204.

Chernis, P.J. 1981. Scanning Electron Microscope Study of the Microcrack Structure of a Granite Sample from Pinawa, Manitoba. Atomic Energy of Canada Limited Technical Record TR-173.

Chernis, P.J. 1984. Comparison of the Pore-Microcrack Structure of Shallow and Deep Samples of the Lac Du Bonnet Granite. Atomic Energy of Canada Limited Technical Record TR-223.

Christiansson, R. and Hamberger, U. 1991. Blasting Damage Investigations in Access Ramp Section 0/256 – 0/565 M. No. 1. Tunnel Excavation and Geological Documentation. Äspö Hard Rock Laboratory Progress Report 25-91-12.

Clarke, D.B., Henry, A.S., and White, M.A. 1998. Exploding xenoliths and the absence of `elephants' graveyards' in granite batholiths. In: Special Issue: Extraction,

Transport and Emplacement of Granitic Magmas, edited by K. Benn, A.R. Cruden and E.W. Sawyer, Journal Of Structural Geology Vol. 20 (9-10), 1325-1343.

Cloos, E. 1946 Lineation: Geological Survey of America, Memoir 18, 122p.

Coates, D.F. and Gyenge, M. 1966. "Suggested test specifications on plate load testing and conventional uniaxial compression testing techniques for rock mechanics"; American Society for Testing and Materials; Special technical publication no. 402; p. 34-34.

Colback, P.S.B. and Wild, B.L. 1965. The influence of moisture content on the compressive strength of rock, Proc. 3rd Canadian Rock Mech. Symp., Toronto, 66-83.

Corthesy, R., Gill, D.E., and Leite, M.H. 1993. Doorstoppers Stress Measurements at the 420 Level of the URL. C.D.T. Project P1596, L'Ecole Polytechnique de Montreal.

Cruden, A.R. 1990. Flow and Fabric Development during the diapiric rise of magma. Journal of Geology, 98, 681-698.

Cruden, A.R. 1998. On the emplacement of tabular granites. Journal of the Geological Society of London, 155, 852-862.

Cruden, A.R. and Lanueau, P. 1994. Structure, magnetic fabric and emplacement of the Archean Lebel Stock, SW Abitibi Greenstone Belt, Journal of Structural Geology, 16, No. 5, 667-691.

Cruden, A.R., Davis D., Menard T., and Robin, P.-Y.F. 1997. Structural and Geochronological relationships between the Winnipeg River and the Wabigoon Subprovinces: Implications for the Terrane Accretion Model. In: Western Superior transect, Lithoprobe Report 63, University of British Columbia.

Cruden, A.R., Koyi H., and Schmeling H. 1995. Diapiric basal entrainment of mafic into felsic magma. Earth and Planetary Science Letters, 131, 321-340.

Cruden, D.M. 1983. Long-term behaviour in compression of Lac Du Bonnet granite. Atomic Energy of Canada Limited Technical Record TR-211.

Dale, T.N. 1923. The commercial granites of new England. I, U.S. Geol. Sur. Bull., 738, 1-97.

Davis, D.W., Corfu, F., and Krogh, T.E. 1986. High precision U-Pb geochronology and implications for the tectonic evolution of the Superior Province. In Workshop on tectonic evolution of greenstone belts. Edited by M.J. deWit and L.D. Ashwal. Lunar and Planetary Institute, Houston, TX, Technical Report 86-10, p. 77-79.

Davis, G.H. 1984. Structural geology of rocks and regions. John Wiley & Sons.

Djouadi, T., Gleizes, G., Ferré, E., Bouchez, J.L., Caby, R., and Lesquer, A. 1997. Oblique magmatic structures of two epizonal granite plutons, Hoggar, Algeria: late-orogenic emplacement in a transcurrent orogen. In: Special Issue: The Adolphe Nicolas Volume , edited by D. Mainprice, F. Boudier and J.-L. Bouchez, [Editorial] , Tectonophysics, Volume 279, Issue 1-4, 15-October-1997 , Tectonophysics Vol. 279 (1-4), 351-374.

Doe,T.W. 1987. Hydraulic fracturing stress measurements in the shaft probe hole at the Underground Research Laboratory, Manitoba . Golder Associates Inc. report to Battelle Memorial Institute, Office of Waste Technology Development.

Doe,T.W. 1989. Hydraulic fracturing stress measurements in horizontal holes at the 240-and 420-m Levels of the Underground Research Laboratory. Golder Associates Inc. report to Atomic Energy of Canada Limited.

Donath, F.A. 1964 Strength variation and deformational behaviour in anisotropic rocks. In: W. Judd (Ed.), State of Stress in the Earth's Crust, Elsevier, New York, p. 281-300.

Duevel, B. and Haimson, B. 1997. Mechanical Characterization Of Pink Lac Du Bonnet Granite: Evidence Of Nonlinearity And Anisotropy. International Journal of Rock Mechanics and Mining Sciences 1997. Vol. 34, No. 3-4, 117.

Duncan, S.E.J. 1987. Mesoscopic scale fractures, microscopic fractures and tensile strength characteristics of the Shield Granite: Southeastern Manitoba. Unpublished M.Sc. thesis, University of Manitoba, Department of Geological Sciences, Winnipeg, Manitoba. 136p.

Engelder, T. 1993. Stress Regimes in the Lithosphere. Princeton University Press. 457p.

Everitt, R.A. 1993a. Orientation and Distribution of Inclusion-Bearing Microcracks in core from the 420m Level of the Underground Research Laboratory, Pinawa, Manitoba. Prepared by Don H. Rousell, Department of Geology, Laurentian University, Sudbury, Ontario, P3E 2C6. URL Library Identifier 01.73.03.

Everitt, R.A. 1993b. Petrography of Granitic Rock Samples from the 420m Level of the Underground Research Laboratory, Pinawa, Manitoba. Prepared by Dana Kelly, David S. Peck and Richard S. James, Department of Geology, Laurentian University, Sudbury, Ontario, P3E 2C6. URL Library Identifier 01.73.03.

Everitt, R.A. 1995. Status of Pegmatite Testing Study. Fracture Initiation and Propagation by Compressive Loading and Unloading in Component Mineral Phases of the Lac du Bonnet batholith. Unpublished internal memorandum. URL-01.84.41, R-3002-07-00.

Everitt, R.A. 1998. The Influence of Rock Fabric on Excavation Damage in the Lac Du Bonnet granite. Report for DS-3, Rock Engineering Studies, URL-G-4200, Memo AGB-98-008.

Everitt, R.A. 2000. Synopsis of natural microcrack work at the Underground Research Laboratory. Unpublished report.

Everitt, R.A. and Brown A. 1986. Subsurface Geology of the Underground Research Laboratory. An Overview of Recent Developments. 25 p. 14 Tables and Figures In: Proceedings of the 20th Information Meeting of the CNFWMP held in Winnipeg, Canada, October, 1985. AECL Technical Record TR-375. p. 146-181.

Everitt, R.A. and Brown A. 1996. Geological Mapping of AECL Research's Underground Research Laboratory. A Cross Section of Thrust faults and Associated Fractures in the Roof Zone of an Archean batholith. Proceedings of Fractured and Jointed rock masses, a regional conference of the International

Society for Rock Mechanics. June 1-6th 1992. Granlibakken, California. Volume 1 , p. 1-11.

Everitt, R.A. and McArthur, J.R. 1994. Petrofabric analysis of natural microfractures in quartz of the Lac du Bonnet Batholith. Unpublished AECL Internal memorandum.

Everitt, R.A. and McGregor, C. 1990. Pilot Petrofabric Study of Natural Microfractures in core from AECL Research's Underground Research Laboratory. Unpublished.

Everitt, R.A. and Passmore, W. 1993. Shaft Extension Data Report - Wall Topography and Geology map. Unpublished AECL internal memorandum.

Everitt, R.A. and Read, R.S. 1989. Geology of the 240 Level of the Underground Research Laboratory - Volume I - General Geology. AECL Technical Record TR-491-1, URL-EXP-006-R001.

Everitt, R.A. and Rousell, D.H. 1994. Orientation and Distribution of Inclusion-Bearing Microfractures in core from the 420m Level of the Underground Research Laboratory, Pinawa, Manitoba. Prepared by Don H. Rousell, Department of Geology, Laurentian University, Sudbury, Ontario. URL Library Identifier 01.73.03.

Everitt, R.A. and Woodcock, D.R. 1994. Contribution to the HFT Characterization Summary Report. Mapping Results for the 600 mm Heated Failure Test Borehole. Unpublished AECL Internal Memorandum. URL-01,84.41, AGB-94-190.

Everitt, R.A. and Woodcock, D.R. 1999 Geology of the Deep Stress Measurement Borehole. OPG Nuclear Waste Management Report 06819-REP-01200-10012-R00. August 1999. 146p.

Everitt, R.A., Brown, A., Davison, C.C., Gascoyne, M., and Martin, C.D. 1990. Regional and local setting of the Underground Research Laboratory. In Proceedings of the Symposium on Unique Underground Structures, Denver, Colorado, p. 64-1 to 64-23.

Everitt, R.A., Brown, D. A., Boychuk, D.M., and Gann, P. 1994. Excavation damage and organic growth in a 1.2m diameter borehole. Poster presentation at the 5th Annual International High-Level Radioactive Waste Management Conference & Exposition. May 22-26th 1994.

Everitt, R.A., Chapman, A.E., Northrop, P., and Brown, A. 1987. Geology of the Underground Research Laboratory Ventilation Raise. Atomic Energy of Canada Limited, Technical Record TR-404.

Everitt, R.A., Chernis, P.J., and Good, D.H. 1989b. Geology of the Room 209 Floor. Contributions to the Excavation Damage Assessment Experiment. 5 p., 4 figures, 4 tables and 2 maps.

Everitt, R.A., Chernis, P.J., Good, D.H., and Grogan, A. 1989. Mapping of the Excavation Damage Zone around the Circular Access Shaft at Atomic Energy of Canada Limited's Underground Research Laboratory. In: Excavation Response in Geological Repositories for Radioactive Waste. Proceedings of an NEA Workshop, April 1988, Winnipeg, Canada, p. 271-282.

Everitt, R.A., Gann, P., and Boychuk, D.M. 1993. Mine-by Experiment : Part 7 - Geological Setting and General Geology. AECL Technical Record RC-1080.1. This report and the following supplements complete the geological characterization of the 420 Level for the Mine-by Experiment and the Connected permeability Experiment.

Everitt, R.A., Gann, P., Brown, A., Woodcock, D.R., Sikorsky, R.I., and Ejeckam, R. B. 1998. Subhorizontal Layering in the "Homogeneous" Lac du Bonnet Batholith at the Underground Research Laboratory, South Eastern Manitoba. In: Special Symposium on Extraction, Transport and Emplacement of Granitic Magmas, Ottawa '97 GAC-MAC Annual Meeting. Journal of Structural Geology. Volume 20, No. 9/10, p. 1291-1304.

Everitt, R.A., Martin, C.D., Brown , A., and Gann, P. 1994. Pop-Ups And Fractures In Granite At The Canital Quarry, Manitoba. Presented at the Geological Association of Canada - Mineralogical Association of Canada Joint Annual Meeting, May 16-18th, 1994.

Everitt, R.A., McMurry, J., Brown, A., and Davison, C. 1996. Geology of the Lac du Bonnet Batholith, Inside and Out: AECL's Underground Research Laboratory, Southeastern Manitoba. Field Excursion B-5: Guidebook,. Geological Association of Canada - Mineralogical Association of Canada Joint Annual Meeting 1996, Winnipeg, Manitoba, Canada. 1996 May 30. Copyright Geological Association of Canada, Winnipeg '96 Committee.

Feves, M. and Simmons G. 1976. Effects of Stress on Cracks on Westerly Granite. Bulletin of the Seismological Society of America. Vol. 66, (5), p. 1755-1765.

Friedman, M. and Bur, T.R. 1974. Investigations of the relations among residual strain, fabric, fracture and ultrasonic attenuation and velocity in rocks. International Journal of Rock Mechanics and Mining Science and Geomechancial Abstracts, Vol. 11, 221-234.

Gerow, M.C. and Bellinger, J.A. 1990. Northwestern region industrial minerals program-1989; in Report of Activities 1989, Resident Geologists, (eds. K.G. Fenwick, P.E. Giblin and A.E. Pitts). Ontario Geological Survey, Miscellaneous Paper 147, 161-179 p.

Gleizes, G., Leblanc, D., Santana, V., Olivier, P., and Bouchez, J.L. 1998. Sigmoidal structures featuring dextral shear during emplacement of the Hercynian granite complex of Cauterets--Panticosa (Pyrenees). In: Special Issue: Extraction, Transport and Emplacement of Granitic Magmas , edited by K. Benn, A.R. Cruden and E.W. Sawyer, Journal of Structural Geology, Volume 20, Issue 9-10, 1229-1245.

Goodman, R.E. 1989. Introduction to Rock Mechanics. 2nd edition. John Wiley and Sons.

Gorski, B. 1987. Post-failure uniaxial strength determinations using a servo-hydraulic test system. Division Report MRL 87-33 (INT), CANMET, Energy, Mines and Resources, Canada, 77p.

Guermani, A. and Pennacchioni, G. 1998. Brittle precursors of plastic deformation in a granite: an example from the Mont Blanc massif (Helvetic, western Alps). In: Special Issue: Structures and Properties of High Strain Zones in Rocks , edited by E.H. Rutter, A. Boriani, H. Brodie and L. Burlini, Journal of Structural Geology, Volume 20, Issue 2-3, -February-1998 , Journal of Structural Geology Vol. 20 (2-3) p. 135-148.

Gyenge, M. 1980. Pit Slope Manual Supplement 3-1- Laboratory Classification Tests; CANMET (Canada Centre for Mineral and Energy Technology, formerly Mines Branch, Energy, Mines and Resources Canada), CANMET Report 77-25; 31p; May 1977. Reprinted May 1980.

Gyenge, M. and Herget G. 1977. Laboratory tests for design parameters. Mining Research Laboratories Pit Slope Manual Canada Centre for Mineral and Energy Technology, Ottawa. Supplement 3-2, p. 1-74. (1977).

Gyenge, M. and Ladanyi B. 1977. Pit Slope Manual Supplement 3-5 – sampling and specimen preparation. CANMET, Report 77-29, 30p.

Haimson, B.C. 1982. Hydrofracturing in situ stress measurements in the Lac du Bonnet batholith drillholes URL-1 and WN-4. A report prepared for Atomic Energy of Canada Limited.

Haimson, B.C. 1990. Stress measurements in the Sioux Falls Quartzite and the state of stress in the midcontinent. In: Proceedings of the 31st U.S. Symposium on Rock Mechanics, Golden, Colorado, June 18th-20th 1990. 31, 397-404.

Haimson, B.C. 1991. Hydraulic fracture stress measurements at the 420 Level, Underground Research Laboratory, AECL. A report to Atomic Energy of Canada Limited.

Haimson, B.C. 1992. Hydraulic fracturing stress measurements in three holes , Room 415, URL. A report to Atomic Energy of Canada Limited.

Hayles, J. G., Stevens, K. M., Serzu, M. H., and Lodha, G. S. 1991. Developments in the Mini-charts system and field trial results in measuring excavation damage in granite. In: Fourth International Symposium on Borehole Geophysics for Minerals, Geotechnical and Groundwater Applications, Toronto, ON, Canada, August 18-22, 1991, International Symposium on Borehole Geophysics for Minerals, Geotechnical, and Groundwater Applications, vol. 4, p. 267-306.

Hayles, J.G., Serzu, M.H., Tomsons D.K., Everitt. R.A., and Lodha G.S. 1994. Cross-hole seismic hole geophysical surveys for characterizing an area of moderately fractured rock. Presented at the CSEG Convention in Calgary Alberta May 10-12th, 1994.

Heuze, F.E. 1980. Scale effects in the determination of rock mass strength and deformability. Rock Mechanics, 12, (3)

Hill, J.R. 1989a. Dimension stone inventory of Islington I.R. No.29; Independent Consultant Report for Rat Portage Indian Band, Kenora, Ontario, January, 1989, 23 p.

Hill, J.R. 1989b. Dimension stone inventory of Swan Lake I.R. No.29; Independent Consultant Report for Rat Portage Indian Band, Kenora, Ontario, January,1989, 22 p.

Hill, J.R. 1990a. Phase II Follow-up Dimension Stone Evaluation of English River I.R. 21 prepared by Northwood Geoscience for The Assin Partnership, Kenora, Ontario, March, 1990, 17 p.

Hill, J.R. 1990b. Phase II Follow-up Dimension Stone Evaluation of Swan Lake I.R. 29 and Islington I.R. 29 prepared by Northwood Geoscience for The Assin Partnership, Kenora, Ontario, March, 1990, 24 p.

Hinz, P., Landry, R.M., and Gerow, M.C. 1994. Dimension stone occurrences and deposits in Northwestern Ontario. Ontario Geological Survey, Open File Report 5890.

Hodgson, K. and Cook, N.G.W. 1970. The effect of size and stress gradient on the strength of rock. Proc. 2nd Congress International Society of Rock Mechanics, Belgrade, Vol. 2, 1970. Paper 3-5.

Hoek, E. and Brown, E.T. 1980. Underground Excavations in Rock. Institute of Mining and Metallurgy, London. 5. Support of Underground Excavations in Hard Rock. A.A. Balkema.

Hoek, E., Kaiser, P.K., and Bawden, W.F. 1995. Support of Underground Excavations in Hard Rock, A.A. Balkema.

Homand-Etienne, F. and Sebaibi, A. 1996. Study of microcracking of the Lac du Bonnet granite. Eurock'96. Barla (ed.), 1996 Balkema, Rotterdam. P. 1353-1360.

Hooker, V.E. and Bickel, D.L. 1974. Overcoring equipment and techniques used in rock stress determination: Information Circular of the U.S. Bureau of Mines, No. 8618.

Hoskins, J.R. and Horino, F.G. 1969. The influence of spherical head size and specimen diameter on the uniaxial compressive strength of rocks. United States Bureau of Mines Report of Investigations, 7234, 16p.

IUGS (International Union of Geological Sciences) Subcommission on the Systematics of Igneous Rocks. 1973. Plutonic rocks, classification, and nomenclature. Geotimes, 18(10): 26-30.

Jaeger, J.C. 1960. Shear Failure of Anisotropic Rocks. Geol. Magazine, 97, 65-72.

Jaeger, J.C. and Cook, N.G.W. 1979. Fundamental of rock mechanics, 3rd edition, Chapman and Hall, London, 593p.

Jang, B., Wang, H.F., Ren X., and Kowallis B.J. 1989. Precambrian paleostress from microcracks and fluid inclusions in the Wolf River batholith of central Wisconsin. Geological Society of America Bulletin, 101: 1457-1464.

Kennedy, M.C. and Shelock, E.J. 1988. Northwestern Region industrial minerals program-1987; in Report of Activities, 1987, Resident Geologists, (ed. C.R. Kustra). Ontario Geological Survey, Miscellaneous Paper 138, 161-174.

Kornfalt, K., Wikman, H., Nordlund, E., and Chunlin, L. 1991. Blasting Damage Investigations in Access Ramp Section 0/256 – 0/565 M. No. 4. Optical

examination of microcracks in thin sections of core samples and acoustic emission of core samples. Äspö Hard Rock Laboratory Progress Report 25-91-15.

Kronenberg, A.K., Russell, J.E., and Carter, N.L. 1990. Anisotropic yielding of rocks at high temperatures and pressures. Final report (Progress report) Texas A and M Univ., College Station. Center for Tectonophysics. Corp. Source Codes: 004736025; 9504864 Sponsor: Department of Energy, Washington, DC. Report No.: DOE/ER/13711-T1 14 Oct 90 15p. Sponsored by Department of Energy, Washington, D.C. Contract No.: FG05-87ER13711.

Kudo, Y., Hashimoto, K, Sano, O., and Nakagawa, K. 1987. Relation between physical anisotropy and microstructures of granitic rock in Japan. In: Proceedings of the Sixth Congress of the International Society for Rock Mechanics, edited by G. Herget and S. Vongpaisal, p. 429-432, A.A. Balkema, Rotterdam, The Netherlands.

Kulander, S.L.D. and Ward B.J. Jr. 1990. Fractured Core Analysis: Interpretation, logging and use of natural and induced fractures in core by. in: Methods in Exploration Series, n.8, American Association of Petroleum Geologists. 1990.

Kusumi, H.; Mine, Y.; and Nishida, K. 1997. Effect of structural anisotropy on deformation properties of granite under cyclic loading. Journal of the Society of Materials Science, Japan v. 46 no. 9 Sep 1997. p 1029-1034.

Lacey, J.K. 1989. Building stone inventory of the Sudbury Resident Geologist's Area. Ontario Geological Survey, Open File Report 5721.

Lajtai, E.Z. 1980. Tensile Strength and its Anisotropy measured by Point – and Line-Loading of Sandstone. Engineering geology, 15, 163-171.

Lajtai, E.Z. 1982. The fracture of Lac du Bonnet Granite. Unpublished report to Atomic Energy of Canada Limited, 126 p.

Lajtai, E.Z. and Dzik, E. 1996. Searching for the Damage Threshold in Intact Rock. In: Proceedings, North American Rock mechanics Symposium.

Lajtai, E.Z., Carter, B.J., and Scott Duncan, E.J. 1991. Mapping the state of fracture around cavities. Eng. Geol., 31, p. 277-289.

Lajtai, E.Z., Schmidtke, R.H., and Bielus, L.P. 1987. The effect of water on the time-dependent deformation and fracture of a granite. International Journal of Rock Mechanics and Mining Sciences & Geomechanics Abstracts, vol. 24, no. 4, p. 247-255.

Lang, P.A., Babulic, P.J., Bilinsky D.M., Everitt, R.A., Spinney, M.H., Kozak, E.T., and Davison, C.C. 1990. Underground Research laboratory Room 209 Instrument Array: Measured Response to Excavation, Volumes 1 and 2, Atomic Energy of Canada Limited Report AECL 9566-3.

Lang, P.A., Everitt, R.A., Kozak, E.T., and Davison, C.C. 1988. Underground Research Laboratory Room 209 Instrument Array: Pre Excavation Information for Modellers. 1988 December, AECL 9566-1.

Lau, J.S.O. and Gorski, B. 1991a. The post- failure behavior of the Lac du Bonnet Grey Granite . Divisional Report MRL 91-079(TR). Canada Mine Technology

Laboratory, Mining Research Laboratories, CANMET, Energy, Mines and Resources Canada, Ottawa, Ontario.

Lau, J.S.O. and Gorski, B. 1991b. The post- failure behavior of the Lac du Bonnet Pink Granite . Divisional Report MRL 91-103(TR). Canada Mine Technology Laboratory, Mining Research Laboratories, CANMET, Energy, Mines and Resources Canada, Ottawa, Ontario.

Lau, J.S.O. and Gorski, B. 1991c. The post- failure behavior of the Lac du Bonnet Granodiorite . Divisional Report MRL 91-098(TR). Canada Mine Technology Laboratory, Mining Research Laboratories, CANMET, Energy, Mines and Resources Canada, Ottawa, Ontario.

Leeman, E.R. 1967. The borehole deformation type of rock stress measuring instrument. The International Journal of Rock Mechanics and Mining Science. Vol. 4, (1), p. 23-34.

Leeman, E.R. 1971. The CSIR "Doorstopper" and triaxial rock measuring instruments: Rock Mechanics, Vol. 3, p. 25-50.

MacLeod, I.N. 1980. A gravity survey of Lac de Bonnet Batholith research area RA-3, Lac du Bonnet, Manitoba. Applied Geoscience Branch, Whiteshell Laboratories, Pinawa, Manitoba, unpublished report.

Marmont, C. 1993. Exploration guidelines and opportunities for dimensional stone in central Ontario. Ontario Geological Survey, Open File Report 5853, 83 p.

Martin C.D. and Kozak, E.T. 1992. Flow measurements in the excavation-disturbed zone of Room 209,. Eurock'92. Thomas Telford. London. Paper 69. p. 402-407.

Martin, C.D. 1989a. Characterizing in-situ stress domains at the Underground Research Laboratory. In Proceedings of the 42nd Canadian Geotechnical Conference, Winnipeg, MB, 1989, 61-74.

Martin, C.D. 1989b. Failure observations and in situ stress domains at the Underground, Research Laboratory. In: International Symposium of Rock Mechanics, Pau, France, Aug. 28-31, 1989, A. A. Balkema, Rotterdam, Netherlands, p. 719-726.

Martin, C.D. 1990. Characterizing in-situ stress domains at the AECL Underground Research Laboratory. Canadian Geotechnical Journal 27: p. 631-646.

Martin, C.D. 1993. The strength of massive Lac du Bonnet Granite around underground openings. University of Manitoba, Winnipeg, MB, Canada. Doctoral Thesis. 304 p.

Martin, C.D., Chandler N.A., and Read, R.S. 1996. The role of convergence measurements in characterizing a rock mass. Canadian Geotechnical Journal, vol. 33, 363-370.

Martin, C.D., Read, R.S., and Lang, P.A. 1990. Seven years of in situ stress measurements at the URL; an overview. In: Proceedings of 31st U.S. Symposium on Rock Mechanics; Contributions and Challenges, Golden, CO, United States, June 18-20, 1990, vol. 31, p. 15-26.

Martino, J.B. 1989. Distometer Convergence Readings in the Shaft Extension of Atomic Energy of Canada Limited's Underground Research Laboratory. Atomic Energy of Canada Limited Technical Report TR-482.

Martino, J.B. 1994. A comparison of fracture growth in intact and Micro-fractured Lac du Bonnet granite. A Masters Thesis submitted to the Department of Civil and Geological Engineering, University of Manitoba.

Martinsen, M. and Wingen, P.T. 1991. Granite dimension stone quarry pre-feasibility study. Prepared for the Sudbury East Municipal Association (SEMA).

Mayo, E.B. 1941. Deformation in the interval Mt. Lyell – Mt. Whitney, California: Geological Survey of America Bulletin, Volume 52, p. 1001-1084.

McCrank, G.F.D. 1985. A Geological Survey of the Lac du Bonnet Batholith, Manitoba. Atomic Energy of Canada Limited Technical Report AECL-7816.

McCrank, G.F.D., Misiura, J.D., and Brown, P.A. 1981. Plutonic Rocks in Ontario. Atomic Energy of Canada Limited, TR-114. Also In: Geological Survey of Canada, G.S.C. Paper 80-23.

McLamore, R.T. 1966. Strength-deformation characteristics of anisotropic sedimentary rocks, Ph.D. thesis, University of Texas, Austin.

McRitchie, W.D. 1971. The petrology and environment of the acidic plutonic rocks of the Wanipigow - Winnipeg Rivers region, southeastern Manitoba. In Geology and geophysics of the Rice Lake region, southeastern Manitoba (Project Pioneer). Edited by W. D. McRitchie and W. Weber. Manitoba Mines Branch, Publication 71-1, p. 7-61.

Mesri, G. and Gibala, R. 1972. Engineering properties of a Pennsylvanian shale, Proceedings, 13th Symposium on Rock Mechanics (ASCE), p. 57-75.

Mogi, K. 1962. The influence of the dimensions of specimens on the fracture strength of rocks. Bulletin Earthquake Research Institute, Tokyo University, Vol. 40, 175-185.

Nur, A. and Simmons, G. 1970. The origin of small cracks in igneous rocks, Int. J. Rock Mech. Min, Sci., vol. 7, p. 307-314.

Obert, L., Windes, S.L., and Duvall, W.I. 1946. Standardized tests for determining the physical properties of mine rock. U.S. Bureau of Mines Report of Investigations, 3891.

Olsson, O. and Conterra AB 1991. Blasting Damage Investigations in Access Ramp Section 0/256 – 0/565 M. No. 2. Geophysical Investigations in Boreholes. Äspö Hard Rock Laboratory Progress Report 25-91-13.

Ontario Ministry of Northern Development and Mines. 1989. Building stone inventory of the Sudbury resident geologist's area. Ontario Geological Survey, Open File Report 5721.

Ontario Ministry of Northern Development and Mines. 1990. Ontario catalogue, dimensional stone.

Ontario Ministry of Northern Development and Mines. 1992. Ontario dimension stone producers directory.

Osmani, I.A. 1991. Proterozoic mafic dike swarms in the Superior Province of Ontario. In: Geology of Ontario, (eds. P.C. Thurston, H.R. Williams, R.H. Sutcliffe and G.M. Stott). Ontario Geological Survey, Special Volume 4, Part 1, 661-682.

Ouchterlony, F., Matsuki, K., Takahashi, H., and Hashida, T. 1991. Experiences from Fracture Toughness Testing of Rock According to the ISRM Suggested Methods. Sponsor: Tohoku Univ., Sendai (Japan). Report No.: DS-1991: 2 Prepared in cooperation with Tohoku Univ., Sendai (Japan).

Papertzian, C. and Farrow, D. 1995. Dimension stone: A guide to prospecting and developing, Ontario Geological Survey, Open File Report 5920.

Park, H.D. 1996. The anisotropy of the granite revealed by tensile tests. 30th international geological congress, Beijing, China, Aug. 4-14, 1996. International Geological Congress, Abstracts vol. 30, Vol. 3 p. 398.

Peng, S. and Johnson, A.M. 1972. Crack growth and faulting in cylindrical specimens of Chelmsford granite. International Journal of Rock Mechanics, vol. 9, p. 37-86.

Plumb, R., Engelder, T., and Yale, D. 1984. Near-surface in situ stress, 3, Correlation with microcrack fabric within the New Hampshire granites, Journal of Geophysical Research. Vol. 89, 9350-9364.

Pratt, H.R., Black, A.D. Brown, W.S., and Brace, W.R. 1972. The effect of specimen size ion the mechanical properties of unjointed diorite. Intnl. J. Rock Mech. Min. Sci., Vol. 9, 513-529.

Price, N.J. and Cosgrove, J.W. 1994. Analysis of geological structures. Cambridge University Press. 502 p.

Protodiakonov, M.M. and Koifman, M.I. 1963. The scale effect in investigations of rock and coal. Proc. 5th Congress International Bureau Rock Mechanics, Leipzig, 1963.

Rawlence, L. 1990. Borehole breakouts: a review of the theory and a discussion of their investigation using seismic methods, #RP005AECL.

Read, R.S. 1994. Interpreting excavation-induced displacements around a tunnel in highly stressed granite. Ph.D. thesis, Department of Civil and Geological Engineering, University of Manitoba, Winnipeg. Manitoba.

Read, R.S. and Martin, C.D. 1990. The Underground Research Laboratory mine-By Experiment - a research perspective on tunnel design. 8th Canadian Tunneling Conference, Oct. 31 - Nov. 02, 1990. Vancouver, B.C.

Read, R.S. and Martin, C.D. 1991. Mine-by Experiment final design report. Atomic Energy of Canada Limited Research Report, AECL-10430.

Read, R.S. and Martin, C.D. 1992. Monitoring the excavation-induced response of granite. In Proceedings of the 33rd U.S. Symposium on Rock Mechanics, Santa Fe, NM. Edited by J.R. Tillerson and W.R. Wawersik, p. 201-210.

Read, R.S. and Martin, C.D. 1996. Technical summary of AECL's Mine-by Experiment, Phase 1: Excavation response. Atomic Energy of Canada Limited Report, AECL-11311.

Read, R.S. and Martino, J.B. 1996. In situ thermal testing at AECL's Underground Research Laboratory. 1487-1494. In: Proceedings of the 2nd North American Rock Mechanics Symposium: Narms' 96, Montreal, Quebec, Canada, June 19-21, (M. Aubertin, F. Hassani, and H. Mitri, Eds.). A. A. Balkema: Rotterdam.

Read, R.S., Martin, C.D., and Dzik, E.J. 1995. Asymmetric borehole breakouts at the URL. In Proceedings of the 35th U.S. Symposium on Rock Mechanics, Lake Tahoe, NV. Edited by J.J.K. Daemen and R.A. Schultz, p. 879-884.

Rehrig, W.A. and Heidrick, T.R. 1972. Regional fracturing in Laramide Stocks of Arizona, Economic Geology. v. 67, #2, 198-213.

Reik, G. A. and Currie, J.B. 1974. A study of relations between rock fabric and joints in sandstone. Canadian Journal of Earth Sciences, Vol. 11, 1253-1268.

Reitan, P.H. and Murphy, J.W. 1983. Influence of metamorphic fabric and residual stresses on joint orientations in basement rock, Adirondack Mountains, New York. In: International Basement tectonics Association Publication No. 4, p.21-34. Oslo, Norway, August 10-14th (1981).

Ren, X., Kowallis, B.J., and Best, M.G. 1989. Paleostress history of the basin and range province in western Utah and eastern Nevada from healed microfracture orientations in granites. Geology, v. 17, p. 487-490.

Richter, D. and Simmons, G. 1977. Microcracks in crustal igneous rocks: Microscopy, In: Heacock, J.G., ed., The Earth's crust: American Geophysical Union monograph, 20: 149-179.

Riller, U., Cruden A.R., and Schwerdtner, W.M. 1996. Magnetic Fabric And Microstructural Evidence For A Tectonothermal Overprint Of The Early Proterozoic Murray Pluton, Central Ontario, Journal Of Structural Geology, V18, N8 (AUG), P1005-1016.

Roman-Berdiel, T., Pueyo-Morer, E-L, and Casas-Sainz, A.M. 1995. Granite emplacement during contemporary shortening and normal faulting: structural and magnetic study of the Veiga Massif (NW Spain), Journal of Structural Geology Vol. 17 (12), 1689-1706.

Rousell, D.H. 1981. A correction factor for contouring planar microfabric data. Tectonophysics, 77, T19-T21.

Rousell, D.H. and Everitt, R.A. 1981. Jointing in the Sudbury Basin, Ontario. In: Proceedings of the Third International Conference on Basement Tectonics, D.W. O'Leary and W.L. Earle, eds. Basement Tectonics Committee, Inc., Denver, Colorado. 381-391.

Rousell, D.H. and Everitt, R.A., 1977. Fracture Analysis of the Sudbury Basin. Abstr. of Paper, Geol. Assoc. Can-Min. Assoc. Can. Annual Meeting, Vancouver, B.C. p. 18.

Sano, O., Kudo, Y., and Mizuta, Y. 1992. Experimental determination of elastic constants of Oshima Granite, Barre Granite, and Chelmsford Granite. Journal of Geophysical Research, B, Solid Earth and Planets vol. 97 no. 3; p. 3367-3379.

Schmidtke, B.E. 1986. Industrial minerals of Southeast Manitoba. Manitoba Dep. Energy and Mines, Winnipeg, MB, Canada, Report of field activities, 1986, (Eds.) Bannatyne, B. B. (editor), Manitoba. Dep. Energy and Mines, Winnipeg, MB, Canada, Report of Field Activities - Mineral Resources Division (Winnipeg), vol. 1986, p. 134-138.

Scholz, C.H. and Koczynski, T.A. 1979. Dilatancy anisotropy and the response of rock to large cyclic loads. Journal of Geophysical Research. Vol. 84, 5525-5534.

Schulmann, K. and Mlcoch, B. 1996. High-temperature microstructures and rheology of deformed granite, Erzgebirge, Bohemian Massif. Journal of Structural Geology, Volume 18, Issue 6, -June-1996, p. 719-733.

Simmons, G., Todd, T., and Baldridge, W.S. 1974. Toward a quantitative relationship between elastic properties and cracks in low porosity rocks, Am. J. Sci., vol. 275, p.318-345.

Simmons, G.R. 1988. Geotechnical Research at Atomic Energy of Canada Limited's Underground Research Laboratory, in: Proceedings of the International Symposium on Uranium and Electricity - The Complete Nuclear Fuel Cycle, Saskatoon, Canada, 1988 September 18-21 (1988), p. 4-7 to 4-20.

Simmons, G.R. 1990a. Introduction to the Underground Research Laboratory. In: Proceedings of the International Symposium on Unique Underground Structures, Denver, Colorado, June 12-15, 1990. p. 63-1 to 63-20.

Simmons, G.R. 1990b. Operating Phase Experiments for Atomic Energy of Canada Limited's Underground Research Laboratory. In: Proceedings of the International Symposium on Unique Underground Structures, Denver, Colorado, June 12-15, 1990. p. 67-1 to 67-19.

Simmons, G.R. and Soonawala N.M. (eds.) 1982. Underground Research Laboratory Experimental Program, Atomic Energy of Canada Limited Technical Record, TR-153.

Sprunt, E.S. and Brace, W.F. 1974. Direct observation of microcavities in crystalline rocks, Int. J. Rock, Mech. Min, Sci. Geomech. Abstr., vol. 11, p. 139-150.

Stecich, J.P., Chin I.R., and Heidbrink F.D. 1992. Testing for thin stone veneers on buildings. Dimensional Stone Magazine, November 1992. p. 28-51.

Stone, D., Kamineni, D. C., and Brown, A. 1984. Geology and fracture characteristics of the Underground Research Laboratory lease near Lac du Bonnet, Manitoba. Atomic Energy of Canada Limited Technical Record TR-243, URL-EXP-00001-R01.

Stone, D., Kamineni, D. C., Brown, A. and Everitt, R.A. 1989. A Comparison of Fracture Styles in Two Granite Bodies of the Superior Province. Canadian Journal of Earth Sciences, Volume 26, p. 387-403.

Svab, M. and Lajtai E. Z. 1981. Microstructural control of crack growth in Lac du Bonnet granite. Proceedings of the 5th Canadian Fracture Mechanics Conference, Winnipeg, Canada. p. 219-228.

Talebi, S. and Young, R.P. 1990. Design of a Microseismic System for the URL Mineby Experiment. Provisional Report #RP006AECL, Department of Geological Sciences, Queen's University.

Talebi, S. and Young, R.P. 1992. Microseismic monitoring in highly stressed granite: Relations between shaft-wall cracking and in situ stress. International Journal of Rock Mechanics, Mineral Science & Geomechanics Abstracts 29, 25-34.

Tammemagi, H. Y. 1982. The Lac du Bonnet Batholith (RA 3); geology and rock properties. In: Geotechnical Research; Proceedings of the Seventh Nuclear Fuel Waste Management Information Meeting, Ottawa, ON, Canada, May 5-6, 1980, p. 261. Atomic Energy of Canada Limited Technical Report TR-190.

Tammemagi, H.Y. 1979. Developing the Data for Nuclear Waste Disposal. Geoscience Canada, 1979, vol. 6, no.4., p.205-208.

Tammemagi, H.Y., Kerford, P.S., Requeima, J.C., and Temple, C.A. 1980. A geological reconnaissance study of the Lac du Bonnet Batholith. Atomic Energy of Canada Limited Report AECL-6439.

Taylor, H.A. 1992. Dimension stone; United States Department of the Interior, Bureau of Mines Annual Report, p.1-17.

Thurston, P.C., Williams, H.R., Sutcliffe, R.H., and Stott, G.M., (eds.). 1991. Geology of Ontario. Ontario Geological Survey, Special Volume 4, Part 1.

Thurston, P.C., Williams, H.R., Sutcliffe, R.H., and Stott, G.M., (eds.). 1992a. Geology of Ontario. Ontario Geological Survey, Special Volume 4, Part 2.

Thurston, P.C., Williams, H.R., Sutcliffe, R.H., and Stott, G.M., (eds.). 1992b. Geology of Ontario. Ontario Geological Survey, Special Volume 4, Part 3, Maps and Charts.

Todd, T., Simmons, G., and Baldridge W.S. 1973. Acoustic double refraction in low-porosity rocks. Bull. Seismol. Soc. Am. Vol. 63, p. 20007-2020.

Tomsons, D.K., Lodha, G.S., Street, P.J., and Auger, J.L.F. 1995. A Bouguer gravity anomaly map and geophysical interpretation of the geometry of the Lac du Bonnet Batholith, Whiteshell Research Area, Southeastern Manitoba. Atomic Energy of Canada Limited, Technical Record TR-633, COG-94-096.

United States National Research Council. 1993. Stability, Failure, and Measurements of Boreholes and other Circular Openings. 1993. U.S. National Committee for Rock Mechanics, Geotechnical Board, Commission on Engineering and technical Systems, National Research Council. National Academy Press, Washington, D.C.

Verschuren, C.P., Kingston, P.W., and Calley, W.F. 1989. Criteria for quarry development in southeastern Ontario. Canadian Institute of Mining and Metallurgy Bulletin, February, 55-60 p.

Verschuren, C.P., Papertzian, V.C., Kingston, P.W., and Villard, D.J. 1986. Reconnaissance survey of building stones of eastern and central Ontario. Ontario Geological Survey, Open File Report 5585.

Verschuren, C.P., van Haaften, S., and Kingston, P.W. 1985. Building stones of eastern Ontario. Ontario Geological Survey, Open File Report 5556, 116 p.

Vos, M.A., Smith, B.A., and Stevenato,R.J. 1981. Industrial minerals of the Sudbury area. Ontario Geological Survey, Open File Report 5329.

Wahlgren, C.-H., Cruden, A.R., and Stephens, M.B. 1994. Kineamatics of a major fan-like structure in the eastern part of the Sveconorwegian orogen, Baltic Shield, south-central Sweden. Precambrian Research, 70, p. 67-91.

West, G. 1991. A note on undulatory extinction of quartz in granite. Quarterly Journal of Engineering Geology, 24: p.159-162.

Whitaker, S.H. 1987. Geoscience research for the Canadian Nuclear Fuel Waste Management Program. Radioactive Waste Management and the Nuclear Fuel Cycle, 8: p. 145-196.

Whitaker, S.H., Davison, C.C., Dormuth, K.W., and Scott, J.S. 1986. The Canadian Approach to Site Characterization for a Nuclear Fuel Waste Disposal Vault, Proceedings of A Symposium on Siting, Design and Construction of Underground Repositories for Radioactive Wastes organized by International Atomic Energy Agency, Hannover, 1986 March 3-7th.

Wijesinghe, A.M. 1987. Extended analysis of constant –height hydraulic fractures for the estimation of in-situ crack-opening modulus from bottom hole pressure records, UCID-200995, Lawerence Livermore National Laboratory.

Young, R.P. and Talebi, S. 1989. Manual of source locations of microseismic events induced by shaft extension at the Underground Research Laboratory #RP002AECL Queen's University, Kingston, ON.

Zarifa, I.H. 1998. Correlation of mineralogical and textural characteristics with engineering properties of selected granitic rocks from Turkey. Engineering Geology, Volume 51, Issue 4, 303-317.

Appendix A

POINT LOAD TESTS

This appendix presents the samples used for and the data obtained from the Point Load Tests. The tables list the specimen characteristics, and the results of the axial Point Load tests described in this report. The figures summarize the fabric and test-induced fractures observed in each of the samples used in the Point Load testing. The symbols used in the sample maps are explained in Figure A1, while the standard format for the sample maps is shown in Figure A2.

Table A1

Axial Point Load Testing Results

Fine Grained Granite, Borehole 421-031-RT1

Sample			Point Load Index		Tensile Strength		Dihedral angle	True orientations		
								Dip	Dip Direction	
fracture / *foliation*	Thickness (mm)	Diameter (mm)	I_s (Mpa)	Normalized I_s (MPa)	(PSI)	(MPa)	loading direction & foliation		Fracture	Foliation
A	19.92	44.88	20.18	21.28	1403.42	9.68	68			
A_G								82		200
B	20.31	44.88	21.57	22.31	1559.35	10.75	60			
B							80			
B_G								65		195
C	20.19	44.88	22.92	23.84	1637.32	11.29	59			
C							25			
C_G								82		200
D	20.15	44.88	21.92	22.84	1559.35	10.75	85			
D_G								82		200
E	20.67	44.88	20.83	21.16	1559.35	10.75	35			
E							85			
E							62			
E_G								90		200
F	20.19	44.88	24.56	25.54	1754.27	12.10	35			
F_G								86		10
G	20.89	44.88	19.88	19.99	1520.37	10.49	90			
G							62			
G_G								82		200
H	20.52	44.88	20.61	21.09	1520.37	10.49	35			
H_G								90		100
I	20.62	44.88	20.93	21.31	1559.35	10.75	58			
I_G								80		188
J	18.94	44.88	24.81	27.50	1559.35	10.75	72			
J							58			
J_G								70		171
J_G								70		180
Count	10.00	10.00	10.00	10.00	10.00	10.00	16.00	11.00		11.00
Maximum	20.89	44.88	24.81	27.50	1754.27	12.10	90.00	90.00		200.00
Median	20.25	44.88	21.25	21.81	1559.35	10.75	61.00	82.00		195.00
Minimum	18.94	44.88	19.88	19.99	1403.42	9.68	25.00	65.00		10.00
Std. dev.	0.54	0.00	1.74	2.33	88.99	0.61	19.78	8.23		59.99

Table A2
Axial Point Load Testing Results
Fine Grained Granite, Borehole 421-031-RT2

Sample			Point Load Index		Tensile Strength		Dihedral angle	True orientations		
								Dip	Dip Direction	
fracture / foliation	Thickness (mm)	Diameter (mm)	I_s (Mpa)	Normalized I_s (MPa)	(PSI)	(MPa)	loading direction & foliation		Fracture	Foliation
A	21.01	44.75	20.16	20.15	1568.42	10.82				
A_{sn}							40	86		59
A_{sn}							40	20		332
A_{sn}							20	45		52
B	20.70	44.75	20.77	21.07	1568.42	10.82				
B_{sn}							30	80		53
B_{sn}							64	83		209
B_{sn}							60	20		332
B_{sn}							0	50		53
B										
B_{sn}							55	80		53
B_{sn}							62	83		209
B_{sn}							60	20		332
B_{sn}							84	50		53
B										
B_{sn}							80	80		53
B_{sn}							80	83		209
B_{sn}							20	20		332
B_{sn}							50	50		53
C	20.46	44.75	19.66	20.18	1450.79	10.01				
C_{sn}							75	80		80
C_{sn}							12	15		23
C_{sn}							25	33		45
D	19.87	44.75	21.41	22.63	1490.00	10.28				
D_{sn}							15	90		59
D_{sn}							58	80		215
D_{sn}							78	20		45
D_{sn}							45	40		45
D										
D_{sn}							50	90		59
D_{sn}							55	80		215
D_{sn}							46	20		45
D_{sn}							75	40		45
D										
D_{sn}							55	90		59
D_{sn}							82	80		215
D_{sn}							38	20		330
D_{sn}							10	40		45
E	21.46	44.75	17.39	17.02	1411.58	9.74				
E_{sn}							80	80		51
E_{sn}							68	82		23
E_{sn}							5	21		51
F	20.86	44.75	18.92	19.04	1450.79	10.01				
F_{sn}							62	80		62
F_{sn}							80	82		10
F	20.86	44.75	18.92	19.04	1450.79	10.01				
F_{sn}							62	80		62
F_{sn}							80	82		10
F_{sn}							18	32		43
G	20.01	44.75	22.22	23.32	1568.42	10.82				
G_{sn}							80	86		57
G_{sn}							82	80		215
G_{sn}							30	30		56
H	20.07	44.75	20.44	21.38	1450.79	10.01				
H_{sn}							65	75		60
H_{sn}							53	61		20
H_{sn}							27	38		50
I	20.96	44.75	16.20	16.24	1254.74	8.65				
I_{sn}							76	78		57
I_{sn}							82	80		27
I_{sn}							20	60		190
I_{sn}							45	44		60
J	20.25	44.75	21.70	22.50	1568.42	10.82				
J_{sn}							88	90		46
J_{sn}							78	74		25
J_{sn}							35	40		163
J_{sn}							50	50		54
Count	10.00	10.00	10.00	10.00	10.00	10.00	50	50.00		50
Maximum	21.46	44.75	22.22	23.32	1568.42	10.82	88	90.00		332
Median	20.58	44.75	20.30	20.63	1470.40	10.14	55	67.50		55
Minimum	19.87	44.75	16.20	16.24	1254.74	8.65	0	15.00		10
Std. dev.	0.52	0.00	1.92	2.36	99.63	0.69	24	25.83		98

Table A3

Axial Point Load Testing Results

Fine Grained Granite, Borehole 421-031-RT3

Sample			Point Load Index		Tensile Strength		Dihedral angle	True orientations		
								Dip	Dip Direction	
fracture / *foliation*	Thickness (mm)	Diameter (mm)	I_s (Mpa)	Normalized I_s (MPa)	(PSI)	(MPa)	loading direction & foliation		Fracture	Foliation
A	22.03	44.87	20.63	19.66	1755.05	12.10	0			
A							0			
A							0			
B	18.38	44.87	27.00	30.85	1599.05	11.03	0			
B							0			
B							0			
C	19.67	44.87	24.15	25.78	1638.05	11.30	0			
D	19.87	44.87	23.10	24.42	1599.05	11.03	0			
E	18.30	44.87	26.57	30.49	1560.05	10.76	0			
F	19.91	44.87	23.57	24.86	1638.05	11.30	0			
F							0			
F							0			
G	23.34	44.87	19.60	17.64	1872.05	12.91	0			
G							0			
H	18.77	44.87	25.89	28.97	1599.05	11.03	0			
H							0			
H							0			
I	22.02	44.87	19.27	18.38	1638.05	11.30	0			
J	19.81	44.87	23.24	24.64	1599.05	11.03	0			
J							0			
J							0			
Count	10.00	10.00	10.00	10.00	10.00	10.00	21.00			
Maximum	23.34	44.87	27.00	30.85	1872.05	12.91	0.00			
[illegible]										
Median	19.84	44.87	23.41	24.75	1618.55	11.16	0.00			
Minimum	18.30	44.87	19.27	17.64	1560.05	10.76	0.00			
Std. dev.	1.70	0.00	2.77	4.78	93.84	0.65	0.00			

NOTE: this borehole is parallel to the most prominent foliation, and the dihedral angles between the fractures and the foliation has been approximated in each case to 0°.

Table A4

Axial Point Load Testing Results

Fine Grained Granite, Borehole 421-031-RT4

Sample			Point Load Index		Tensile Strength		Dihedral angle	True orientations		
								Dip	Dip Direction	
fracture *foliation*	Thickness (mm)	Diameter (mm)	I_s (Mpa)	Normalized I_s (MPa)	(PSI)	(MPa)	loading direction & foliation		Fracture	Foliation
A	20.50	44.96	20.65	21.15	1514.96	10.45				
A_{G1}							55		55	5
B	21.35	44.96	20.50	20.16	1631.50	11.25				
B_{G1}							55		50	20
C	19.89	44.96	20.81	21.97	1437.27	9.91				
C_{G1}							84		46	27
D	20.70	44.96	20.77	21.07	1553.81	10.72				
D_G							88		46	27
D_G							60		70	200
E	19.00	44.96	22.19	24.52	1398.43	9.64				
E										
E_{G1}							65		85	43
F	21.29	44.96	18.65	18.40	1476.12	10.18				
F_{G1}							50		40	33
F_G							75		90	334
G	21.81	44.96	17.30	16.66	1437.27	9.91				
G_G							32		71	133
G_G							65		55	244
H	20.55	44.96	20.55	21.00	1514.96	10.45				
H_{G1}							65		70	344
H_{G2}							48		65	57
I	19.09	44.96	22.59	24.85	1437.27	9.91				
I_{M1}							38		80	74
J	19.52	44.96	21.02	22.61	1398.43	9.64				
J_{G1}							36		80	300
K	18.56	44.96	23.25	26.31	1398.43	9.64				
K_{G1}							20		70	290
K_{G2}							10		76	143
L	21.05	44.96	19.08	19.03	1476.12	10.18				
L_{G1}							55		56	160
M	22.34	44.96	19.17	18.02	1670.34	11.52	20			
M							10			
M_G									90	335
Count	13.00	13.00	13.00	13.00	13.00	13.00	19.00		18.00	18.00
Maximum	22.34	44.96	23.25	26.31	1670.34	11.52	88.00		90.00	344.00
Mean	20.51	44.96	20.70	21.07	1514.96	10.45	55.00		70.00	138.00
Median	20.55	44.96	20.65	21.07	1476.12	10.18	55.00		70.00	138.00
Minimum	18.56	44.96	17.30	16.66	1398.43	9.64	10.00		40.00	5.00
Std. dev.	1.16	0.00	1.65	2.85	87.42	0.60	23.24		15.62	125.34

Table A5

Axial Point Load Testing Results

Medium Grained Granite, Borehole 417-071-RT4

Sample			Point Load Index		Tensile Strength		Dihedral angle	True orientations		
								Dip	Dip Direction	
fracture *foliation*	Thickness (mm)	Diameter (mm)	I_s (Mpa)	Normalized I_s (MPa)	(PSI)	(MPa)	loading direction & foliation		Fracture	Foliation
A	21.49	44.80	16	16	1291	9		32	135	
B	21.16	44.80	14	14	1095	8		20	177	
C	19.53	44.80	21	23	1408	10		50	118	
D	20.29	44.80	17	17	1213	8		18	194	
E	20.47	44.80	15	16	1135	8	75	22	219	
E			15	16	1135	8	26	45	259	
E			15	16	1135	8	60	48	116	
E_{M1}			15	16	1135	8		20		250
F	21.11	44.80	15	15	1213	8	12	20	177	
F_{M1}			15	15	1213	8		10		195
Count	6	6	10	10	10	10	4	10	8	2
Maximum	21.49	44.80	21	23	1408	10	75	50	259	250
Mean	20.68	44.80	16	16	1197	8	43	29	174	223
Median	20.79	44.80	15	16	1174	8	43	21	177	223
Minimum	19.53	44.80	14	14	1095	8	12	10	116	195
Std. dev.	0.72	0.00	2	2	94	1	29	14	50	39

Table A6
Axial Point Load Testing Results
Medium Grained Granite, Borehole 417-071-RT5

Sample			Point Load Index		Tensile Strength		Dihedral angle	True orientations		
								Dip	Dip Direction	
fracture *foliation*	Thickness (mm)	Diameter (mm)	I_s (Mpa)	Normalized I_s (MPa)	(PSI)	(MPa)	loading direction & foliation		Fracture	Foliation
A	22.39	44.68	13.76	12.90	1219.34	8.41		30	100	
A_{G1}							70	25		15
A_{G2}							86	15		21
A_{G3}							82	55		251
B	21.42	44.68	15.52	15.21	1258.67	8.68		0	100	
B_{G1}							25	20		100
B_{G2}							70	46		293
B								48	280	
B_{G1}							60	20		100
B_{G2}							15	46		293
C	19.59	44.68	17.39	18.64	1180.01	8.14		5	100	
C_G							30	60		5
C_G							86	90		330
D	22.45	44.68	15.01	14.04	1337.34	9.22		20	100	
D_{G1}							65	80		145
D_{G2}							75	75		184
E	20.89	44.68	15.29	15.37	1180.01	8.14		30	100	
E_{G1}							75	75		184
E_{G2}							75	75		20
E_{G3}							88	75		213
F	20.51	44.68	15.87	16.24	1180.01	8.14		10	100	
F								45	100	
F								50	280	
G	19.52	44.68	17.52	18.84	1180.01	8.14		25	100	
G_1							90	77		215
H	19.40	44.68	16.55	17.92	1101.34	7.60		90	100	
H_G							65	25		100
I	20.62	44.68	14.65	14.92	1101.34	7.60		20	100	
I_{G1}							57	90		127
J	20.81	44.68	16.44	16.59	1258.67	8.68		25	100	
J_G							0	25		100
J_G							75	80		295
K	18.66	44.68	17.89	20.13	1101.34	7.60		25	100	
K_{G2}							4	0		0
K_{G1}							74	75		290
K								25	100	
K_{G2}							35	0		0
K_{G1}							75	75		290
L	21.71	44.68	15.10	14.61	1258.67	8.68		10	100	
L_G							67	55		285
L_{G2}							0	10		100
L_{M1}							65	75		100
M	18.73	44.68	19.66	22.04	1219.34	8.41		10	100	
M_{G1}							60	20		100
M_{G2}							0	90		280
M_G							80	60		280
N	19.87	44.68	16.34	17.27	1140.67	7.87		10	100	
N_{G1}							70	40		280
N_{G2}							82	88		176
N_{G3}							10	20		100
N_{G1}							60	90		100
Count	14.00	14.00	14.00	14.00	14.00	14.00	33	51	18	33
Maximum	22.45	44.68	19.66	22.04	1337.34	9.22	90	90	280	330
Mean	20.47	44.68	16.21	16.77	1194.05	8.23	57	44	120	163
Median	20.57	44.68	16.10	16.42	1180.01	8.14	67	40	100	145
Minimum	18.66	44.68	13.76	12.90	1101.34	7.60	0	0	100	0
Std. dev.	1.24	0.00	1.53	2.54	70.04	0.48	29	30	58	106

Table A7
Axial Point Load Testing Results
Coarse Grained Granite, Borehole 418-051-RT2

Sample			Point Load Index		Tensile Strength		Dihedral angle	True orientations		
								Dip	Dip Direction	
fracture *foliation*	Thickness (mm)	Diameter (mm)	I_s (Mpa)	Normalized I_s (MPa)	(PSI)	(MPa)	loading direction & foliation		Fracture	Foliation
A	19.6	45.1	16.2	17.3	1083.3	7.5		56	147	
A_{G1}							60	0		0
B	20.6	45.1	16.7	17.0	1238.1	8.5		57	124	
B								57	159	
B_{G1}							65	5		228
C	18.6	45.1	16.0	18.1	967.3	6.7		56	145	
C_{G1}							90	0		0
D	21.7	45.1	13.8	13.3	1122.0	7.7		62	180	
D_{G1}							48	22		215
D_{G1}							40	18		228
E	22.1	45.1	13.6	12.9	1160.7	8.0		56	140	
E_{G1}							45			
F	22.8	45.1	15.4	14.2	1392.8	9.6		68	196	
F_{G1}							52	15		208
F_{G2}							35	80		26
G	20.7	45.1	13.6	13.8	1005.9	6.9		58	165	
G_{G1}							45	78		240
G_{G2}							45	78		150
H	21.0	45.1	14.6	14.6	1122.0	7.7		57	154	
H_{A2}							30			
H_{A2}							45			
H_{G1}							45			
I	21.2	45.1	13.9	13.8	1083.3	7.5		58	160	
I_{G1}							13	72		158
J	20.9	45.1	15.3	15.4	1160.7	8.0		52	133	
J_{G1}							16	56		165
J'	20.6	45.1	16.8	17.1	1238.1	8.5		58	160	
J_{G1}							50			
K	21.9	45.1	14.9	14.3	1238.1	8.5		61	180	
K_{G1}							45	20		230
L	19.6	45.1	15.6	16.7	1044.6	7.2		54	178	
L							0	54		178
L							46	75		342
M	20.7	45.1	15.5	15.7	1160.7	8.0		68	197	
M_{G1}							18	88		190
N	21.6	45.1	13.4	13.0	1083.3	7.5		56	153	
N								90	53	
N								68	197	
N_{G1}							10	85		188
O	19.8	45.1	16.0	17.0	1083.3	7.5		90	54	
O_{G1}							20	90		92
O_{G2}							35	90		92
O	19.8	45.1	16.0	17.0	1083.3	7.5		90	54	
O_{G1}							72	90		92
O_{G2}							60	90		92
O	19.8	45.1	16.0	17.0	1083.3	7.5		90	54	
O_{G1}							55	90		92
O_{G2}							75	90		92
O	19.8	45.1	16.0	17.0	1083.3	7.5		90	54	
O_{G1}							72	90		92
O_{G2}							60	90		92
O	19.8	45.1	16.0	17.0	1083.3	7.5		90	54	
O_{G1}							55	90		92
O_{G2}							75	90		92
Count	10	10	10	10	10	10	27	43	21	22
Maximum	22.8	45.1	16.7	18.1	1392.8	9.6	90.00	90	197	342
[illegible]										
Median	20.9	45.1	15.0	14.4	1122.0	7.7	45.00	61	154	162
Minimum	18.6	45.1	13.6	12.9	967.3	6.7	0.00	0	53	0
Std. dev.	1.2	0.0	1.2	1.8	119.7	0.8	21.03	n/a	n/a	n/a

Table A8

Axial Point Load Testing Results

Coarse Grained Granite, Borehole 418-051-RT3

Sample			Point Load Index		Tensile Strength		Dihedral angle	True orientations		
								Dip	Dip Direction	
fracture *foliation*	Thickness (mm)	Diameter (mm)	I_s (Mpa)	Normalized I_s (MPa)	(PSI)	(MPa)	loading direction & foliation		Fracture	Foliation
A	20.6	44.6	14.1	14.3	1065.3	7.3		40	110	
A_{G1}							43	65		63
B	20.5	44.6	15.9	16.2	1183.7	8.2		48	93	
B_{G1}							18	54		75
C	20.5	44.6	13.8	14.1	1025.9	7.1		70	69	
C_{G1}							12	61		75
D	20.0	44.6	14.5	15.3	1025.9	7.1		70	69	
D_{G1}							10	63		64
D_{G1}							34	43		70
D	20.0	44.6	14.5	15.3	1025.9	7.1		48	83	
D_{G1}							32	56		47
D_{G1}							15	56		47
E	20.7	44.6	14.6	14.8	1104.8	7.6		55	84	
E_{G1}							20			
F	20.0	44.6	13.4	14.0	947.0	6.5		65	72	
F_{G1}							5			
Count	7	7	7	7	7	7	9	9	14	7
Maximum	20.7	44.6	15.9	16.2	1183.7	8.2	43.00	43	70	110
[illegible]										
Median	20.5	44.6	14.5	14.8	1025.9	7.1	18.00	18	56	83
Minimum	20.0	44.6	13.4	14.0	947.0	6.5	5.00	5	40	69
Std. dev.	0.3	0.0	0.8	0.8	74.6	0.5	12.64	13	10	15

Table A9

Axial Point Load Testing Results

Coarse Grained Granite, Borehole 418-051-RT4

Sample			Point Load Index		Tensile Strength		Dihedral angle	True orientations		
								Dip	Dip Direction	
fracture *foliation*	Thickness (mm)	Diameter (mm)	I_s (Mpa)	Normalized I_s (MPa)	(PSI)	(MPa)	loading direction & foliation		Fracture	Foliation
A	22.3	44.5	13.4	12.7	1189.6	8.2		35	85	
A_{G1}							25	20		160
A_{G}							75	88		10
B	21.0	44.5	14.2	14.2	1110.3	7.7		20	125	
B_{G1}								20		136
C	19.9	44.5	17.5	18.5	1229.2	8.5		48	73	
C_{G1}							45	20		136
C_{G2}							62	25		322
D	19.8	44.5	15.9	16.9	1110.3	7.7		32	124	
D_{G1}							45			
D_{G1}							45			
E	20.7	44.5	14.5	14.7	1110.3	7.7		27	95	
E_{G1}							15	22		122
E_{G1}							45	65		142
E_{G2}							50	30		348
F	21.0	44.5	16.2	16.2	1268.9	8.8		28	85	
F_{G1}							0	71		79
F_{G2}							45			
Count	5	5	5	5	5	5	10	13	5	8
Maximum	21.0	44.5	17.5	18.5	1268.9	8.8	75.00	88	125	348
[illegible]										
Median	20.7	44.5	15.9	16.2	1110.3	7.7	45.00	28	95	136
Minimum	19.8	44.5	14.2	14.2	1110.3	7.7	0.00	20	73	10
Std. dev.	0.6	0.0	1.3	1.7	77.3	0.5	21.31	23	23	116

Table A10

Axial Point Load Testing Results

Coarse Grained Granite, Borehole 418-051-RT5

Sample			Point Load Index		Tensile Strength		Dihedral angle	True orientations		
								Dip	Dip Direction	
fracture *foliation*	Thickness (mm)	Diameter (mm)	I_s (Mpa)	Normalized I_s (MPa)	(PSI)	(MPa)	loading direction & foliation		Fracture	Foliation
A	19.1	44.6	13.8	15.2	892.1	6.2		0	0	
A_{G1}							10			
B	19.7	44.6	14.1	15.1	971.1	6.7		20	87	
B							15	25		90
C	20.1	44.6	13.2	13.9	943.4	6.5		25	53	
C_{G1}							8	65		90
D	19.9	44.6	13.4	14.2	943.4	6.5		15	53	
D_{G1}							72	18		54
E	20.0	44.6	17.8	18.7	1263.2	8.7		71	53	
E_{G1}							5	20		160
F	20.9	44.6	14.0	14.1	1089.5	7.5		0	0	
F_{G1}							10			
G							10	15	233	
G							35	12	53	
G							83	10	233	
G_{G1}								13		230
H	21.8	44.6	14.0	13.5	1184.2	8.2		50	233	
H_{G1}							45			
I	20.5	44.6	18.0	18.5	1342.1	9.3		30	53	
I_{G1}							10	28		75
J	20.4	44.6	16.1	16.6	1184.2	8.2		5	233	
J_{G1}							5	8		187
K	20.2	44.6	15.3	15.9	1105.3	7.6		15	233	
L	20.6	44.6	16.8	17.1	1263.2	8.7	30	77	233	
L	20.6	44.6	16.8	17.1	1263.2	8.7	35	5	233	
L	20.6	44.6	16.8	17.1	1263.2	8.7	82	45	53	
L_{G1}								75		228
Count	7	7	7	7	7	7	15	24	16	8
Maximum	21.8	44.6	18.0	18.5	1342.1	9.3	83.00	77	233	230
Median	20.6	44.6	16.8	17.1	1263.2	8.7	15.00	19	70	125
Minimum	20.2	44.6	14.0	13.5	1105.3	7.6	5.00	0	0	54
Std. dev.	0.5	0.0	1.3	1.5	77.0	0.5	28.17	24	98	71

Sample A

Structure	Relative Orientation *(strike / dip & dip direction)*
F	100°/90° NE
G_1	100°/20° NE
G_2	190°/60° NW
M_1	190°/60° NW
A	100°/30° E
^{30}┤	strike & dip with dip direction

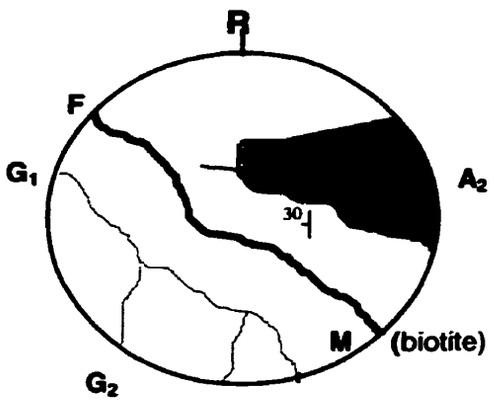

Downhole View
Dwg. No.

where:

R	core reference line
F	fracture induced by loading
G_1	gneissic foliation type 1
G_2	gneissic foliation type 2
M_1	mineral alignment, type indicated on figure
A_1	axial plane of fold
A_2	axis of fold
▬	biotite > 10% or some compositional heterogeneity as indicated by text.

Note: All orientations shown in the drawings are relative to the section shown, with the core reference line representing an interim North. These have been converted to true orientations in the report.

Figure A1. Key to symbols used on the sample maps.

Rock name **Test type (Brazilian or Point load)**

Borehole name (e.g. 401-123-rt2) **Core size (alphanumeric and in mm).**

Sample a

Structure	Relative Orientation
F	strike (0-360) / dip (0-90)
G_1	strike (0-360) / dip (0-90)
G_2	strike (0-360) / dip (0-90)

Comments
Brief description of rock including anything noteworthy about the foliations present and the affect (if any) this had on testing.

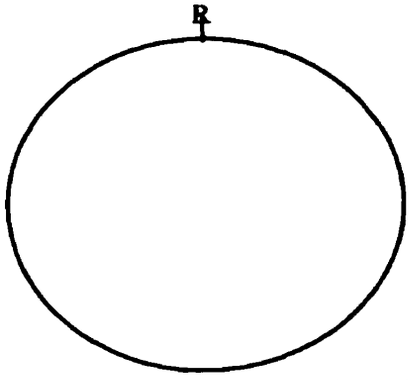

Downhole View
Dwg. No.

Sample b

Structure	Relative Orientation
F	strike (0-360) / dip (0-90)
G_1	strike (0-360) / dip (0-90)
G_2	strike (0-360) / dip (0-90)

Comments
Brief description of rock including anything noteworthy about the foliations present and the affect (if any) this had on testing.

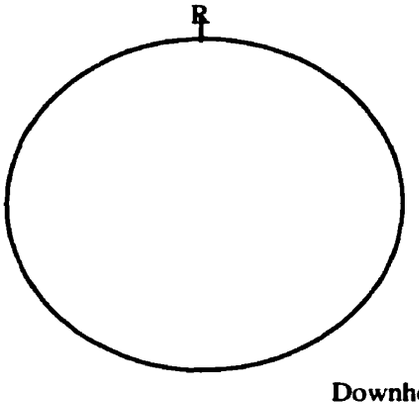

Downhole View
Dwg. No.

Sample c

Structure	Relative Orientation
F	strike (0-360) / dip (0-90)
G_1	strike (0-360) / dip (0-90)
G_2	strike (0-360) / dip (0-90)

Comments
Brief description of rock including anything noteworthy about the foliations present and the affect (if any) this had on testing.

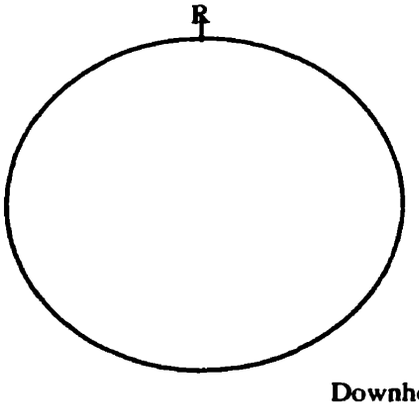

Downhole View
Dwg. No.

Figure A2: Standard format for the fabric maps constructed for each of the samples selected for testing. The rock name, the borehole from which the sample came, the size of the borehole, and the test type are indicated at the top of each sheet. Up to three sample maps are shown per page, at their actual size. The reference line marked on the top of the core is shown, and all views are downhole unless otherwise indicated.

Medium Grained Granite
Borehole 417-071-RT4

Test Type (Point Load)
Core Size: NQ-3, 45 mm

Sample A

Structure	Relative Orientation
F	065°/90°

Comments

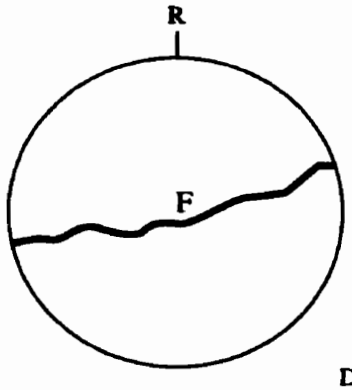

Downhole View
Fig. 2_071

Sample B

Structure	Relative Orientation
F	085°/90°

Comments

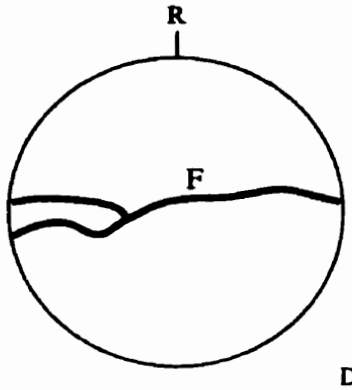

Downhole View
Fig. 2_072

Sample C

Structure	Relative Orientation
F	045°/90°

Comments

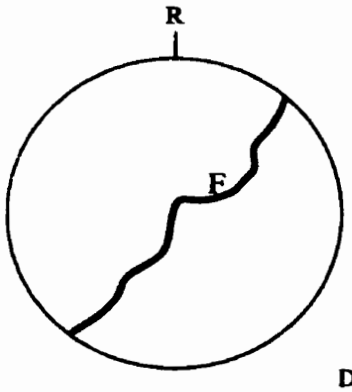

Downhole View
Fig. 2_073

Medium Grained Granite
Borehole 417-071-RT4

Test Type (Point Load)
Core Size: NQ-3, 45 mm

Sample D

Structure	Relative Orientation
F	090°/90°

Comments

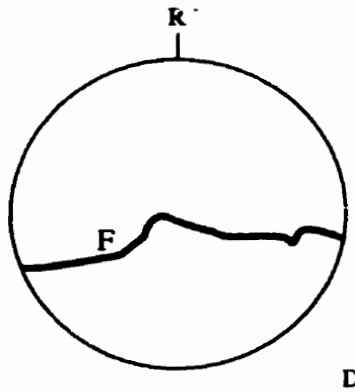

Downhole View
Fig. 2_074

Sample E

Structure	Relative Orientation
F	000°/90°
	130°/90°
	225°/90°
M_1	105°/80°N

Comments
Triple point fracture

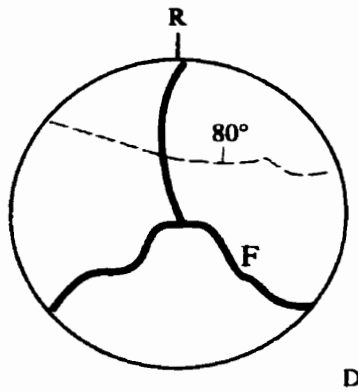

Downhole View
Fig. 2_075

Sample F

Structure	Relative Orientation
F	085°/90°
M_1	088°/80°N

Comments

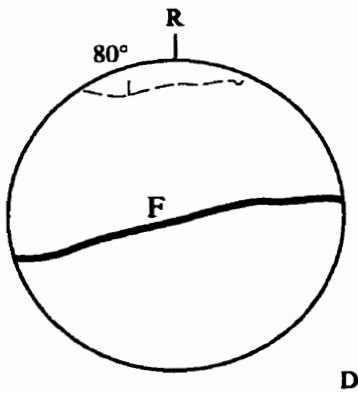

Downhole View
Fig. 2_076

Medium Grained Granite
Borehole 417-072-RT5

Test Type (Point Load)
Core Size: NQ-3, 45 mm

Fig. 2_077

Sample A

Structure	Relative Orientation
F	067°/90°
G_1	080°/25°NW
G_2	025°/35°NW

Comments

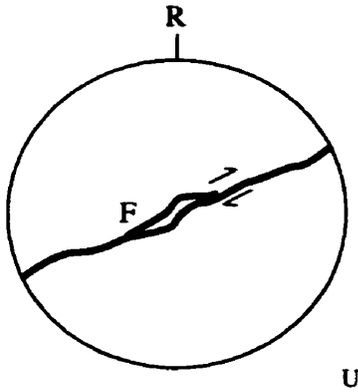

Uphole View

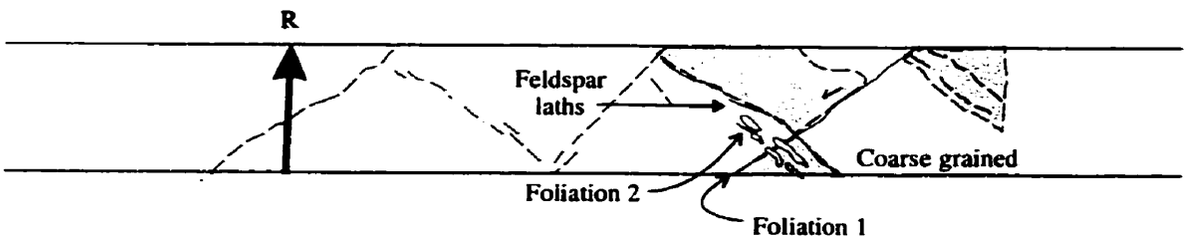

Perimeter View

Structure	Relative Orientation

Comments

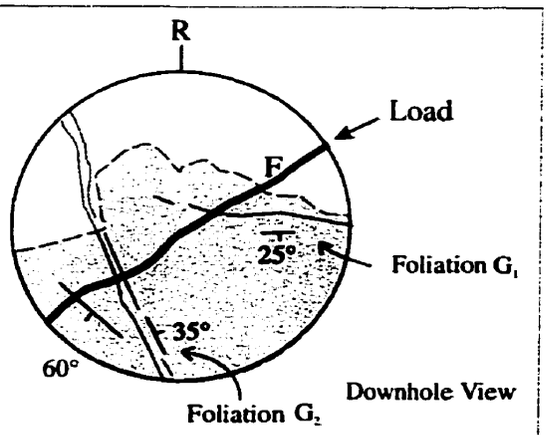

Downhole View

Medium Grained Granite
Borehole 417-072-RT5

Test Type (Point Load)
Core Size: NQ-3, 45 mm

Fig. 2_079

Sample B'

Structure	Relative Orientation
F	090°/90°
F	110°/90°
F	320°/80°NE
G_1	060°/25°SE
G_2	140°/80°NE

Comments

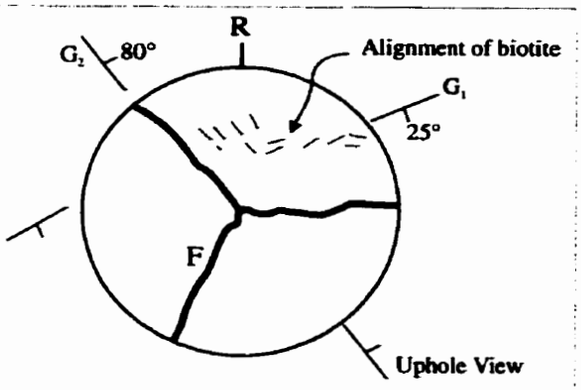

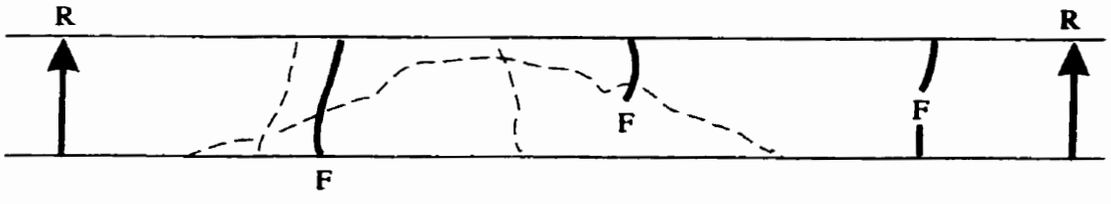

Perimeter View

Medium Grained Granite
Borehole 417-072-RT5

Test Type (Point Load)
Core Size: NQ-3, 45 mm

Fig. 2_078

Sample C

Structure	Relative Orientation
F	070°/90°
M_1	180°/40°E
M_2	060°/60°SE

Comments

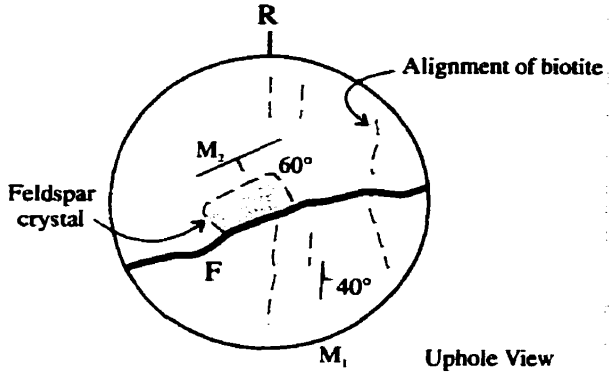

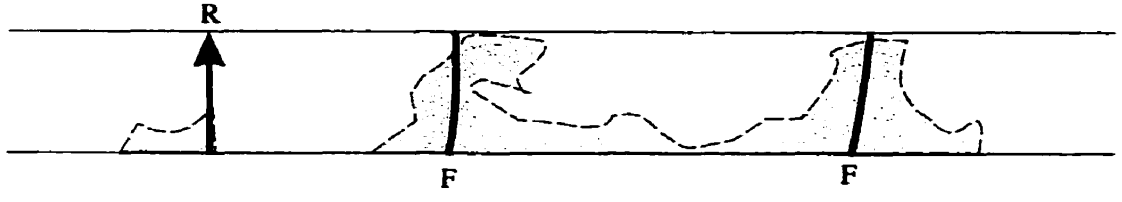

Perimeter View

Medium Grained Granite
Borehole 417-072-RT5

Test Type (Point Load)
Core Size: NQ-3, 45 mm

Fig. 2_081

Sample D

Structure	Relative Orientation
F	067°/90°
M_1	025°/45°SE
M_2	067°/15°SE

Comments

Two Foliations;
Relative Orientations as shown

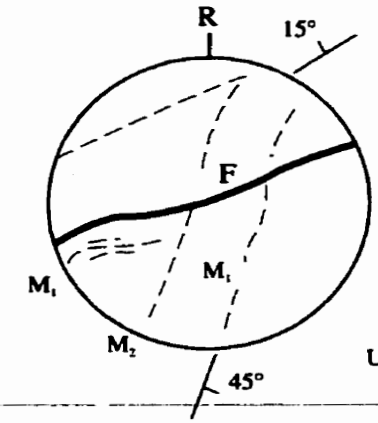

Uphole View

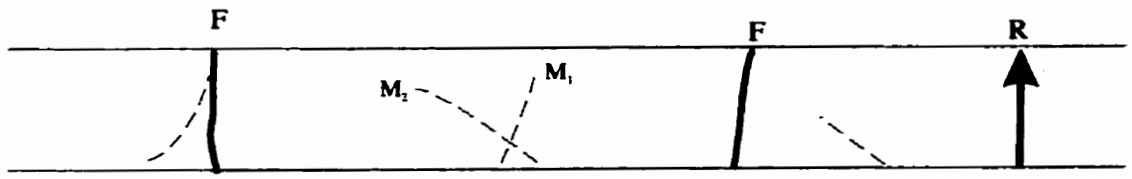

Perimeter View

Medium Grained Granite
Borehole 417-072-RT5

Test Type (Point Load)
Core Size: NQ-3, 45 mm

Fig. 2_082

Sample E

Structure	Relative Orientation
F	065°/90°
M_1	160°/35°SW
M_1	070°/15°SW

Comments

Two foliations; orientations as shown

Sample appears to resemble boudin structure with white areas (feldspar) separated by greyish quartzose areas

Steeper foliation is marked by weak banding and offsets of boudins. Fracture as shown.

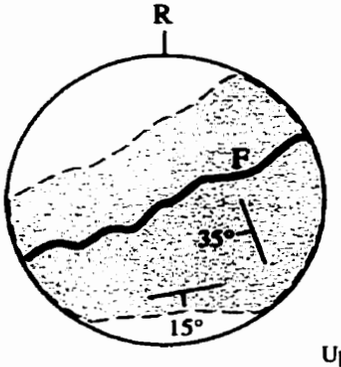

Uphole View

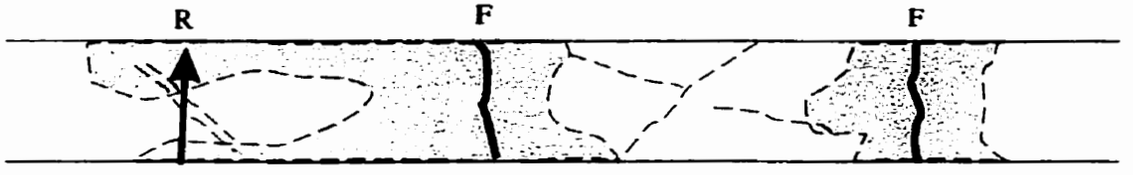

Perimeter View

Medium Grained Granite
Borehole 417-072-RT5

Test Type (Point Load)
Core Size: NQ-3, 45 mm

Fig. 2_083

Sample F

Structure	Relative Orientation
F	085°/90°
F	140°/90°
F	040°/90°

Comments
This sample is essentially massive

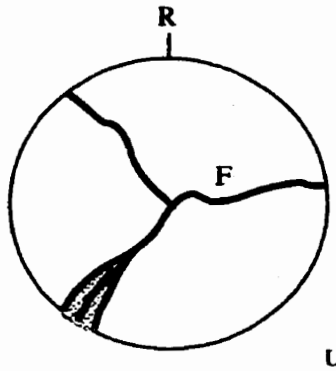

Uphole View

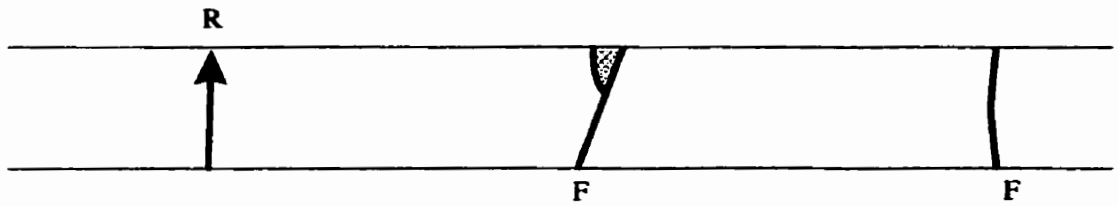

Perimeter View

Medium Grained Granite
Borehole 417-072-RT5

Test Type (Point Load)
Core Size: NQ-3, 45 mm

Sample G

Structure	Relative Orientation
F	065°/90°
G_t	145°/85°NE
G_t	145°/30°SW

Comments

Weak mineral alignment
The shallow dipping foliation is more coarsely defined, with irregular bands which are several grains in width

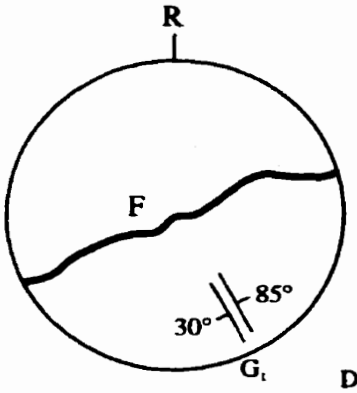

Downhole View
Fig. 2_084

Sample H

Structure	Relative Orientation
F	175°/90°
G_t	065°/60°NW

Comments

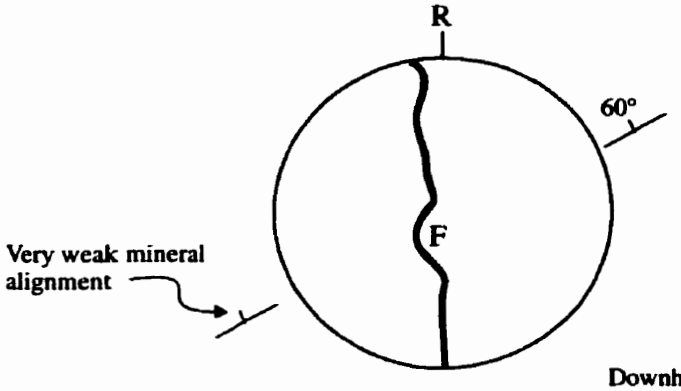

Downhole View
Fig. 2_085

Sample I

Structure	Relative Orientation
F	080°/90°
G_t	015°/60°NW

Comments

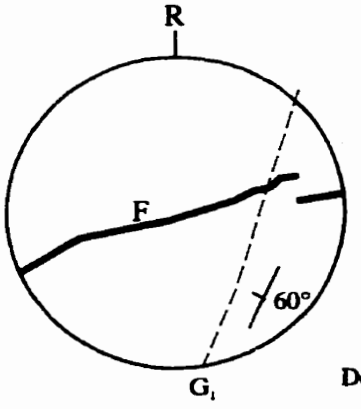

Downhole View
Fig. 2_086

Medium Grained Granite
Borehole 417-072-RT5

Test Type (Point Load)
Core Size: NQ-3, 45 mm

Sample J

Structure	Relative Orientation
F	065°/90°
G_1	170°/75°E
G_2	065°/90°SE

Comments

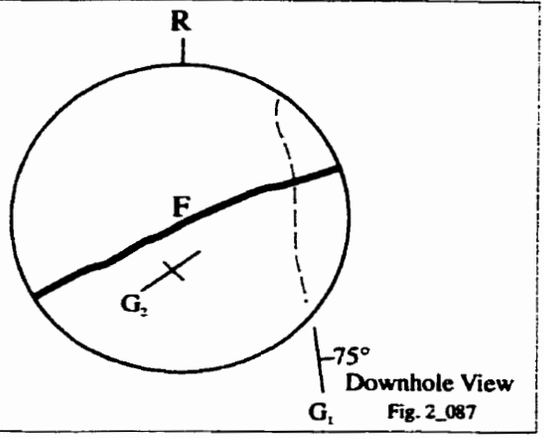

Fig. 2_087

Sample K

Structure	Relative Orientation
F	060°/90°
G_1	150°/80°NE
G_2	090°/90°

Comments

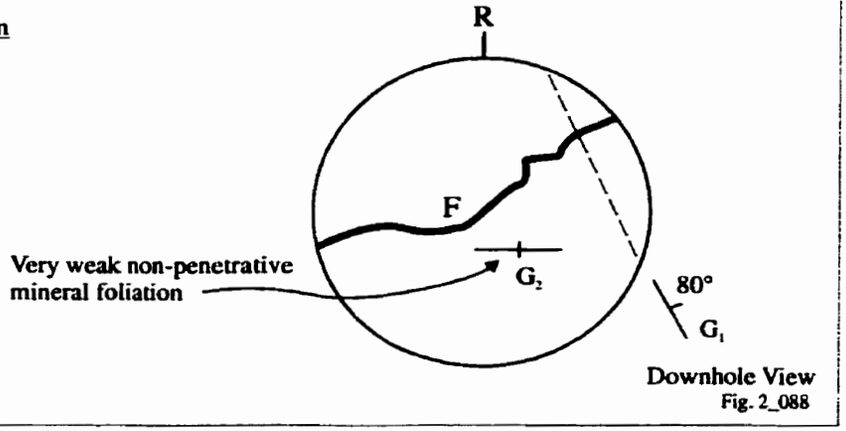

Fig. 2_088

Sample L

Structure	Relative Orientation
F	085°/90°
G_1	145°/85°NE
G_2	060°/80°NW

Comments

Non-penetrative lineament in matrix between feldspar phenocrysts

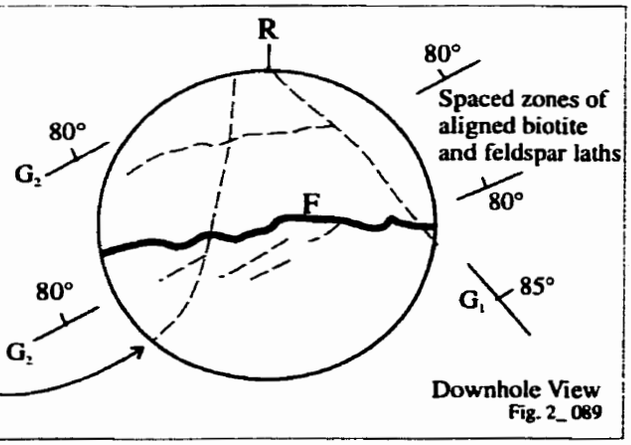

Fig. 2_089

Medium Grained Granite
Borehole 417-072-RT5

Test Type (Point Load)
Core Size: NQ-3, 45 mm

Sample M

Structure	Relative Orientation
F	070°/90°
G_1	130°/80°NE
M_1	130°/90°
M_2	145°/90°

Comments: Broken feldspar laths with quartz filling, also alteration veins in feldspar and biotite

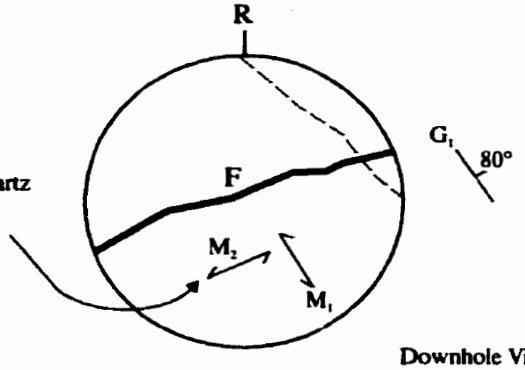

Downhole View
Fig. 2_090

Sample N

Structure	Relative Orientation
F	065°/90°
G_1	130°/80°NE
G_2	090°/15°
M_2	065°/90°

Comments: Weak mineral alignments and bleached alteration along microcracks

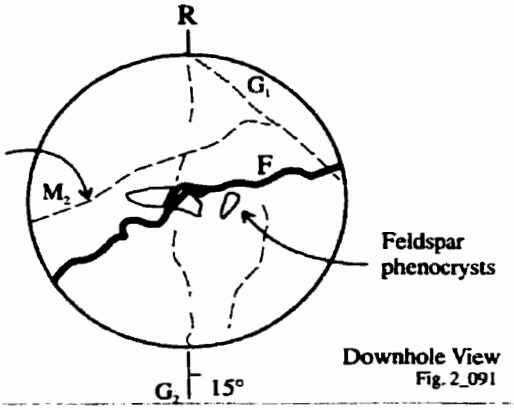

Downhole View
Fig. 2_091

Coarse Grained Granite
Borehole 418-051-RT2

Test Type (Point Load)
Core Size: NQ-3, 45 mm

Fig. 2_092

Sample A

Structure	Relative Orientation
F	090°/90°
G_t	090°/30°N

Comments

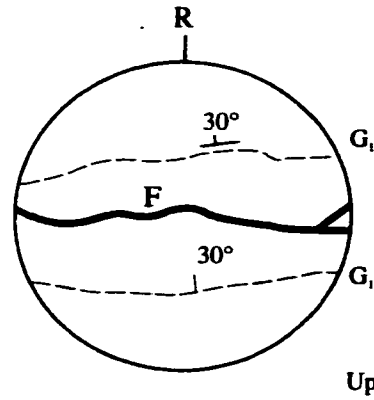

Uphole View

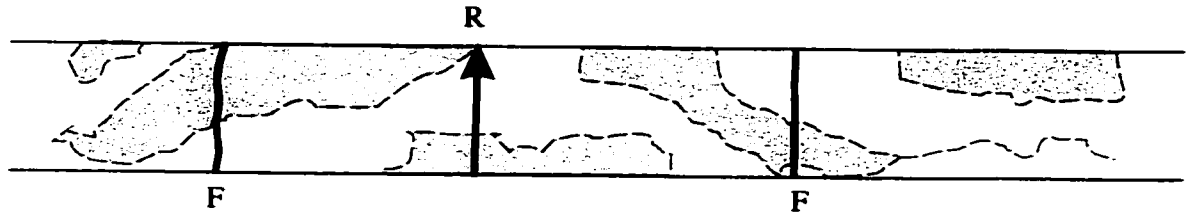

Perimeter View

Structure

Comments

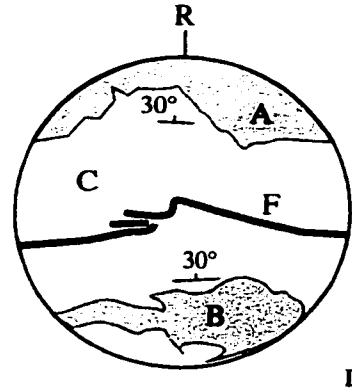

Downhole View

Coarse Grained Granite
Borehole 418-051-RT2

Test Type (Point Load)
Core Size: NQ-3, 45 mm

Fig. 2_093

Sample B

Structure	Relative Orientation
F	070°/90°
F	100°/90°
G_i	100°/30°N

Comments

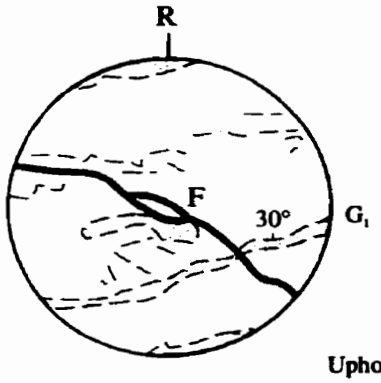

Uphole View

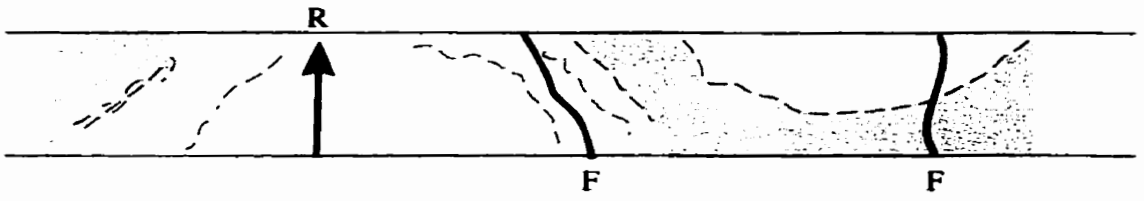

Perimeter View

Structure

Comments

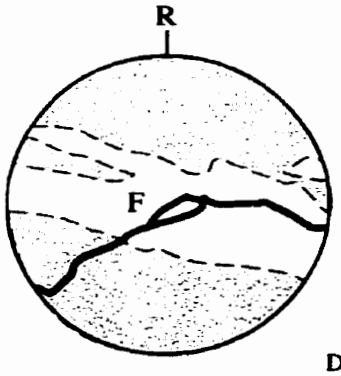

Downhole View

Coarse Grained Granite
Borehole 418-051-RT2

Test Type (Point Load)
Core Size: NQ-3, 45 mm

Fig. 2_094

Sample C

Structure	Relative Orientation
F	090°/90°
G_1	090°/35°N

Comments

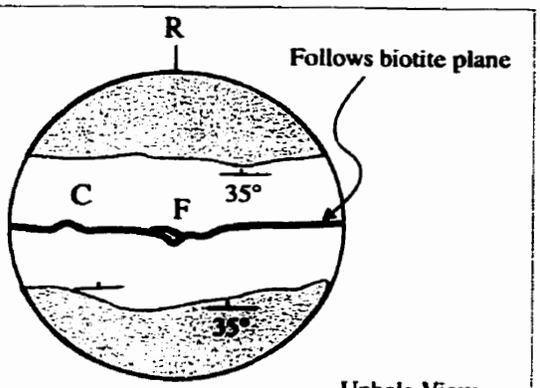

Uphole View

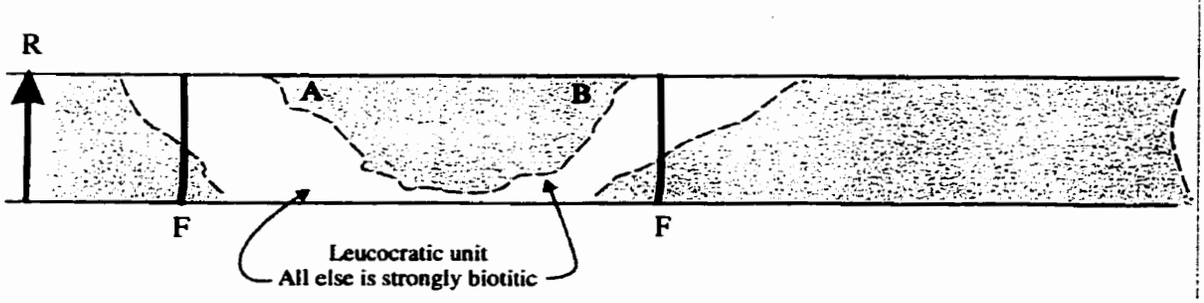

Perimeter View

Structure

Comments

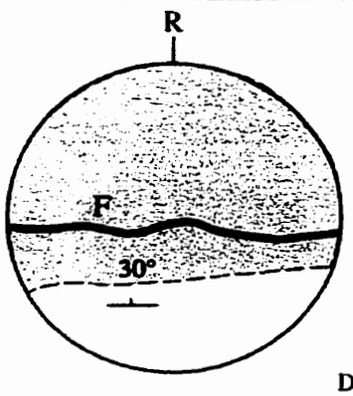

Downhole View

Coarse Grained Granite
Borehole 418-051-RT2

Test Type (Point Load)
Core Size: NQ-3, 45 mm

Fig. 2_094

Sample C

Structure	Relative Orientation
F	090°/90°
G_1	090°/35°N

Comments

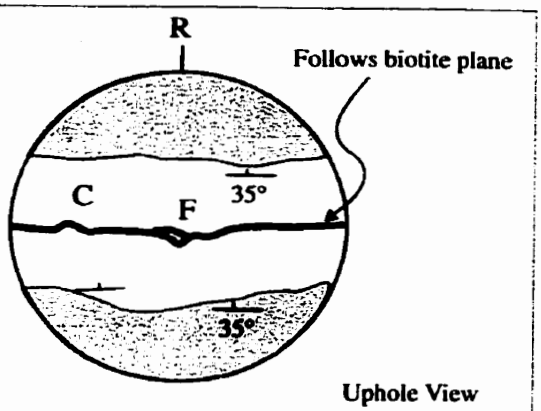

Uphole View

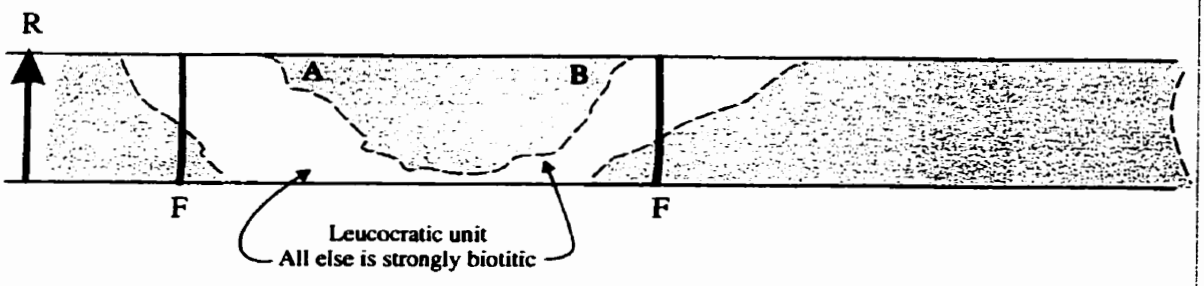

Perimeter View

Structure

Comments

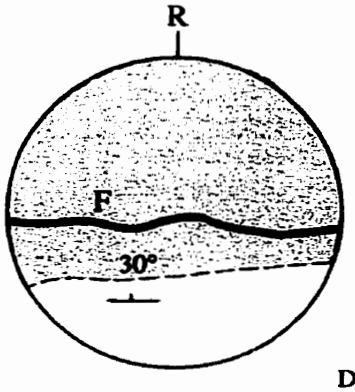

Downhole View

Coarse Grained Granite
Borehole 418-051-RT2

Test Type (Point Load)
Core Size: NQ-3, 45 mm

Sample D

Structure	Relative Orientation	
F	120°/90°	Fracture
G_1	120°/45°NE	Gneissosity
G_2	120°/40°NE	Thrusts

Comments

Sample is a classic fabric type 4 with well demarcated layers of alternating biotite and leucocratic granite. Some of the biotitic lenses are slip surfaces (like miniature thrust faults)

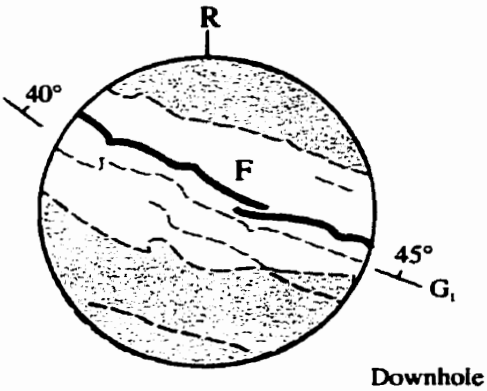

Downhole View
Fig. 2_095

Sample E

Structure	Relative Orientation
F	085°/90°
G_1	080°/ 45°N

Comments

Sample is strongly layered, biotitic schlieren alternating with leucocratic and intermediate layers.

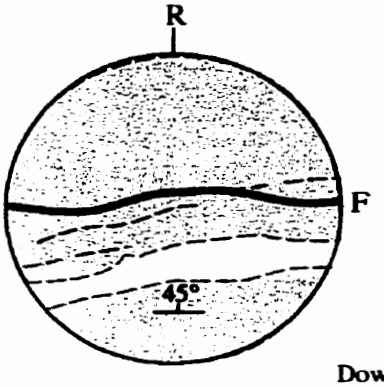

Downhole View
Fig. 2_096

Sample G

Structure	Relative Orientation	
F	105°/90°	
G_1	105°/45°N	Gneissic Banding
G_2	105°/45°S	Thrusts

Comments

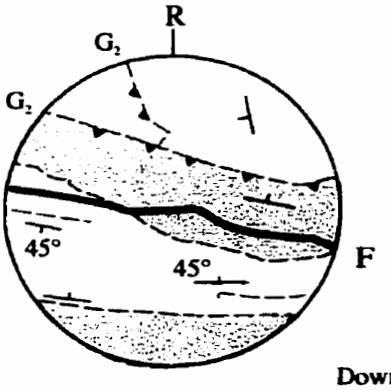

Downhole View
Fig. 2_098

Coarse Grained Granite
Borehole 418-051-RT2

Test Type (Point Load)
Core Size: NQ-3, 45 mm

Fig. 2_099

Sample H

Structure | Relative Orientation

Comments

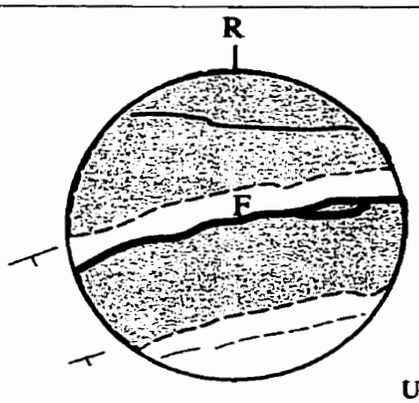

Uphole View

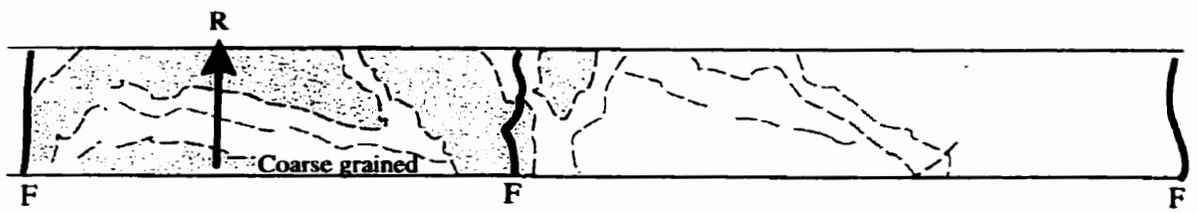

Perimeter View

Structure	Relative Orientation	
F	100°/90°	Fracture
G_1	100°/45°NE	
A_2	100°/60°SW	Fold axial plane
A_2	100°/45°NE	Fold axial plane

Comments

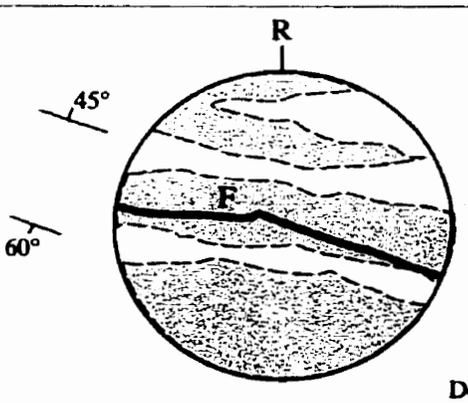

Downhole View

Coarse Grained Granite
Borehole 418-051-RT2

Test Type (Point Load)
Core Size: NQ-3, 45 mm

Fig. 2_100

Sample I

Structure | Relative Orientation

Comments

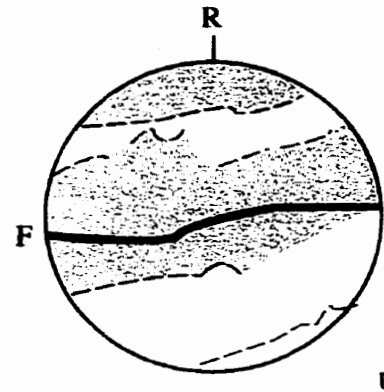

Uphole View

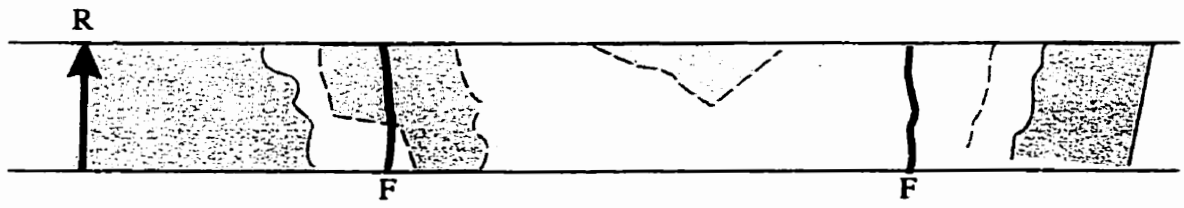

Perimeter View

Structure	Relative Orientation
F	100°/88°S
G_1	100°/75°S

Comments

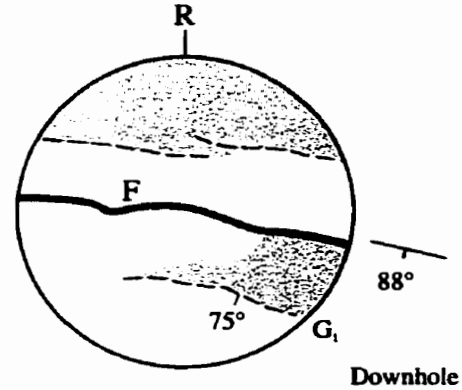

Downhole View

Coarse Grained Granite
Borehole 418-051-RT2

Test Type (Point Load)
Core Size: NQ-3, 45 mm

Fig. 2_101

Sample J

Structure | Relative Orientation

Comments

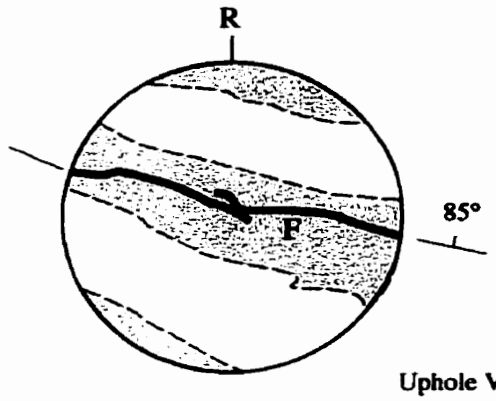

Uphole View

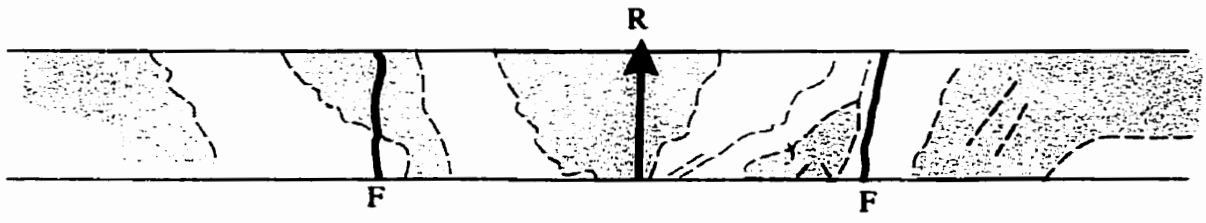

Perimeter View

Structure	Relative Orientation
F	080°/85°N
G_1	080°/70°N

Comments

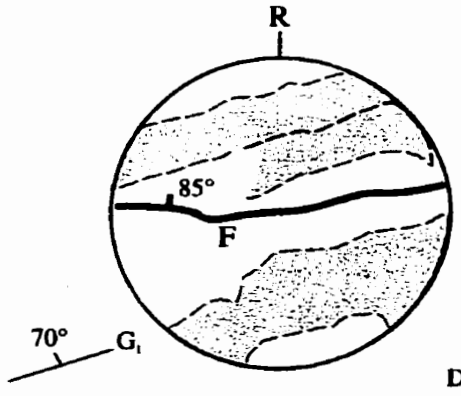

Downhole View

Coarse Grained Granite
Borehole 418-051-RT2

Test Type (Point Load)
Core Size: NQ-3, 45 mm

Fig. 2_102

Sample J*

Structure Relative Orientation

Comments

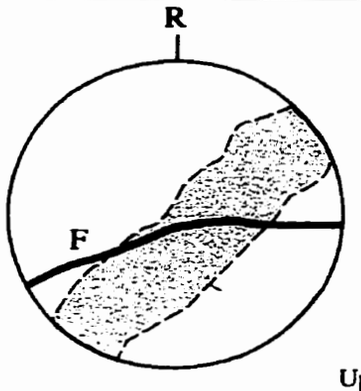

Uphole View

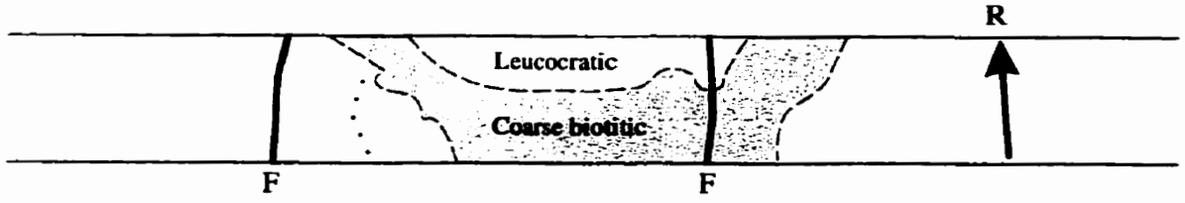

Perimeter View

Structure	Relative Orientation	
F	100°/90°	Fracture
G_t	120°/45°NE	

Comments

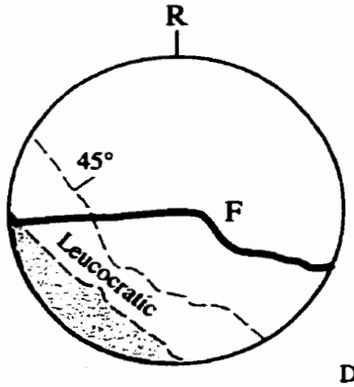

Downhole View

Coarse Grained Granite
Borehole 418-051-RT2

Test Type (Point Load)
Core Size: NQ-3, 45 mm

Fig. 2_103

Sample K

Structure Relative Orientation

Comments

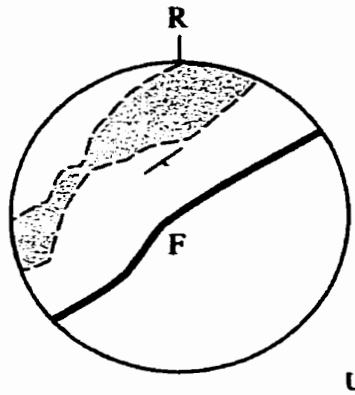

Uphole View

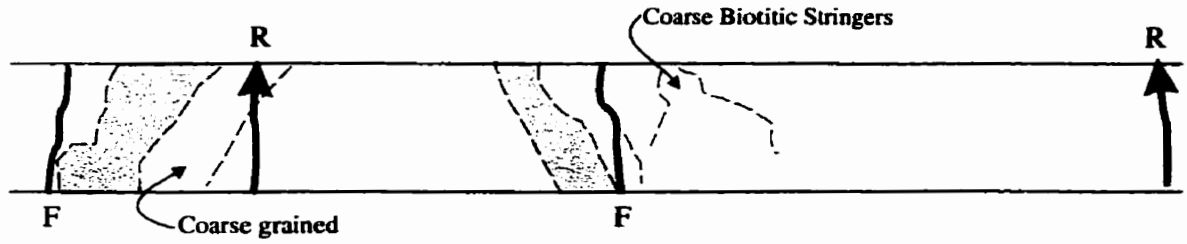

Perimeter View

Structure	Relative Orientation
F	120°/ 90°
G_1	120°/45°NE

Comments

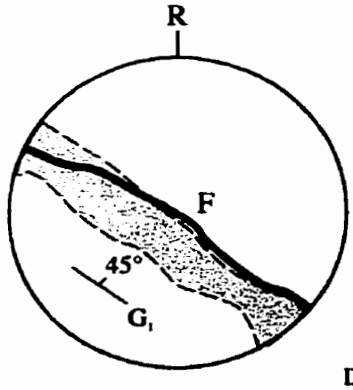

Downhole View

Coarse Grained Granite
Borehole 418-051-RT2

Test Type (Point Load)
Core Size: NQ-3, 45 mm

Fig. 2_104

Sample L

Structure Relative Orientation

Comments

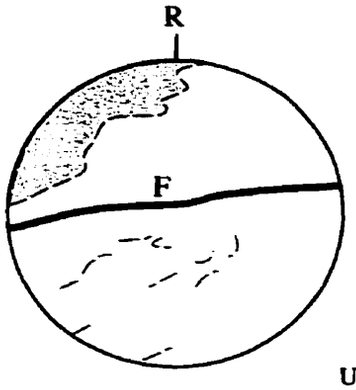

Uphole View

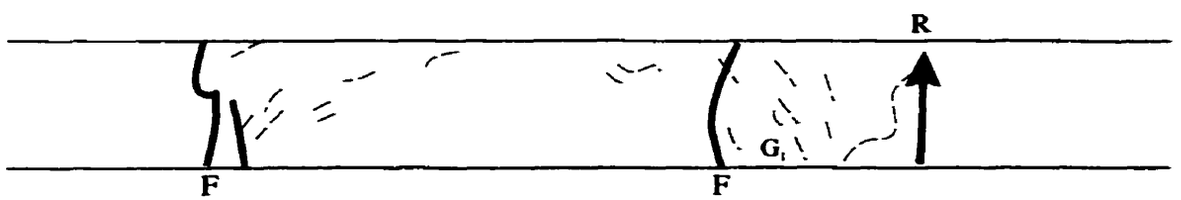

Perimeter View

Structure	Relative Orientation
F	115°/85°NE
G_1	115°/85°NE
G_2	115°/48°SW

Comments

Sample contains two distinct gneissic layers, one biotitic, the other coarse to medium grained leucocratic granite. Biotite grains within the latter have a preferred orientation trending same but with opposite dip direction.

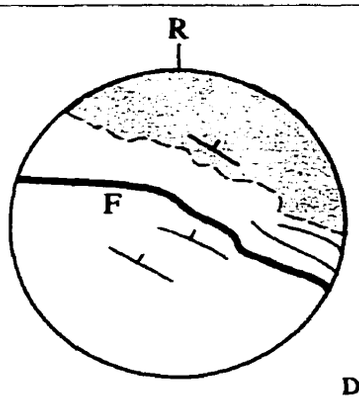

Downhole View

Coarse Grained Granite
Borehole 418-051-RT2

Test Type (Point Load)
Core Size: NQ-3, 45 mm

Sample M

Structure	Relative Orientation	
F	135°/90°	Fracture
G_1	140°/75°NE	Gneissic foliation

Comments

Fracture developed in coarse granite leucocratic segment of sample but nearly along foliation. Crack appears to be along grain boundaries.

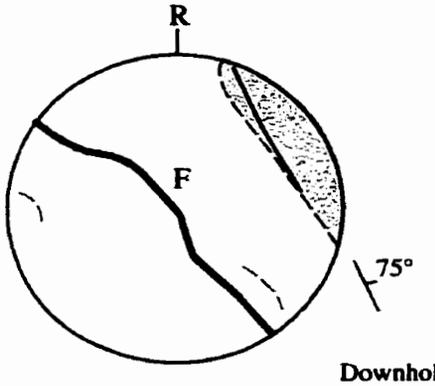

Downhole View
Fig. 2_105

Sample N

Structure	Relative Orientation
F	100°/90°
F	180°/90°
F	135°/90°
G_1	135°/80°NE

Comments

Sample is entirely leucocratic granite with ill-defined banding distinguished by variations in relative abundance of quartz. Coarse grained.

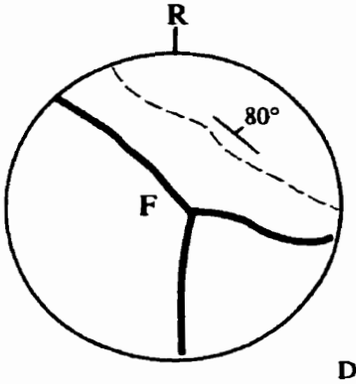

Downhole View
Fig. 2_ 106

Sample O

Structure	Relative Orientation
F	105° /90°
F	235°/90°
F	000°/90°
G_1	125°/90°
G_2	105°/55°NE

Comments

Sample is entirely coarse grained leucocratic granite with no biotitic lenses to impart layering. Instead, layering is indicated by variations in quartz content. Sample may show incipient discing.

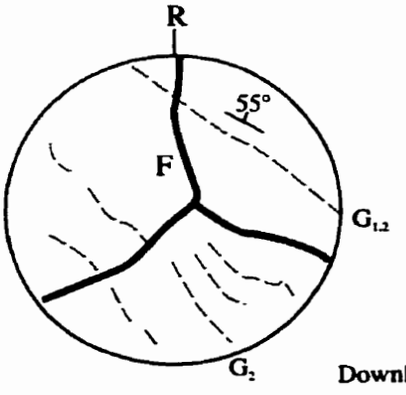

Downhole View
Fig. 2_ 107

Coarse Grained Granite
Borehole 418-051-RT3

Test Type (Point Load)
Core Size: NQ-3, 45 mm

Sample A

Structure	Relative Orientation
F	068°/90°
G_1	025°/80°NW

Comments

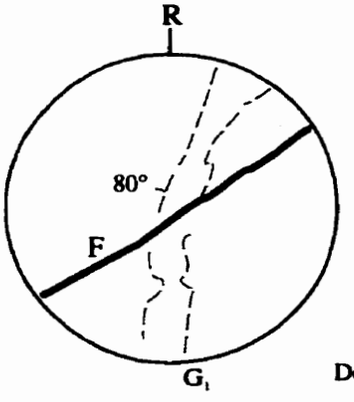

Downhole View
Fig. 2_121

Sample B

Structure	Relative Orientation
F	055°/90°
G_1	040°/80°NW

Comments

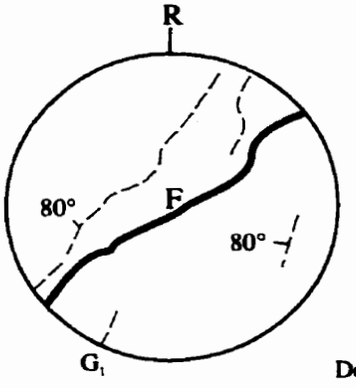

Downhole View
Fig. 2_122

Sample C

Structure	Relative Orientation
F	025°/90°
G_1	035°/85°NW

Comments

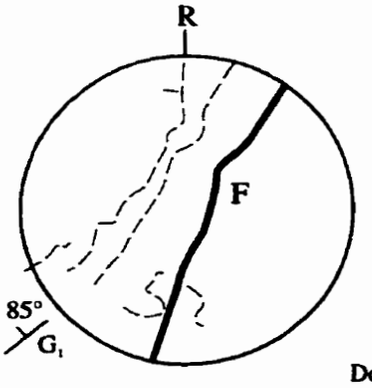

Downhole View
Fig. 2_123

Coarse Grained Granite
Borehole 418-051-RT3

Test Type (Point Load)
Core Size: NQ-3, 45 mm

Sample D

Structure	Relative Orientation
F	025°/90°
	055°/90°
G_t	025°/ 81°NW
	055°/75°NW

Comments

Fracture follows change in foliation

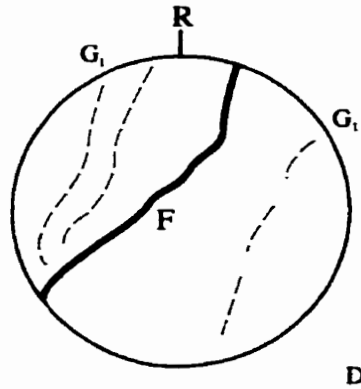

Downhole View
Fig. 2_124

Sample E

Structure	Relative Orientation
F	055°/90°
F	082°/90°
F	025°/90°
F	055°/90°
G_t	055°/70°NW
G_t	082°/70°NW
G_t	025°/65°NW
G_t	115°/60°NW

Comments

Layering in sample folded in a complex manner.

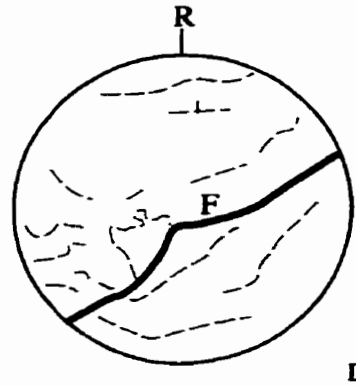

Downhole View
Fig. 2_125

Sample F

Structure	Relative Orientation
F	010°/90° to 025°/90°
G_t	010°/85°NW
G_t	030°/85°NW

Comments

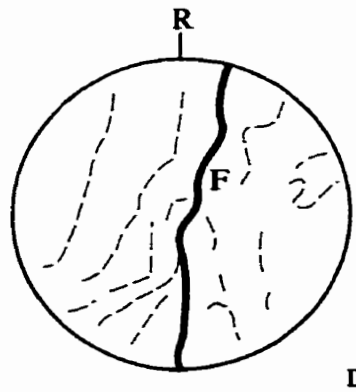

Downhole View
Fig. 2_126

Coarse Grained Granite
Borehole 418-051-RT4

Test Type (Point Load)
Core Size: NQ-3, 45 mm

Sample A

Structure	Relative Orientation	
F	060°/90°	
G_1	085°/90°	Coarse layering
G_2	165°/60°SW	Boudin plane

Comments

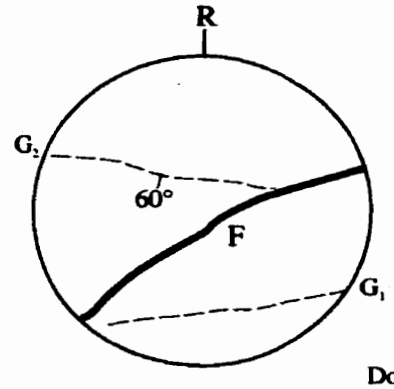

Downhole View
Fig. 2_127

Sample B

Structure	Relative Orientation
F	085°/90°
G_1	085°/90°

Comments

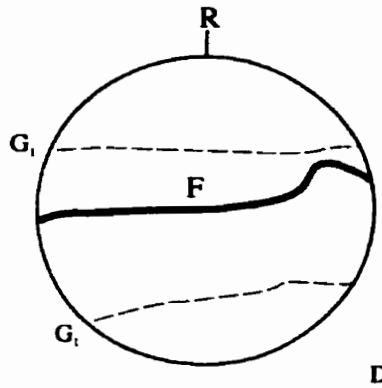

Downhole View
Fig. 2_128

Sample C

Structure	Relative Orientation
F	045°/90°
G_1	090°/90°
G_2	090°/45°N

Comments

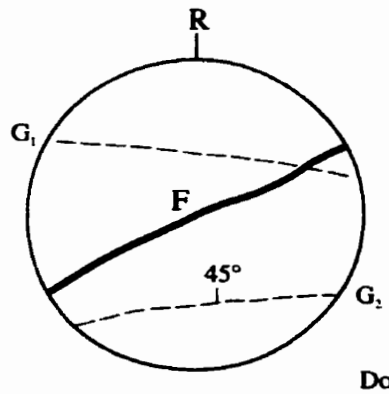

Downhole View

Coarse Grained Granite
Borehole 418-051-RT4

Test Type (Point Load)
Core Size: NQ-3, 45 mm

Sample D

Structure	Relative Orientation
F	080°/90°
G_1	060°/50°S
G_2	060°/90°

Comments

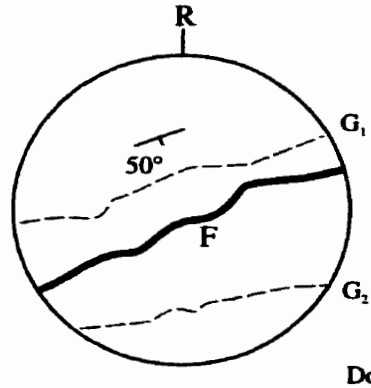

Downhole View
Fig. 2_129

Sample E

Structure	Relative Orientation
F	070°/90°
G_1	085°/90°
G_2	070°/45°N
G_1	090°/45°S

Comments

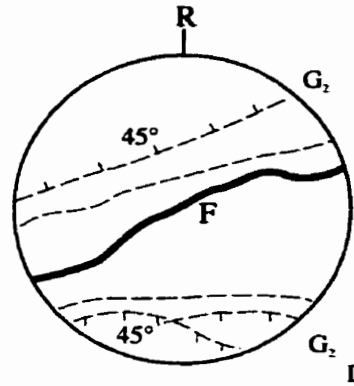

Downhole View
Fig. 2_ 130

Sample F

Structure	Relative Orientation
F	070°/90°
G_1	070°/90°
G_2	030°/75°S

Comments

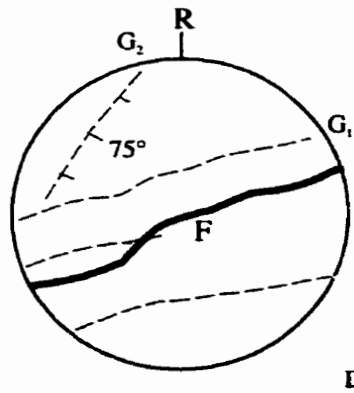

Downhole View
Fig. 2_ 131

Coarse Grained Granite
Borehole 418-051-RT5

Test Type (Point Load)
Core Size: NQ-3, 45 mm

Sample A

Structure	Relative Orientation	
F	090°/90°	
G_1	090°/80°S	Very irregular at this grain size

Comments

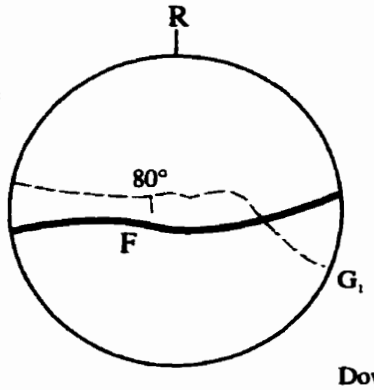

Downhole View
Fig. 2_108

Sample B

Structure	Relative Orientation	
F	070°/–70°NE	Fracture has broken along grain
G_1	070°/–75°NE	boundaries at the contact

Comments

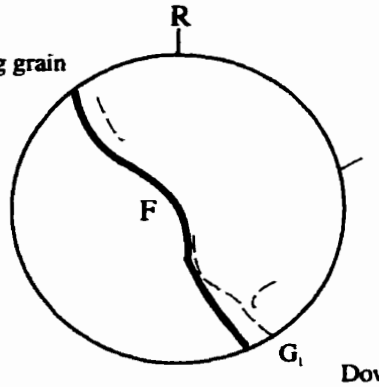

Downhole View
Fig. 2_109

Sample C

Structure	Relative Orientation	
F	065°/90°	Broke along contact
G	065°/90°	Grain boundary irregularity due to coarse grain size.

Comments

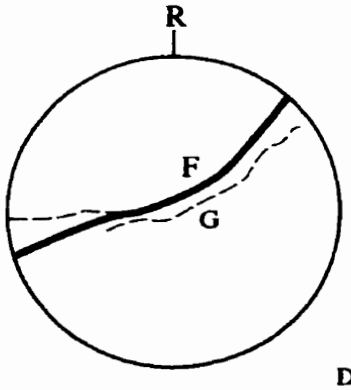

Downhole View
Fig. 2_110

Coarse Grained Granite
Borehole 418-051-RT5

Test Type (Point Load)
Core Size: NQ-3, 45 mm

Sample D

Structure	Relative Orientation	
F	085°/90°	Follows contact
G_1	080°/85°S	

Comments

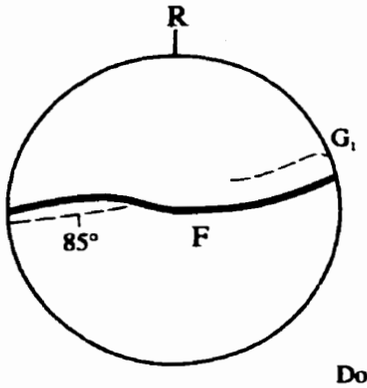

Downhole View
Fig. 2_111

Sample E

Structure	Relative Orientation
F	020°/90°
G_1	090°/70°S

Comments

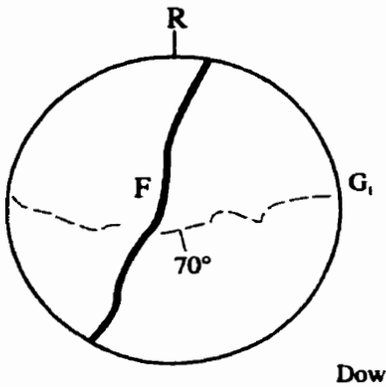

Downhole View
Fig. 2_112

Sample F

Structure	Relative Orientation
F	090°/90°
G	090°/85°S

Comments

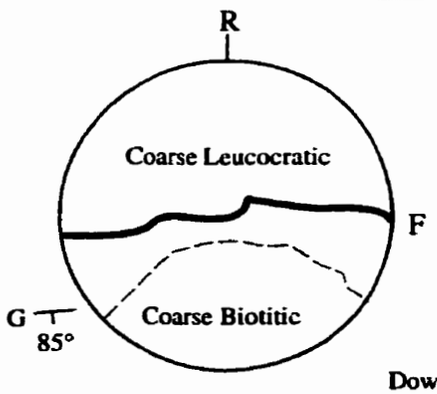

Downhole View
Fig. 2_113

Coarse Grained Granite
Borehole 418-051-RT5

Test Type (Point Load)
Core Size: NQ-3, 45 mm

Sample G

Structure	Relative Orientation	
F	105°/90°	Runs along contact
F	075°/90°	
F	190°/90°	
G_1	105°/80°S	Very coarsely crystalline, slight variations in mineralogy define layering

Comments

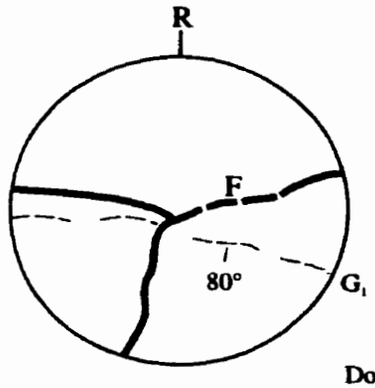

Downhole View
Fig. 2_114

Sample H

Structure	Relative Orientation
F	140°/90°
G_1	095°/80°S

Comments

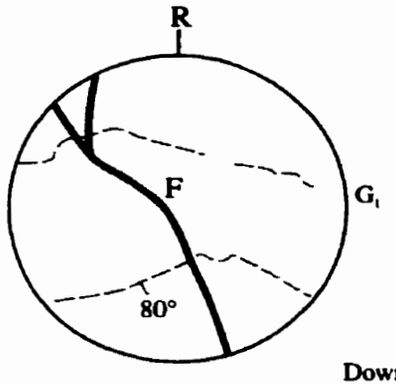

Downhole View
Fig. 2_115

Sample I

Structure	Relative Orientation	
F	060°/90°	Nearly concordant with layering
G	065°/80°S	

Comments

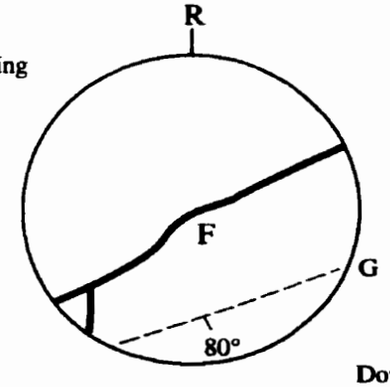

Downhole View
Fig. 2_116

Coarse Grained Granite
Borehole 418-051-RT5

Test Type (Point Load)
Core Size: NQ-3, 45 mm

Sample J

Structure	Relative Orientation	
F	095°/90°	Concordant with local layering
G_1	095°/85°S	

Comments

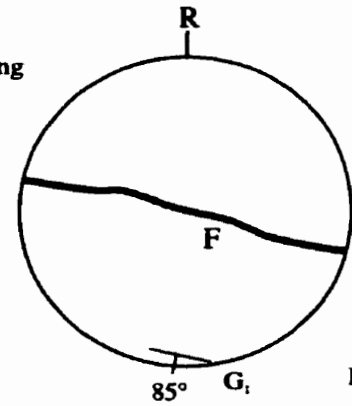

Downhole View
Fig. 2_117

Sample K

Structure	Relative Orientation
F_1	115°/90°

Comments

Sample is massive

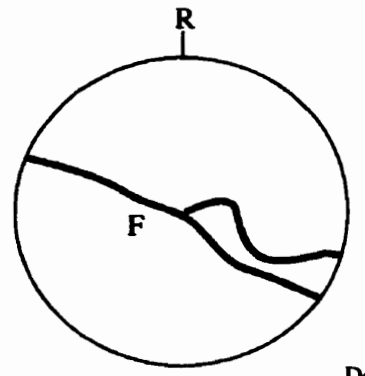

Downhole View
Fig. 2_ 118

Sample L

Structure	Relative Orientation
F	010°/90°
F	125°/90°
F	260°/90°
G	160°/90°

Comments

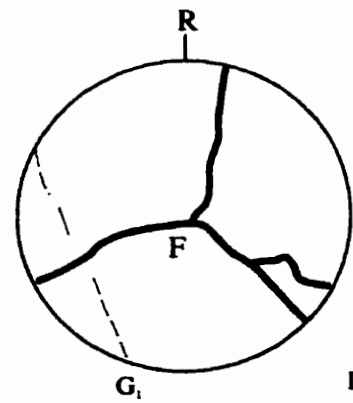

Downhole View
Fig. 2_ 119

Fine Grained Granite
Borehole 421-032-RT1

Test Type (Point Load)
Core Size: NQ-3, 45 mm

Sample A

Structure	Relative Orientation
F	055°/90°
G_t	170°/65°SW

Comments

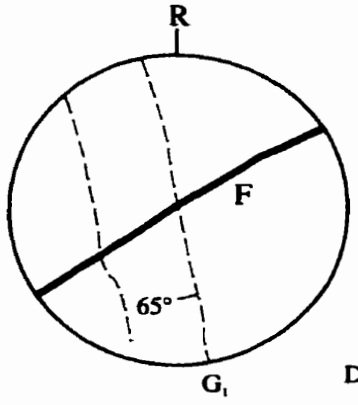

Downhole View
Fig. 2_134

Sample B

Structure	Relative Orientation
F	090°/90°
F	070°/90°
G_t	150 °/65°SW

Comments

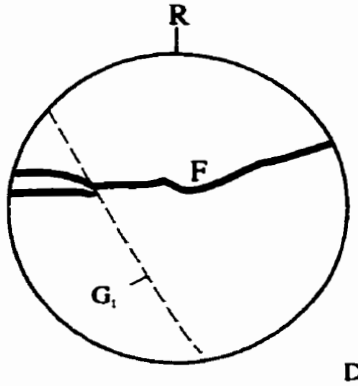

Downhole View
Fig. 2_133

Sample C

Structure	Relative Orientation
F	045°/90°
F	175°/90°
G_t	170°/ 65°W

Comments

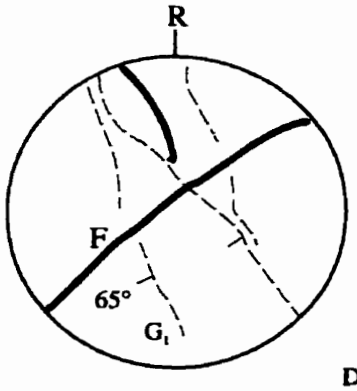

Downhole View
Fig. 2_135

Fine Grained Granite
Borehole 421-032-RT1

Test Type (Point Load)
Core Size: NQ-3, 45 mm

Sample D

Structure	Relative Orientation
F	085°/90°
G_1	170°/65°W

Comments

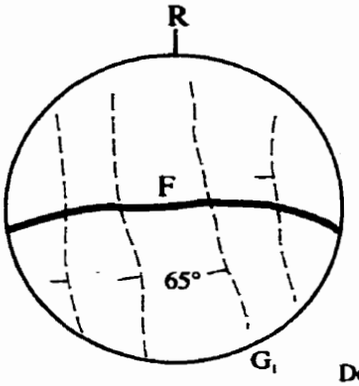

Downhole View
Fig. 2_136

Sample E

Structure	Relative Orientation
F	000°/90°
F	090°/90°
F	060°/90°
G_1	005°/55°W

Comments

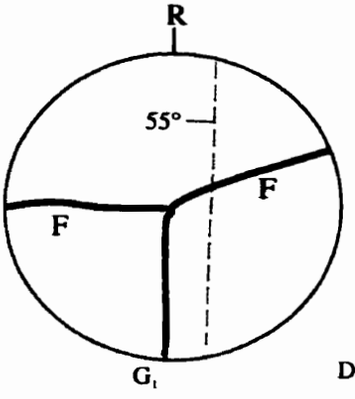

Downhole View

Sample F

Structure	Relative Orientation
F	000°/90°
G_1	000°/65°W

Comments

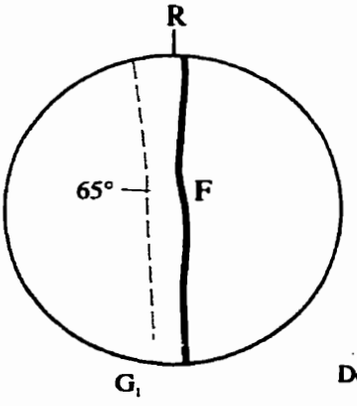

Downhole View
Fig. 2_137

Fine Grained Granite
Borehole 421-032-RT1

Test Type (Point Load)
Core Size: NQ-3, 45 mm

Sample G

Structure	Relative Orientation
F	085°/90°
F	050°/90°
G	170°/65°W

Comments

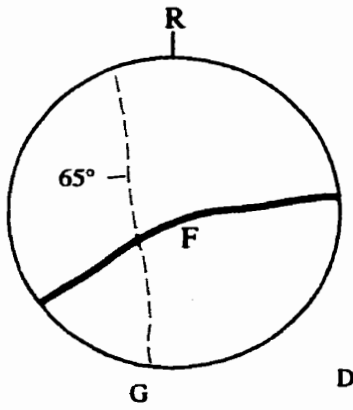

Downhole View
Fig. 2_ 138

Sample H

Structure	Relative Orientation
F	120°/90°
G	140°/65°W

Comments

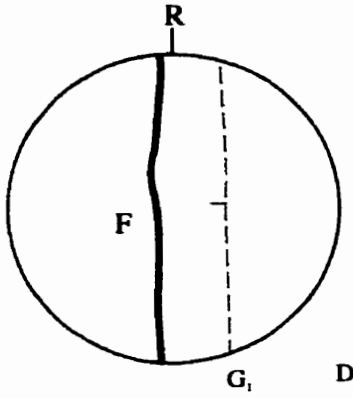

Downhole View

Sample I

Structure	Relative Orientation
F	090°/90°
G	145°/40°SW

Comments

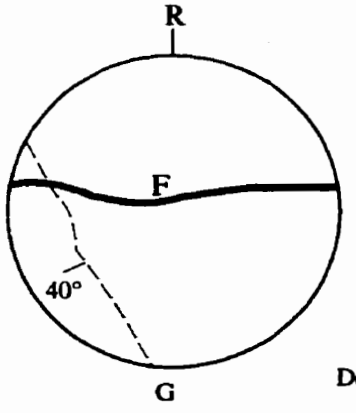

Downhole View
Fig. 2_ 132

Fine Grained Granite
Borehole 421-032-RT1

Test Type (Point Load)
Core Size: NQ-3, 45 mm

Sample J

Structure	Relative Orientation
F	085°/90°
G_t	150°/50°W
G	030°/70°W

Comments

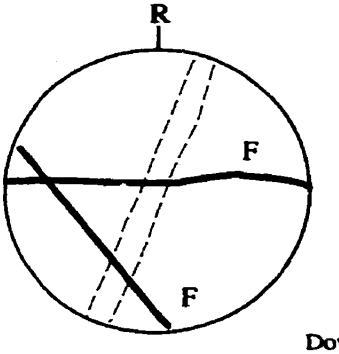

Downhole View

Sample I-2

Structure	Relative Orientation
F	170°/90°
G_t	170°/55°

Comments

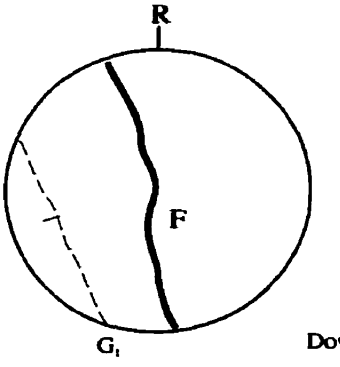

Downhole View

Fine Grained Granite
Borehole 421-032-RT2

Test Type (Point Load)
Core Size: NQ-3, 45 mm

Sample A

Structure	Relative Orientation
F	045°/90°
M_1	005°/80°W
M_2	
M_3	088°/70°N
M_4	045°/80°NW

Comments

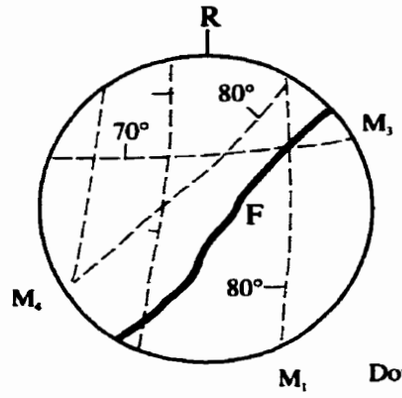

Downhole View
Fig. 2_139

Sample B

Structure	Relative Orientation
F	040°/80°NW
F	140°/80°NE
F	270°/90°
M_1	010°/75°W
M_2	165°/40°W
M_3	088°/70°S
M_4	040°/88°W

Comments

most prominent banding
mineral alignment
distinct non-penetrative banding

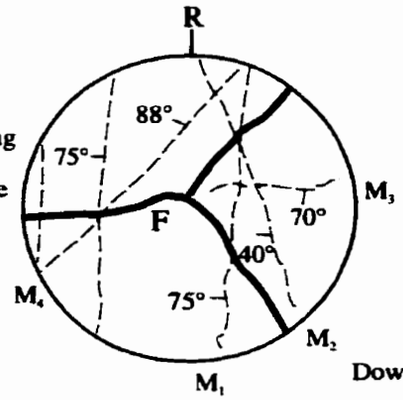

Downhole View
Fig. 2_140

Sample C

Structure	Relative Orientation
F	085°/90°
M_1	010°/80°W
M_2	
M_3	080°/80°S
M_4	060°/80°NW

Comments

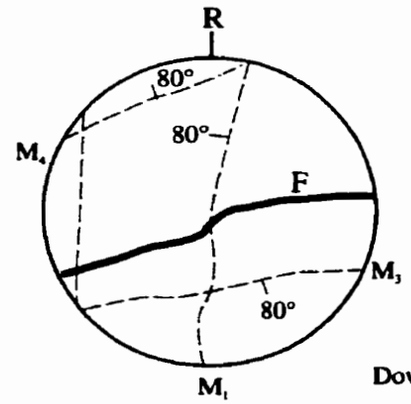

Downhole View
Fig. 2_141

Fine Grained Granite
Borehole 421-032-RT2

Test Type (Point Load)
Core Size: NQ-3, 45 mm

Sample D

Structure	Relative Orientation
F	010°/90°
F	120°/90°
F	055°/90°
M_1	000°/80°W
M_2	155°/40°W
M_3	088°/70°S
M_4	055°/80°W

Comments

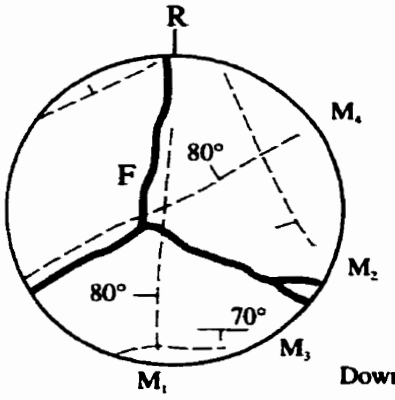

Downhole View
Fig. 2_142

Sample E

Structure	Relative Orientation
F	070°/90°
M_1	010°/75°W
M_2	010°/45°W
M_3	
M_4	070°/85°NW

Comments

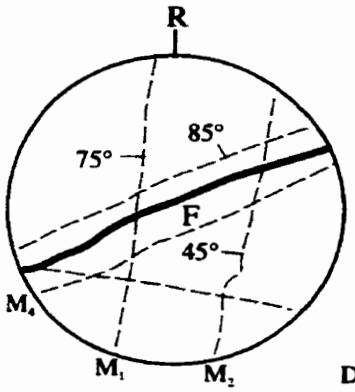

Downhole View
Fig. 2_143

Sample F

Structure	Relative Orientation
F	070°/85°NW
M_1	010°/85°W
M_2	010°/40°W
M_3	
M_4	055°/85°NW

Comments

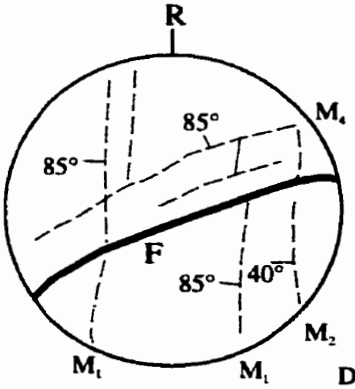

Downhole View
Fig. 2_144

Fine Grained Granite
Borehole 421-032-RT2

Test Type (Point Load)
Core Size: NQ-3, 45 mm

Sample G

Structure	Relative Orientation
F	090°/90°
M_1	
M_1	010°/80°W
M_2	010°/45°W
M_4	060°/85°W

Comments

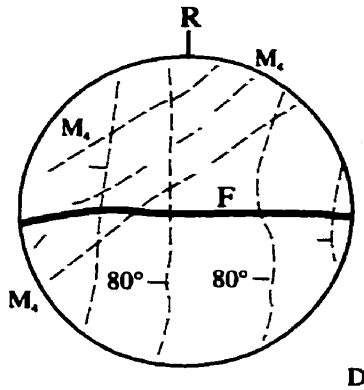

Downhole View
Fig. 2_145

Sample H

Structure	Relative Orientation
F	080°/90°
M_1	015°/85°W
M_2	040°/50°NW
M_3	
M_4	055°/80°SE

Comments

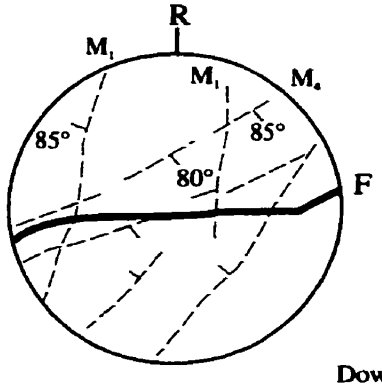

Downhole View
Fig. 2_146

Sample I

Structure	Relative Orientation
F	090°/90°
M_1	012°/80°W
M_2	010°/50°W
M_3	085°/70°S
M_4	045°/85°N

Comments

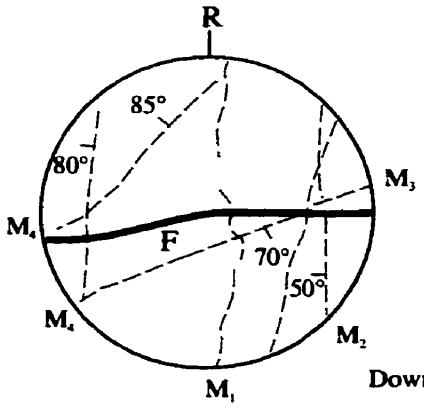

Downhole View
Fig. 2_147

Fine Grained Granite
Borehole 421-032-RT2

Test Type (Point Load)
Core Size: NQ-3, 45 mm

Sample J

Structure	Relative Orientation
F	090°/85°S
M_1	000°/80°W
M_2	020°/50°NW
M_3	095°/50°S
M_4	040°/80°NW

Comments

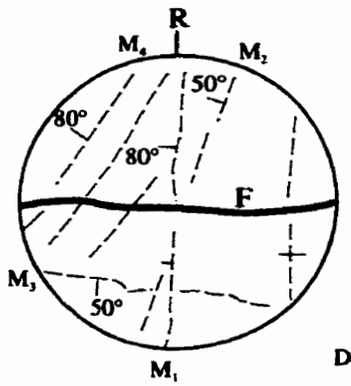

Downhole View
Fig. 2_148

Fine Grained Granite
Borehole 421-032-RT3

Test Type (Point Load)
Core Size: NQ-3, 45 mm

Sample A

Structure	Relative Orientation
F	000°/90°
F	075°/90°
F	052°/90°

Comments

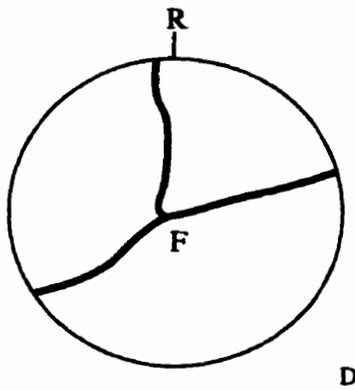

Downhole View
Fig. 2_149

Sample B

Structure	Relative Orientation
F	000°/90°
F	145°/90°
F	070°/90°

Comments

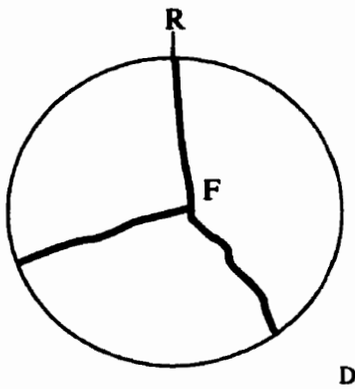

Downhole View
Fig. 2_ 150

Sample C

Structure	Relative Orientation
F	070°/90°

Comments

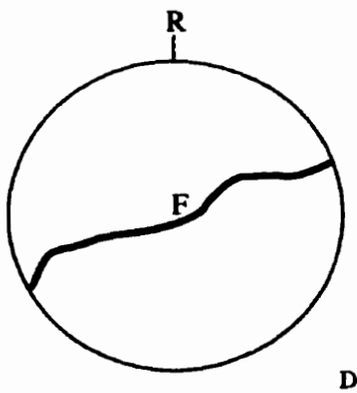

Downhole View
Fig. 2_ 151

Fine Grained Granite
Borehole 421-032-RT3

Test Type (Point Load)
Core Size: NQ-3, 45 mm

Sample D

Structure	Relative Orientation
F	070°/90°

Comments

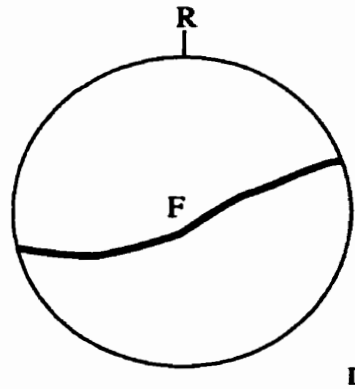

Downhole View
Fig. 2_ 152

Sample E

Structure	Relative Orientation
F	050°/90°

Comments

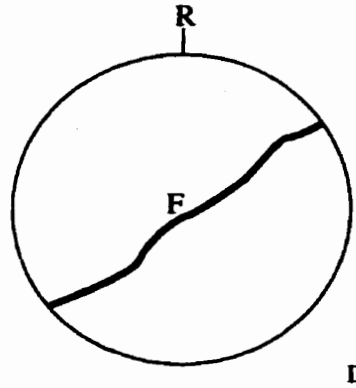

Downhole View
Fig. 2_153

Sample F

Structure	Relative Orientation
F	080°/90°
F	020°/90°
F	160°/90°

Comments

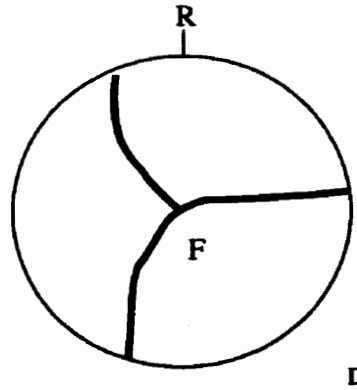

Downhole View

Fine Grained Granite
Borehole 421-032-RT3

Test Type (Point Load)
Core Size: NQ-3, 45 mm

Sample G

Structure	Relative Orientation
F	045°/90°
F	020°/90°

Comments

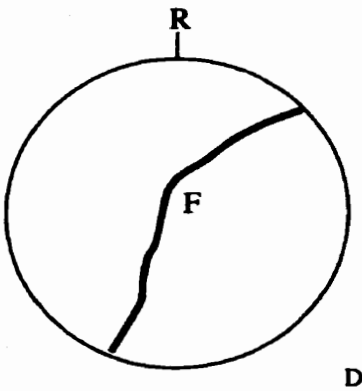

Downhole View

Sample H

Structure	Relative Orientation
F	080°/90°
F	045°/90°
F	135°/90°

Comments

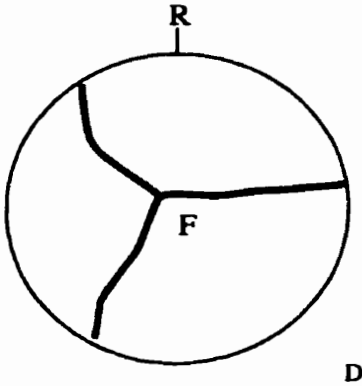

Downhole View

Sample I

Structure	Relative Orientation
F	175°/90°

Comments

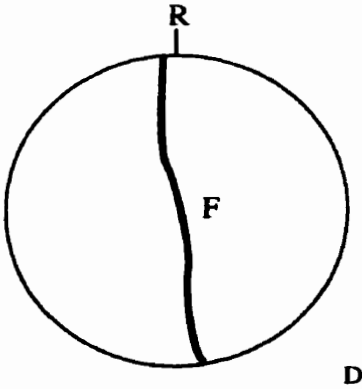

Downhole View
Fig. 2_154

Fine Grained Granite
Borehole 421-032-RT3

Test Type (Point Load)
Core Size: NQ-3, 45 mm

Sample J

Structure	Relative Orientation
F	045°/90°
F	070°/90°
F	145°/90°

Comments

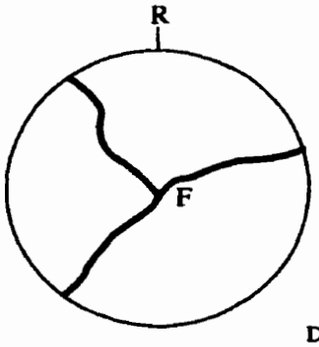

Downhole View
Fig. 2_ 155

Fine Grained Granite
Borehole 421-034-RT4

Test Type (Point Load)
Core Size: NQ-3, 45 mm

Sample A

Structure	Relative Orientation
F	180°/90°
G_t	170°/35°W

Comments

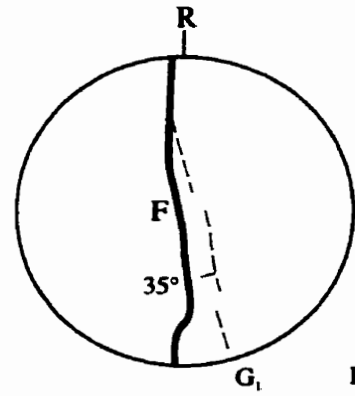

Downhole View
Fig. 2_156

Sample B

Structure	Relative Orientation
F	180°/90°
G_t	180°/40°W

Comments

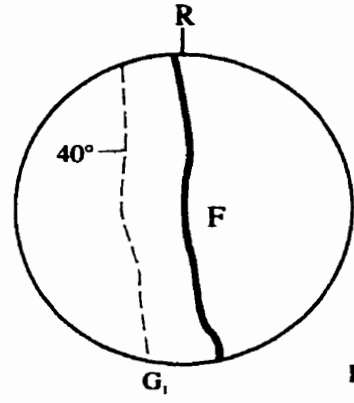

Downhole View
Fig. 2_157

Sample C

Structure	Relative Orientation	
F	075°/90°	
G_t	175°/45°W	Gneissosity much less distinct, and heterogeneous even at this scale

Comments

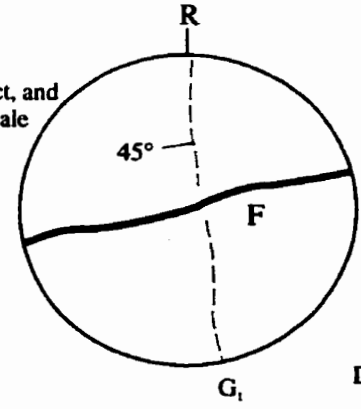

Downhole View
Fig. 2_158

Fine Grained Granite
Borehole 421-034-RT4

Test Type (Point Load)
Core Size: NQ-3, 45 mm

Sample D

Structure	Relative Orientation	
F	085°/ 90°	
G_1	~170°/45°W	Very weak & ill defined,
G	~090°/30°S	not penetrative

Comments

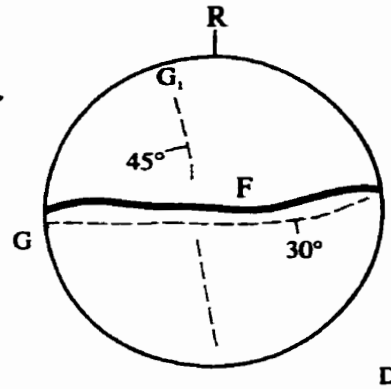

Downhole View
Fig. 2_ 159

Sample E

Structure	Relative Orientation	
F	~010°/ 90°	Triple fracture, orientation approximate
F	~090°/ 90°	
G_1	~010°/25°W	Very weak & only partially penetrative

Comments

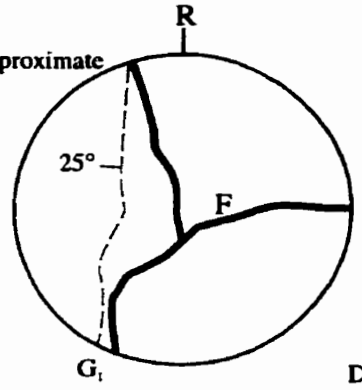

Downhole View
Fig. 2_ 160

Sample F

Structure	Relative Orientation	
F	070°-090°/90°	
G_1	075°/40°N	Very ill defined & non-penetrative
G	000°/45°E	Very ill defined & non-penetrative

Comments

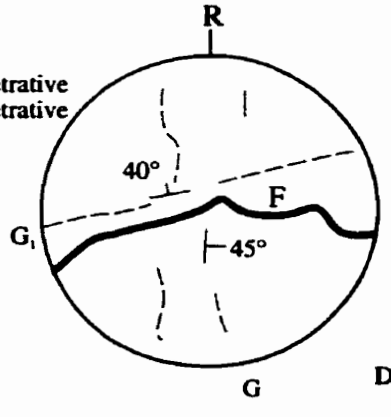

Downhole View
Fig. 2_161

Fine Grained Granite
Borehole 421-034-RT4

Test Type (Point Load)
Core Size: NQ-3, 45 mm

Sample G

Structure	Relative Orientation
F	175°/90°
G	020°/70°SE
G	135°/35°NW

Comments

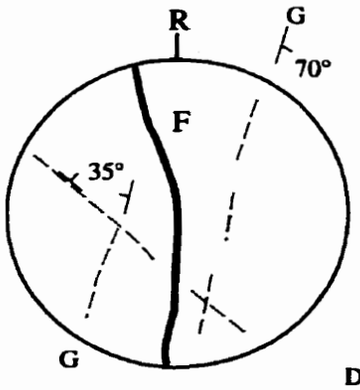

Downhole View
Fig. 2_ 162

Sample H

Structure	Relative Orientation
F	015°/90°
G_1	145°/40°NE
G_2	035°/45°NW

Comments

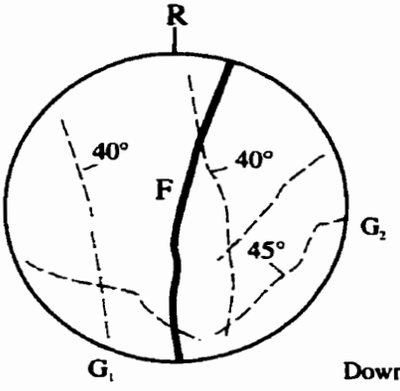

Downhole View
Fig. 2_ 163

Sample I

Structure	Relative Orientation
F	175°/90°
M_1	010°/55°W

Comments

Fracture partially follows foliation

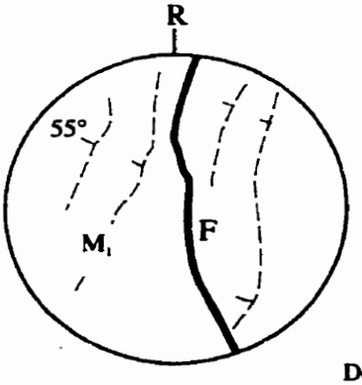

Downhole View
Fig. 2_ 163

Fine Grained Granite
Borehole 421-034-RT4

Test Type (Point Load)
Core Size: NQ-3, 45 mm

Sample J

Structure	Relative Orientation	
F	025°/90°	Numerous en echelon steps parallel to G
G_1	170°/80°NE	Sample appears otherwise homogeneous, possible highly irregular foliation approximately normal to core axis
Comments		

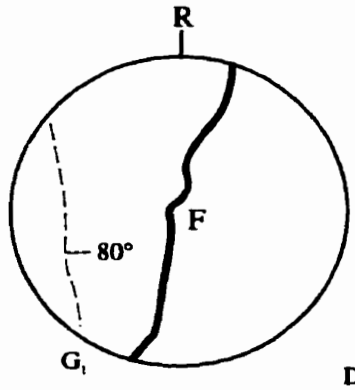

Downhole View
Fig. 2_165

Sample K

Structure	Relative Orientation	
F	090°/ 90°	
G_1	160°/90°?	Well defined mineral alignment (aggregate alignment in cross section but ill defined around perimeter
G_2	190°/70°SE	Non-penetrative foliation, no offset but appears to cross-cut
Comments		

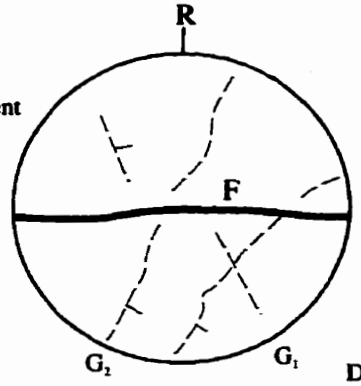

Downhole View
Fig. 2_ 166

Sample L

Structure	Relative Orientation	
F	075°/ 90°	Very irregular, only partially
G	00°-90°SE	Numerous sub-domains marked by grain alignments

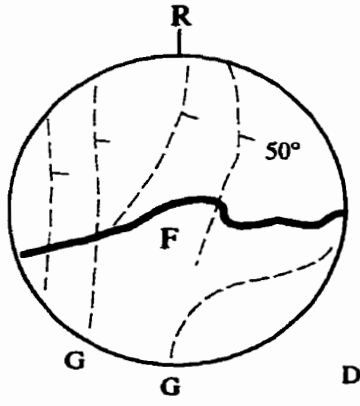

Downhole View

Fine Grained Granite
Borehole 421-034-RT4

Test Type (Point Load)
Core Size: NQ-3, 45 mm

Fig. 2_167

Sample M

Structure	Relative Orientation	
F	070°/90°	
F	175°/90°	
G	180°/45°E	Non-penetrative domains with varying grain & grain aggregate orientations.

Comments

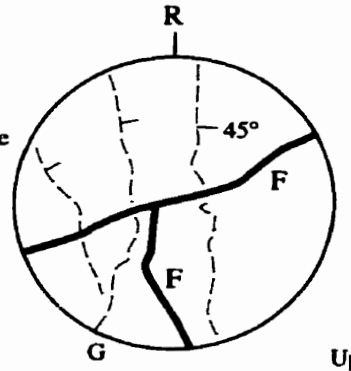

Uphole View

Structure	Relative Orientation
F	110°/90°
F	200°/90°
F	130°/90°
G	005°/45°

Comments

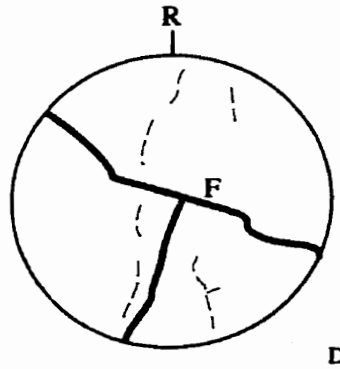

Downhole View

Appendix B

BRAZILIAN TESTING

This appendix presents the samples used for and the data obtained from the Brazilian testing. The tables list the specimen characteristics, and the results of the Brazilian tests described in this report. The figures summarize the fabric and test-induced fractures observed in each of the samples used in the Brazilian tests. The symbols used in the sample maps are explained in Figure B1, while the standard format for the sample maps is shown in Figure B2.

Table B1
Brazilian test results
Fine Grained Granite from boreholes 421-032-RT1, 2, 3, 4.

Borehole	Sample	Density	Loading angle relative to low-dipping compositional layering	Minimum Tensile Strength (Crack Initiation) (MPa)	Maximum Tensile Strength (Failure) (MPa)
RT1	D	2.64	90		3.01
	A	2.59	57		3.26
	B	2.64	70		2.26
	C	2.65	70		2.76
RT2	A	2.66	30		2.50
	B	2.61	65		3.00
	C	2.67	75		1.91
	D	2.66	80	1.34	2.79
	F	2.65	70		2.21
	E	2.65	45		3.12
RT3	A	2.64	0		
	B	2.64	0		2.12
	C	2.64	52		2.38
	D	2.62	25		1.65
	E	2.65	25		2.86
RT4	A	2.62	45		2.82
	B	2.65	70		2.66
	C	2.63	45		2.14
	D	2.62	20		1.98
	E	2.64	80		1.84
	F	2.63	80		2.68

Table B2
Brazilian Test Data
Medium Grained Granite (Borehole 417-071-RT4,5)

Borehole	Sample	Density	Loading angle relative to low-dipping compositional layering	Minimum Tensile Strength (Crack Initiation) (MPa)	Maximum Tensile Strength (Failure) (MPa)
RT1, 2,3	- not suitable due to core discing -				
RT4	A	2.62	90		1.49
RT4	B	2.60	90		1.79
RT4	C	2.60	70	0.91	1.14
RT4	D	2.63	45		1.33
RT4	A'	2.62	90	1.03	1.22
RT5	A	2.63	90		1.32
RT5	B	2.61	30		1.09
RT5	C	2.62	0	0.87	1.07
RT5	D	2.63	60		0.87

Table B3
Brazilian Test Data.
Coarse Grained Granite (Borehole 418-051-RT2,3,4,5)

Borehole	Sample	Density	Loading angle relative to low-dipping compositional layering	Minimum Tensile Strength (Crack Initiation) (MPa)	Maximum Tensile Strength (Failure) (MPa)
RT1	- not suitable due to core discing -				
RT2	A	2.67	90		1.70
	B	2.70	75		1.75
	C	2.68	90		2.07
	D	2.67	0		1.49
	E	2.66	45		1.69
	F	2.68	0		1.11
	G	2.63	10		1.17
	H	2.67	0	0.60	1.39
RT3	B	2.70	45		1.45
	C	2.69	75	0.67	2.01
	D	2.67	90		2.53
	E	2.70	85		2.49
	F	2.71	0		1.88
	A'	2.68	55		1.56
	G	2.65	60	0.60	1.65
RT4	A	2.61	50		0.96
	B	2.59	45		1.21
	C	2.60	45		1.04
	D	2.56	15		1.33
	E	2.60	20		1.53
	F	2.60	38	0.62	0.88
	G	2.61	52	0.54	1.42
RT5	A	2.62	0		0.93
	B	2.54	25	0.52	1.18
	C	2.65	45		1.52
	D	2.64	85		1.65

Sample A

Structure	Relative Orientation *(strike / dip & dip direction)*
F	100°/90° NE
G_1	100°/20° NE
G_2	190°/60° NW
M_1	190°/60° NW
A	100°/30° E
^{30}┤	strike & dip with dip direction

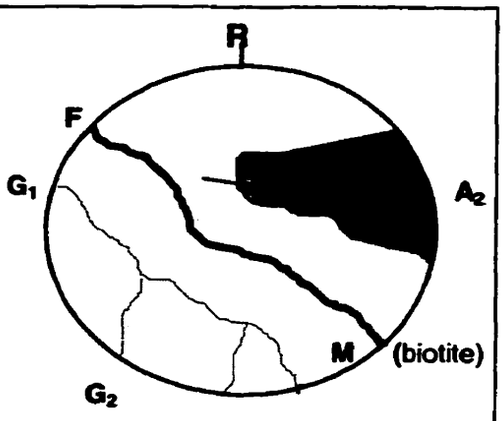

where:

R	core reference line
F	fracture induced by loading
G_1	gneissic foliation type 1
G_2	gneissic foliation type 2
M_1	mineral alignment, type indicated on figure
A_1	axial plane of fold
A_2	axis of fold
	biotite > 10% or some compositional heterogeneity as indicated by text.

^{30}┤

Downhole View
Dwg. No

Note: All orientations shown in the drawings are relative to the section shown, with the core reference line representing an interim North. These have been converted to true orientations in the report.

Figure B1. Key to symbols used on the sample maps.

Rock name **Test type (Brazilian or Point load)**

Borehole name (e.g. 401-123-rt2) **Core size (alphanumeric and in mm).**

Sample a

Structure	Relative Orientation
F	strike (0-360) / dip (0-90)
G_1	strike (0-360) / dip (0-90)
G_2	strike (0-360) / dip (0-90)

Comments
Brief description of rock including anything noteworthy about the foliations present and the affect (if any) this had on testing.

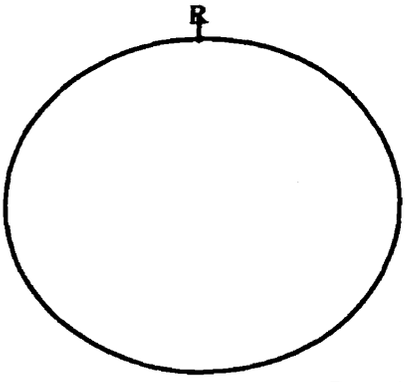

Downhole View
Dwg. No.

Sample b

Structure	Relative Orientation
F	strike (0-360) / dip (0-90)
G_1	strike (0-360) / dip (0-90)
G_2	strike (0-360) / dip (0-90)

Comments
Brief description of rock including anything noteworthy about the foliations present and the affect (if any) this had on testing.

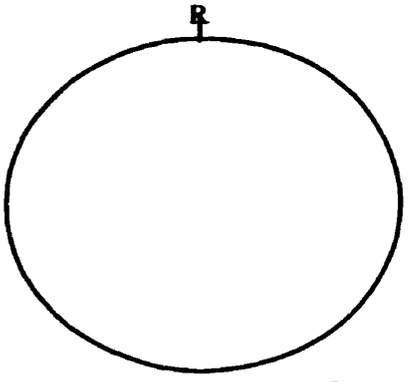

Downhole View
Dwg. No.

Sample c

Structure	Relative Orientation
F	strike (0-360) / dip (0-90)
G_1	strike (0-360) / dip (0-90)
G_2	strike (0-360) / dip (0-90)

Comments
Brief description of rock including anything noteworthy about the foliations present and the affect (if any) this had on testing.

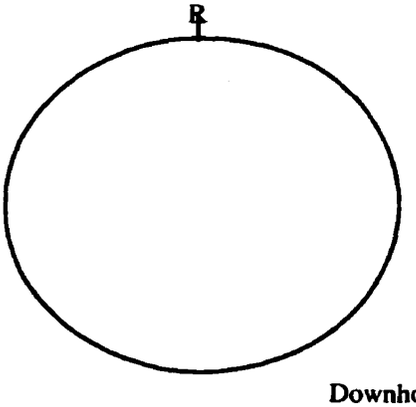

Downhole View
Dwg. No.

Figure B2: Standard format for the fabric maps constructed for each of the samples selected for testing. The rock name, the borehole from which the sample came, the size of the borehole, and the test type are indicated at the top of each sheet. Up to three sample maps are shown per page, at their actual size. The reference line marked on the top of the core is shown, and all views are downhole unless otherwise indicated.

Medium Grained Granite
Borehole 417-071-RT4

Test Type (Brazilian)
Core Size: NQ-3, 45 mm

Sample A'

Structure	Relative Orientation	
L	000°/26°	Aligned mineral aggregates. Probably in the other samples as well.
F	180°/90°	

Comments

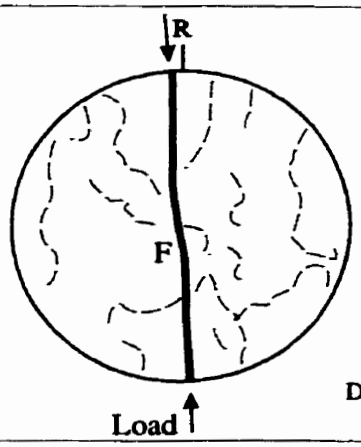

Downhole View
Fig. 2_066

Structure Relative Orientation

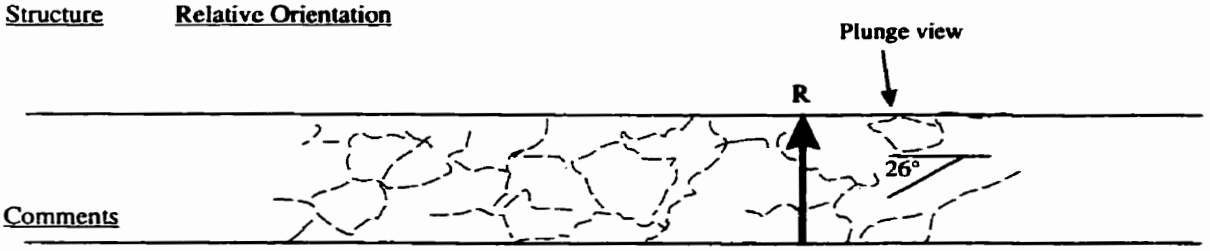

Comments

Downhole View

Sample B

Structure	Relative Orientation
F	170°/90°

Comments

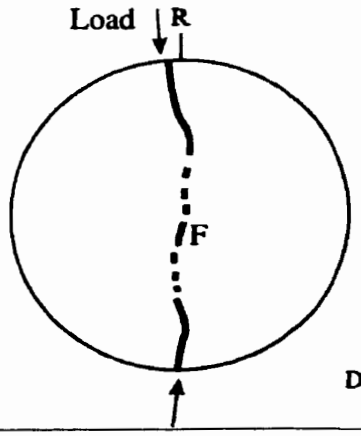

Downhole View
Fig. 2_069

Medium Grained Granite
Borehole 417-071-RT4

Test Type (Brazilian)
Core Size: NQ-3, 45 mm

Sample C

Structure	Relative Orientation
F	105°/90°

Comments

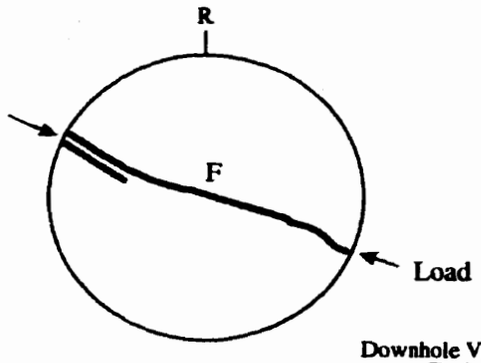

Downhole View
Fig. 2_070

Sample D

Structure	Relative Orientation
F	065°/90°

Comments

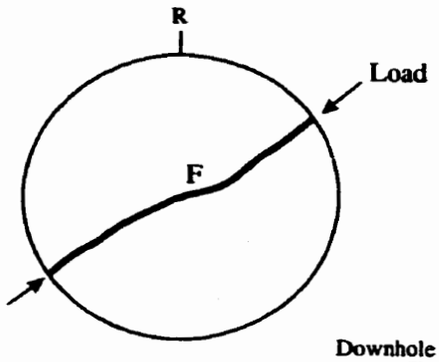

Downhole View
Fig. 2_067

Medium Grained Granite
Borehole 417-072-RT5

Test Type (Brazilian)
Core Size: NQ-3, 45 mm

Sample A

Structure	Relative Orientation
F	000°/ 90°
M_1	010°/45°E Aligned mineral aggregates
M_2	110°/60°NE

Comments

Massive

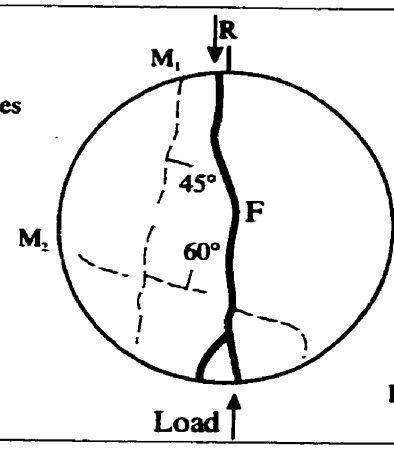

Downhole View
Fig. 2_062

Sample B

Structure	Relative Orientation
F	120°/ 90°
M_1	025°/45°SE

Comments

Nearly massive at this scale

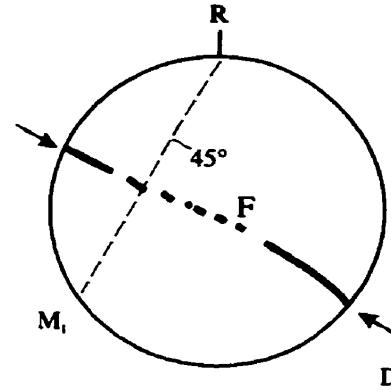

Downhole View
Fig. 2_063

Sample C

Structure	Relative Orientation
F	088°/90°
M_1	000°/45°NE

Comments

Nearly massive at this scale

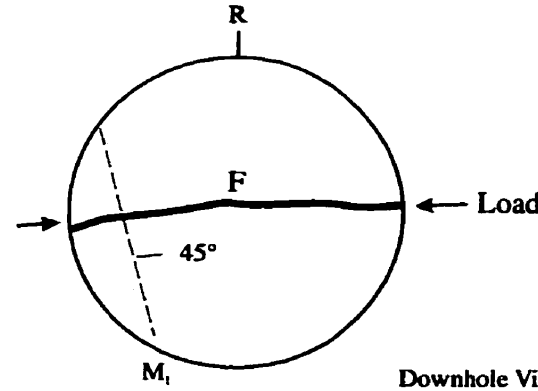

Downhole View
Fig. 2_064

Medium Grained Granite
Borehole 417-072-RT5

Test Type (Brazilian)
Core Size: NQ-3, 45 mm

Sample D

Structure	Relative Orientation	
F	035°/90°	Many splays deviated by foliation
G_t	000°/45°E	

Comments

Nearly massive at this scale

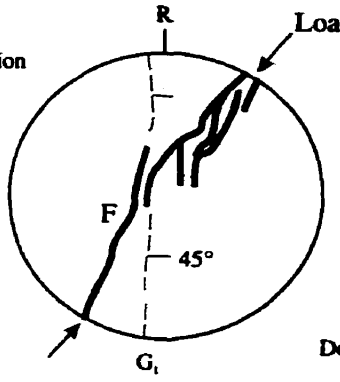

Downhole View
Fig. 2_065

Coarse Grained Granite
Borehole 418-051-RT2

Test Type (Brazilian)
Core Size: NQ-3, 45 mm

Fig. 2_053

Sample A

Structure	Relative Orientation
F	000°/90°
G_1	090°/33°S
M_1	~090°/35°S

Comments

1. Note gap in fracture is in quartz/feldspar layer
2. 35° gneissosity and biotite

Loading angle to G_1 ~80°-90°

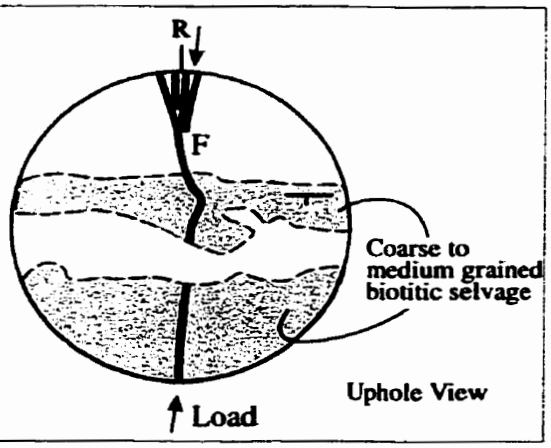

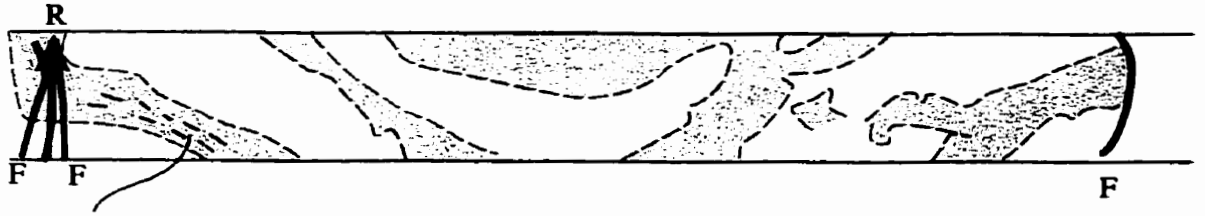

Perimeter View

Structure Relative Orientation

Foliation 2: Coarse biotite in selvages guides fracture

Comments

Vertical microcracks in quartz

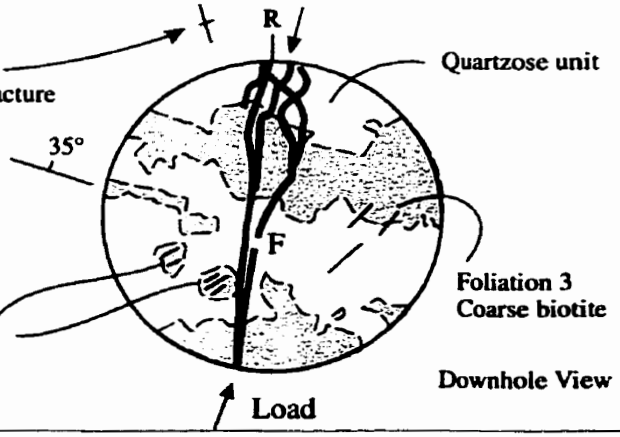

Coarse Grained Granite
Borehole 418-051-RT2

Test Type (Brazilian)
Core Size: NQ-3, 45 mm

Fig. 2_054

Sample B

Structure Relative Orientation

Comments (Perimeter View)

- Fine grained biotitic granite (A,C,E below)
- Leucocratic granite (B,D,G)
- Biotite selvage, (F)

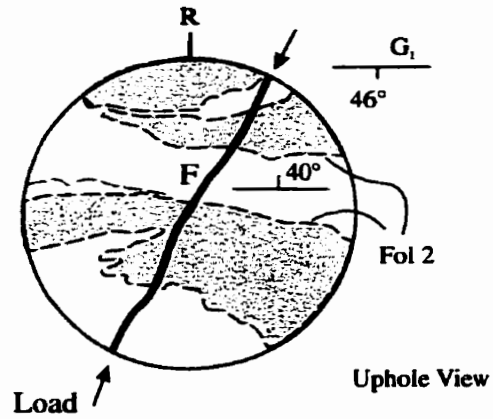

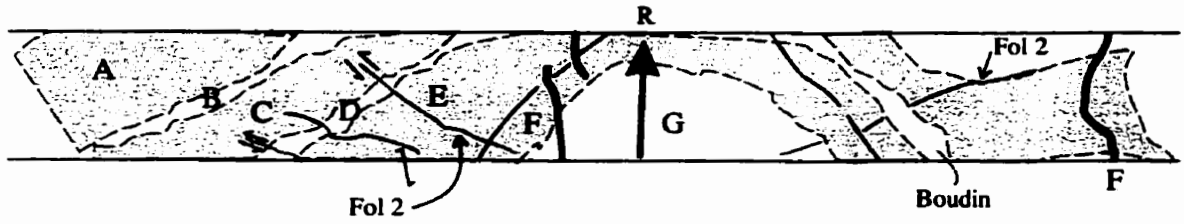

Perimeter View

Structure	Relative Orientation	
G_1	180°/40°N	
G_2	180°/40°S	but opposite dip direction, resembles small semi-ductile faults, leaves leucosome boudined
F	160°/90°	

Comments

Fracture direction may coincide with intersection of the two foliations

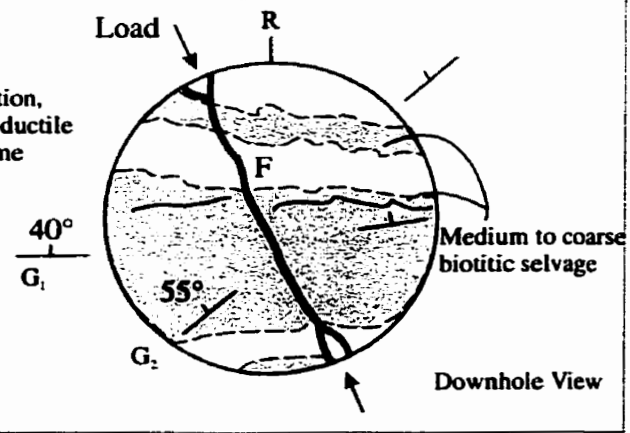

Coarse Grained Granite
Borehole 418-051-RT2

Test Type (Brazilian)
Core Size: NQ-3, 45 mm

Fig. 2_055

Sample C

Structure | Relative Orientation

Comments

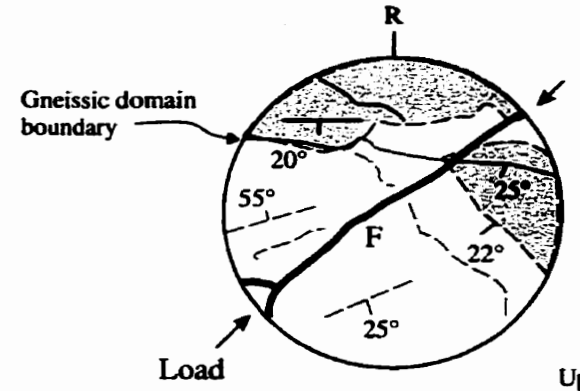

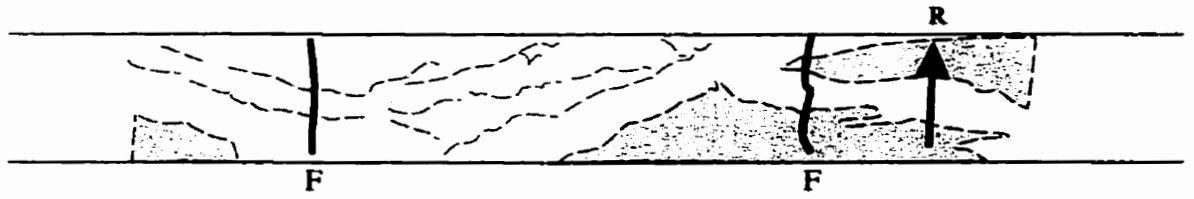

Perimeter View

Structure	Relative Orientation
G_1	045°/25°N
F	140°/90°

Comments

Angles relative to loading

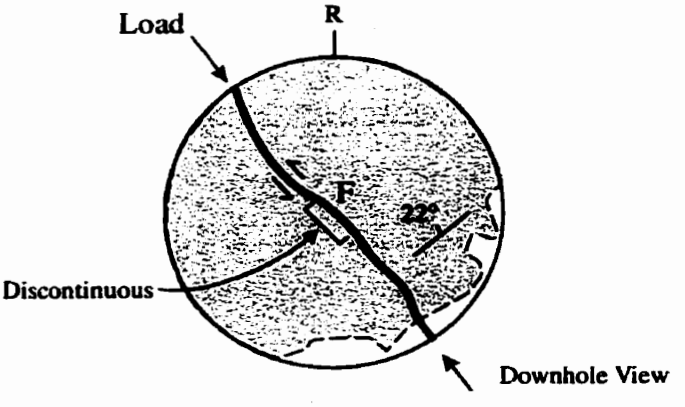

Coarse Grained Granite
Borehole 418-051-RT2

Test Type (Brazilian)
Core Size: NQ-3, 45 mm

Fig. 2_056

Sample D

Structure Relative Orientation

Comments

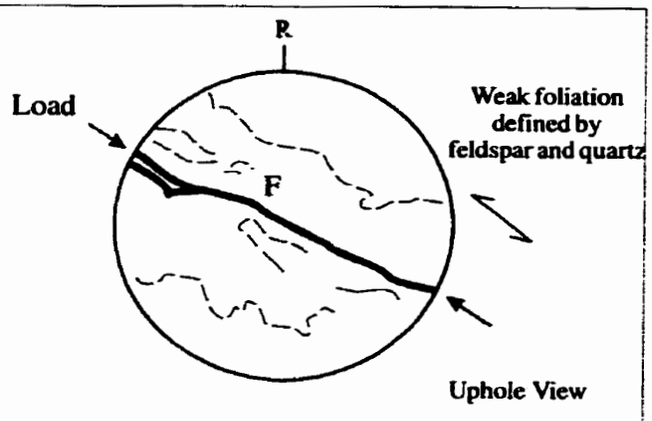

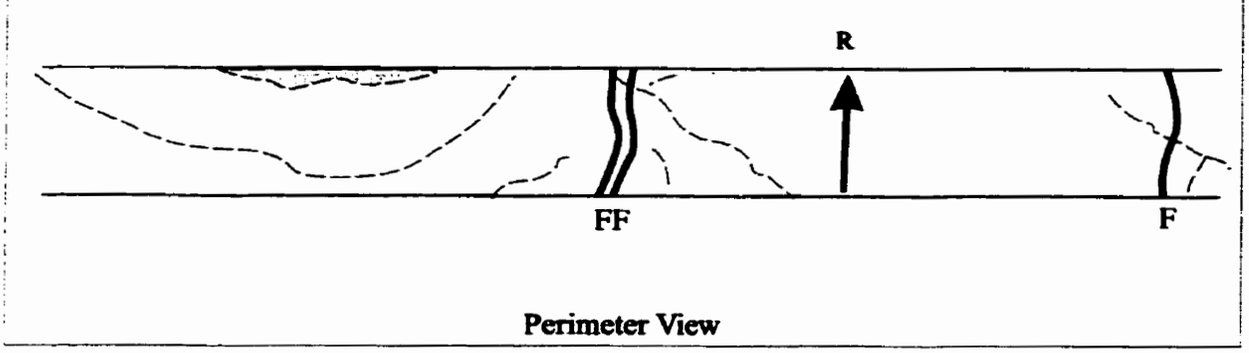

Structure Relative Orientation

G_i 020° to 55° (1) and 025° (2) dips

Comments

Angles relative to loading

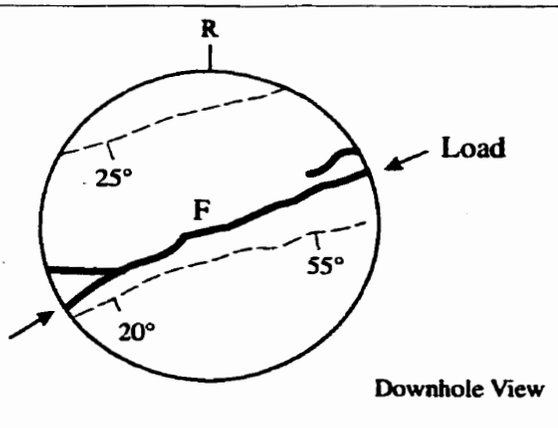

Coarse Grained Granite
Borehole 418-051-RT2

Test Type (Brazilian)
Core Size: NQ-3, 45 mm

Fig. 2_057

Sample F

Structure	Relative Orientation
F	120°/ 90°
G_1	120°/45°NE
G_2	120°/50°SW
Load	120°/00

Comments

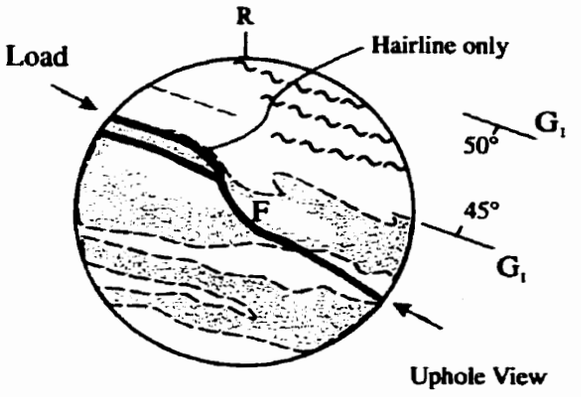

Uphole View

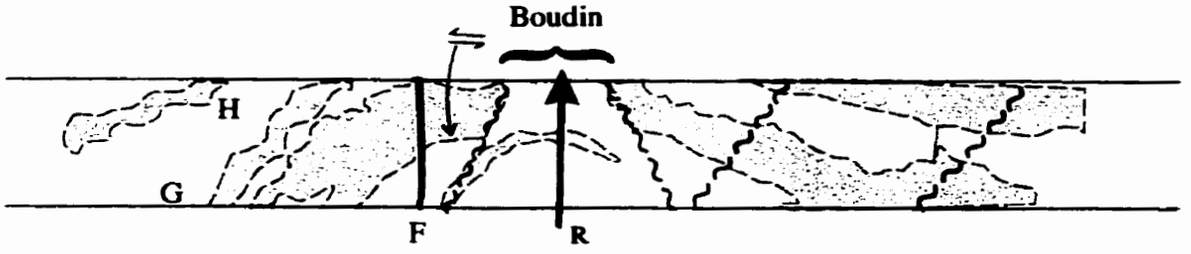

Perimeter View

Structure	Relative Orientation

Comments

- Fracture partially follows banding and biotitic alignment.
- Biotite parallels compositional layering
- Cross-cutting spaced foliation cuts G_1 into poorly defined boudins foliation type.....(biotitic lenses)

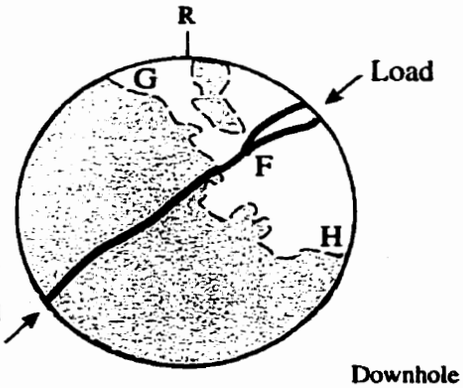

Downhole View

Coarse Grained Granite
Borehole 418-051-RT2

Test Type (Brazilian)
Core Size: NQ-3, 45 mm

Fig. 2_058

Sample G

Structure | Relative Orientation

Comments

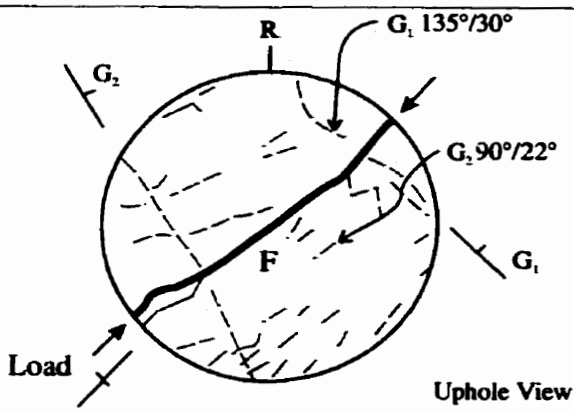

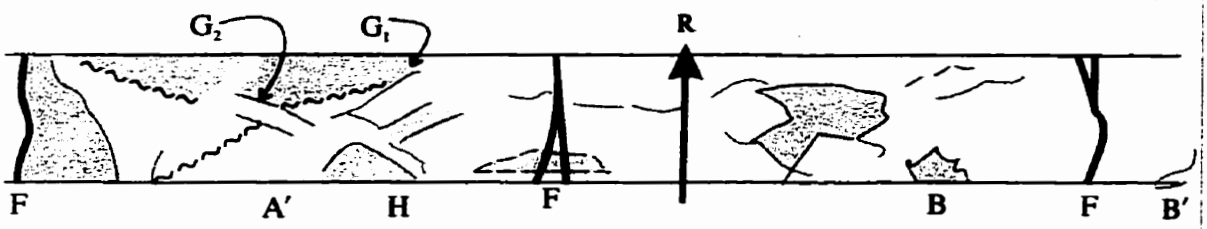

Perimeter View

Structure	Relative Orientation
F	130°/90°
G_1	120°/45°NE
G_2	120°/50°SW
Load	130°/00°

Comments

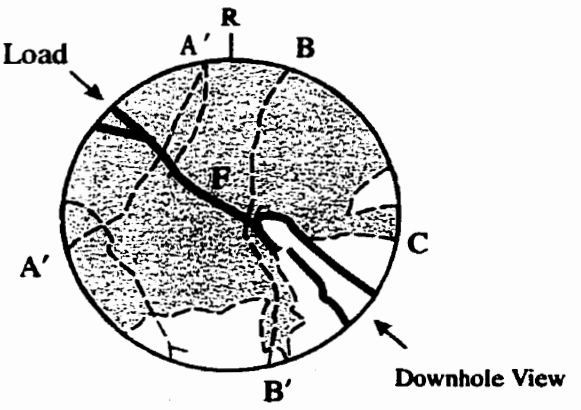

Coarse Grained Granite
Borehole 418-051-RT2

Test Type (Brazilian)
Core Size: NQ-3, 45 mm

Fig. 2_059

Sample H

Structure | Relative Orientation

Comments

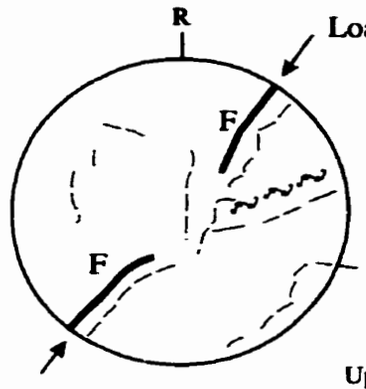

Uphole View

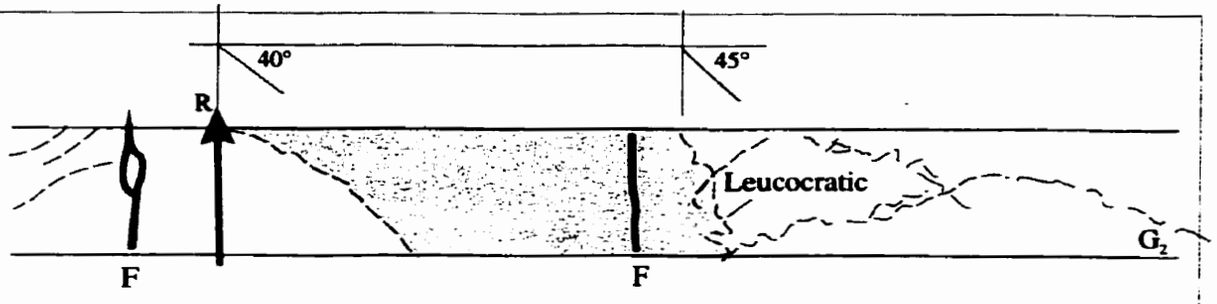

Perimeter View

Structure	Relative Orientation
F	145°/90°
G_1	135°/45°NE
G_2	100°/30°SW
Load	145°/00

Comments

Homogenous textural domain from this view. Weakly developed foliations.

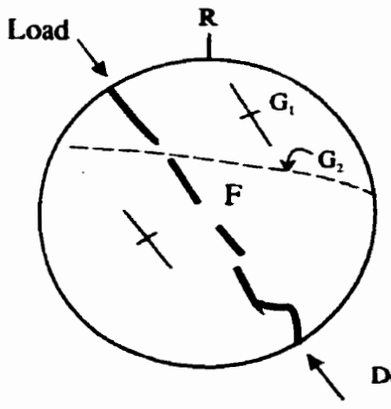

Downhole View

Coarse Grained Granite
Borehole 418-051-RT3

Test Type (Brazilian)
Core Size: NQ-3, 45 mm

Sample A

Structure	Relative Orientation
F	080°/90°
G_1	035°/85°NW

Comments

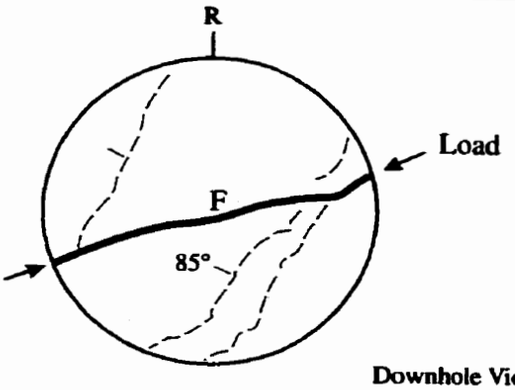

Downhole View
Fig. 2_047

Sample B

Structure	Relative Orientation
F	100°/90°
G_1	050°/50°NW
	090°/90°SE
A_1	070°/70°SW ?
A_2	135°/90°

Comments

Sample shows at least two fold generations. One (A_1) tightly isoclinal and steeply plunging (in this relative orientation) and the later second (A_2), generation broad and open.

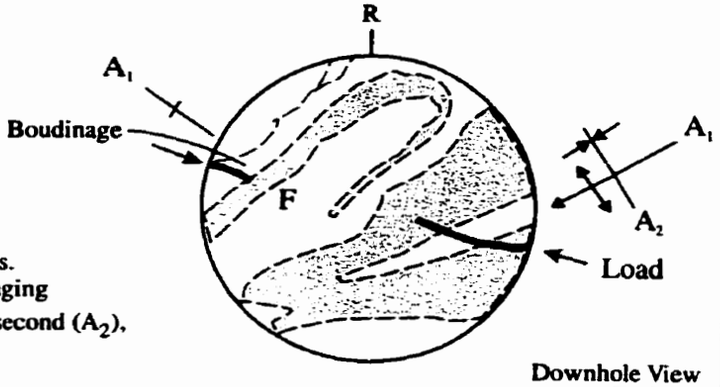

Downhole View
Fig. 2_048

Sample C

Structure	Relative Orientation	
F	100°/90°	Fractures
G_1	045°/75°NW	Schlieric layering
G_2	065°/ 85°NW	Schlieric layering

Comments

Xenolithic granite. Schlieric, fabric type 5

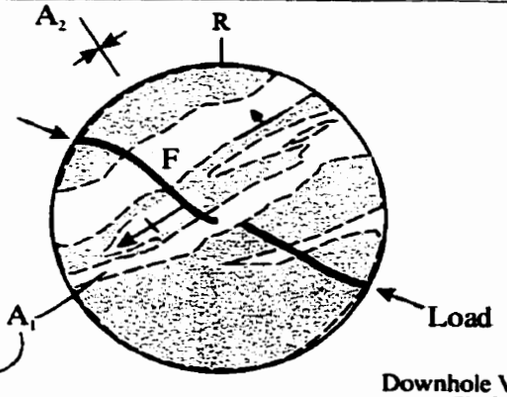

Downhole View
Fig. 2_049

Coarse Grained Granite
Borehole 418-051-RT3

Test Type (Brazilian)
Core Size: NQ-3, 45 mm

Sample D

Structure	Relative Orientation	
F	130°/90°	
G_1	045°/55°NW	
A_1	045°/90°	Axial plane
A_2	130°/90°	Axial plane

Comments

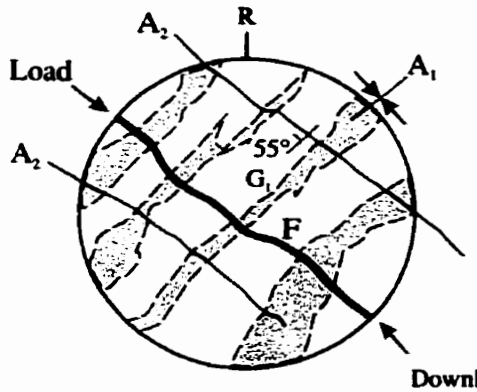

Fig. 2_050

Sample E

Structure	Relative Orientation
F	150°/90°
G_1	045°/65°NW

Comments

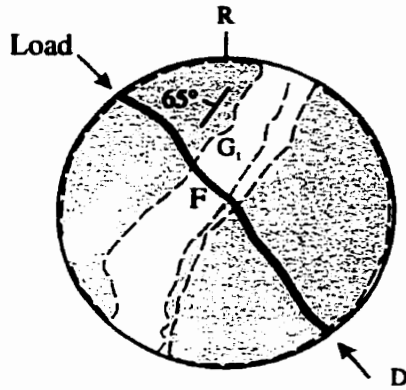

Fig. 2_051

Sample F

Structure	Relative Orientation
F	040°/90°
G_1	045°/85°NW

Comments

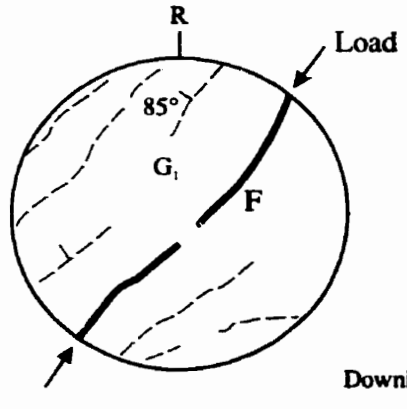

Fig. 2_052

Coarse Grained Granite
Borehole 418-051-RT3

Test Type (Brazilian)
Core Size: NQ-3, 45 mm

Sample G

Structure	Relative Orientation	
F	005°/90°	Folded on mm scale with crenulations and kinks
G_1	040° /80°N	
G_1	080° / 75°N	
A	135°/??	Axis

Also folded normal to core axis

Comments

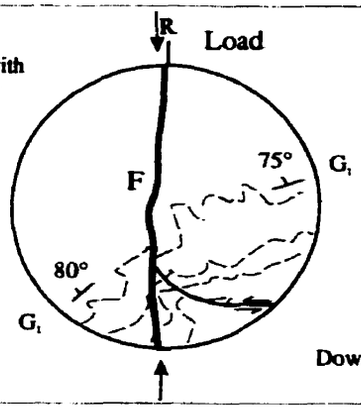

Downhole View
Fig. 2_060

Coarse Grained Granite
Borehole 418-051-RT4

Test Type (Brazilian)
Core Size: NQ-3, 45 mm

Sample A

Structure	Relative Orientation	
F	135°/90°	
G_1	090°/90°	

Comments

Very coarse grained therefore boundaries somewhat irregular..

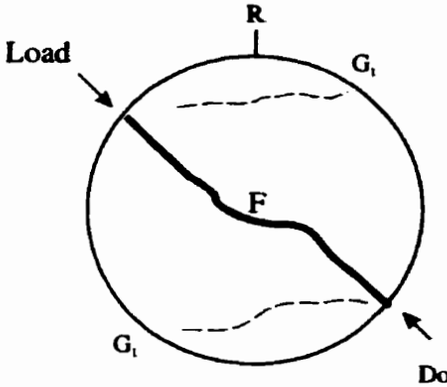

Fig. 2_038

Sample B

Structure	Relative Orientation	
F	130°/90°	
G_1	080°/90°	
G_2	070°/80°N	Boudin Planes

Comments

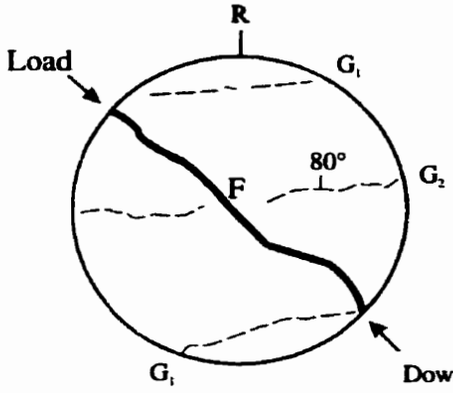

Fig. 2_039

Sample C

Structure	Relative Orientation	
F	125°/90°	
G_1	085°/ 90°	Coarse Layering
G_1	085°/90°	Boudin Planes
G_2	075°/90°	Boudin Planes

Comments

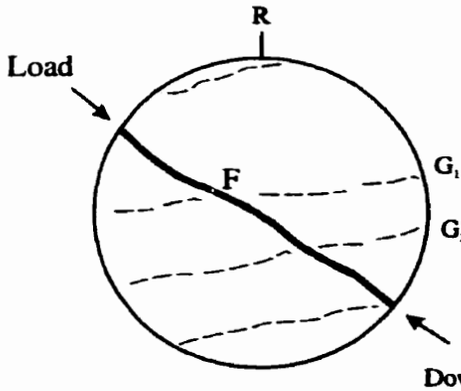

Fig. 2_040

Coarse Grained Granite
Borehole 418-051-RT4

Test Type (Brazilian)
Core Size: NQ-3, 45 mm

Sample D

Structure	Relative Orientation
F	080°/90°
G_1	090°/90°
G_2	080°/45°N

Comments

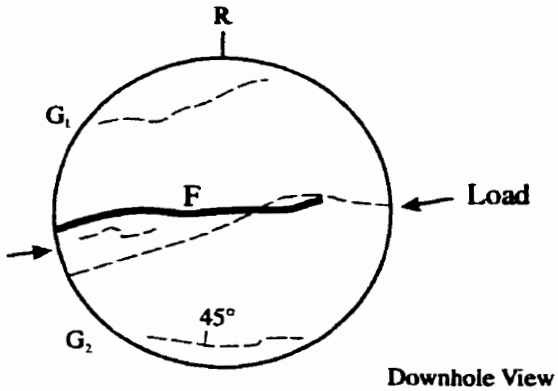

Downhole View
Fig. 2_041

Sample E

Structure	Relative Orientation
F	055°/90°
G_1	070°/90°
G_2	050°/45°NW

Comments

Boudin structure

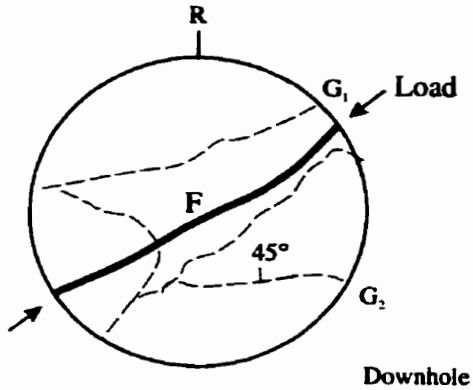

Downhole View
Fig. 2_042

Sample F

Structure	Relative Orientation
F	105°/90°
G_2	060°/45°SE

Comments

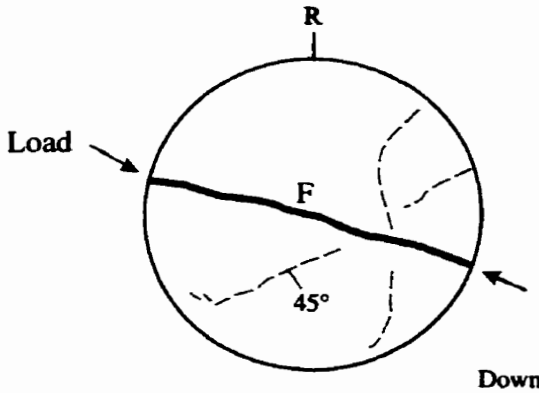

Downhole View
Fig. 2_037

Coarse Grained Granite
Borehole 418-051-RT4

Test Type (Brazilian)
Core Size: NQ-3, 45 mm

Sample G

Structure	Relative Orientation
F	130°/90°
G_2	075°/45°SE

Comments

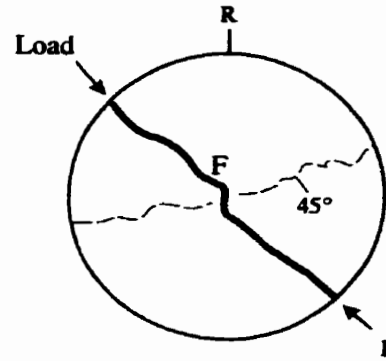

Fig. 2_036

Coarse Grained Granite
Borehole 418-051-RT5

Test Type (Brazilian)
Core Size: NQ-3, 45 mmm

Sample A

Structure	Relative Orientation
F	100°/90°
G_1	100°/65°S

Comments

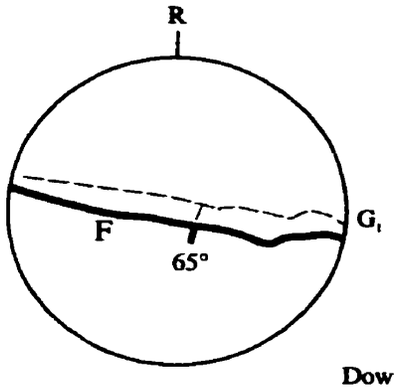

Downhole View
Fig. 2_043

Sample B

Structure	Relative Orientation
F	120°/ 90°
G_1	090°/80°S

Comments

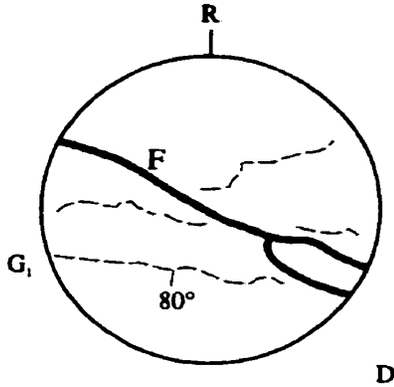

Downhole View
Fig. 2_044

Sample C

Structure	Relative Orientation
F	135°/90°
G_1	090°/80°N
G_2	135°/30°NE

Comments

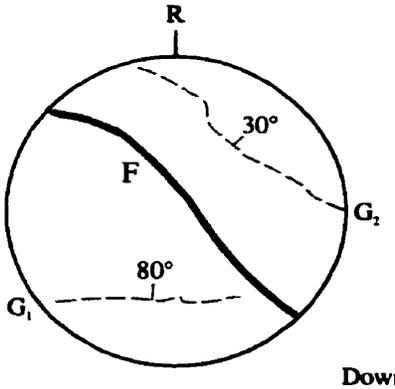

Downhole View
Fig. 2_045

Coarse Grained Granite
Borehole 418-051-RT5

Test Type (Brazilian)
Core Size: NQ-3, 45 mmm

Sample D

Structure	Relative Orientation
F	000°/90°
G_1	085°/80°S
G_2	085°/30°N

Comments

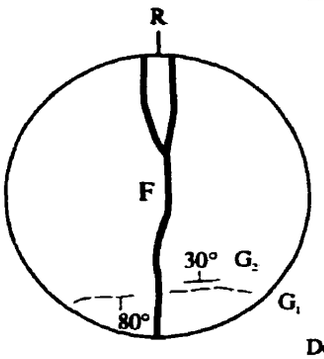

Downhole View
Fig. 2_046

Fine Grained Granite
Borehole 421-032-RT1

Test Type (Brazilian)
Core Size: NQ-3, 45 mm

Sample A

Structure	Relative Orientation
F	175°/90°
G_1	035°/45°W
G_2	175°/75°E

Comments

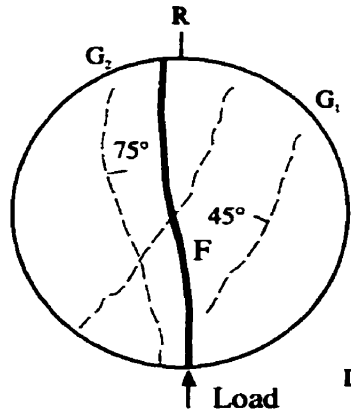

Downhole View
Fig. 2_005

Sample B

Structure	Relative Orientation
F	135°/90°
G	015°/45°W

Comments

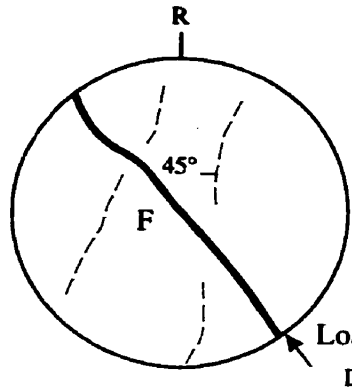

Downhole View
Fig. 2_006

Sample C

Structure	Relative Orientation
F	115°/90°
G_1	175°/45°W

Comments

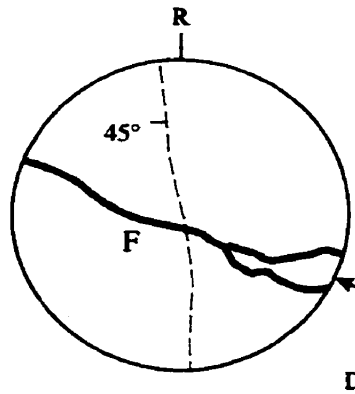

Downhole View
Fig. 2_007

Fine Grained Granite
Borehole 421-032-RT1

Test Type (Brazilian)
Core Size: NQ-3, 45 mm

Sample D

Structure	Relative Orientation
F	090°/90°
G	180°/45°W

Comments

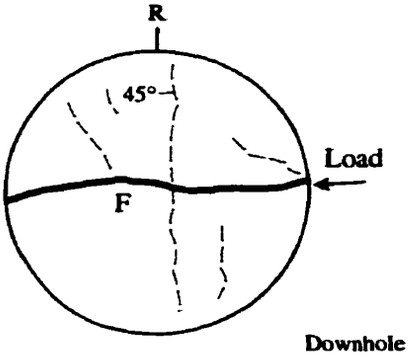

Downhole View
Fig. 2_008

Fine Grained Granite
Borehole 421-032-RT2

Test Type (Brazilian)
Core Size: NQ-3, 45 mm

Sample A

Structure	Relative Orientation	
F	000°/85°W 010°/85°W	} partially along banding
G_1	015°/70°W	flow banding
	015°/55°W	mineral alignment within banding

Comments

Loading nearly parallel to foliation

Failure at 7.0 MPa

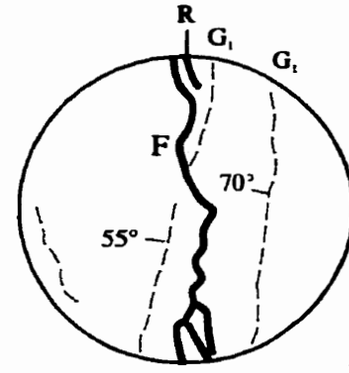

Downhole View
Fig. 2_014

Sample B

Structure	Relative Orientation	
F	135°/90°	loading direction
G_1	010°/45°W	

Comments

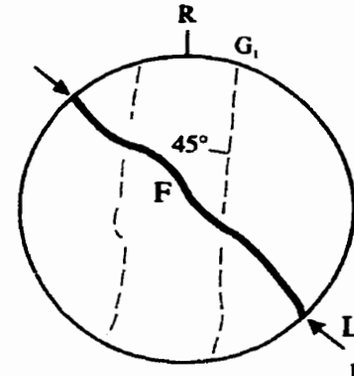

Downhole View
Fig. 2_016

Sample C

Structure	Relative Orientation
F	105°/90°
G	000°/70°W

Comments

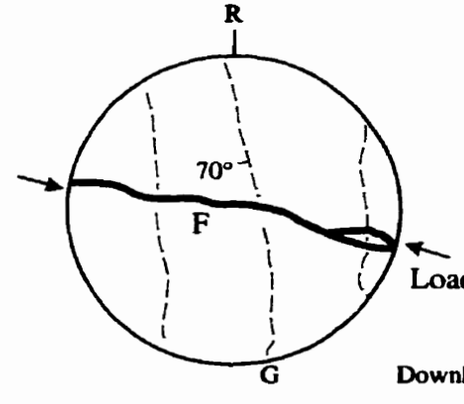

Downhole View
Fig. 2_017

Fine Grained Granite
Borehole 421-032-RT2

Test Type (Brazilian)
Core Size: NQ-3, 45 mm

Sample D

Structure	Relative Orientation
F	075°/90°
G	005°/65°W
G	005°/20°W

Comments

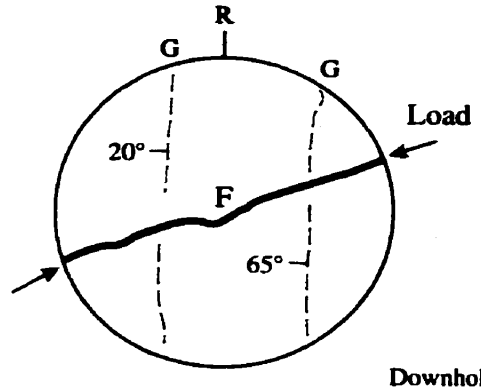

Downhole View
Fig. 2_018

Sample E

Structure	Relative Orientation	
F	000°/70°	
G	000°/70°W	banding
G_1	020°/70°W	banding
G_2	000°/45°W	mineral alignment

Comments

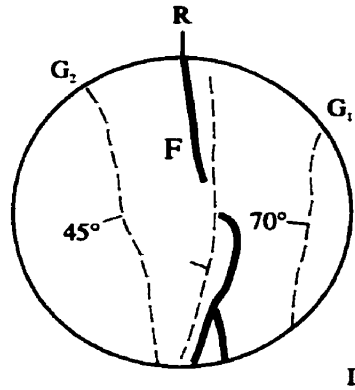

Downhole View
Fig. 2_015

Sample F

Structure	Relative Orientation	
F	116°/90°	
G_1	175°/70°W	banding
G_2	165°/45°W	mineral alignment

Comments

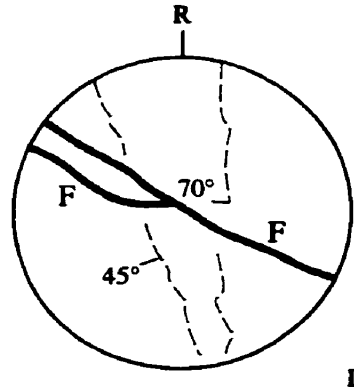

Downhole View
Fig. 2_013

Fine Grained Granite
Borehole 421-032-RT3

Test Type (Brazilian)
Core Size: NQ-3, 45 mm

Sample A

Structure	Relative Orientation
F	000°/90°
G_1	000°/40°W

Comments

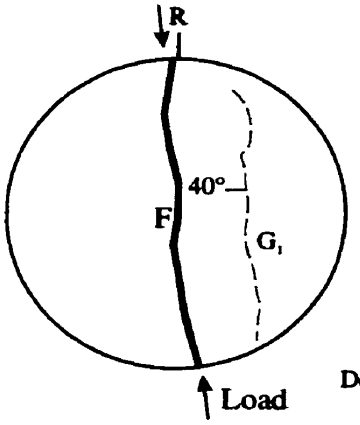

Downhole View
Fig. 2_024

Sample B

Structure	Relative Orientation
F	150°/90°
G_1	150°/75°W
G_2	045°/45°SE

Comments

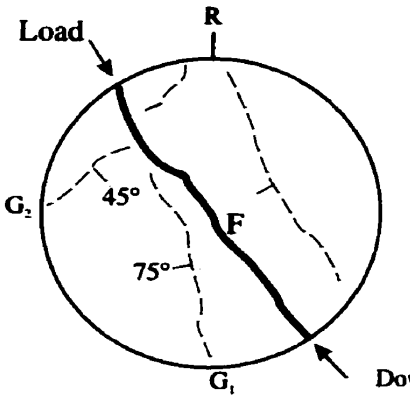

Downhole View
Fig. 2_025

Sample C

Structure	Relative Orientation
F	120°/90°

Comments

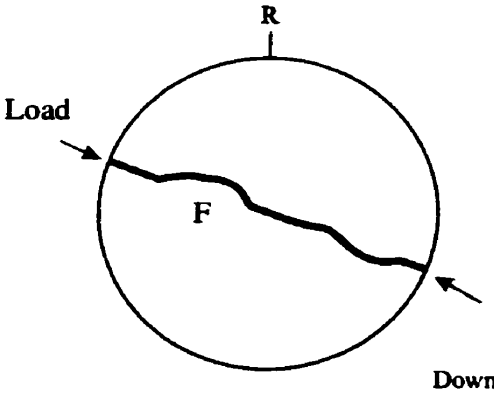

Downhole View
Fig. 2_026

Fine Grained Granite
Borehole 421-032-RT3

Test Type (Brazilian)
Core Size: NQ-3, 45 mm

Sample D

Structure	Relative Orientation
F	070°/90°
G	175°/75°W

Comments

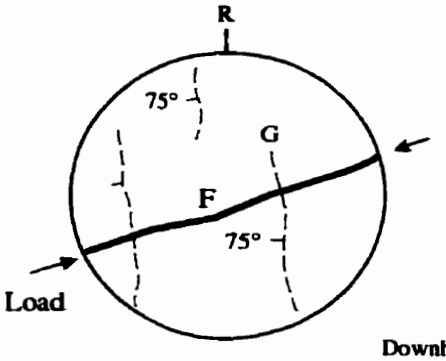

Downhole View
Fig. 2_027

Sample E

Structure	Relative Orientation
F	175°/90°

Comments

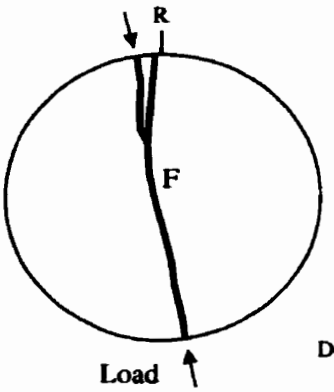

Downhole View
Fig. 2_023

Fine Grained Granite
Borehole 421-034-RT4

Test Type (Brazilian)
Core Size: NQ-3, 45 mm

Sample A

Structure	Relative Orientation
F	000°/90°
G	010°/45°SW

Comments

Angle between strike of foliation and fracture	05°
Dihedral angle between planes	46°

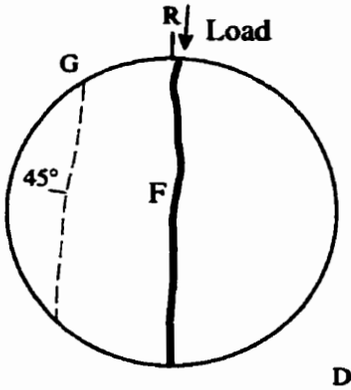

Downhole View

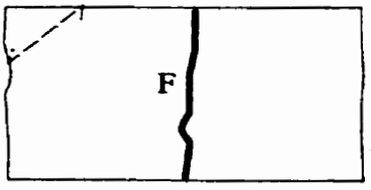

Section Normal to Fracture & Foliation

Sample B

Structure	Relative Orientation
F	140°/90°
G	170°/45°SW

Comments

Angle between strike of foliation and fracture	30°
Dihedral angle between planes	52°

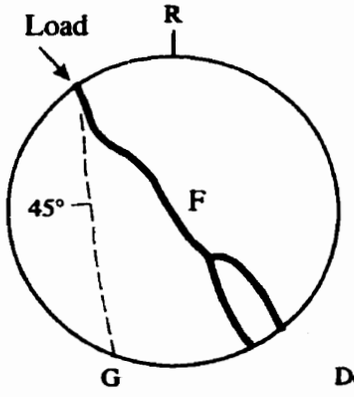

Downhole View
Fig. 2_034

Fine Grained Granite
Borehole 421-034-RT4

Test Type (Brazilian)
Core Size: NQ-3, 45 mm

Sample C

Structure	Relative Orientation
F	120°/90°
G	170°/45°SW
Lineation	120°/00°

Comments

Angle between strike of foliation and fracture	50°
Dihedral angle between planes	62°

This sample is virtually massive although a non-penetrative lineation is observed. The foliation orientation is from Sample B.

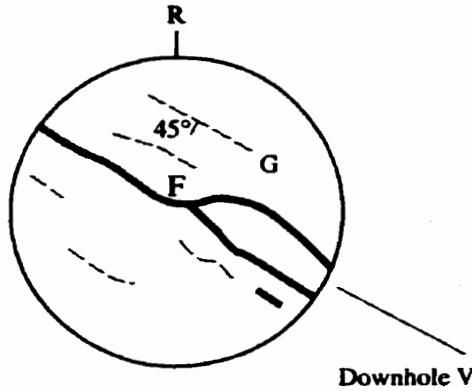

Downhole View
Fig. 2_035

Sample D

Structure	Relative Orientation
F	070°/90°
G	170°/45°SW

Comments

Angle between strike of foliation and fracture	~80°
Dihedral angle between planes	83°

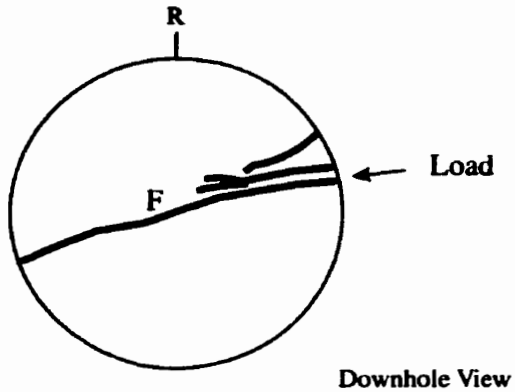

Downhole View
Fig. 2_035

Sample E

Structure	Relative Orientation
F	085°/90°
G	010°/45°W

Comments

Angle between strike of foliation and fracture	75°
Dihedral angle between planes	80°

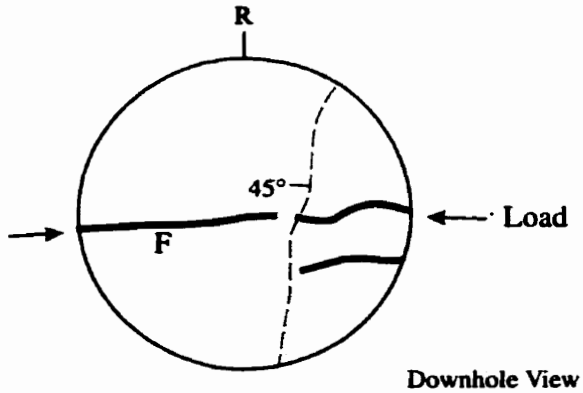

Downhole View
Fig. 2_033

Fine Grained Granite
Borehole 421-034-RT4

Test Type (Brazilian)
Core Size: NQ-3, 45 mm

Sample F

Structure	Relative Orientation
F	085°/90°
G	010°/45°W

Comments

Angle between strike of foliation and fracture	75°
Dihedral angle between planes	80°

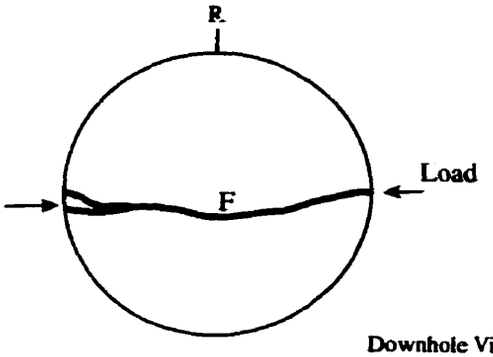

Downhole View
Fig. 2_033

Appendix C

UNIAXIAL COMPRESSION TESTS

This appendix presents the data obtained from the uniaxial compression testing conducted to define fabric-related anisotropy within the granite of the Lac Du Bonnet Batholith. The stress strain graphs and the original loading / strain data files are included. The stress strain diagrams show the axial, lateral and volumetric strains under accumulating load, and the associated data tables, listing the loads and corresponding strains as recorded by data acquisition system for each gauge. Volumetric strain was computed by using the following equation:

$$\varepsilon_v = \varepsilon_a + 2\varepsilon_c$$

where ε_v = volumetric strain, ε_a = axial strain, and εc = circumferential strain.

The inflection points on the stress-strain curves were determined manually and are listed in the tables in Chapter 9 of this report.

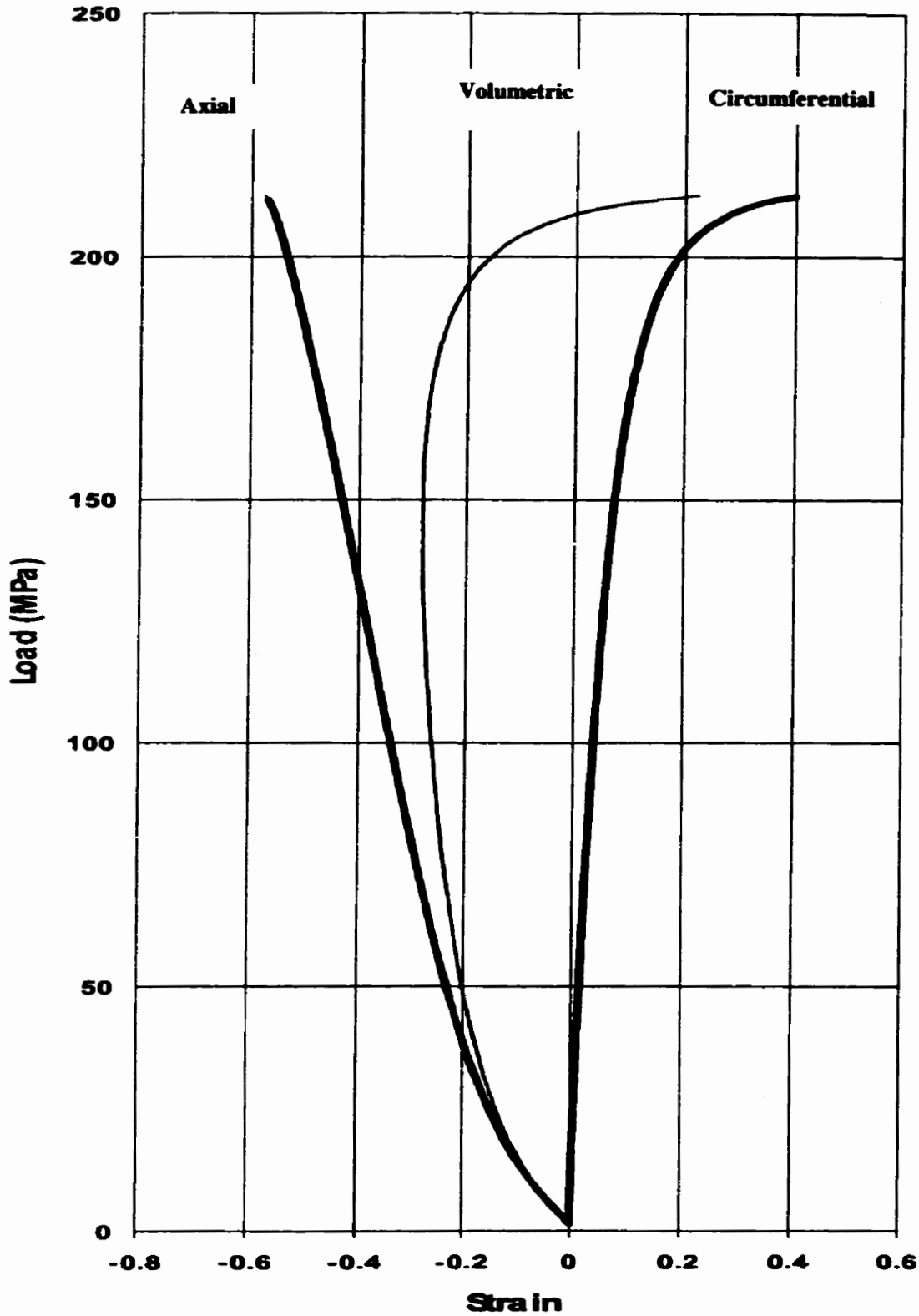

Figure C1. Stress-strain diagram obtained from a single uniaxial compression test of the fine-grained granite, borehole 421-032-RT1 (#1188).

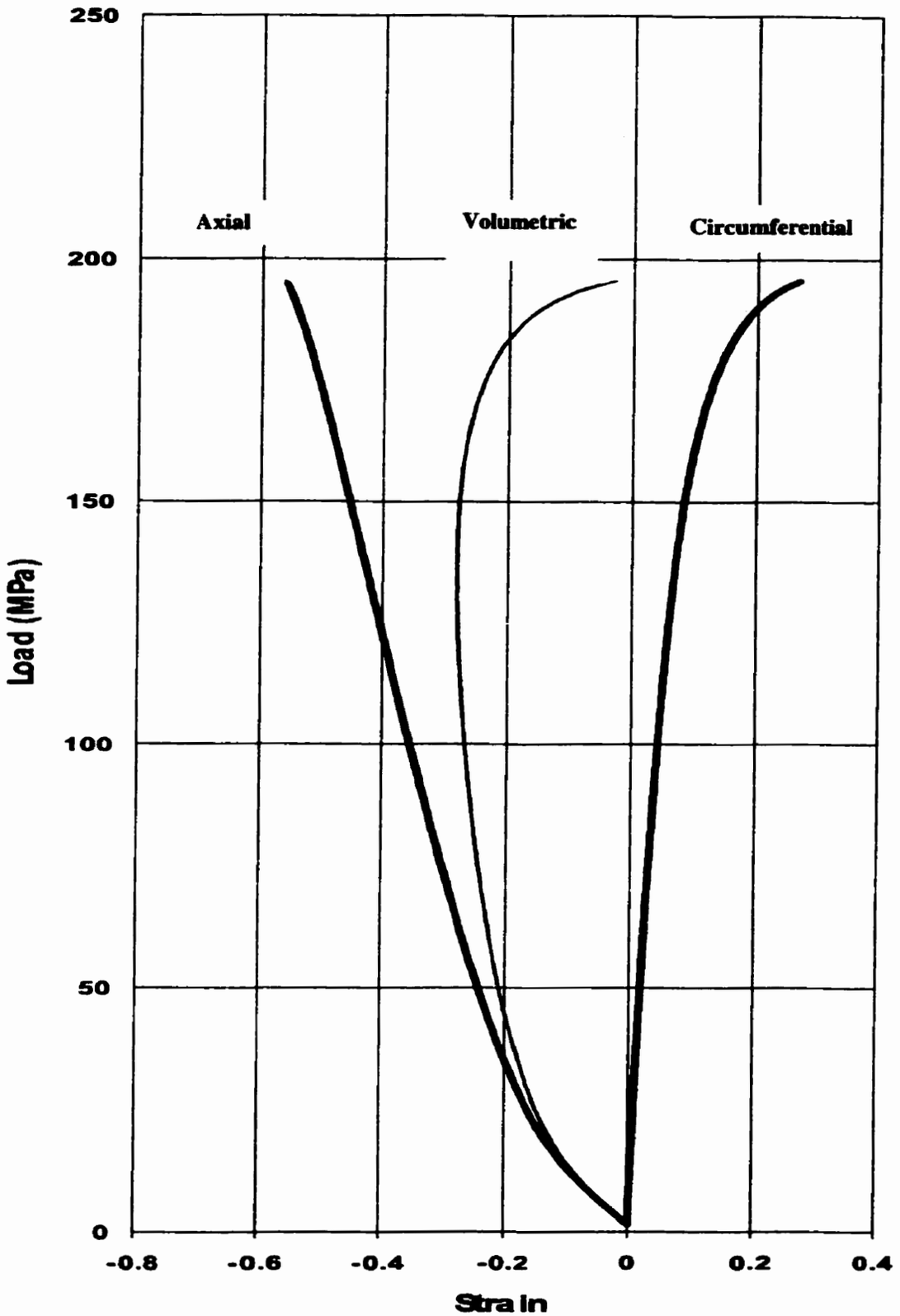

Figure C2. Stress-strain diagram obtained from a single uniaxial compression test of the fine-grained granite, borehole 421-032-RT2 (#1275).

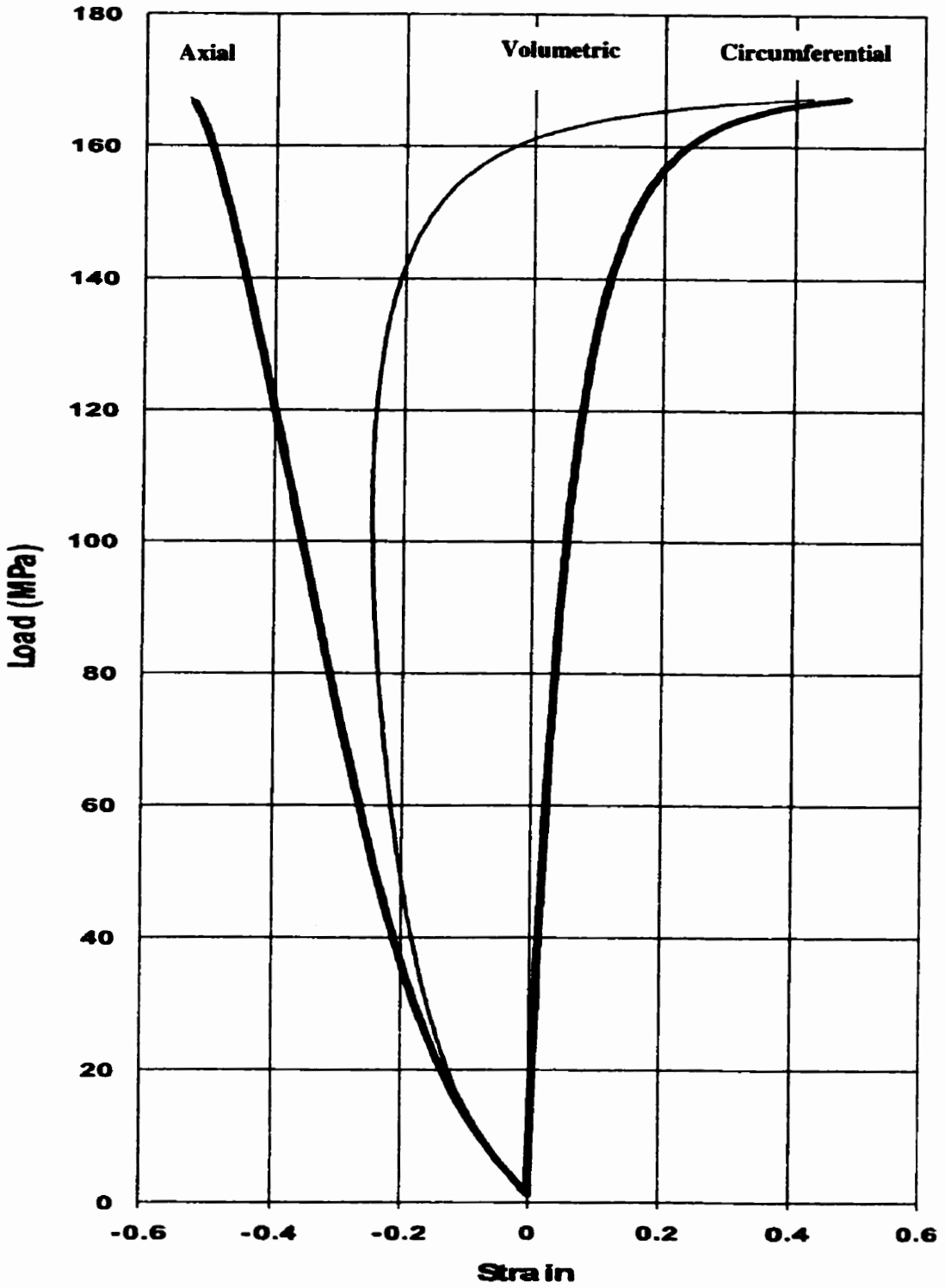

Figure C3. Stress-strain diagram obtained from a single uniaxial compression test of the fine-grained granite, borehole 421-032-RT3 (#1555).

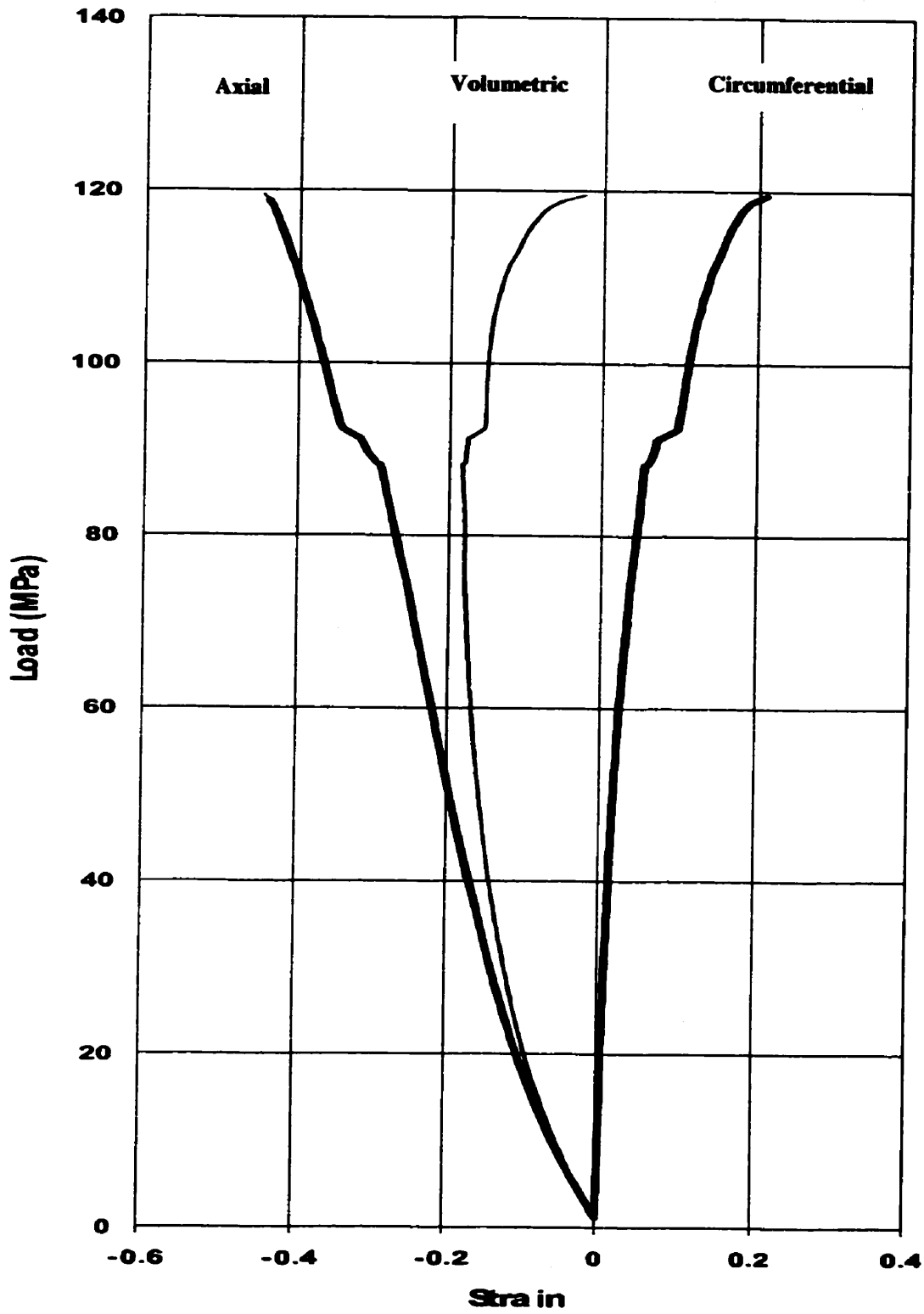

Figure C4. Stress-strain diagram obtained from a single uniaxial compression test of the fine-grained granite, borehole 421-032-RT4 (#1710).

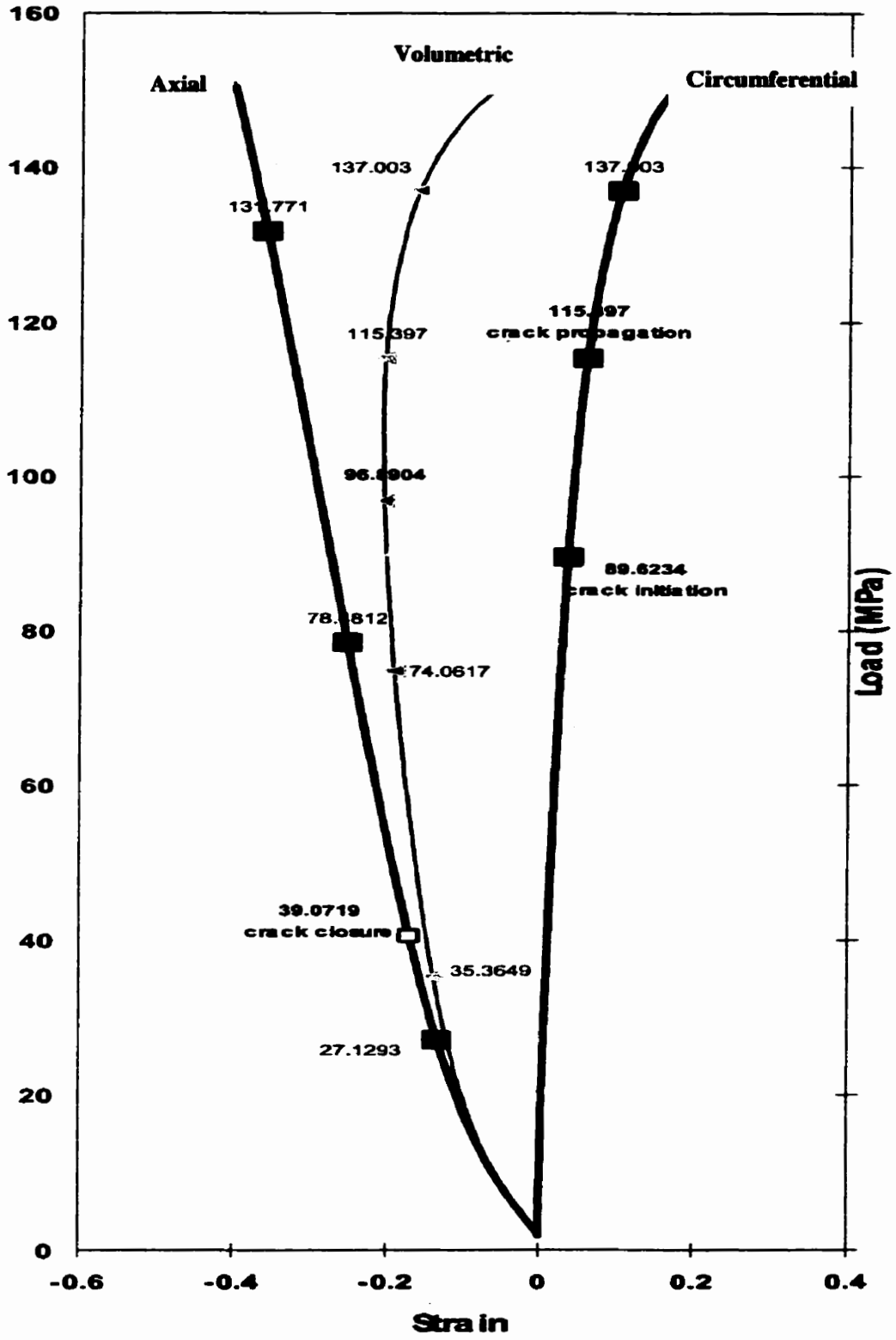

Figure C5. Stress-strain diagram obtained from a single uniaxial compression test of the medium-grained granite, borehole 417-071-RT4 (#1052).

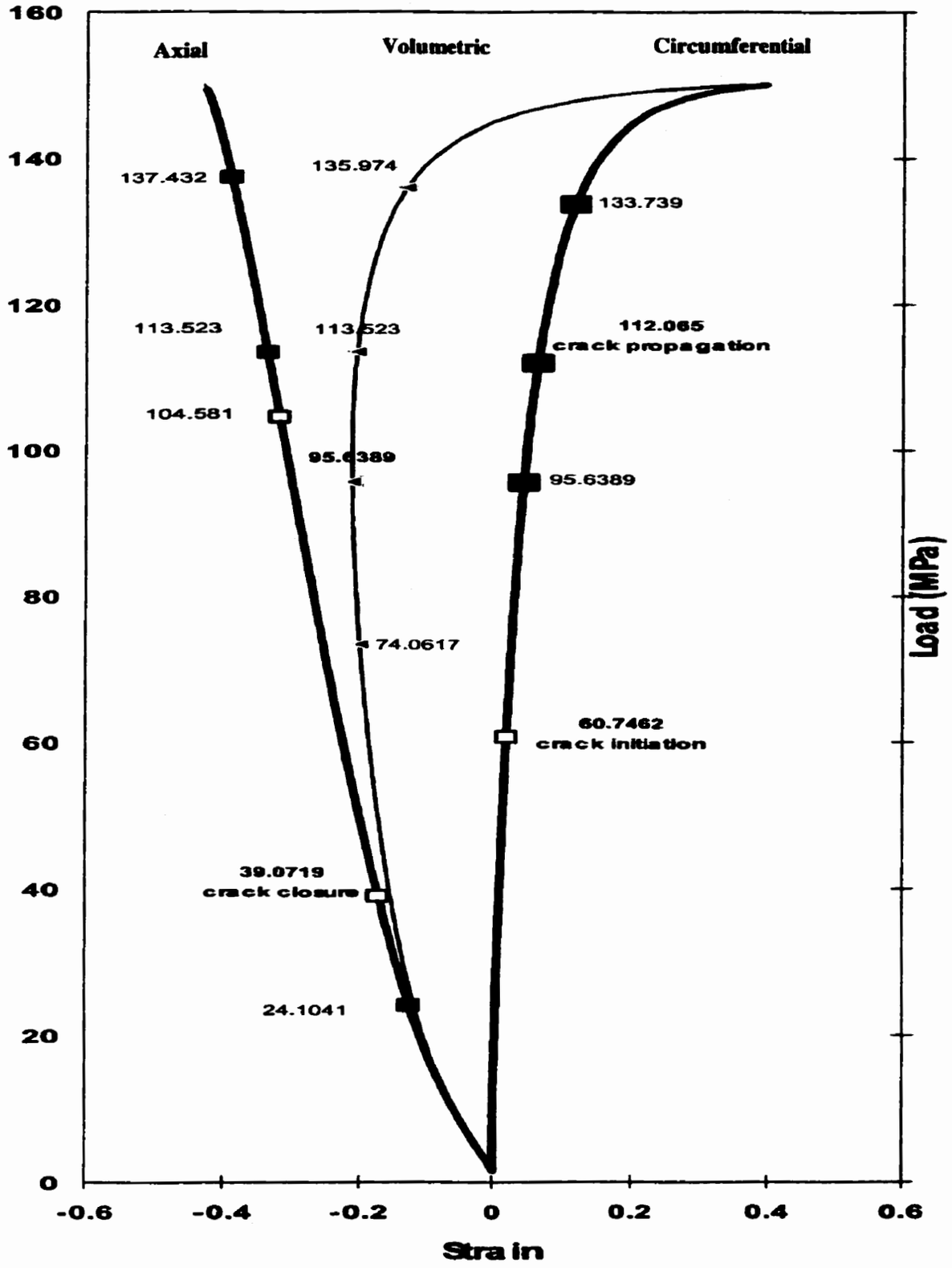

Figure C6. Stress-strain diagram obtained from a single uniaxial compression test of the medium-Grained granite, borehole 417-071-RT5 (#0831).

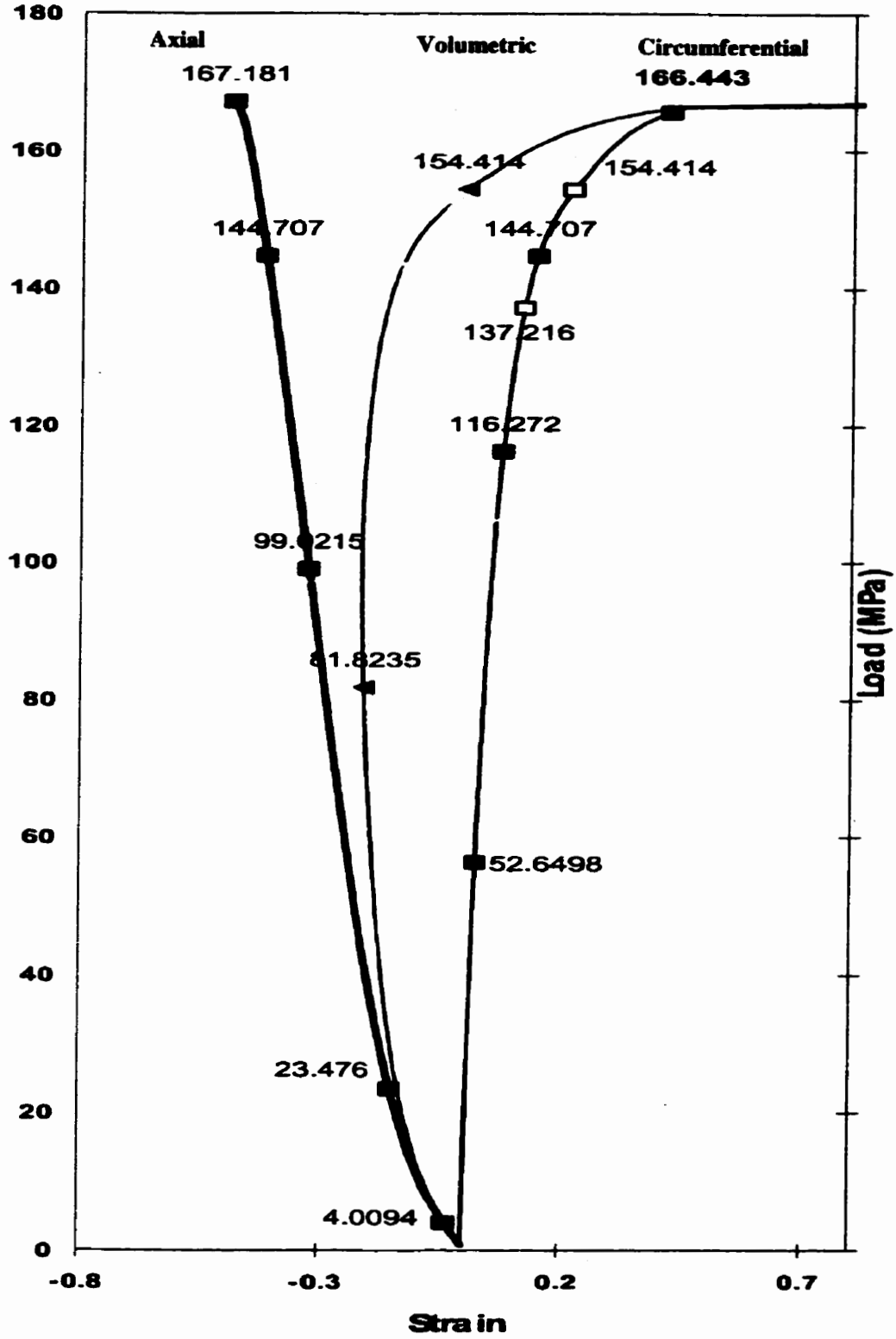

Figure C7. Stress-strain diagram obtained from a single uniaxial compression test of the medium grained granite, borehole 403-014-MB2 (#695).

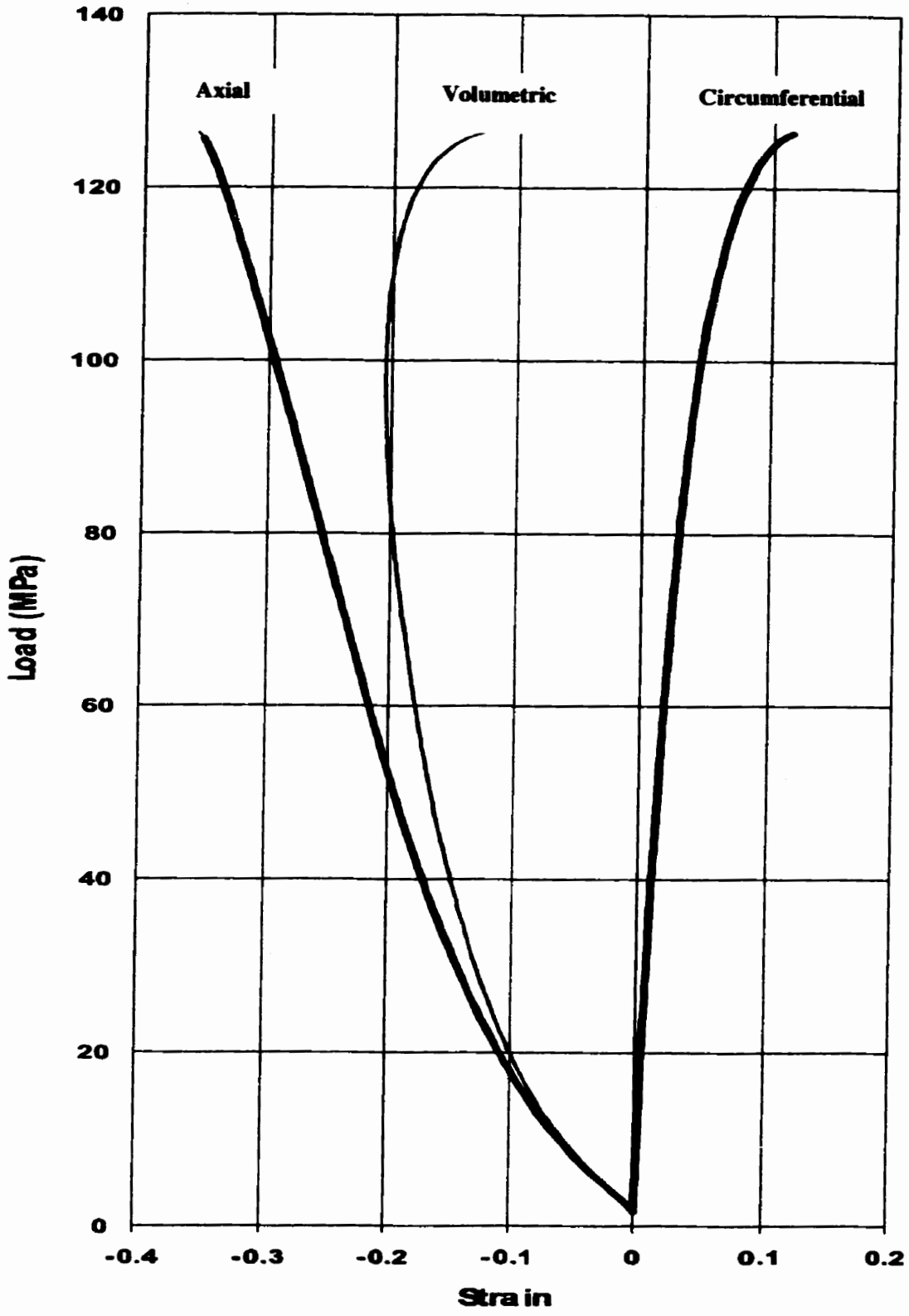

Figure C8. Stress-strain diagram obtained from a single uniaxial compression test of the coarse-grained granite, borehole 418-051-RT3 (#1335).

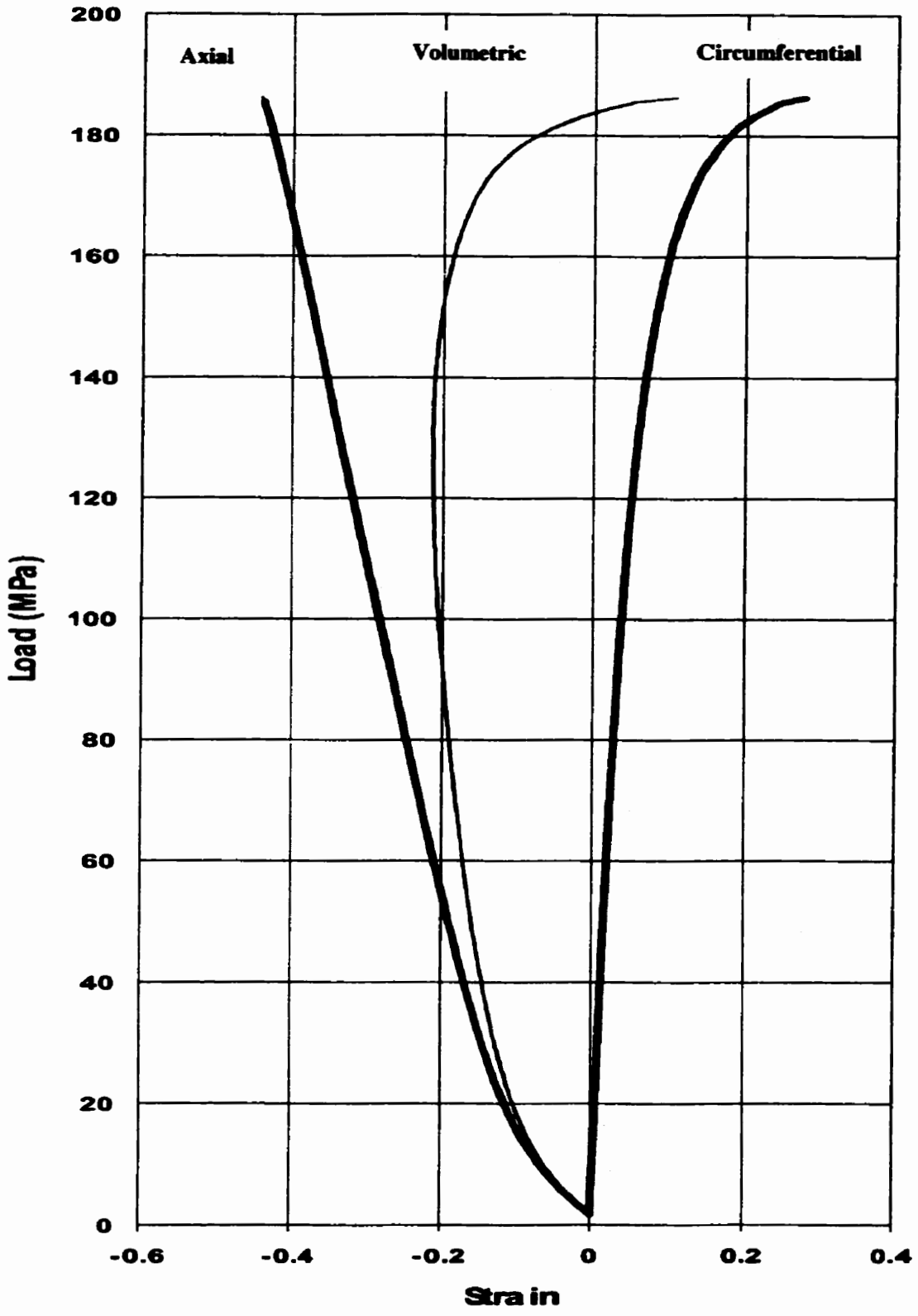

Figure C9. Stress-strain diagram obtained from a single uniaxial compression test of the coarse-grained granite, borehole 418-051-RT4 (#1342).

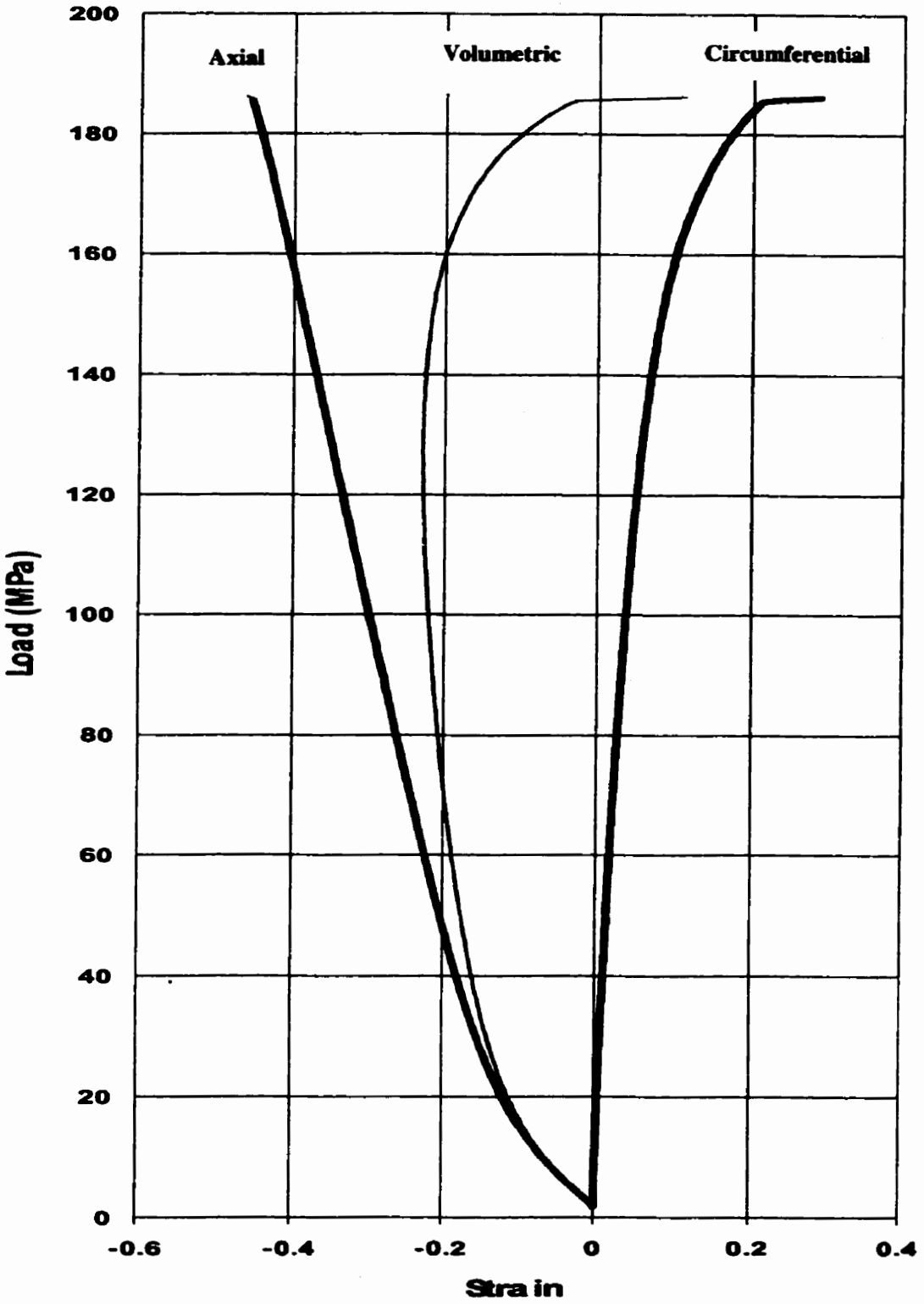

Figure C10. Stress-strain diagram obtained from a single uniaxial compression test of the coarse-grained granite, borehole 418-051-RT5 (#1114).